Award Number: W81XWH-11-C-0095

TITLE: Development of an Ocular and Craniofacial Trauma Treatment Training System

PRINCIPAL INVESTIGATOR: Mark P. Ottensmeyer, Ph.D.

CONTRACTING ORGANIZATION: Massachusetts General Hospital
Boston, MA 02114

REPORT DATE: May 2015

TYPE OF REPORT: Final

PREPARED FOR: U.S. Army Medical Research and Materiel Command
Fort Detrick, Maryland 21702-5012

REPORT DOCUMENTATION PAGE

Form Approved
OMB No. 0704-0188

1. REPORT DATE	**2. REPORT TYPE**	**3. DATES COVERED**
May 2015	Final	11JUL2011 - 10FEB2015

4. TITLE AND SUBTITLE
Development of an Ocular and Craniofacial Trauma Treatment Training System

5a. CONTRACT NUMBER
W81XWH-11-C-0095

5b. GRANT NUMBER

5c. PROGRAM ELEMENT NUMBER

6. AUTHOR(S)
Mark P. Ottensmeyer, Ph.D.,
Gianluca De Novi, Ph.D., Gregory Loan

E-Mail: mottensmeyer@partners.org

5d. PROJECT NUMBER

5e. TASK NUMBER

5f. WORK UNIT NUMBER

7. PERFORMING ORGANIZATION NAME(S) AND ADDRESS(ES)

Massachusetts General Hospital
55 Fruit St., LND-209
Boston, MA 02114

8. PERFORMING ORGANIZATION REPORT NUMBER

9. SPONSORING / MONITORING AGENCY NAME(S) AND ADDRESS(ES)
U.S. Army Medical Research and Materiel Command
Fort Detrick, Maryland 21702-5012

10. SPONSOR/MONITOR'S ACRONYM(S)

11. SPONSOR/MONITOR'S REPORT NUMBER(S)

12. DISTRIBUTION / AVAILABILITY STATEMENT
Approved for Public Release; Distribution Unlimited

13. SUPPLEMENTARY NOTES

14. ABSTRACT

A prototype of a novel simulator of ocular and facial trauma was developed for training and skills maintenance of eye surgeons and first responders in treating injuries to the face and eyes. The simulator fills a needs gap in the ophthalmological training domain between VR-based systems for cataract and retinal repair and part task trainers without quantitative measurement capabilities and offers an alternative to animal-based training. The prototype combines physical anatomical modules with instrument tracking sensors and a data acquisition, scoring and feedback system in a portable bench-top structure. The head/neck form can further be mounted to a commercial full-body mannequin to support first-responder training. We conducted user testing primarily in conjunction with the annual USUHS Ocular Trauma Course and as part of a Simulator Validation Program study and through demonstrations to local expert surgeons. Posters and oral presentations were given at local and national conferences/workshops. Options for commercialization continue to be investigated and further funded research extending this work with new features is under way.

15. SUBJECT TERMS
Medical modeling and simulation; ophthalmic surgical training; ocular trauma; facial trauma

16. SECURITY CLASSIFICATION OF:			**17. LIMITATION OF ABSTRACT**	**18. NUMBER OF PAGES**	**19a. NAME OF RESPONSIBLE PERSON**
a. REPORT	**b. ABSTRACT**	**c. THIS PAGE**			USAMRMC
U	U	U	UU	182	**19b. TELEPHONE NUMBER** *(include area code)*

Table of Contents

1. Introduction

This research program addressed an unmet need in the training for treatment of head trauma, focusing on ocular, peri-ocular and facial trauma. While improvements in armor systems have reduced injuries to the trunk and extremities, the face and head remain relatively vulnerable. Opportunities for medics to learn the treatment of facial and head trauma are limited due to the lack of realistic training simulators for this area of the body. For military ophthalmologists, critical trauma skills such as microsurgical suturing are no longer routinely taught in US residencies. Consequently, the burden of developing and maintaining these essential trauma skills is on the ophthalmologists themselves. We addressed these dual needs by creating a new prototype training system to simulate injuries of the orbit and peri-orbital tissues, including elements addressing the mandible, maxilla, and upper airway. The system functions as a procedural training system and was also designed for integration into a mannequin-based trauma simulator to support advanced, multiple trauma scenarios. It was designed to incorporate performance measurement sensors and algorithms together with physical mannequin components, conventional displays and augmented presentations of teaching content, and to provide meaningful feedback to enhance learning. The research was performed in three overlapping phases: improvement of an earlier proof-of-principle eye trauma system for preliminary user testing; substantial revision and expansion of the eye trauma system to form a full face/neck trauma system with additional eye trauma and face trauma components; and development and integration of a mannequin-compatible version of a selected set of relevant components to enable more comprehensive trauma scenarios.

This program was originally conceived as a two year research and development effort; no cost extensions supported the continuing work through an additional 18 months, accounting for initial delays and personnel changes during the first two years.

This final report summarizes the accomplishments of the entire program.

2. Body

2.1. Project background: proof-of-principle simulator development

The origin of this research program was a proof-of-principle system developed in our laboratory in response to training needs expressed by our subject matter expert, Dr. Robert Mazzoli, M.D. now of the Vision Center of Excellence. In that earlier research, Dr. Paul Neumann, Ph.D. and colleagues created a physical silicone head form with a simple replaceable left eye module, and coupled it to a pair of magnetic position tracking sensors attached with Velcro straps to the surgeon's index fingers. In performing lid laceration repair, the index figure motions were measured, with performance statistics previously employed in a laparoscopy trainer that we developed, including total exercise duration, instrument path length, an indication of motion smoothness, and a measure of amount of hand reorientation. The original project included demonstrations for the subject matter experts and others,

but did not extend to the level of collecting expert and novice performance data to create a means for distinguishing the groups and determining when a novice reached some threshold of acceptable performance.

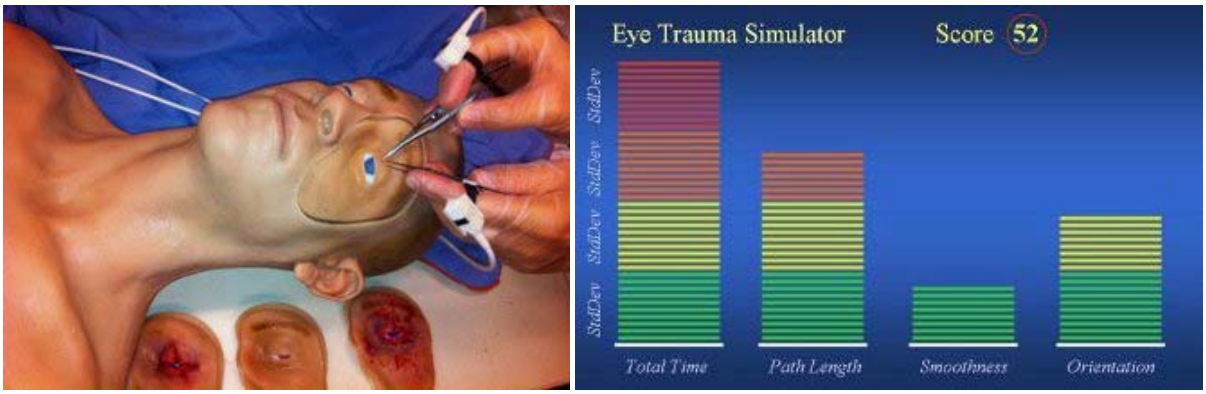

Figure 1. Proof-of-principle physical mannequin, motion tracking system, sample results plot, circa 2010.

While a promising beginning, numerous desirable changes were identified by Dr. Mazzoli and others. Anatomically, the eye lid consisted of only one layer of silicone; real lids have two major layers of differing biomechanical character and additional structures and landmarks important to correct surgical repair. A hollow eye globe was filled with a simulated vitreous humor substitute, however the cornea was opaque and the anterior chamber was a solid structure; for realism and to allow simulated injury of the globe, a transparent, thin cornea is necessary, together with an iris/pupil, which ideally should indicate light response or pathology. The lid lacerations were manually created, with limitations on how repeatable the simulated injury could be generated; a training system with standardized, replicable scenarios would be more useful and reliable as a measurement/testing system. The tracking sensors were attached to the user's fingers, providing at best a poor approximation of the motions of the instrument tips; revision of this and the expansion of the instrument suite were requested. Lastly, while the laparoscopy simulator-based scoring system used has been shown to be able to distinguish expert from novice laparoscopic surgeons (on a suitable simulator), it is a post-performance score and cannot easily be used to make detailed recommendations for improvement – a more detailed evaluation and feedback system is desirable.

In addition to addressing these system improvements, the original vision was to create a larger suite of scenarios, to be supported by a series of replaceable eye trauma modules: globe laceration (scleral and/or corneal), more complex lid lacerations, and retrobulbar hemorrhage.

The current research also extends the simulator to create a system that supports training of first responders in management of eye trauma as well. As ocular injuries are typically addressed surgically only after life threatening conditions are managed, it is essential that first responders properly protect the injured eye prior to transport, avoid causing additional damage (typically by applying inappropriate pressure), and in the case of retrobulbar hemorrhage, quickly identify the condition and take

appropriate steps to relieve pressure on the optic nerve to avoid permanent loss of vision. For this reason, developing capabilities to present eye injuries to medics and detect interventions was deemed to be important for ongoing development. Because eye trauma is often accompanied by face trauma, including additional facial trauma elements and airway management features were also considered, together with integration of a revised/improved simulator with a full-body mannequin-based simulator for combined head/body trauma capabilities.

These needs lead to the current research effort, which seeks to address them in three overlapping phases:

- Revision and evaluation of the proof-of-principle eye trauma system, including user testing
- Expansion of the eye trauma system to include additional ocular elements, facial trauma components and upper airway management elements
- Integration of the procedural trainer components into a mannequin system

Over the course of these phases, we created a substantially more advanced prototype that includes many of the desired features and developed proof-of-concept models to examine the rest.

For the evaluation and testing elements of this project, we have brought the system to the annual Ocular Trauma course offered at USUHS to obtain feedback and direction for ongoing development as well as to help in the training of ophthalmology residents

We have further been involved in a simulator validation program associated with the Ocular Trauma course, representing a near-commercial level simulator to be used in comparison with the current standard of education, namely live animal and animal-tissue-based training.

Based on these developments, we applied for and were awarded additional funding to create additional features for irreparable globe injuries, facial fracture response training and modification of the system for compatibility with an additional full-body mannequin system.

The accomplishments, described by the various milestones related to these phases, are detailed in the sections below.

2.2. Quarterly Report Administrative Details

The prior quarterly report covered the period up to and including 15 December 2014. The following details cover the remainder of the program, up to the end date of 10 February 2015.

1. Contract No.: __ W81XWH-11-C-0095 _____

2. Report Date: _3/28/2016_____

3. Reporting period from __16 December 2014__ to __10 February 2015__

4. PI: _Mark P. Ottensmeyer, Ph.D._____

5. Telephone No.: _617-768-8783__

6. Institution:__Massachusetts General Hospital_____

7. Project Title:_Development of an Ocular and Craniofacial Trauma Treatment Training System__

8. Current staff, with percent effort of each on project (applies to final quarter prior to final month for reporting):

Mark P. Ottensmeyer, Ph.D. P.I. 35%

Gianluca De Novi, Ph.D. Computer Scientist, Post-Doc 35%

Gregory J. Loan Clinical Engineer, Fabrication Lead 35%

Steven L. Dawson, M.D. co-I, SME 0%[1]

Maria J. Troulis, D.D.S. SME 0%[1]

9. Contract expenditures to date (as applicable):

	11/30/14-02/10/15	/	Cumulative
Personnel:	$ 16,852.60	/	$ 1,140,881.80
Fringe Benefits:	6176.84	/	409,544.33
Supplies:	554.32	/	71,577.24
Travel:	2866.04	/	35,997.06
Equipment:	0.00	/	139,858.50
Non-capital equipment:	-430.32[2]	/	28,342.08
Consultants:	0.00	/	15,346.40
Other:	-9896.18[3]	/	81,086.57
Subtotal:	$16,123.30	/	$1,922,633.98
Indirect Costs:	11,931.27	/	1,329,335.02
Fee:	0.00	/	0.00
Total:	$28,054.57	/	$3,251,969.00
Budget			3,251,969.00

[1] Dr. Dawson and Dr. Troulis continued to serve as SMEs and advisors during the period of the no-cost extension, with no further salary component requested.

[2] Return/refund of incompatible graphics card for primary software development workstation purchased in prior quarter

[3] Final journal entry adjustments to correct for differences between financial reporting intervals and contract end date.

10. Comments on administrative and logistical issues.

This document summarizes the full research program that lead to the development of the Ocular-Craniofacial Trauma Training Simulator, and goes into additional detail for the period following the penultimate quarterly report.

This final report was completed and submitted after the specified deadline, due primarily to issues related to first time parenthood of the PI coincident with the no-cost extension (NCE) period and underestimation of the requirements of parallel grants that began as this program reached its conclusion. The PI recognizes the importance of the submission of the final report and regrets the complications that have resulted from the delinquency of this document.

Personnel:

During the final reporting period, our staff remained stable, comprising Dr. Ottensmeyer (PI, mechanical engineering), Dr. Gianluca De Novi (software architecture) and Mr. Gregory Loan (anatomical modeling, fabrication).

Review of significant non-personnel expenses during final reporting period

During the final reporting period, the following significant expenses were incurred:

Equipment/Supplies:

- None. Only minor expenses were incurred, related to preparation of the simulator for demonstration at the 2015 International Meeting on Simulation in Healthcare conference in New Orleans, LA, 10-14 January, 2015

Travel:

- Dr. Ottensmeyer and Dr. De Novi presented the simulator at the 2015 International Meeting on Simulation in Healthcare conference in New Orleans, LA, 10-14 January, 2015 in the context of the TATRC demo area.

IRB/Human use protocol status:

There was no IRB/Human Use activity during the final months of the program. Following the end of this research effort, the protocol that had been approved by the IRB at Massachusetts General Hospital was extended to enable continuing use of the simulator at the annual USUHS Ocular Trauma Course. The continuing review documentation was forwarded to HRPO with information regarding the end of the program. They determined that no further review would be necessary by HRPO in relation to this program.

SME[4] and other expert interactions:

[4] Subject Matter Expert

On 15 December 2014, Mr. John James of Sawbones (Pacific Research Laboratories) visited the Simulation Group facility to review the Ocular Trauma simulator to evaluate whether the system or components thereof would be of interest to his company. No immediate efforts towards licensing elements of the system were pursued, however we will continue to maintain contact and explore future options as the project continues with additional support (see below).

Following our presentation at the TATRC "Corral" at the 2015 IMSH conference, we were contacted by the Center for Learning Clinical Attitudes and Skills (Centre d'Apprentissage des Attitudes et Habilites Cliniques), a CAE Healthcare-affiliated Simulation Center in Montreal, Canada, to inquire regarding the cost of acquiring one of the simulators. We have replied to their medical director and await a further response.

Lastly, also in relation to the presentation at IMSH, we made contact with Markus Schill of VR Magic, makers of the Eyesi Cataract and Vitreoretinal VR-based simulators. We have scheduled a conference call for shortly after the end of this program to discuss application of our gesture-recognition algorithms and our interchangeable instrument designs to their system.

Funding Proposals

There were no new proposals for funding initiated during this final reporting interval.

A grant from the Center for Integration of Medicine and Innovative Technology (CIMIT) awaits the arrival of our new post-doctoral research fellow to initiate an effort to develop an enucleation component, enhanced mid-facial fracture components, and modification of the head form to be compatible with other mannequin-based simulators.

The USUHS Ocular Trauma course is involved in a Simulator Validation Program effort in which our simulator is being compared with the standard animal-tissue based training. Expenses to transport and operate our system and for the consumable facial trauma modules at the 2015 Course will be reimbursed through the SVP program.

As the period of performance ended, we had scheduled discussions with SimQuest Solutions, Inc. to discuss whether our physical models and sensorized canthotomy/cantholysis components might be suitable to support an SBIR application by SimQuest, (DHP15-001, "Lateral Canthotomy and Cantholysis Training System") and will pursue the discussions further.

2.3. Research Accomplishments by Milestone

For each of the individual milestone tasks, the accomplishments over the whole of the program will be summarized, with final elements of the effort highlighted in additional detail where relevant.

The "Month #" reference follows the language of the contract, although progress proceeded in parallel across multiple milestones and completion times of the milestones varied from that of the original calendar, in part due to extension of the program during the periods of the no-cost extensions.

In the proposal, certain separate milestones were listed for completion in the same month, but were combined in the contract language. In this report, such items are separated as parts a, b, etc. where relevant.

2.3.1. "Month 1" - Review of craniofacial trauma training needs with Subject Matter Experts (SMEs), creation of specifications, limitations, detailed analysis for trauma cases.

This milestone, relevant to the Phase I work, was completed in year 1. This milestone was accomplished through multiple discussions with our SMEs, their colleagues, contacts established through TATRC and at the 2011 AFSIM meeting, and review of multiple literature sources including standard military medical training and civilian eye trauma references. Personnel consulted included Dr. Robert Mazzoli (SME), and his colleagues at MAMC, Dr. (LTC) Adam Buchanan and Dr. (MAJ) Jeffrey Shere; Dr. Jeffrey Cain; Dr. (COL) Robert Hale and his colleage Dr. Anthony Johnson at AISR; and surgeons at the Massachusetts Eye and Ear Infirmary (MEEI) Drs. Suzanne Freitag, Justin Kanoff and Daniel Lefebvre. In addition to discussions, we were able to closely observe the MEEI surgeons perform multiple ocular procedures, including lid laceration repair, suborbital fracture repair, enucleation (a procedure also mentioned by Dr. Hale), and a procedure to remove a dislodged artificial lens. Dr. Maria Troulis, one of our MGH SMEs, is a maxillofacial reconstructive surgeon; with her we reviewed photographs and CT reconstructions of examples of severe facial trauma resulting from multiple causes, as well as typical classes of upper and lower facial fractures (e.g. Le Fort fractures, typical jaw fractures).

As a whole, no changes were made to the plans for the types of injuries simulated by the system. Corresponding with preliminary discussions that lead to the original project scope, the desired scope of injury scenarios that the system address included:

For surgical scenarios:

- Full thickness lid lacerations
- Lid laceration with canalicular damage
- Intact globe with retrobulbar hemorrhage
- Globe laceration (scleral and corneal)
- Combinations of the above

For first responders:

- Protection of the eye using an eye shield and stabilization of penetrating objects
- Intact globe with retrobulbar hemorrhage
- Removal of non-penetrating foreign bodies
- Facial hemorrhage control
- Management of airway with severe damage to the lower face
- Surgical airway

Retrobulbar hemorrhage appeared in both lists as this is a condition that requires recognition and urgent response whether in the field or at a medical facility, namely lateral canthotomy and cantholysis, is included both in surgical training and also in the SOF Medical Handbook.

Our observations showed that for oculoplastics and facial procedures, magnifying loupes would be worn by physicians, so they would be able to make use of video displays showing teaching/feedback content placed near the simulator. For corneal and scleral procedures, an operating microscope would be in use and the physician would be "heads-down" for much a procedure – this suggested that an augmented reality system to provide content through the microscope would be desirable.

During this period, we also began to gather the list of necessary and desirable instruments that should be provided to the trainees and which would need to be tracked in position, orientation and actuation/force to provide quantitative data for evaluation and providing context-sensitive feedback.

Dr. Cain and others recommended that facial trauma presented should be either relatively minimal, so that intubation would be the preferred choice for establishing an artificial airway, or so severe that trainees would be faced with no alternative by to perform a cricothyroidotomy.

While facial fractures were included as part of the damage calling for hemorrhage control and management of complicated airway, surgical repair and/or stabilization of the bone fragments was outside of the scope of this simulation system program. Similarly, enucleation was been recommended as a valuable scenario. In Year 3, a proposal for funding to create modules for both of these scenarios was submitted and approved for funding by the Center for Integration of Medicine and Innovative Technology (CIMIT), as one of a series of proposals supporting the Joint Warfighter Medical Research Program. Work on this project will follow after the completion of this contract.

Of the scenarios listed above, we created a fully-developed scenario to teach repair of full-thickness lid laceration including content, tracking and realistic physical components. We created an animatronic system to generate proptosis for retrobulbar hemorrhage; an electronic valve system that has the capacity to direct fake blood to multiple sites; a series of eye globe models that support creation of incisions in the cornea and sclera for teaching repair; facial trauma modules that can be interchanged to show more or less injury to the face; a highly realistic oral/nasal/tracheal airway that can be intubated; an augmented reality simulator system that can be used to present both traditional graphical displays of information as well as projected imagery on the anatomy and graphics merged with a direct microscope view of the silicone anatomy; sensing systems to detect cuts through simulated tissue at the lateral canthus of the eye and the skin over the larynx; "unlockable" facial fracture components that can present palpable mobility of jaw and facial "bone" structures; and a software architecture that quantitatively measures and responds to the performance of the trainee, which can be adapted to a wide range of procedures. Lastly, we modified the procedural head/neck form of the system to be mounted in a commercial full-body mannequin to support the capability for use in a multiple trauma/first responder scenario. Many of these features have been demonstrated to elicit expert opinion, and the lid laceration scenario and features have been used for three years at the USUHS

Ocular Trauma course, including as part of a comparison study between training on animal tissue and on our silicone-based simulator, which is ongoing at the conclusion of this phase of our research program.

2.3.2. "Month 2" –

2.3.2.a. Review of treatment modes and potential error modes to be detected

This milestone, relevant to the Phase I work, was completed in Year 1. Based on discussions with the SMEs, primarily Dr. Mazzoli and Dr. Freitag, we developed a series of measurements relevant to the treatment modes appropriate for the scenarios described above. These measurements have thresholds or criteria that will allow for the determination of success or error states.

For the surgical interventions, the primary source of performance information is the 6 degree of freedom (DOF) magnetic position trackers described in more detail below. With instrument motion data, we measure global criteria including path length, performance time, motion smoothness, and amount of instrument reorientation and can derive additional global measurements. While useful from an overall scoring perspective, more detailed measures are needed to provide useful immediate feedback for improvement. As a result, we determined that detection of the sequence of surgically relevant gestures is an important element of evaluation of treatment and errors. Performing gestures out of sequence or missing elements of a procedure can be flagged as errors or deviations from the ideal. Surgical gesture recognition and analysis methods that we developed are described in sections 2.3.2.b.v, 2.3.5.b, and 2.3.7.c.iv. Analysis of the gestures allows detection of numbers and types of suture throws, knot types, potentially size of needle "bites," and sequencing of these. As a parallel measure of performance, multiple eye surgeons mentioned that with increasing stress or also through inexperience, trainees may grasp instrument with excessive force; we are able to measure this in part through sensors installed on the surgical instrument (strain gages to measure instrument deformation). Feedback can be given to the user immediately, allowing him or her to improve performance during the course of a scenario, rather than receiving such feedback only after completion and receipt of a final score.

For general management of the head, relative positioning of the head can be sensed using the magnetic tracking system. This is especially important when cervical spinal injury scenarios are considered and it also allows the system to synchronize the motion of the head and hand gestures during data acquisition.

Additional measurement and sensor systems that were identified and studied to the level of proof-of-concept but that were not implemented in the final prototype version of the system include:

- Sensing of force/pressure applied directly to the globe, indicating incorrect application of an eye shield
- Detection of water-tightness of globe suturing and establishment of hemostasis
- Sensing direct pressure applied to simulated facial wounds/bleeding

Measurements identified for consideration in future versions include:

- Automatic measurement of alignment of geometric/anatomical landmarks, e.g. lid margins, corneo-scleral margin
- Detection of the presence of a scleral shield, placed on the globe to protect it during lid repair, but left behind after completion of the scenario

The system can accommodate the implementation of such features in future developments should they be required. An electronic valve system includes components to pressurize the eye globes, the selected microcontroller system has sufficient analog and digital input lines to sense multiple pressure and force sites, an improved/repositioned video camera could detect anatomical alignments, and inclusion of the scleral shield insertion suction device among the position-tracked ophthalmological instrument suite will allow for tracking the insertion and removal of the shield.

2.3.2.b. Implement improvements for upgraded proof-of-concept stand-alone eye trauma simulator based on feedback from preliminary user testing by CIMIT[5] project advisors.

This phase of the work comprised the largest element of the Phase I work, and focused on improvements to the simulated anatomy, the suite of instruments available to the surgeon/trainee, position and additional sensing capabilities, development of a functional, structural system for the simulator, a versatile user interface and data collection architecture, and development of didactic content and a presentation architecture appropriate to the scenarios under development.

Accomplishments in these areas are described as chronological developments to provide context. Additional modifications to the design based on later phases of the work are described in later sections.

2.3.2.b.i. Eye globe anatomy

Improvements to the original, proof-of-principle system eye globe are numerous. The original globe had an opaque, tinted cornea, no lens or iris, and a preliminary estimate of scleral thickness. In year 1 we:

- Created clear, anatomically sized lens; more accurate scleral thickness with integrated nylon mesh to resist silicone fracturing and enable anchoring of sutures; colored irises of anatomical thickness; transparent corneas with open (rather than solid) anterior chamber
- Evaluated, with assistance from our SMEs, a series of viscoelastic materials for use as the vitreous humor within the globe, including polyvinyl acetate “slime”, egg white (as suggested through contact with Phillips Studio, a potential commercial contact for production of anatomical components), and a series of silicone and water-based personal lubricant materials
- Modified the globe design to approach compatibility with actively driven actuation of eye motion and integration with an internal pupil contraction mechanism, pressure/force sensing.

Further developments in later years are described below in the context of development of the eye motion mechanism, exploration of pupil contraction mechanisms and development of the full-face replaceable modules.

[5] Center for Integration of Medicine and Innovative Technology, Massachusetts General Hospital, Boston, MA

Figure 2: Top row: original eye globe with opaque cornea; new transparent lens; molded, mesh-reinforced sclera; molding of iris; iris installed on new globe. Middle row: molded transparent corneas; assembled globe with normal sclera thickness, iris, cornea and lens; samples of gel/lubricant materials compatible with silicone anatomy evaluated for similarity to vitreous humor. Bottom row: "stringiness" property of Astroglide shown as fingers are separated, similar to vitreous humor characteristic; new globe concept with rigid backing for use with animatronic eye module (Phase II).

We also made contact with Phillips Studio, UK, who creates commercial globe models for training vitreo-retinal surgery, cataract surgery and strabismus. They did not have trauma simulation products, and their globe models were not directly compatible with our concepts for the Phase I or Phase II systems.

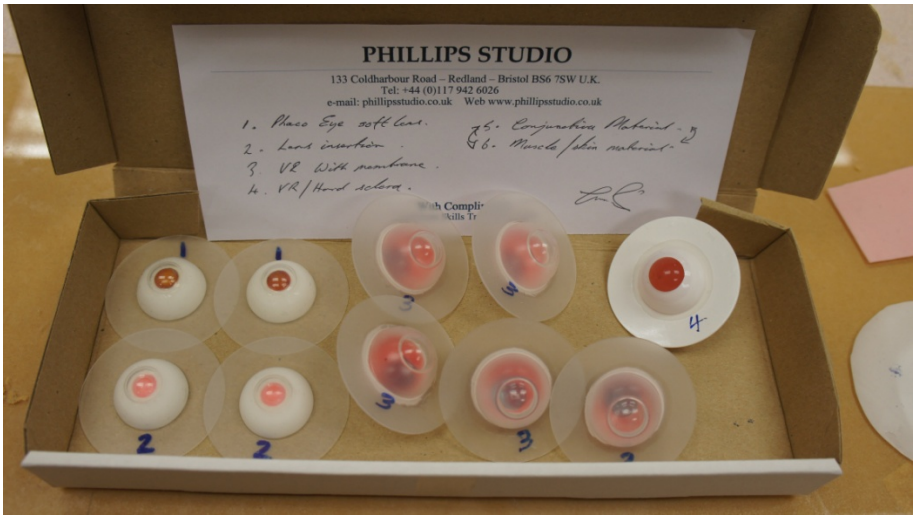

Figure 3: Samples of vitreo-retinal surgery simulation globes from Phillips Studio.

2.3.2.b.ii. Eyelid and periocular module anatomy

The overall module structure for the Phase I system was retained during the early portions of the work for compatibility with the original head form. Numerous modifications and improvements were implemented during Y1 of the program, however.

- A series of experiments to evaluate production techniques, materials, cost-effectiveness of varying levels of artistic moulage features were conducted. We reached a stable selection of silicones for casting the skin elements (Smooth-On, Inc., Macungie PA, EcoFlex 0030 tinted with SilcPig for skin/eyelids). Installation of realistic eyelashes is desirable to the surgeons (to replicate the tangling that often occurs with suture threads), however it is a highly labor intensive process.
- Additional anatomical features were added, notably a tarsal plate layer in response to the SMEs' criticism of the original single-layer eyelid (Smooth-On, Dragon Skin 10). The tarsal plate underwent a series of revisions, to include reinforcing mesh and multiple tests of different durometer silicones to better approximate the correct feel of a needle penetrating the tissue
- The head-form skin layer was modified to correct a gap between facial skin and the module skin in the original system.

Figure 4: Top row: experiments with use of alternate silicone materials to produce correct palpation response of skin, explore cost-benefit relationship of increased realism (e.g. eye lashes, brows); original gap in face/module margin. Bottom row: modified molds showing pre-molded tarsal plate installed for overmolding process; back side of lid laceration module showing higher stiffness tarsal plate structure; front side of lid laceration module after suturing the full thickness "wound".

During Q4, initial efforts focused on preparations for conducting user data collection at the USUHS eye trauma course:

- A standardized lid laceration feature was built into the molds to ensure repeatability in creation of the trauma modules (allowing for more direct numerical comparison between trainees).
- Small "dimples" were added to the skin surface to provide calibration points for the tracking system to allow registration between the physical module and the mathematical model used to

define Regions of Interest (see section2.3.2.b.v) relevant for different phases of a surgical procedure.

- Positive attachment points were added to improve repeatability in module installation and eliminate the possibility of module shifting during the course of a scenario.
- Molds were revised to streamline the casting and module production process
- A set of 25 modules was produced for use in the data collection trials at the annual Eye Trauma course at USUHS in May 2012.

Figure 5: (left to right) Y1 module design with dimples for position calibration – instruments contact at each location to confirm position and orientation; attachment/alignment features to maintain stability of module during scenario; installation of module; 25 modules prepared for USUHS user testing.

2.3.2.b.iii. Sensorized surgical instruments

The original proof-of-principle system made use of four available stainless steel instruments lent to the team by Dr. Mazzoli, and a pair of Ascension model 800 sensors attached to the user's fingers using Velcro straps. It was clear from discussions with the ocular surgeons that a larger suite of instruments was necessary, with different instruments available for oculoplastics (lid repair) and for the corneoscleral procedures (typically finer tipped, smaller instruments). Further, attachment of the position sensors to the user's index fingers was of limited usefulness in measuring the gestures performed by the surgeon – estimating instrument tip position and orientation would be essentially impossible, since (in our observations of live operations) surgeons often reposition, rotate and even invert the instruments in their hands.

Over Y1, we broadened the set of instruments available from 4 to 9 plus a surgical sponge "spear". We created rigid attachments for the position tracking sensors (now smaller) to the instruments, but added additional sensing capabilities, signal conditioning, hot-swappability, and automated instrument identification by the data acquisition system.

We continued to make use of the Ascension trakSTAR magnetic tracking system, however we did consider alternate sensing technologies. The primary alternative is optical tracking. These systems, to achieve measurement of instrument position and rotation, typically require the attachment of an array of optical markers or retro-reflectors, arranged in a known, 3D arrangement, and ideally the mounting of multiple tracking cameras around the system. For our purposes, and given the observed instrument

manipulations, we concluded that the tracking markers would interfere with the surgeon's normal manipulations more than the attachment of a flexible cable, and that mounting multiple cameras would be more complex for ultimate end users than a single magnetic field emitter. The clear advantage of optical systems over magnetic is immunity to sensing distortion from the presence of nearby ferrous materials, however we designed the system with as few ferrous elements as possible.

Described in later sections, we also reviewed the main competitor, the Polhemus (Colchester, VT) FASTTRAK system, to evaluate alternative sensor cable properties. During most of this program, Polhemus did not have a micro sensor available to match the small sizes of Ascension's system, however their cables were substantially more pliable. Only at the end of the project did Polhemus release an equivalent sensor, however as described below, the Ascension price structure continued to be more advantageous and the difference in cable compliance was determined by users to be not of sufficient significance to warrant changing technologies.

The following figures show:

- Expansion of the instrument suite from four to nine (with additional instruments added in later years) and acquisition of titanium instruments (vs. steel) to minimize field distortion due to the instruments (see Figure 6)
- CAD modeling of the instruments to provide graphical models for integration into the data acquisition/user interface software and support development of connectors/sensor holders and finite element analysis of the instruments (Figure 7)
- Attachment of strain gages at critical locations to measure the flexing of the instruments as the jaws are closed, and measure the deflection of forceps tips when grasping tissue or upon closure, and a prototype signal conditioning system and interface to the data acquisition software with the current, miniaturized equivalent version. The finest tipped forceps have been equipped with a silicon strain gage sensor (not shown), much smaller than conventional foil gages, so that force sensing can be made even on the very gentle manipulations during corneo-scleral manipulations (Figure 8)
- A series of tracking sensor mounts, from an early fixed system for testing (which would require nine separate tracking sensors - Figure 9), an initial version allowing interchangeability of the tracking sensors between instruments (allowing for just three position tracking sensors to be necessary - Figure 11), a later version integrating an onboard signal conditioning circuit sending a pre-amplified signal back to the data acquisition system, a revision of the miniature circuit board to minimize self-heating and single drift (Figure 10), and a version which includes an array of mounting points so that the user can interchange the connector using only one hand (Figure 11 – later versions are described in 2.3.4.c).
- An initial prototype data acquisition board using an Arduino kit microcontroller system, followed by an improved, USB-compatible custom board which is expandable to allow multiple functions to be sensed or controlled over the single USB connection (Figure 10).
- Elastic wrist straps with cable-management clips attached. We developed these for the users to wear to help minimize sensor cable tangling during a scenario. One sensor cable would run

through the clip on each arm, with the third sensor cable available for instruments left on the array tray (Figure 9 and Figure 11). This cable configuration was retained throughout development of the system.

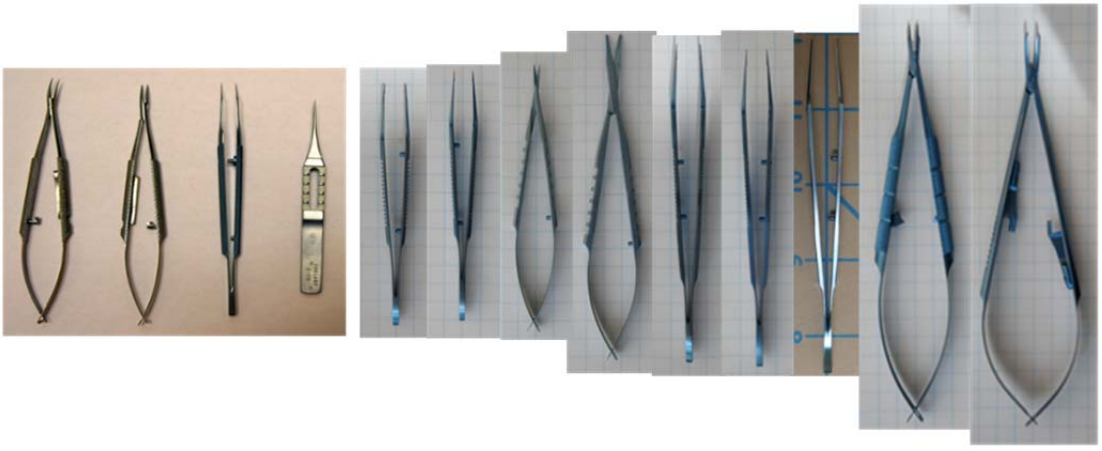

Figure 6: (left) Original steel instrument suite. (right) New titanium instrument suite (to scale)

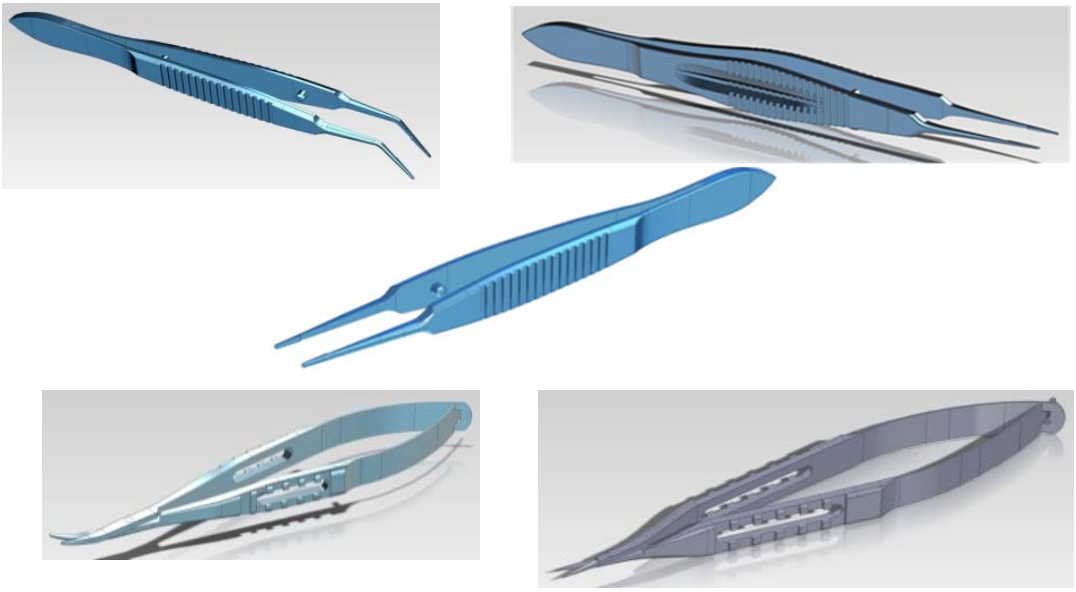

Figure 7: CAD models of instruments for use in visualization tools, finite element analysis

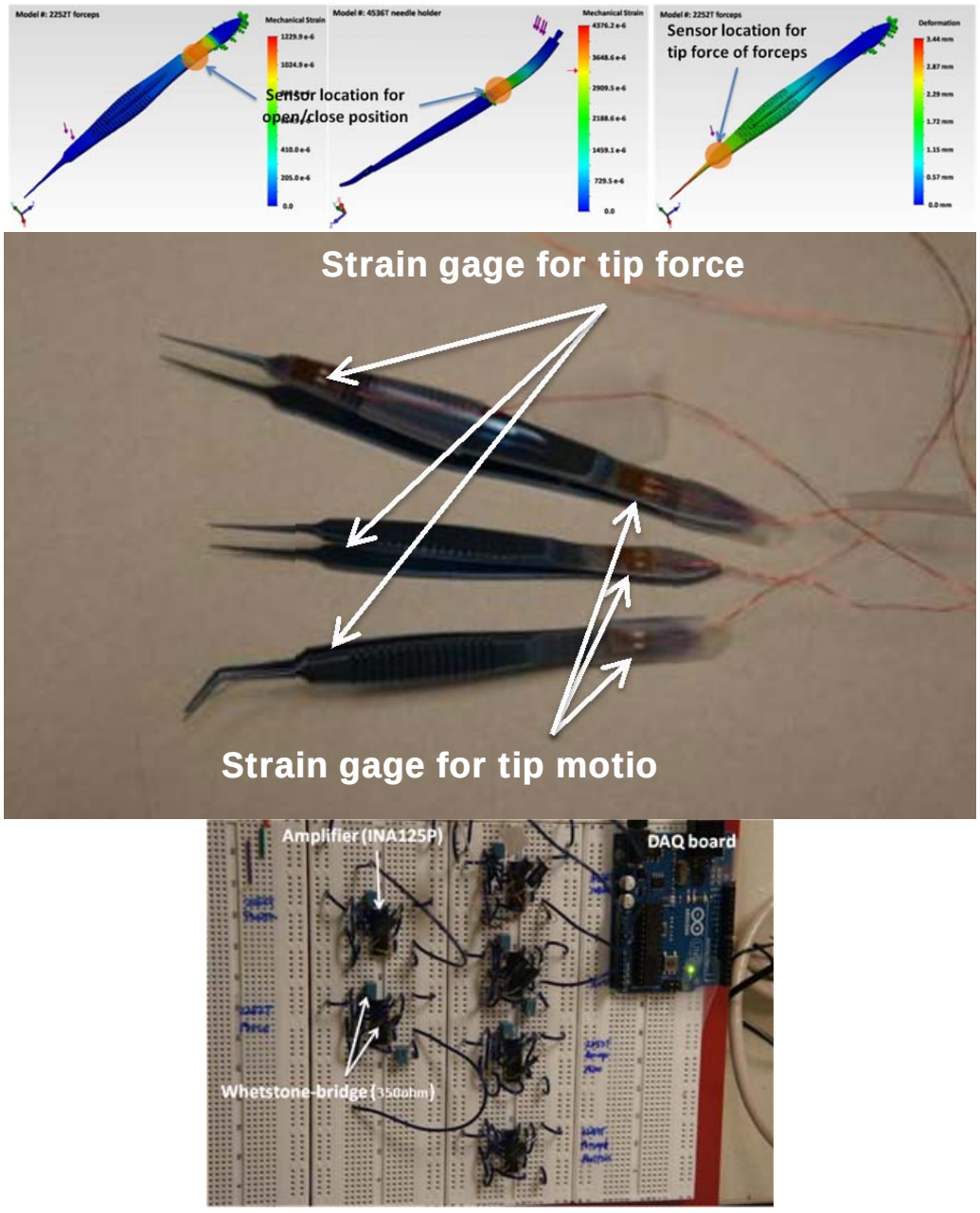

Figure 8: (top left, center) Finite element analysis (FEA) of forceps and scissors showing locations of high strain, optimal for strain gauge placement for measuring grasping/closure action. (top right) FEA showing location of high strain under tip loading for measuring applied force. (bottom) Strain gauges attached to three forceps; breadboard test circuit for amplifying strain gauge output signals.

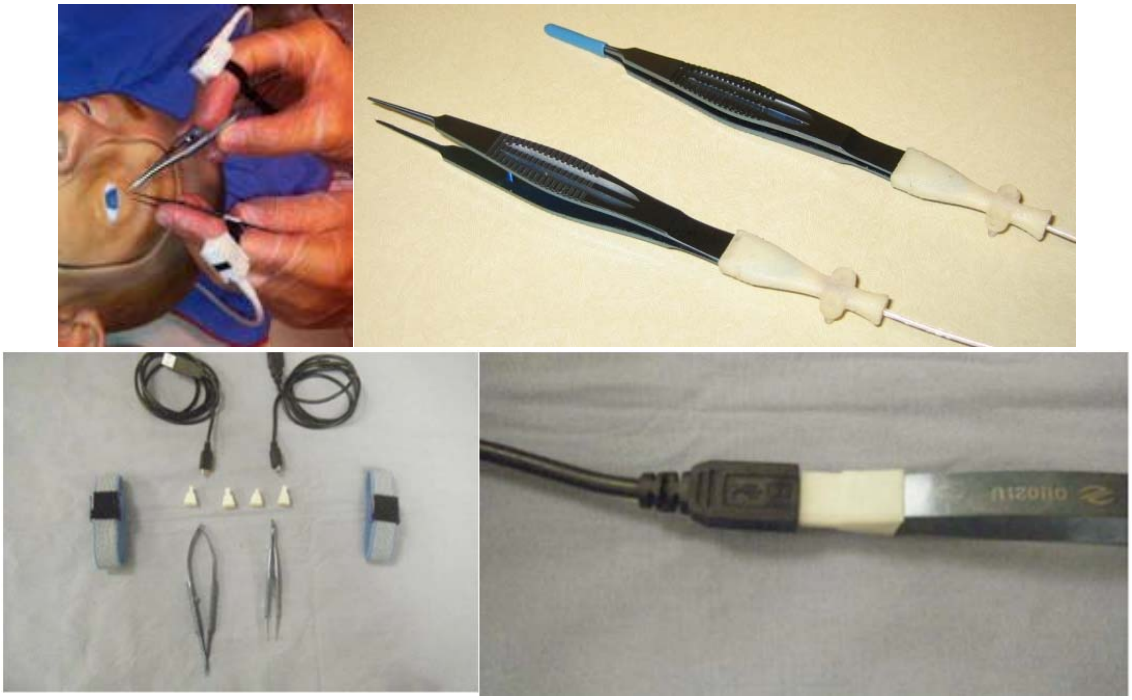

Figure 9: (Top) Original finger-mounted position tracking sensors; version 1 of sensor mounting rigidly attached to instruments directly for improved tracking accuracy. (Bottom) Version 2 of sensor mounting fixtures with swappable connectors and wrist straps for cable management; detail of version 2 connector to needle holder.

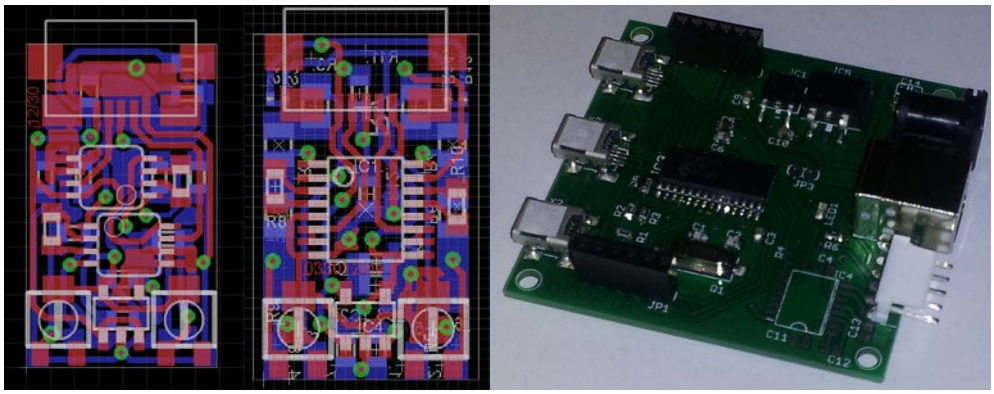

Figure 10: Miniature circuit boards for strain gauge amplification and instrument identification (larger than actual size); Data acquisition board for strain gauge signals, board identification.

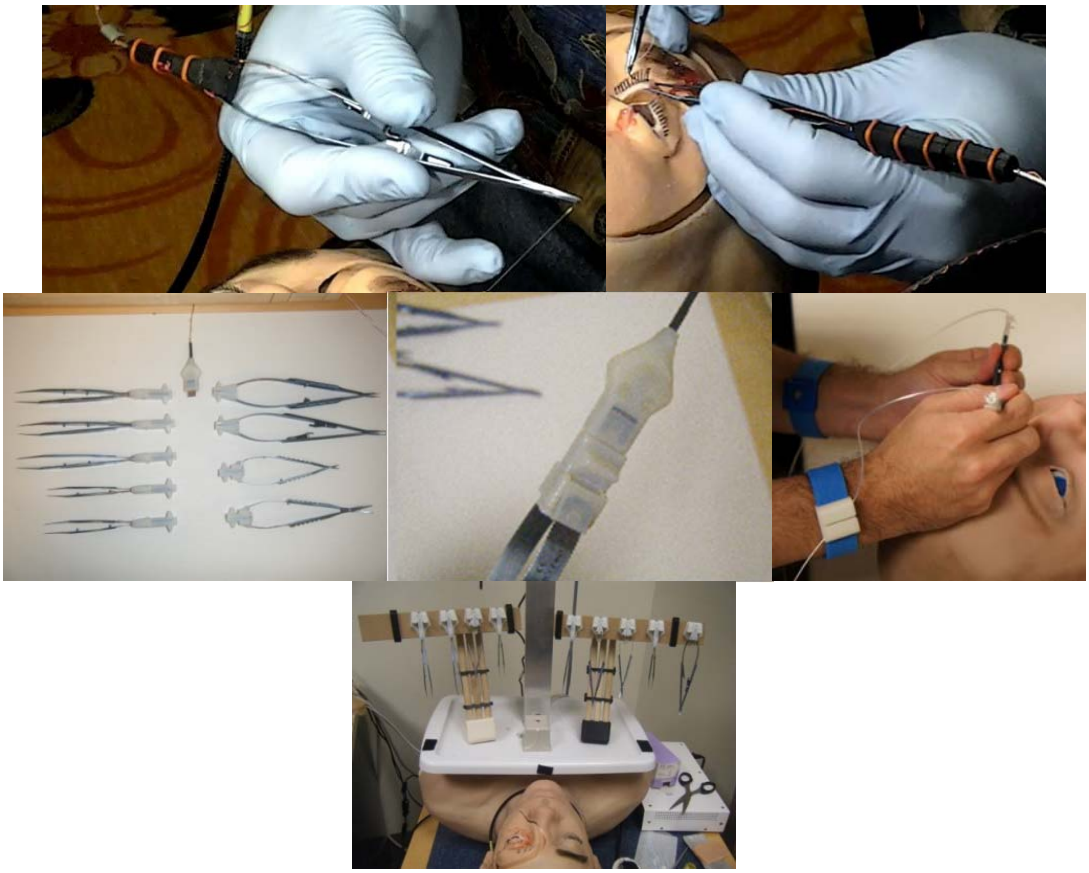

Figure 11: (top) Version 3 connectors with mini circuit boards in use by Dr. Mazzoli at MMVR 2012. (middle) Suite of instruments with swappable, auto-ID instruments; detail of connector sensors connect to all instruments regardless of instrument configuration (i.e. forceps vs. scissors vs. needle holder); wrist strap provides some improvement to prevent cable tangling. (bottom) Simulator with rack of instruments ca. 2012.

Following the 2012 USUHS testing, we identified areas of connector weakness and instability of the sensor with respect to some of the instruments. In addition, this iteration of the one-handed instrument holder tray was found to allow the user to poke themselves on the sharp, downward pointing instruments. Further, the prismatic features that mate between the instrument connectors and the holder tray can jam if the user angles an instrument while picking it out of the tray – a somewhat non-intuitive grasp and removal technique is necessary to avoid jamming, with the potential for breaking the connector shell. Further evolution to address these issues is described in later sections.

2.3.2.b.iv. Simulator stand, camera/kinect/projector/web cam mounting

The original proof of principle system integrated the magnetic field emitter (Ascension Technology, short range emitter) into the throat area of the head form. This was not optimal as it placed the most sensitive area of the magnetic field above the mannequin's forehead rather than near the eyes. In addition, our improved system supplements the position tracker with video recording, possible optical hand motion sensing using a Kinect sensor (available, and partially integrated into the full gesture detection system), a video projector for feedback and augmented reality applications. For this reason,

we developed and incrementally improved a framing system that holds the head form in place relative to the repositioned field emitter.

Early testing made use of convenient office furniture as mounting hardware for a miniature video projector and a miniDV video recorder, followed by development of the first version of the a mounting stand, initially with adjustable height projector/Kinect mounting and instrument tray, and later with an adjustable brightness lighting system, the improved instrument holding array described above, and a mounting for a web cam video input (for simplified synchronization of video recording and sensor inputs, vs. later synchronization of mini-DV tape recordings that would need to be reimported for analysis).

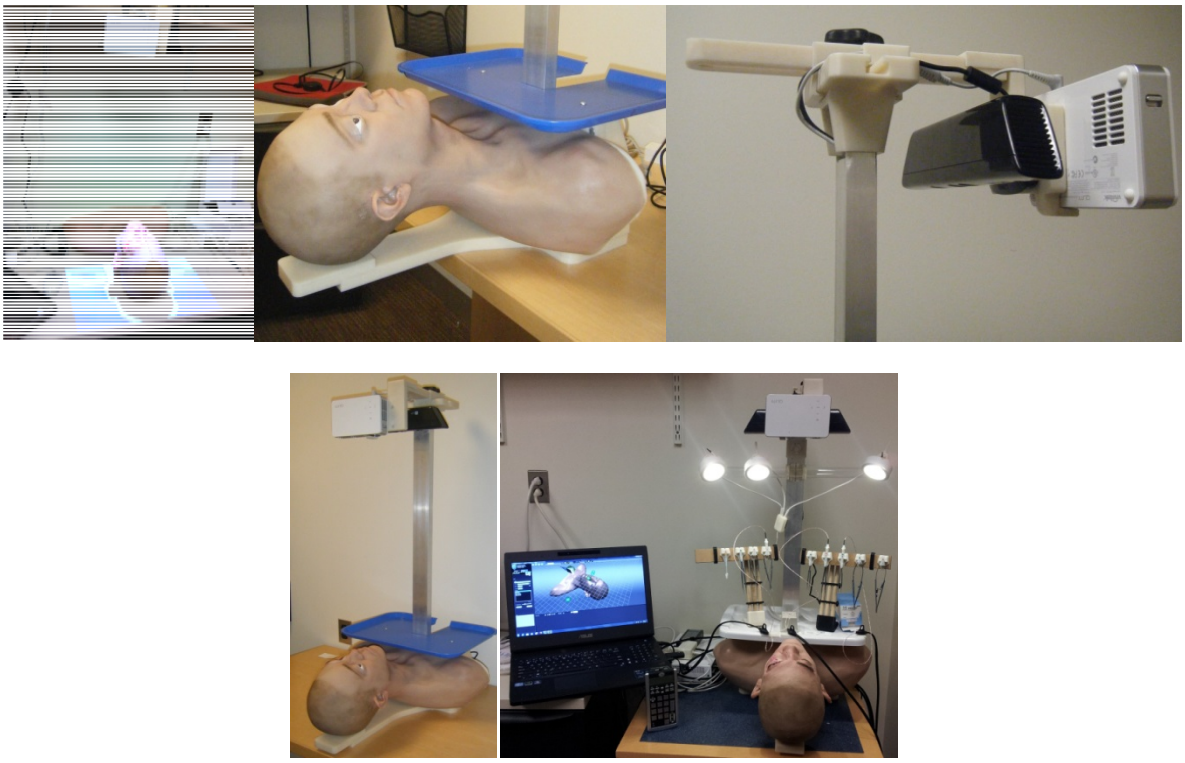

Figure 12: (top) Early test configuration; initial stand design with rigid mounting of head form; Kinect and projector mounting above head form. (bottom) First assembly of stand; configuration of system used at USUHS user trials.

At the end of Y1, the stand had reached an initial design freeze for the USUHS trials. In response to observations and feedback at the trials, modifications were made and additional features continued to be added throughout the program, as described in section 2.3.4.a.

2.3.2.b.v. Data collection user interface development, calibration, linearization, development of Event-Driven Gesture Segmentation and Task Recognition system (EDGSTR)

The initial suite of software tools and architecture that enable data acquisition, recording, playback, and analysis, and that controls the projection and lighting systems were rewritten from the ground up, compared with the original proof-of-principle system. As the system hardware evolved, from a small number of fixed position tracking sensors, to a large number of sensors (one per instrument), to three

interchangeable sensors, to the inclusion of the strain gage sensors, to an increasingly capable system for defining surgical gestures and events and providing meaningful displays of data, the software continued to evolve with it. The series of images below shows various phases of the revisions of the software system:

- Basic reimplementation of 6 degree of freedom tracking system data acquisition and synchronization of virtual representation with physical head form and instruments (Figure 13)
- Definition of Regions of Interest (ROIs), spherical zones centered at surgically relevant sites (to be defined by surgical trainers/experts) to allow detection of events such as entry or exit from these zones (Figure 14)
- Graphical display of strain gage sensor inputs, representation of three tools tracked simultaneously (Figure 14)
- Refinement of data stream presentation (orientation, grasping, force) for all nine instruments simultaneously, creation of dynamic playback system for use in post-processing and performance analysis (Figure 15)
- Example of identifiable events based on raw strain gage information, showing applied force during needle insertion (red, upper band), and cutting of suture (short red blocks, lower band) (Figure 15)
- Revision to track swappable instruments, using the automatic instrument identification function of the miniature circuit boards attached to each instrument – fewer distinct bands of data are presented on the streaming display as the identity corresponding with the input data switches depending on the instrument in use. All data, including instrument identity, are recorded to file for later analysis at this phase (Figure 16)
- Integration of the Kinect data stream into the user interface (blue/gray window at left of screen shot) (Figure 16)
- Results plot showing example of global performance variable levels (time, path length, motion smoothness, orientation datum) (Figure 17)
- Wireless numeric keypad used for manual event recording for system training. To develop event/gesture detection algorithms, we provided a means to manually identify events/gestures, for comparison with sequences of automatically detected low-level events and determination of relevant numerical thresholds. (Figure 17)
- Screen shot showing low level event detection window (text window at left), complex set of Regions of Interest overlaid on head-form representation. The EDGSTR system is described in more detail below, and in the IMIASH workshop paper [De Novi et al., 2012] in section 7.4 of the Appendices (Figure 18).

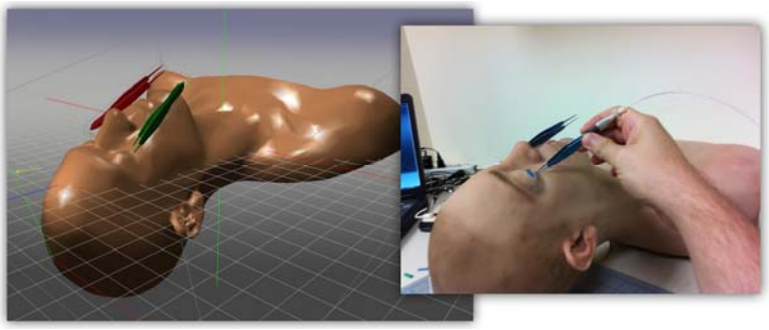

Figure 13: instrument-mounted sensors and correspondence between real and virtual

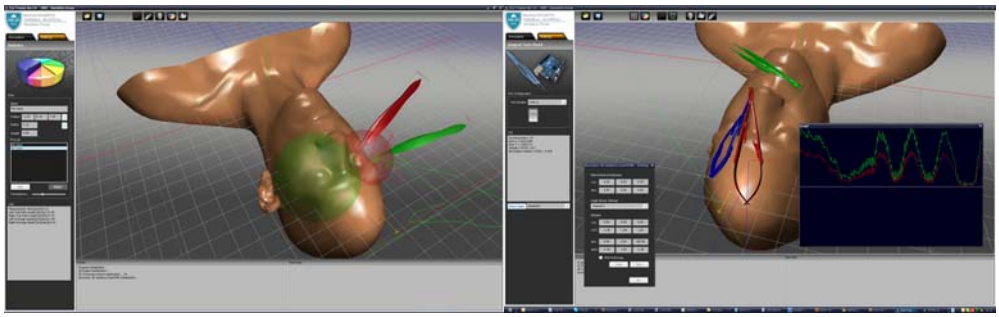

Figure 14: Regions of interest defined near eye zones; measurement and display of grasping/cutting action and force measurement

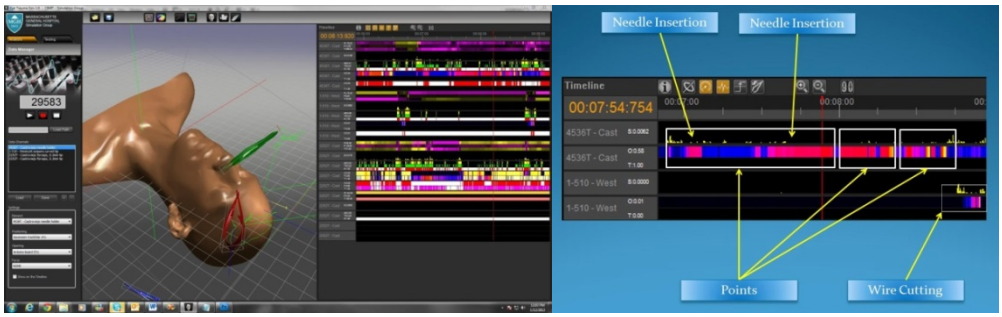

Figure 15: Data acquisition interface showing parallel tracks of orientation, force, grasping/cutting actions; Detail of tracks showing forceps (top color bar) grasp (red) and release (blue), scissors cutting (lower color bar, red)

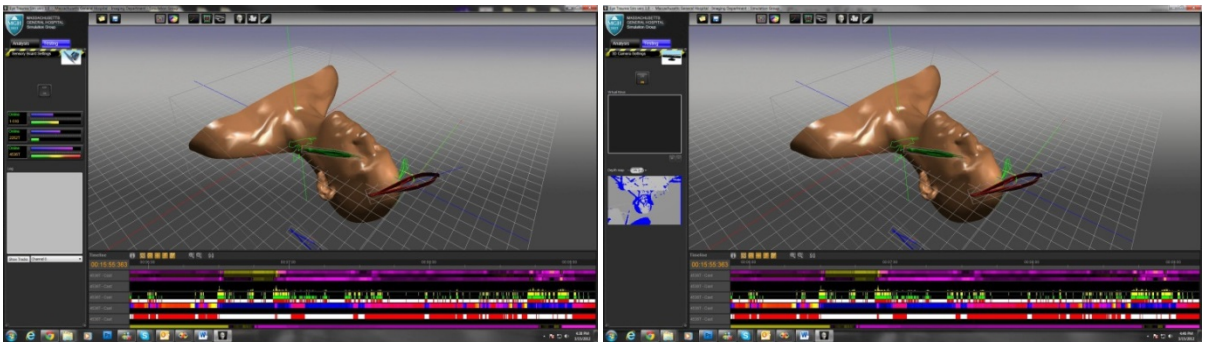

Figure 16: Reduced display of tracks for 3 swappable instrument measurements. Interface with addition of Kinect depth map measurement/display

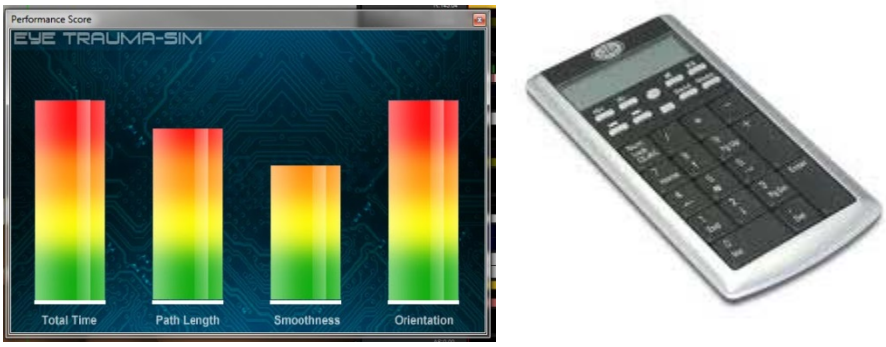

Figure 17: Early global score output screen; manual input keypad.

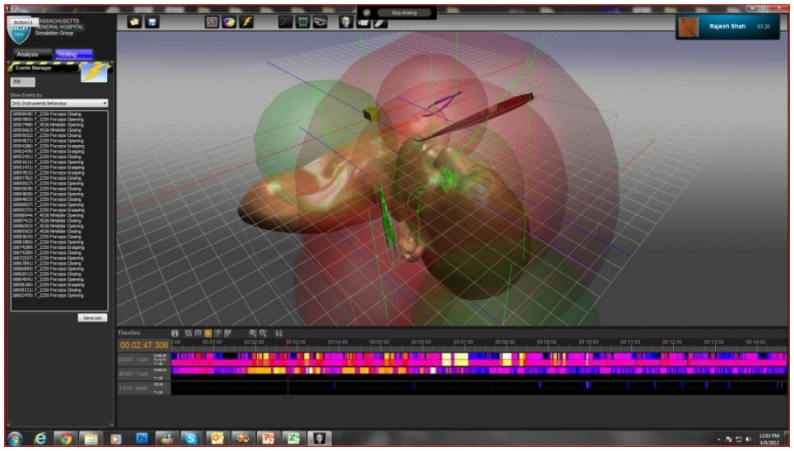

Figure 18: Recent interface screenshot showing regions of interest around eye, around instrument tray, with timestamped listing of ROI transitions recorded at left.

In addition to data collection functions, software tools allow calibration of the sensors within the magnetic field and compensation of the sensor measurements against distortions caused by static environmental influences (large, nearby volumes of metal). A sensor mounting frame is shown, together with a representation of the physical grid used for calibration (green "block") and the measured apparent positions of the sensor. By mapping the measured results back to the known geometric positions, an improved estimation of instrument positions can be obtained.

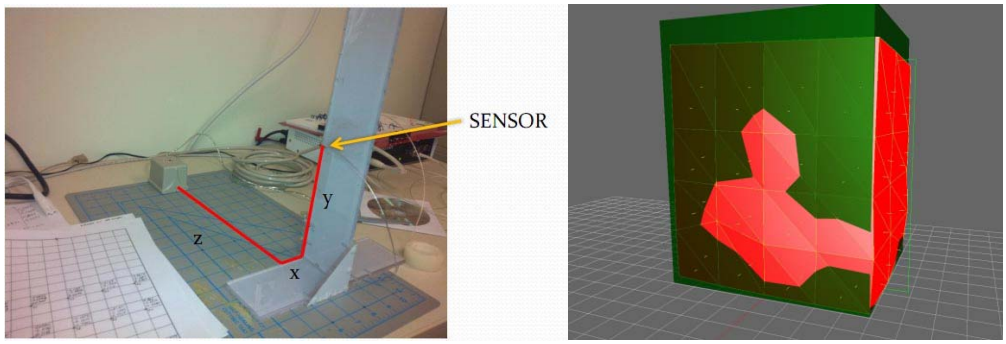

Figure 19: Magnetic tracker calibration system; graphical display of nominal positions (green) and measured positions (red) to be mathematically remapped to correct locations.

Towards the end of Year 1, following the Course, we began integrating these elements of the software to make best use of the video and instrument motion data collected at the 2012 USUHS Ocular Trauma Course and in future tests.

A software library was under development to allow recording of video sequences together with data collection, using a web-cam as a source, or to import separately recorded video from a miniDV camcorder. Video is stored in compressed AVI format and can be displayed with playback of the raw data to provide a complete picture of the recorded procedure. After the 2012 Course, we completed synchronized display of the video stream with the rest of the data acquired during the procedure in order to provide a consistent playback, despite differences in sampling rates of the instrument paths, instrument grasping/force sensing and the frame rate of the video.

During this period, we developed the initial versions of our analysis tools, presenting the streamed data in the form of the multi-track time line. Shown below, the first track shows the event labels for the manually input keystrokes that were recorded during the trials corresponding with a set of specific events (cuts, grasps, throws, etc.) Displaying keystrokes in the timeline makes it is easy to find specific segments of a given scenario to extract useful information for analysis as we identified the geometric and activity thresholds for later automatic detection. Data manipulation capabilities were added to the timeline, allowing the user to cut, clean, segment, and export sections of data. The data manipulation feature was important to create to extract and analyze specific sections with appropriate statistical tools, leading to creation of libraries of patterns that would later be used to generate the gesture recognition engine. All the segmented data can be exported in several file formats that can be loaded by different commercial applications (e.g. Microsoft Excel).

With segmented data identified, we implemented functions to measure parameters including total task time, total instrument path length, and compactness of motion, both in global terms and also by instrument.

We also refined the position tracking system calibration process, developing code that makes use of instrument motions centered at the calibration “dimples” on the lid laceration portal (section 2.3.2.b.ii). This ensured accuracy and precision of tracking for the scenario in the vicinity of the eye, eliminating any shifting between the ideal location of the magnetic field emitter and the physical head due, for example, to transportation or bumping the structure.

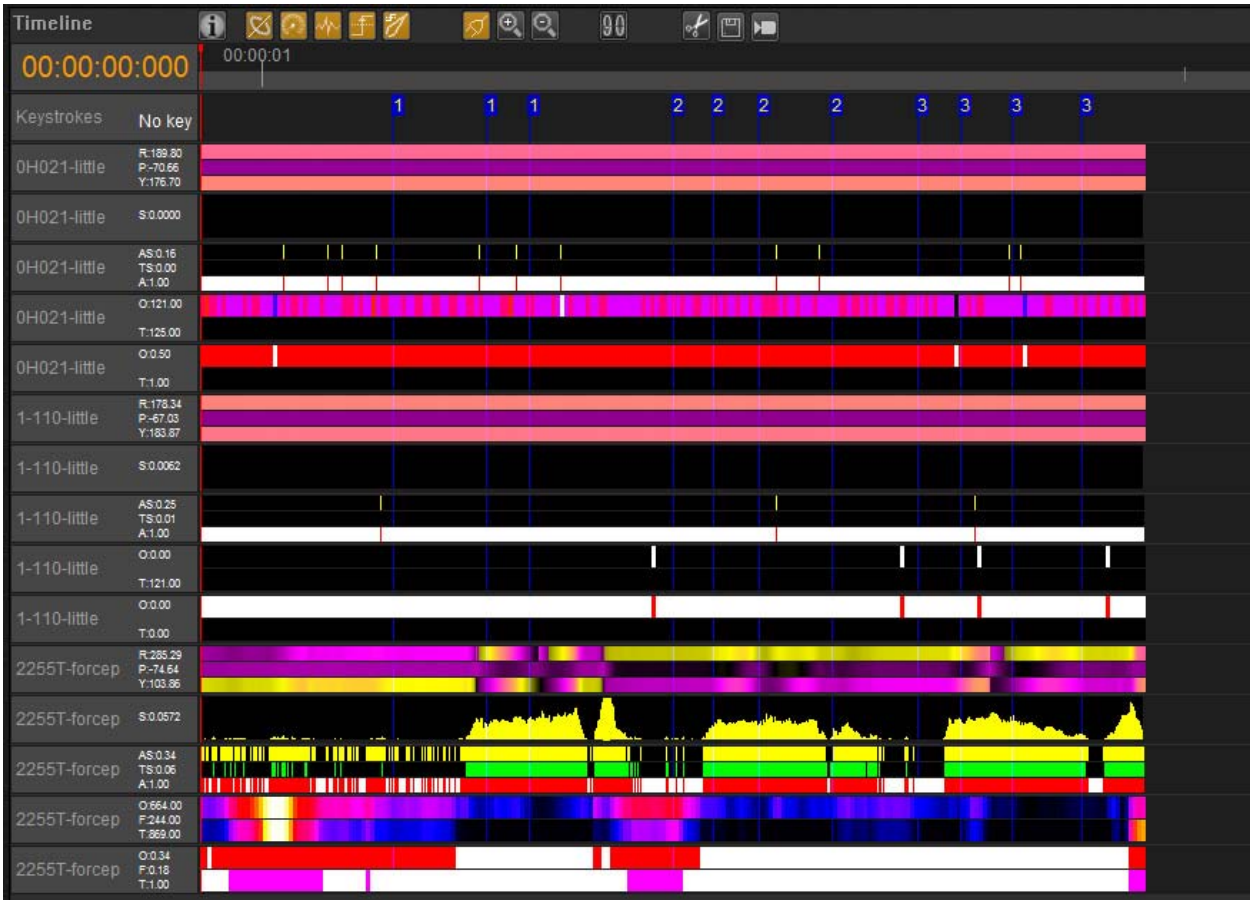

Figure 20: Detail of instrument closure traces with new indication (top row "Keystrokes") of manually entered events to facilitate comparison of surgical gestures with measured data.

2.3.2.b.vi. Content presentation architecture and content development

During Y1, we began to develop a learning architecture to integrate the simulator with curricular elements. We conducted a review of the prior codebase used for the user interface of the CELTS system, a Computer Enhanced Laparoscopy Training System that we developed in the mid-2000s [Stylopoulos et al, 2004]. The CELTS interface was developed in Java Server Pages (JSP). JSP technology has now been superseded by more common scripting languages such as PHP and the advent of the newer HTML5. Therefore, we redesigned the interface architecture around these newer languages while retaining some of the structure of the content used in the earlier system.

The overarching goal of this effort was to coherently link our simulation development efforts with military and civilian learning objectives. We aimed to provide an architecture that supports familiarizing practitioners with the correct understanding of the tools, steps, tasks and procedures specific to ocular and facial trauma, both simple and complex.

Figure 21 shows the early evolution of our concepts for progression through a scenario, storage of performance data, tools for scenario and scenario library development. Figure 22 shows an example of an instructional screen for display during the simulator set-up process.

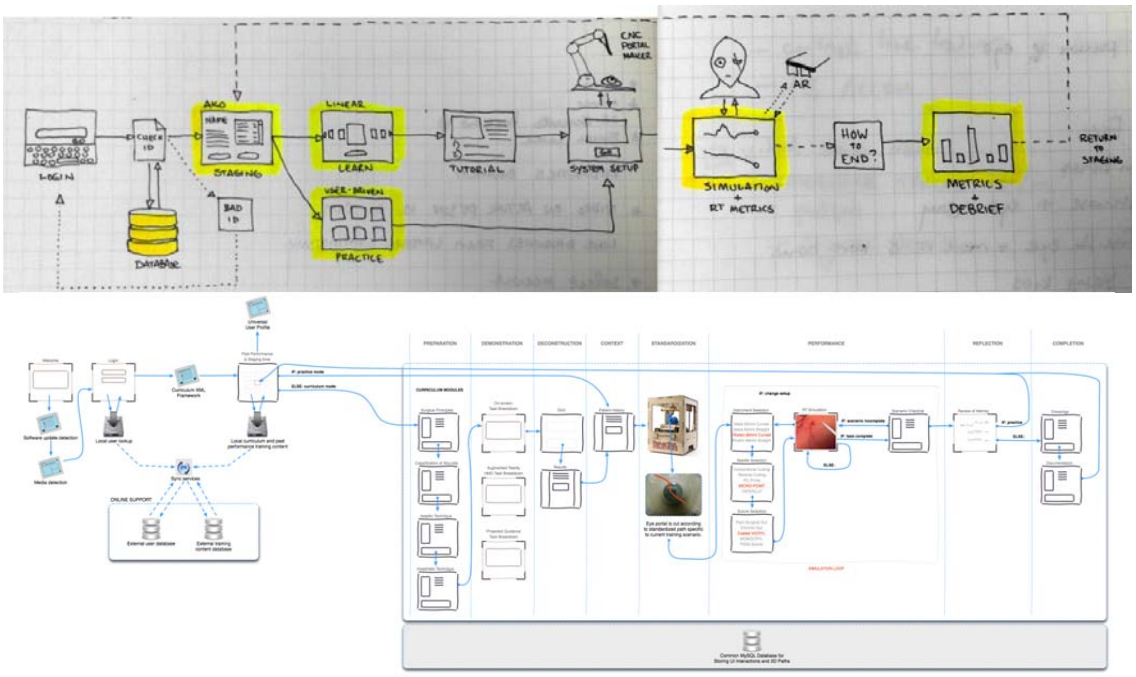

Figure 21: (top) early concept sketches for scenario generation, storage, presentation, branching sequences of measurement and feedback, recording of performance data, analysis and scoring of performance. (bottom) refinement of concepts guiding Year 2 development.

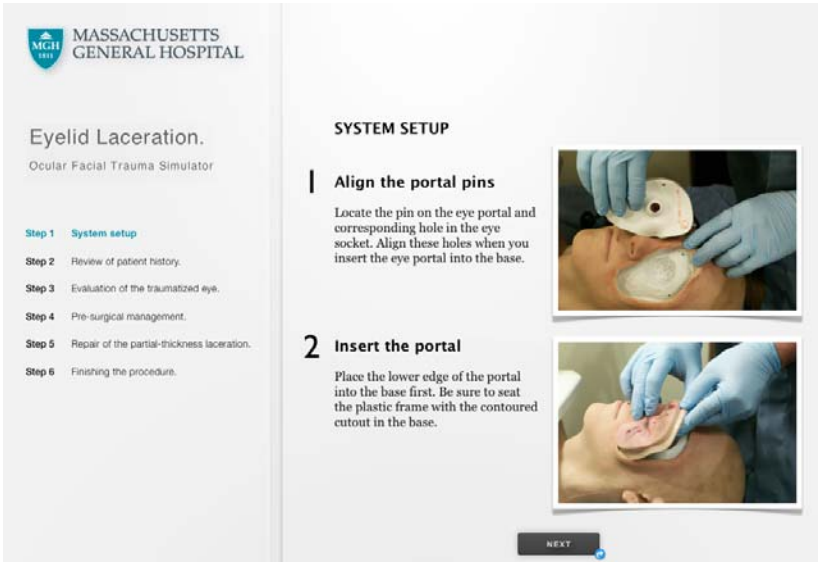

Figure 22: Typical instructional screen in the Year 1 era, with progress through scenario highlighted at left.

2.3.3. "Month 4" -

2.3.3.a. Perform user evaluation at USUHS TriService Ophthalmology courses.

One of the most important accomplishments of year 1 was conducting our first major user testing exercise. The original calendar for this research program envisioned a start date in January of 2011, testing of the revised prototype would occur early in the program.

Contact established at the 2011 AFSIM meeting with Mr. Shad Deering lead ultimately to contact with Dr. (COL) Richard Stutzman, the then ophthalmology program director at WRNNMC. Early discussions with Dr. Stutzman indicated that user testing might be conducted during regularly scheduled academic days at WRNNMC and/or Ft. Belvoir, when staff, fellow and resident participation would not interfere with patient duties. The human studies protocol that drafted by Dr. Paul Neumann, formerly of our group for testing the original proof-of-concept system, was adapted to reflect these plans and the approval process was commenced. Working with the MGH IRB, Dr. Jeffrey Stephenson at TATRC and the ORP HRPO, we made changes to the protocol, consent form, procedure for recruiting subjects and information presented to potential participants. As this process continued, Dr. Stutzman proposed that ultimately it would be most efficient and practical to conduct our testing exclusively at USUHS during the annual Ocular Trauma course in May, which allowed sufficient time to prepare the simulator for such use and to obtain all of the necessary approvals.

The MGH IRB determined that the protocol constitutes minimal risk to participants and processed it using expedited review. The ORP HRPO conducted a similar review. USUHS determined that since the trauma course was being conducted on campus, but that no USUHS personnel would be directly involved in the conduct of the study except as subjects, the USUHS IRB would not require review. A vendor agreement was established to permit the transport of the simulator to the USUHS campus and describe the permissions and responsibilities of the parties involved.

2.3.3.a.i. Preliminary user testing with SMEs

In the period prior to the formal user testing at USUHS, we conducted a series of demonstrations to our SMEs (Drs Freitag, Kanoff and Lefebvre of MEEI, Dr. Mazzoli) and their colleagues, to obtain early feedback for system improvement, to define the nature of the exercises to be performed by users, and to ensure that all of the necessary supplies would be available to users (e.g. type and number of sutures, auxiliary supplies such as gloves). During these demonstrations, we asked the experts to perform the complete process of full thickness upper eye lid laceration repair, from exploration of the simulated injury through to ensuring neatness of cut ends of sutures at the end of the procedure. We also asked them to perform a series of 15 elemental exercises so that we could collect data on the performance of different knot styles, suture needle handling technique and other gestures/tasks we expected to observe during the full laceration scenario. These tests allowed us to estimate the time required to complete different scenario combinations, which lead to the determination that at the USUHS user testing, we would ask participants to perform only the lid laceration repair, without additional elemental exercises, as this would place an undue demand on participants' time during the tightly scheduled course agenda.

2.3.3.a.ii. User data collection at 2012 USUHS Ocular Trauma courses

The first set of user trials were conducted over 23-24 May 2012, during which time 21 participants started the data collection exercises, and 20 completed the full consent and scenario sequence. These included 12 attending surgeons of various disciplines, two fellows and six residents. We planned to have a larger representation of earlier-career surgeons in the study, however the time limitations of the Course did not permit them significant availability away from their small-group lectures and wet-lab sessions. The senior surgeons and instructors had significantly more availability.

During the sessions, only skill level and handedness were recorded as demographic data, consistent with the anonymization process of the protocol. In later years, described below, we expanded upon the list of participant characteristics. We collected 6DOF instrument motion data, instrument exchanges, video recordings of hand motions in the area of the mannequin's face (Figure 23), and then manually entered surgical event keypad entries. We separately made notes when users made comments or suggestions on how to improve or alter the system, without attaching name or rank information to those comments. Observations of the ease or difficulty of use of the system, system failure modes and system damage were made so that we would be able to improve future iterations of the system.

Figure 23: Video frames from USUHS trial participant.

2.3.3.a.iii. Other user trial outcomes

At the trial, Dr. Mazzoli observed that we were collecting a series of used trauma modules, which showed suture patterns for experts and novices, all on identical injuries. As multiple physicians would never all be able to perform surgery on identical injuries, even in cadaver or animal lab situations, Dr. Mazzoli suggested performing an analysis on our trauma modules to determine if there are measureable differences in suture patterns. We created a lighting/mounting jig to allow us to generate aligned photographs of all of the used modules, however the ongoing development requirements and shifts in analysis methods took precedence over this analysis.

2.3.3.b. Locate and coordinate commercial partner to manufacture first version of the stand-alone eye trauma simulator.

This section describes most of the efforts towards commercialization that were made throughout the program, not only those in the early months of the program.

Initial commercialization discussions comprised contact with simulator vendors, including Laerdal (Wappingers Falls, NY) and CAE-Healthcare (Sarasota, FL), in the context of acquiring one of their mannequin systems for the Phase 3 element of this work, with the intent of developing a trauma head extension for the systems of the mannequin manufacturers. In the case of Laerdal, they conveyed that they have worked with developers creating systems compatible with their own, working closely when the systems align with their own interests. We continued to maintain contact with Laerdal in the context of integration of our software and their mannequin application programmer's interface (API), although their interest in the system did not increase. Resulting from the acquisition of METI by CAE-Healthcare early during this program, discussions with CAE were with the METI team rather than the earlier Caesar development team we came to know during the MGH licensing and tech transfer of our

COMETS system [Bardsley et al, 2014]. Early conversations showed that there is no equivalent software tool to Laerdal's API for the METI mannequins, however should they be interested at a later time integrating our head form and software with theirs, our final system has well documented interface protocols and physical connectivity that simplifies any modifications that they would find necessary.

We evaluated the use of Phillips Studio (Redland, Bristol, UK) products for our system and also discussed their manufacturing capabilities, however Phillips was not in a position to pursue a simulator with advanced computing and sensing capabilities.

As described in 2.3.5.b, with respect to the augmented reality microscope system, Scan Optics Pty Ltd (Adelaide, Australia) expressed interest in helping us to develop the optics for the integrated display, however their market focus appeared to be production of microscopes for the surgical end user, rather than entering the training/simulation space. As described below, we made significant progress in developing augmented display optics for our prototype.

An invention disclosure was filed on the original (pre-phase 1) proof-of-concept system, although MGH had not pursued a patent application as Year 1 came to a close. The original system had been publicly disclosed prior to the commencement of this work, and early improvements to the stand-alone system were considered to be relatively obvious to one skilled in the art, in light of simulators for other procedures that also use tracking technology and anatomical models. Value to a vendor at this stage would have been primarily in the know-how generated in the course of system development. MGH has previously licensed technology in which know-how is a substantial portion of the value, so we did not see this as an obstacle at this time, but did continue to record and report the development of novel technological elements of the system.

Subsequently, in support of a strong licensing agreement when a commercial partner is identified, a provisional patent application was submitted to the USPTO prior to the 2013 MHSRS meeting to allow us to present new features and inventive content. At the end of Year 3, we were working with patent attorneys to make the conversion to full patent application.

At the 2012 USUHS user trials**,** some of the eye trauma specialists indicated that they would find the eye lid modules useful in their training responsibilities, so we began to contemplate alternative commercialization options, including sales of the trauma modules as consumables for the instrument tracking and simulation system or as individual components.

After the 2012 USUHS user trials, we analyzed the current commercial trainer product lines available for ocular surgery training. This analysis served to help evaluate our options for transitioning the current research prototype to a marketable product. Throughout the course of the project, we informally asked the end users which training systems they currently use. The most advanced simulator that trainers referred to was the Eyesi Surgery Simulator (VRmagic Holding AG, Germany). At approximately $200k per unit, this simulator is substantially more expensive than the next type of simulator used, namely, the silicone eyes models manufactured by Phillips Studio. The disposable eye models from Phillips can be used in the Eyesi unit and cost approximately $75 each. It can be clearly seen that there is a substantial gap in the current product offering. However, due to the comparatively small number of ocular

surgeons, the number of commercial players in this market is correspondingly small. This does not diminish the opportunity to deliver a mid-range hybrid simulator that combines realistic disposable anatomical modules with tracked instruments and dynamic guidance.

Following inquiry with FCI Ophthalmics (Pembroke, MA), an instrument and device company specializing in ophthalmology, in regards to ordering canalicular stents, we established an NDA with Ms. Anne Bozak and FCI in Q9. This allowed us to have discussions with Ms. Bozak and her colleague Michele Joyce in Q11. Their position at the time was that there were no good commercial simulators that could support canalicular repair training, and they expressed interest in evaluating our system as it evolved. A follow-up meeting with Ms. Bozak and Mr. Jim Perez, their director of sales for North America was held at the end of Year 3. Subsequently, as described below, they were present for a review of the anatomical modules in the final months of the program and remain interested and await a number of minor modifications that we intend to make following completion of this project.

A confidentiality agreement process was established with NVIS, Inc. (Reston, VA), a company that develops VR and augmented reality head mounted displays and binoculars, in July 2014. They saw the abstract for our MMVR 2014 poster but were unable to meet us at the conference. A conference call was held in November 2014 with Minoo Bablani, CTO and VP Product Development, to discuss the technology that we developed. They have interest in developing medically-related products, having previously bid on the development of a VR-based cataract surgery simulator. Our prototype system, which by 2014 combined graphical and directly observed real imagery, sparked interest for NVIS in regards to a variety of microsurgery applications. Contact with NVIS will be made again following the final changes to the microscope system and demonstration interface.

An NDA established with Lantos Technologies, Inc. (Wakefield, MA) in Year 2, towards applying the technology and methods we developed for fabricating the realistic head form, lead to a sponsored research agreement to fabricate a new simulator for training in the use of an ear canal 3D scanning instrument. That relationship was ongoing at the end of the program. One useful benefit of the work with Lantos was the opportunity to make use of small touch-screen monitors as part of the interface for a simulator. Following application of a touch-screen to the Lantos system, we adapted the software used for that element of the Lantos simulator and the same touch screen monitor for use in this system.

On 13 August 2014, we met with Dr. David Hunter, Ophthalmologist-in-Chief of Boston Children's Hospital and his colleague Dr. Gena Heidary, who is responsible for their strabismus course. They expressed interest in viewing the completed system and discussing the development of a strabismus surgery training module. This is likely to be compatible with the enucleation module that will be developed under CIMIT funding that was awarded in part as a result of the successes of the current program.

We met with John James, Director of Engineering at Sawbones (Pacific Research Labs), on 15 December 2014 to discuss possibilities for fabrication and commercialization of this and other simulators. Sawbones has developed some additional electronics fabrication capabilities since we worked with them on our Virgil Chest Trauma simulator [Ritter & Bowyer, 2005] however the Ocular-Facial Trauma system

remains outside their area of specialty. They have had some limited experience developing an eye surgery system, which included an eye globe which could pivot on its base, suggesting that they could be a potential supplier of the anatomical components of the system for another system integrator.

At the 2015 USUHS Ocular Trauma Course, following the formal end of this program, Dr. Marcus Colyer, the course director, introduced our team to that of Simulation Systems, Inc. (Hummelstown, PA) (Dr. Joseph Sassani and Mr. Brian Smith), leading to extended discussions regarding how the software libraries that the MGH Simulation Group staff have developed may be applied to solve certain remaining issues of Dr. Sassani's virtual reality-based system. In addition, we began to explore the possibility of taking advantage of the commercial status of Simulation Systems (vs. the non-profit academic hospital status of the Simulation Group) as a route towards commercialization of the Simulation Group simulator. A confidentiality agreement was completed in June, 2015, followed by Dr. Ottensmeyer being named as a scientific advisor for SimSys, and ongoing efforts towards preparation of an STTR grant proposal to verify and validate the system.

2.3.4. "Month 6" - Revise design and fabricate improvements based upon USUHS Spring evaluation.

This section describes not only the revisions made after the first round of user testing at the 2012 USUHS Ocular Trauma Course, but also those made throughout the program based on user feedback and observations of the system in use.

In Year 1 preliminary expert testing and the USUHS trials were very instructive in terms of identifying elements for system improvement, calling for system modification and revision to the testing process for future user trials.

After Year 1, our task list for redesign included the following, most elements of which were addressed by the completion of the final prototype iteration:

- Strengthen instrument connectors to prevent damage during extended use, modify connectors to make connector/instrument orientation more obvious and mating easier
- Provide adjustable height seating and alternate loupe magnification/working distance for users of different heights
- Broaden web-camera field of view to include instrument tray to support identification of surgical actions away from vicinity of surgical site
- Add anatomical features to modules, including eyelashes if possible, softer tarsal plate
- Eyelid tissue should include redundant tissue, which typically buckles and rolls under when the eyes open, rather than the taught, more fixed version of our current modules. Versions of this were developed to test blinking, but not implemented in the modules provided for the USUSH courses, as not essential for the selected laceration training scenarios.
- The division between tarsal plate and skin should include a pigmented layer representative of the orbicularis orbis muscle, used as a landmark for suturing
- The tool tray should be reconfigured so that sharp ends of instruments point away from the user, that the alignment/retention features of the tray should allow for "unwinding" of the

sensor cable, which can become twisted (as with a telephone handset cord), that the alignment/retention features should allow for simpler, quicker engagement/disengagement, with reduced possibilities for jamming and potentially breaking the jammed instrument connector

- A means for identifying when sutures penetrate through the palpebral conjunctiva (inner lining of eyelid), which would scratch and irritate the patient's eye surface (not implemented).
- The system stand should be reconfigured to improve the location of the magnetic field emitter, instrument tray location.
- Additional consideration for the participation of two trainees, one serving as surgeon, the other as first assistant or nurse, should be made, considering the preparation and hand-off of instruments (not implemented – training scenarios focused on signal participants only).
- Novices tended to "merely survive" the scenario by suturing the eyelid closed with any type of suture and without any form of guidance as to what the proper way to do it was. As sequencing of suture type should correspond with the phase of a scenario (e.g. when to use silk vs. Vicryl, what size suture to use), a suture dispenser with sensors to detect when a new suture is selected and its type/size, is a desirable feature (not implemented – later advice from SMEs was to eliminate an integrated suture rack).
- There is a distinct pattern to the sequence of gestures an expert uses to repair the laceration presented on our eye portal. This should be incorporated into our didactic teaching material to better inform a novice performance. (This forms part of the AR training system in Phase II)
- Occasionally, experts performed maneuvers outside of the nominal pattern, commenting that their additional actions were part of their "personal style" (e.g. tying additional, temporary, sutures in the brow to hold the loose ends of the suture neatly out of the surgical field). Use of the ROI concept should allow exclusion of extraneous motions from analysis.
- Sessions in 2012 were recorded with a video camera, but the video was not synced with the recorded 3D paths of the user. Future system modification will need to combine these features to ensure synchronized video and performance data.

2.3.4.a. Stand-alone simulator structure revisions

In the Q5 report, we presented a series of concept drawings were prepared by one of our student interns pursuing a masters degree in design, that began to address limitations of the system used at the first user testing exercise.

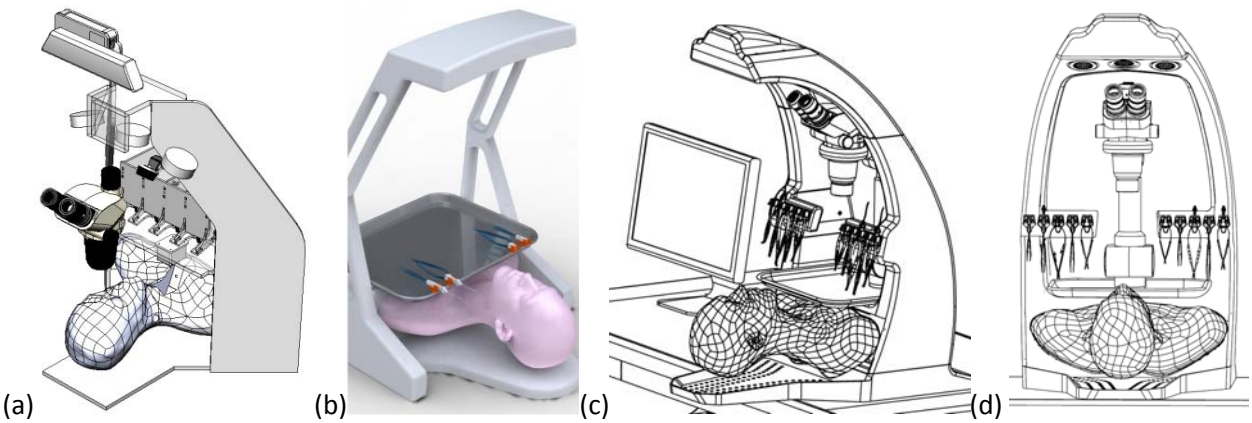

Figure 24: Design concepts for revised stand-alone system. Preliminary concept (a) for blocking out system components; (b-d) student concept designs: (a) early revision for instrument tray and integrated overhead lighting system; (c-d) views of more advanced concepts including mobile arm to support microscope head.

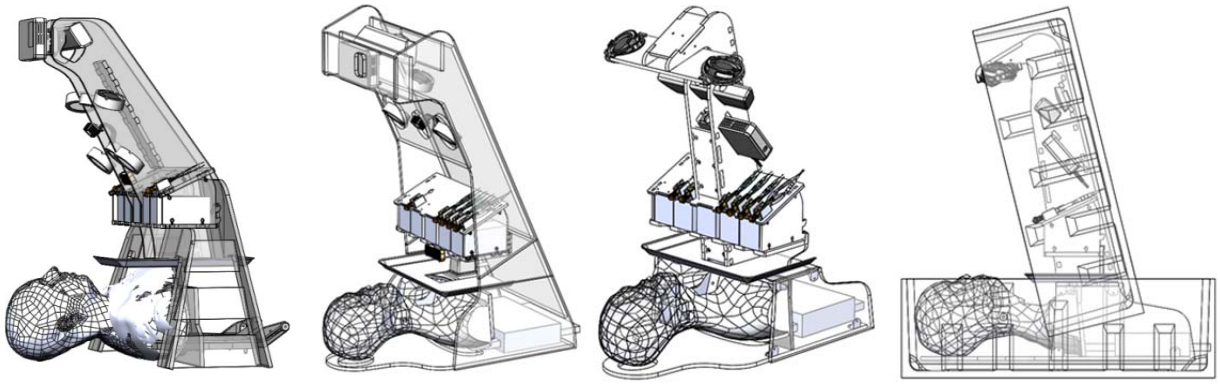

Figure 25: Evolution of panel-based frames, including analysis of break-down for transportation in standard Pelican cases.

These designs integrated new means for mounting the surgical instruments, improved the positioning of the magnetic and optical tracking systems and the display field of the projector system, and notably supported ease of assembly/packing/shipping.

At the close of Year 2, the structure had reached the state shown below (middle panel, Figure 26), as was used at that 2013 USUHS Ocular Trauma course. It is primarily assembled from laser-cut acrylic panels, using a tab and slot method [e.g. Big Blue Saw, 2015] that has become common with the growing availability of laser cutters in the commercial and private domain. The method supports relatively easy prototyping, assembly (and disassembly for repair/packing) requires only a single screw driver, and modification and replacement of components does not require wholesale modification – new slots/holes can be added to existing parts, as has been done frequently during development. The method also supports the use of threaded inserts to provide for secure connections between removable components without relying to threaded holes tapped directly into the plastic (which may wear or be stripped through continued use).

Regarding the Year 2 version, one of the criticisms noted was that non-sterile boxes of sutures are not found within the sterile field of a procedure, so the placement of the suture boxes beneath the instrument holder rack was in appropriate. In Year 3, the instrument rack was modified for the 2014 course, removing the suture boxes and lowering the instrument tray for easier access. In addition, as will be described in more detail in sections 2.3.5.b, 2.3.7.c and 2.3.8, a touch-screen display mount and integrated mount for the augmented reality microscope were added to the system.

Of note, the head and shoulders, retained from the original proof-of-concept system, were mounted such that they can be removed and replaced with alternate anatomy, particularly that of the later CT-derived head form, described in section 2.3.5.a.

Figure 26: (left) Early Year 2 stand, ca. 1/2013. (middle) Year 2 stand, ca. 5/2013 for 2nd USUHS Ocular Trauma Course. (right) Year 3 stand ca. 6/2014, with modified instrument rack, integrated touch-screen display and augmented reality microscope. The 6/2014 version allows for drop-in replacement of the head form with the more advanced version described below.

2.3.4.b. Force sensing strain gages for scissors and needle holders, characterization of sensing

In Year 2, we installed strain gages on all grasping (beyond forceps) and cutting instruments to extract not only open/close positioning, but also grasp/cutting forces. This enabled the detection not only of instrument action, but also interaction with the silicone tissues, sutures and other objects, and the detection of their relative stiffness and/or strength properties. Finite element analysis of the region near instrument fulcrums was performed to show where the ideal locations for strain gage placement would occur, and for some instruments we had professionally installed silicon strain gages installed.

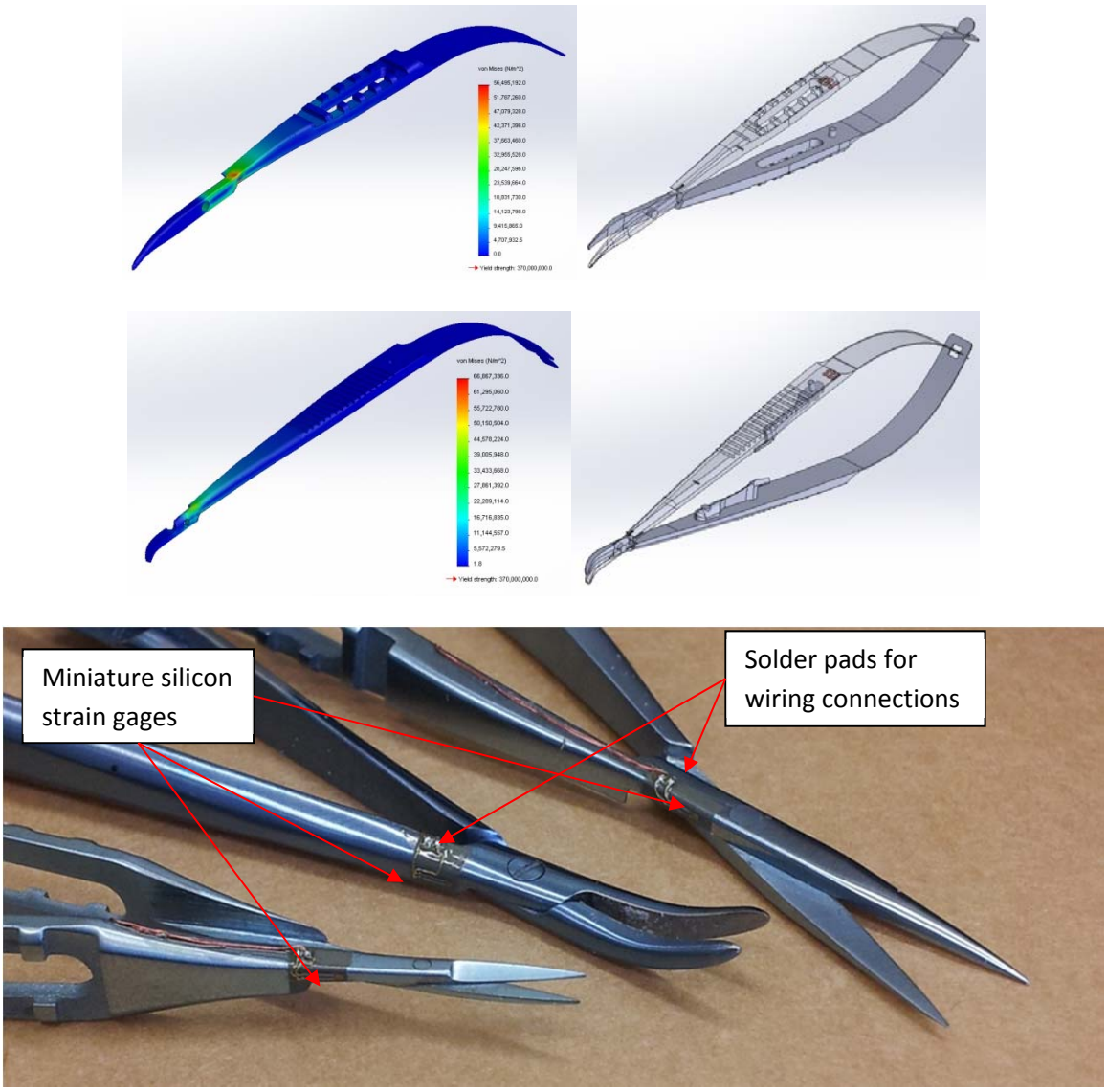

Figure 27: FEA of scissors and needle holders showing optimal placement for strain gages; instruments showing design positions of gages for force sensing and inactive gage for temperature compensation. Top: curved Westcott scissors. Middle: Castroviejo needle holder. Bottom: Detail of scissors and needle holder with silicon strain gages installed

Detection of relative stiffness of grasped or cut objects, for example, allows discrimination between grasping of tissue vs. grasping of a suture needle vs. closure on empty space. This distinction can be recognized by the event-based gesture recognition system, as the force-displacement response of the instrument changes.

In empty space, the position sensing gage registers the user squeezing the instrument closed, without an initial response from the force sensing gage, located close to the instrument tip. Once the tips come together, the force sensing gage begins to respond, and the two responses plotted against each other generate a curve that is related to the instrument's own spring stiffness. If an object is grasped, the position at which the force response begins occurs earlier than for the empty instrument, giving

information about approximate size of the object grasped. This shifts the break-point in the force-displacement curve accordingly. The slope of the characteristic curve also changes, as the response is now a combination of the stiffness of the instrument and the object grasped.

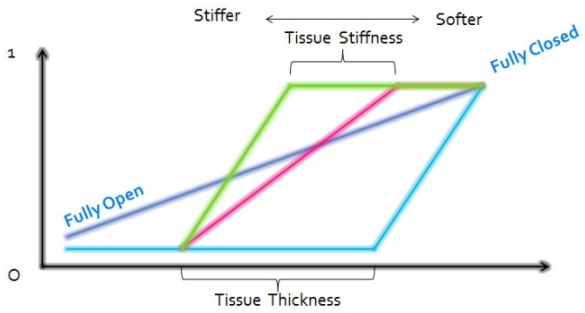

Figure 28: Schematic of force-displacement curves for use of grasping instruments in open space and grasping different stiffness tissues.

A simple jig was designed to repeatably close the forceps (Figure 29). In testing, strain gage outputs were collected for each full turn of the lead screw. For scissors and the needle holder, digital calipers were locked at a series of closure positions.

In the graphs below (Figure 30), taken using the forceps, the shifts in break point and overall slope are clearly shown.

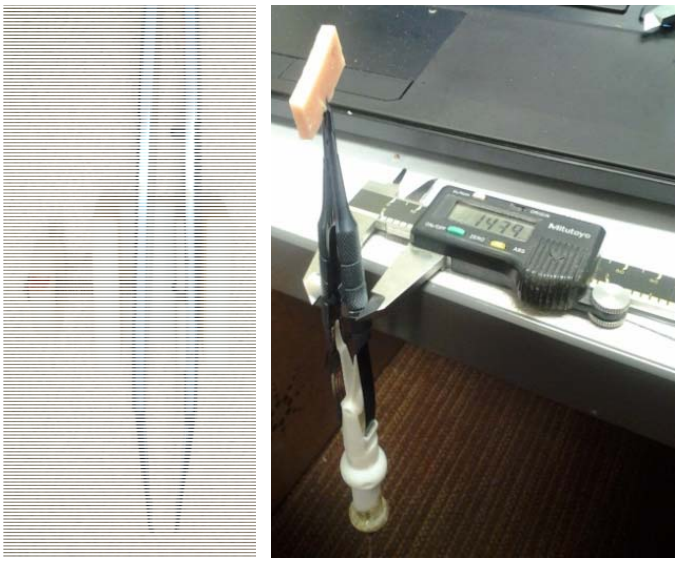

Figure 29: Forceps force-displacement test rig.

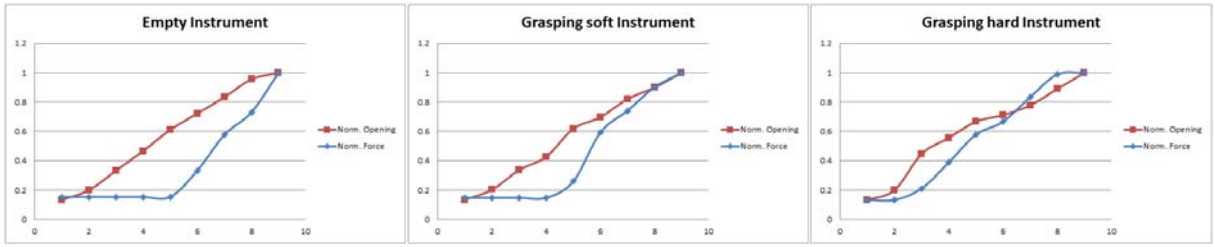

Figure 30: Normalized strain gage output vs. instrument closure: red curve – closure sensor, blue curve – grasp force sensor. (Left) Closing instrument, with tips coming together at 5mm displacement of lead screw, with force increasing as forceps are squeezed further. (Center) Grasping soft object, with initial deviation from baseline curve at 4mm displacement, difference in force slope with additional squeezing. (Right) Large, hard object, with contact detected at 2mm.

These same data sets were collected for each of the instruments used at the 2013 Ocular Trauma Course tests. Different instrument types show different characteristic responses. The needle holders are of a locking variety, with a spring-loaded mechanism that holds the jaws closed after the user has squeezed the instrument far enough. This results in a momentary reversal of the force curve at the locking point and an analogous signal appears in the closure position sensing response. Similarly, the scissors show almost no output force in empty space until complete closure is achieved, while force increases during cutting, as the shearing forces generated by the scissors increase while cutting through an object. In the cutting case, as the scissors close the cutting point shifts away from the scissor axis, increasing the bending moment on the scissors (force x distance increases), and the angle between the cutting edges becomes smaller, so a larger section of the material is being sheared. This results in the non-linear increase in the response observed.

Described below, these curves were built into the gesture recognition architecture, supplementing the earlier, position-based (Region of Interest) event detection algorithms.

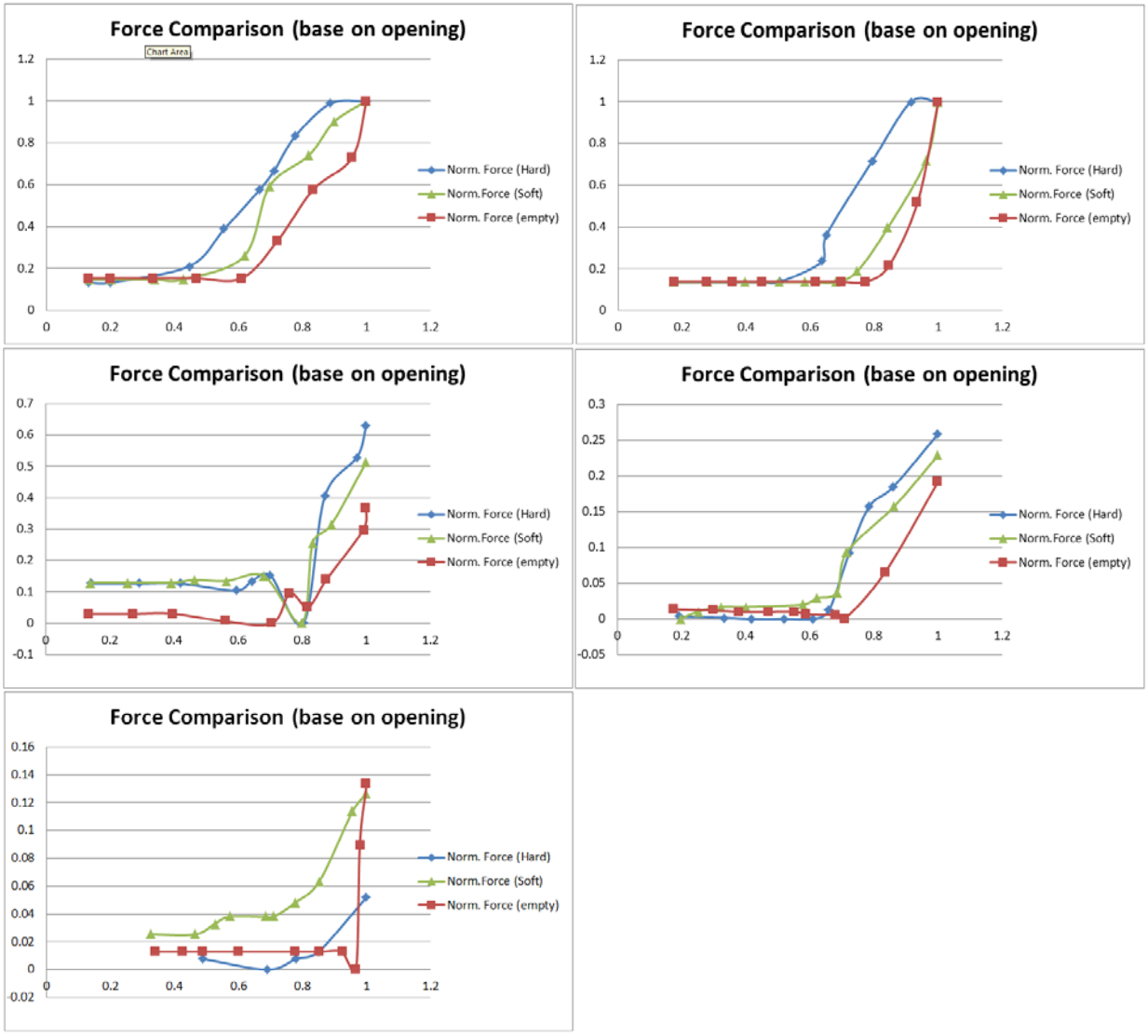

Figure 31: Strain gage response curves: (upper left) 0.5mm jaw grasping forceps; (upper right) 0.3mm jaw grasping forceps; (center left) large jaw needle holder; (center right) small jaw needle holder; (lower left) curved scissors.

2.3.4.c. Revision of instrument connector shells, stabilization of instrument/sensor orientation

In Q7 we began work to replace the earlier iteration of the housing that connects the Ascension sensor, the strain gage amplifiers and the instruments together. The version used at the 2012 USUHS eye trauma course data collection exercise was subject to accidental misalignment of the connector, which prevented proper mating and distraction to the surgeon/trainee. The new design includes spiral “ramp” features to guarantee that during plug insertion, the force of insertion between the instrument and plug causes them to rotate towards the correct connector alignment. In addition, spherical features allow for mating of an instrument with the holding rack in any orientation about the instrument’s axis. This design was retained through the remainder of the development of the system, with new instruments having custom fittings designed to be compatible with this form-factor.

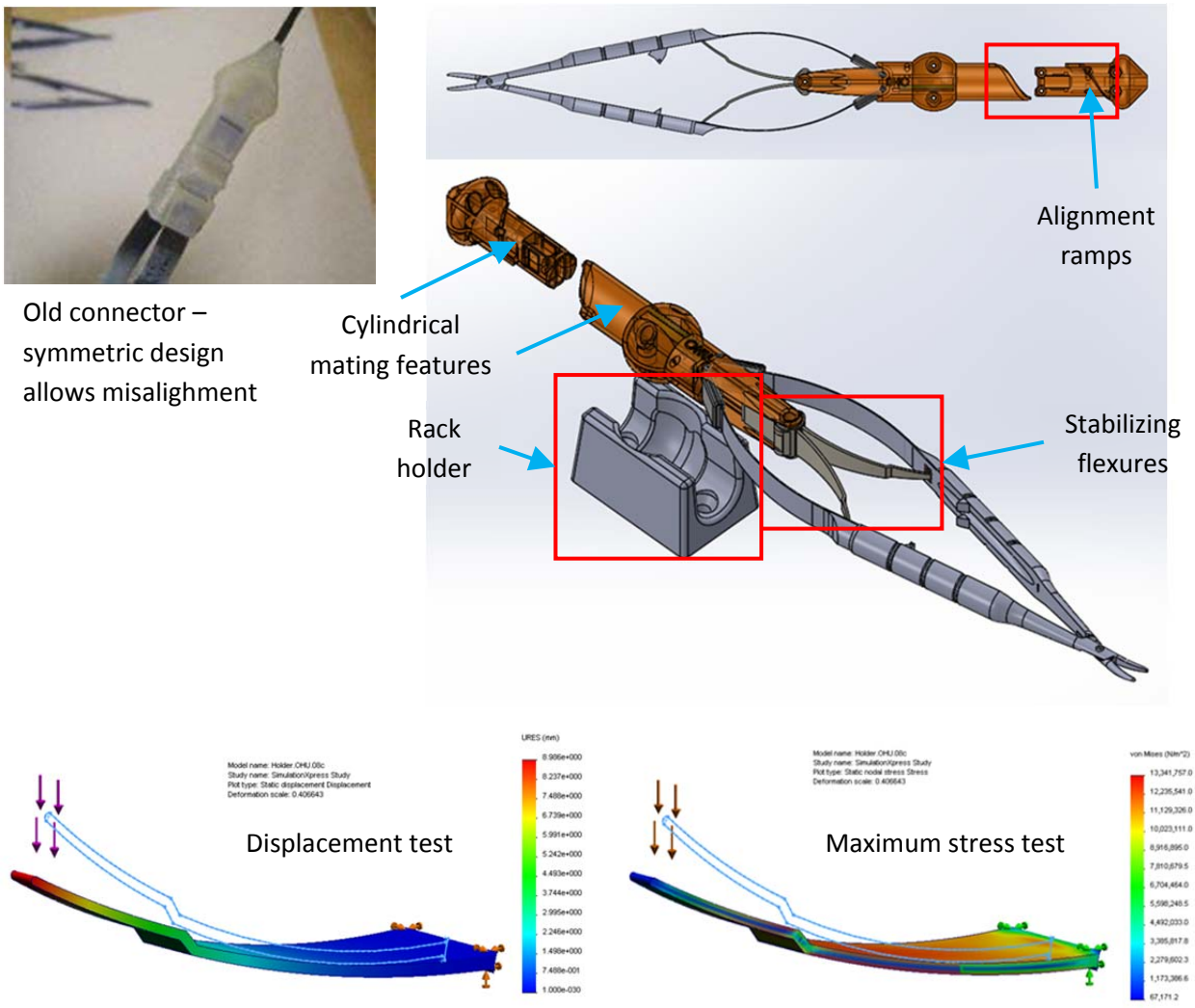

Figure 32: New design for instrument/sensor interconnect format with features to make insertion/removal intuitive and resistant to misalignment. For scissor/needle holder instruments, FEA of concepts for flexural beams for holding connector/sensor housing aligned with long axis of each instrument. Not necessary for forceps.

For the scissors and needle holders, the pivoting action of the proximal ends allows the housing to bend away from the axis of the instrument, causing position sensing (in the housing) to miscalculate the tip location. To prevent this, stabilizing cantilever flexures (leaf springs) were designed into the housings to hold the scissor/needle holder arms apart. Early versions were printed as part of the housing using the Polyjet process of our Objet rapid prototyping system. This material suffers from creep deformation when held under continuous load (e.g. needle holder locked closed); a solution was found in the form of combining parts from both of our rapid prototyping systems – the high resolution Polyjet parts for the rigid elements of the housing, with a flexible cantilever fabricated using our FDM system, which uses a different plastic that appears to be substantially less subject to creep.

In Year 3, in response to recommendations from SMEs and expert users at the USUHS Ocular Trauma course, we acquired a punctal dilator for canalicular repair scenarios, Mini Monoka stents (FCI Ophthalmics, Pembroke, MA – see also section 2.3.3.b) for such procedures, and alternate cotton swabs

for use with the suite of instruments. New designs for the associated instrument holders were created and fabricated. The detailed design of the holders for the miniature tying forceps and fabrication were completed during Year 3 for potential future use in corneo-scleral repair scenarios.

At the 2014 USUHS Eye Trauma course, requests were made to add straight-jaw locking needle holders and a standard cotton swab to the suite of available instruments. Over the following months, new instrument holders were designed for these instruments.

The final suite of instruments is shown in Figure 33 (earlier set shown in Figure 6).

Figure 33: Instrument holder designs for new devices (cotton swab, punctal dilator), earlier devices for globe surgery (straight and bent tying forceps)

In addition, the mini-circuit board installed in the holders was redesigned, replacing fixed gain and ID resistors with potentiometers, making adjustment and set up simpler for future work. In earlier periods, we found that the growing number of instrument meant finer divisions in the ID signal to identify each device. An analog voltage, ranging from 2.5V to 5V was the original signal corresponding to each instrument – a two surface mount resistors, one at approximately 8k ohms, the other varying depending on the device, were used to set the value. This restricts the available signal range, which could in principle be as low as 0V, given the power and ground inputs to the instruments. The "miniboards" were redesigned to replace the fixed resistors for ID with potentiometers. This caused the current drawn by the ID signal to be the same for each board, and allows outputs from 0-5V.

Further, the strain gage placement on each instrument and the normal range of deformation of each instrument is different, so the instrumentation amplifier chip (the single chip at the heart of each board) needs to have a different gain setting. Gain can only be set experimentally, so installing and removing SMT components repeatedly is a challenge. Potentiometers replaced the fixed gain resistors for both the open/close sensing portion of the circuit and the force sensing portion. Finally, the zero-offset of the amplifier also varies depending on slight differences in the installation process of the strain gages

and on the relative values of the fixed resistors in the Wheatstone bridge circuit in use. Potentiometers were already in use in the original boards, and these were retained in their positions in the new version.

To access the potentiometers, small ports were added to the holder shell, aligned with the potentiometers on both the top and bottom of the board. A jeweler's slot screwdriver is used to make adjustments without requiring disassembly of the holder (a process that also tended to shift ideal gain and offset values). The new boards were installed for the cotton swab, lacrimal dilator, straight needle holder and the straight and bent tying forceps. The remaining instruments will have replacement boards installed following the current end of the period of performance, likely in conjunction with preparations for the 2015 USUHS Eye Trauma course.

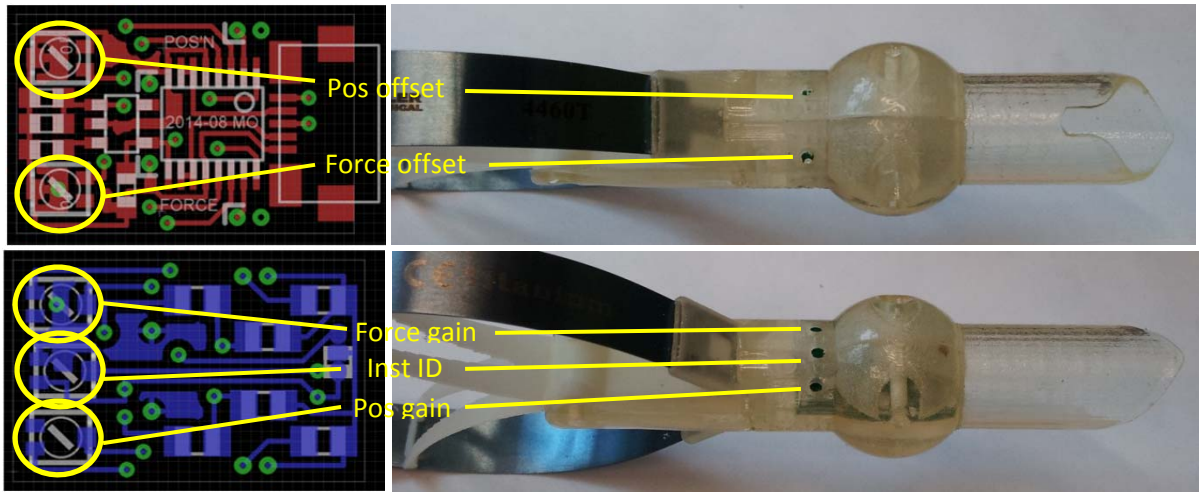

Figure 34: Adjustment access ports in latest instrument holder version.

At the 2014 USUHS Eye Trauma course, requests were made to add straight-jaw locking needle holders and a standard cotton swab to the suite of available instruments. Over the following months, new instrument holders were designed for these instruments. In addition, the holder for the lacrimal dilator previously acquired was completed.

2.3.4.d. Polhemus sensor evaluation completion

As mentioned above, we evaluated the Polhemus position/orientation tracking sensors available in 2012 following contact established with the company at the TATRC booth at the Medicine Meets Virtual Reality conference. We found the increased cable flexibility to be a desirable feature as compared with that of the Ascension Technologies system, however the available sensor was too large for the ophthalmic instruments and we observed additional noise added to the strain gage sensor signals. Subsequently, we held discussions with Ascension and evaluated material samples in regards to the possibility of creating cabling with enhanced flexibility and with integrated conductors to support our force/grasp strain gages, however at that time we chose not to make modifications as the expense of the engineering work was not justified for a relatively small improvement to our prototype.

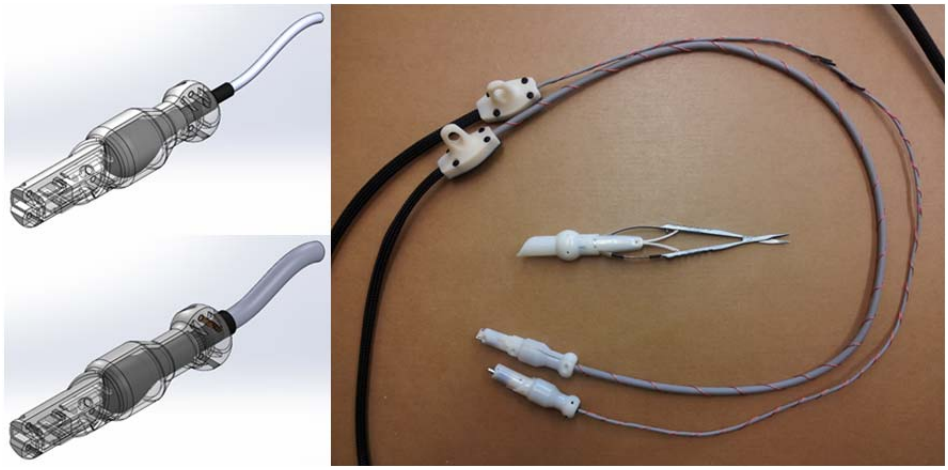

Figure 35: (left) designs for Polhemus sensor holders for teardrop sensor style, with standard and thin cable implementations. (right) Sensor cabling implemented for physical testing.

2.3.5. "Month 7" –

2.3.5.a. Design of skeletal structure, docking points, sensor/actuator interfaces with ocular and craniofacial trauma modules.

2.3.5.a.i. Creation of anatomically accurate data sets to support system design

The basis for this phase of the work was the development of a base anatomical data set, upon which all of the complex biological contours would be based, and which was modified as we added the engineering systems to actuate and sense from the trauma modules and the main structure of the simulator. We initially attempted to achieve this result by identifying a high resolution CT or MR dataset from the MGH patient data archives with anatomy including the base of the neck through the top of the head. When de-identified (stripped of any patient information outside of the images), it would be possible to use this kind of data as a design tool. Unfortunately, after significant searching by our SME Dr. Dawson, by Drs. Hugh Curtin (Massachusetts Eye and Ear Infirmary Chief of Radiology) and Troulis, we were unable to find a suitable scan. As a result, we attempted to generate our own data set from CT and MR imaging and physically molding a cadaver head in silicone. IRB clearance was obtained (determined to be not human studies research), and biosafety committee approval was acquired.

Figure 36: Process of silicone casting of cadaver head and neck anatomy; CT scanning of head. Images of MR scan unavailable due to restrictions on metallic objects in MR suite.

We performed a trial run of the molding/imaging procedure using the first available cadaver sample that was reasonably close to our target demographic (nominally male, average height, 20-30 years of age, normal to muscular body habitus, no pathology of the head/neck region), however the tissue available was from an overweight individual in his mid-50s. We discovered further that the CT scanner was unable to clearly distinguish the boundary between skin and the silicone, so segmentation, even with an advanced software tool that we licensed on an evaluation basis (Mimics, 3-Matic, by Materialize NV, Leuven, Belgium), was found not to be possible.

While developing refined molding/imaging methods to conduct a second set of scans and waiting for a more ideal candidate donor, we began to work with a high resolution deidentified CT data set used previously for a neuroendovascular simulation system developed by our group in the mid-2000s (Luboz et al, 2005). Use of this data set was determined to be Not Human Use. While this data set did not have matching MR imagery or a physical mold, it was created with thin slice spacing. Skin and bone contours and a number of the soft tissue elements could be segmented directly while final treatments, such as skin textures, were included after 3D printing of the relevant sections of the reconstructed head form. Figure 37 shows segmented skeletal features and skin surface, and preliminary imagery of how the face sections would be segmented so that elements could be removed and replaced. The precise division of facial/eye trauma zones continued to evolve as we designed in the necessary mobility and functional features. Figure 39 shows sections of the segmented anatomy reproduced in rigid plastic and a semi-flexible rubber, which we created to explore the capabilities of the Objet 3D fabrication system, which we acquired through this program and which came online in early 2012.

In addition to the structural design elements described above, we worked toward subdividing tissue types and experimenting with molding techniques to generate the various portals. Towards the end of Year 1, to support compatibility with COTS components and commercial mannequin systems, we examined elements such as the Laerdal airway model to use as a platform for testing the sensors prior to developing our own versions with improved anatomy, but with common connection points.

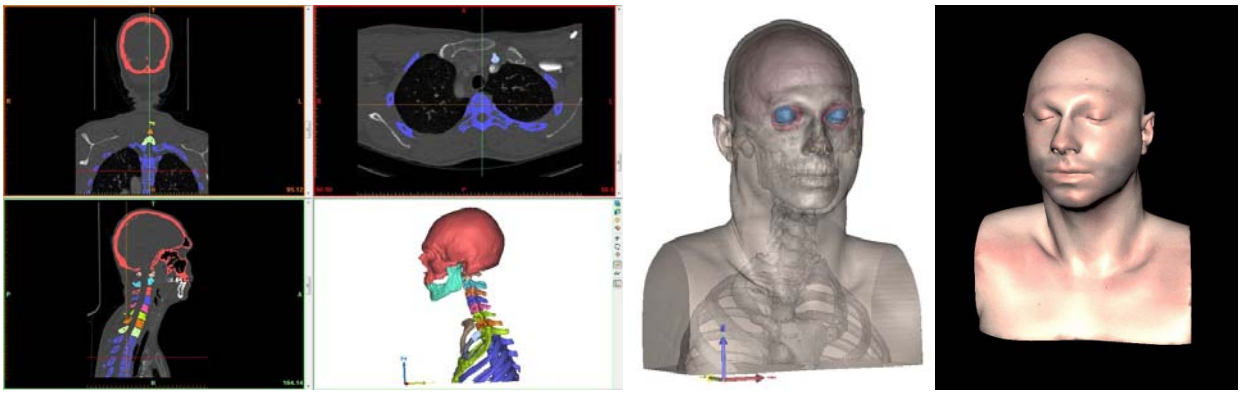

Figure 37: Segmented CT images from prior simulator project; reassembled surface models of skin, bone, eye globes; rendering of reconstruction with flesh tones applied. Skin textures would be applied during creation of physical molds

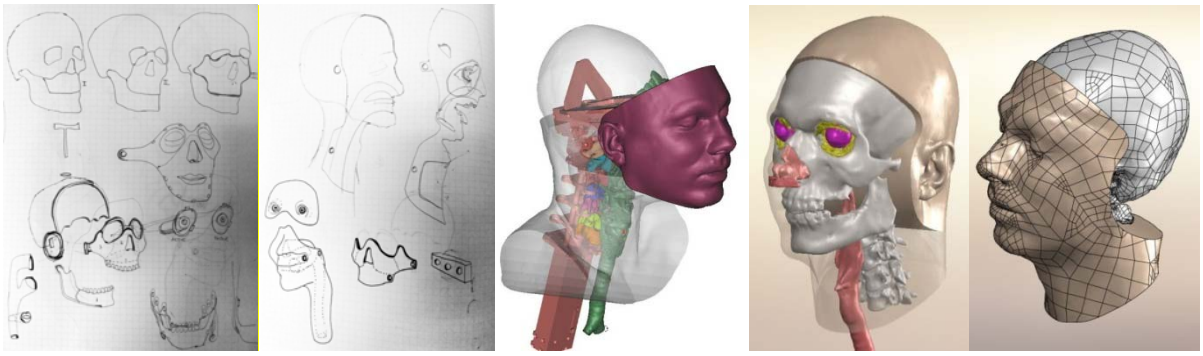

Figure 38: Early concept sketches and later CAD models of methods for dividing structural elements of the head/skull to permit creation of modular injury components and recent scans and combinations of COTS and custom components.

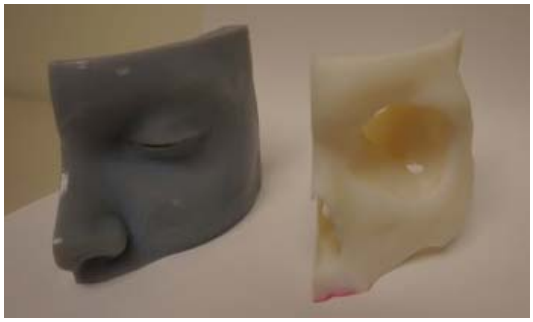

Figure 39: Early concept for division of head elements using Solidworks CAD tools; rapid prototyped rubber and hard plastic sections created from CAD models.

2.3.5.a.ii. Eye motion mechanism

Eye globe motion, both passive and controlled, was an important improvement over the fixed globe of the proof-of-principle system. For the unconscious patient, the globe should be movable when manipulated with surgical instruments, and for the conscious patient, the globe should allow for controlled motion. For conditions including retrobulbar hemorrhage, the eye ceases to be mobile due to the increased pressure; when relieved, some of the motion returns. In addition, retrobulbar hemorrhage causes the globe to be pushed forwards (proptosis), so an additional mechanism needed to be included to generate this motion. The measurement of intraocular pressure or force loading onto the globe must also be measured to detect (a) when retrobulbar hemorrhage is successfully treated through lateral canthotomy and cantholysis and (b) when eye shields or other coverings are applied around the eye, to verify that inappropriate pressures are not applied to the globe during the treatment of nearby bleeding.

In year 1, we developed initial prototypes to investigate motion systems are shown below. They used a pivoting joint at the center of the globe and cable and linkage mechanisms to link to actuators. The actuation and transmission systems were envisioned to reside within the permanent structure of the mannequin head, with interchangeable eye globe modules to represent different conditions (e.g. lacerated globe, undamaged globe). The actuation mechanisms were designed to be “backdrivable”, so that external surgical manipulation would move the eye.

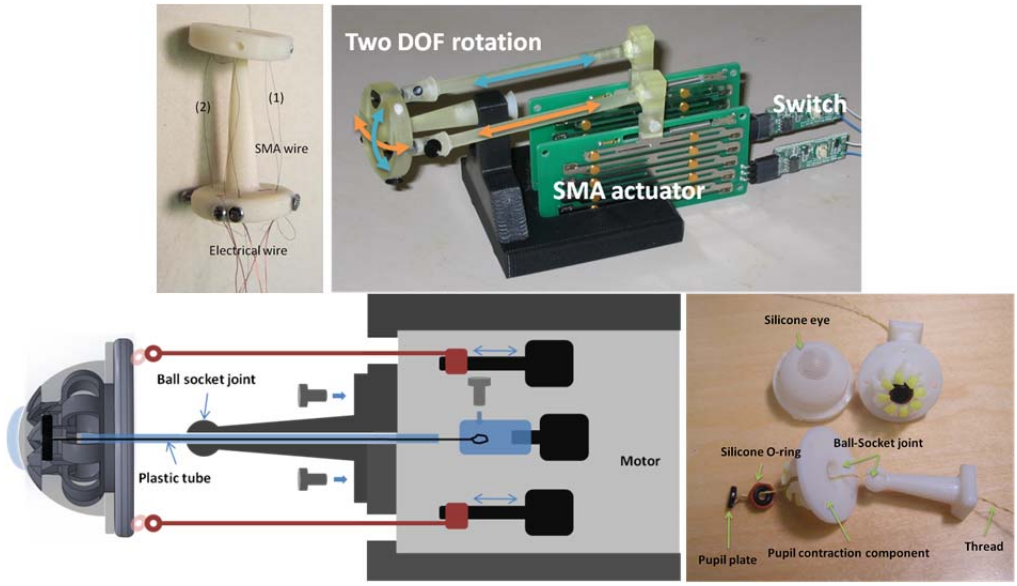

Figure 40: Concepts and prototypes for eye motion mechanism. Includes early concept test of mechanical, petal-based pupil contraction mechanism.

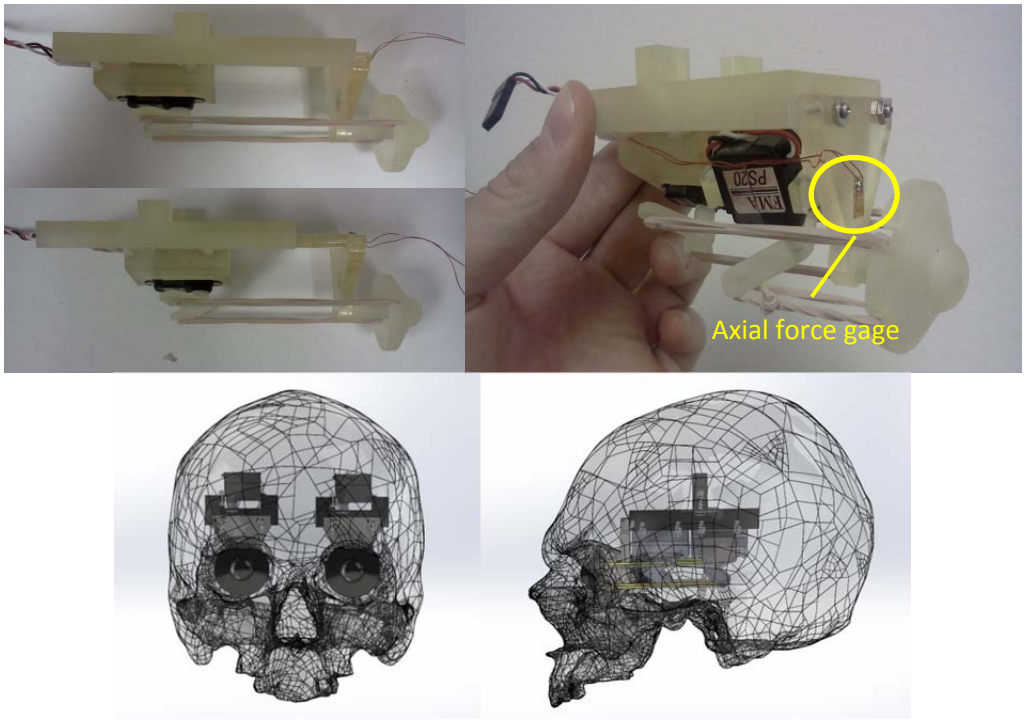

Figure 41: Eye motion module for pitch, yaw and proptosis, with backdriveability in globe motion. Sizing of internal components relative to skull model.

In year 2 building on earlier design concepts, we designed and prototyped a mechanism that includes all of the globe motion features to be included in the eye modules: eye pitch and yaw, proptosis, backdriveability in pitch and yaw (to allow the surgeon to manipulate the eye) and sensing of applied

force to detect pressure/load applied to the globe and the reduction of force on the eye expected on successful canthotomy/cantholysis.

The mechanism shown in Figure 41 was the first iteration that supported the mechanical motions and compliance features analogous to normal eye motions, and relative sizes of the components in reference to our CT-derived skull model.

To allow for attachment of replaceable eye globe models and provide fluid and signal connectivity, we included fluid channels that protrude into the space of the globe. These serve the dual purpose of providing mechanical connection through a tight friction fit. The fluid channels connect the globe to a blood simulant supply for simulation of bleeding and/or hemorrhagic chemosis – bleeding behind the conjunctiva creating a red zone around the cornea, one of the common signs of retrobulbar hemorrhage. They would also provide channels for fluid for testing of suture water-tightness and future capabilities such as control of pupil contraction. Figure 42 shows modifications, including reduction in thickness (to accommodate large angular motion without collision between fluid connections and the supporting post), the fluid channels with connection points front and back and corrections to the central spherical joint design from the earlier version. It also integrated a first test at a revision to the elastic member connection, replacing the latex rubber bands with neoprene o-ring material for improved reliability and lifetime vs. latex rubber. The original hook/loop attachment mechanism was replaced with a version no longer subject to the possibility of the elastic member becoming dislodged, as set screws maintain the connections.

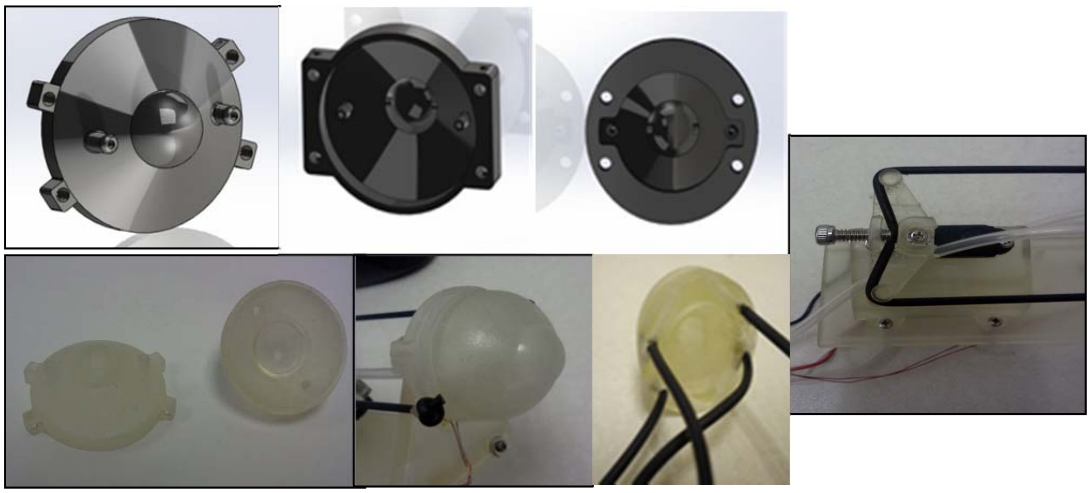

Figure 42: base plate modifications, rapid prototyped test versions of plate and globe showing plate and globe segment separately and assembled. Features include bosses for neoprene cords to replace latex rubber bands. Modified elastic transmission components: o-ring cord threaded through servo arm, initial baseplate attachment.

During Q6, examination of sections through the model of the skull was done to verify accommodation of the mechanism within the skull contour while maintaining a reasonable thickness of skull structure external to the motion mechanism. The initial orthogonal arrangements of eye motion mechanisms would violate the outer contour of the skull, so they were angled inwards and the servo/cord

arrangements and contour of the globe base plates modified to retain the normal forward looking orientation of the globe.

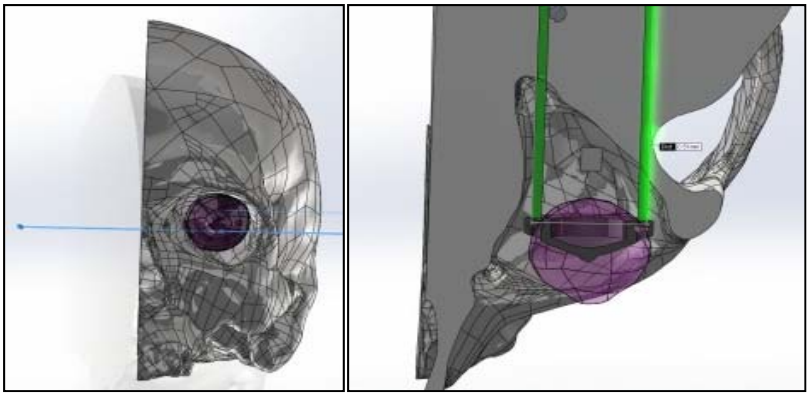

Figure 43: Sectioning of skull with prototype motion mechanism showing excursion of elastic cords from surface of skull in zygomatic/sphenoid region.

A proptosis mechanism designed early in Q5 reached a functional test model by the end of the quarter, demonstrating a range of motion of approximately 10mm, more than sufficient to generate the protrusion of the globe necessary to indicate retrobulbar hemorrhage. Shown below is proof of principle design and the sliding carriage shown in the extended configuration.

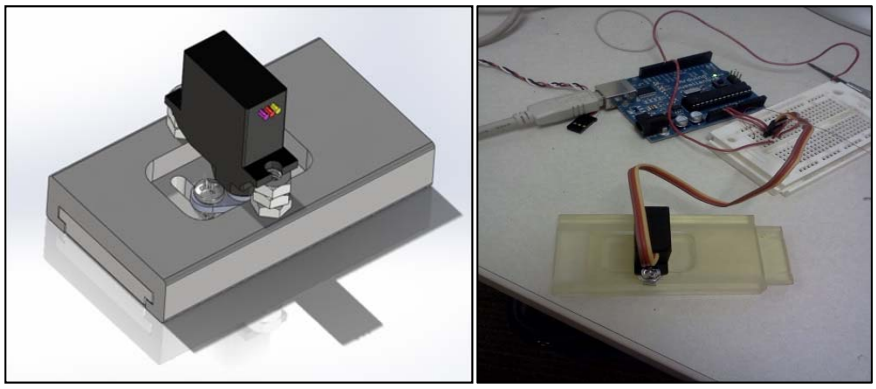

Figure 44: Proptosis mechanism (separate from pitch/yaw components)

Further revisions to the design included selection of smaller servo motors, unification of the structure into fewer separate components, and flipping the orientation of one servo of each pair to reduce size of the mechanism and prevent collision between the control arms. These changes enabled the mechanism to be rotated 15 degrees from the original position to better align with the eye socket and preserve orbital wall thickness. A prototype of the compact version of the eye motion system was built, shown below.

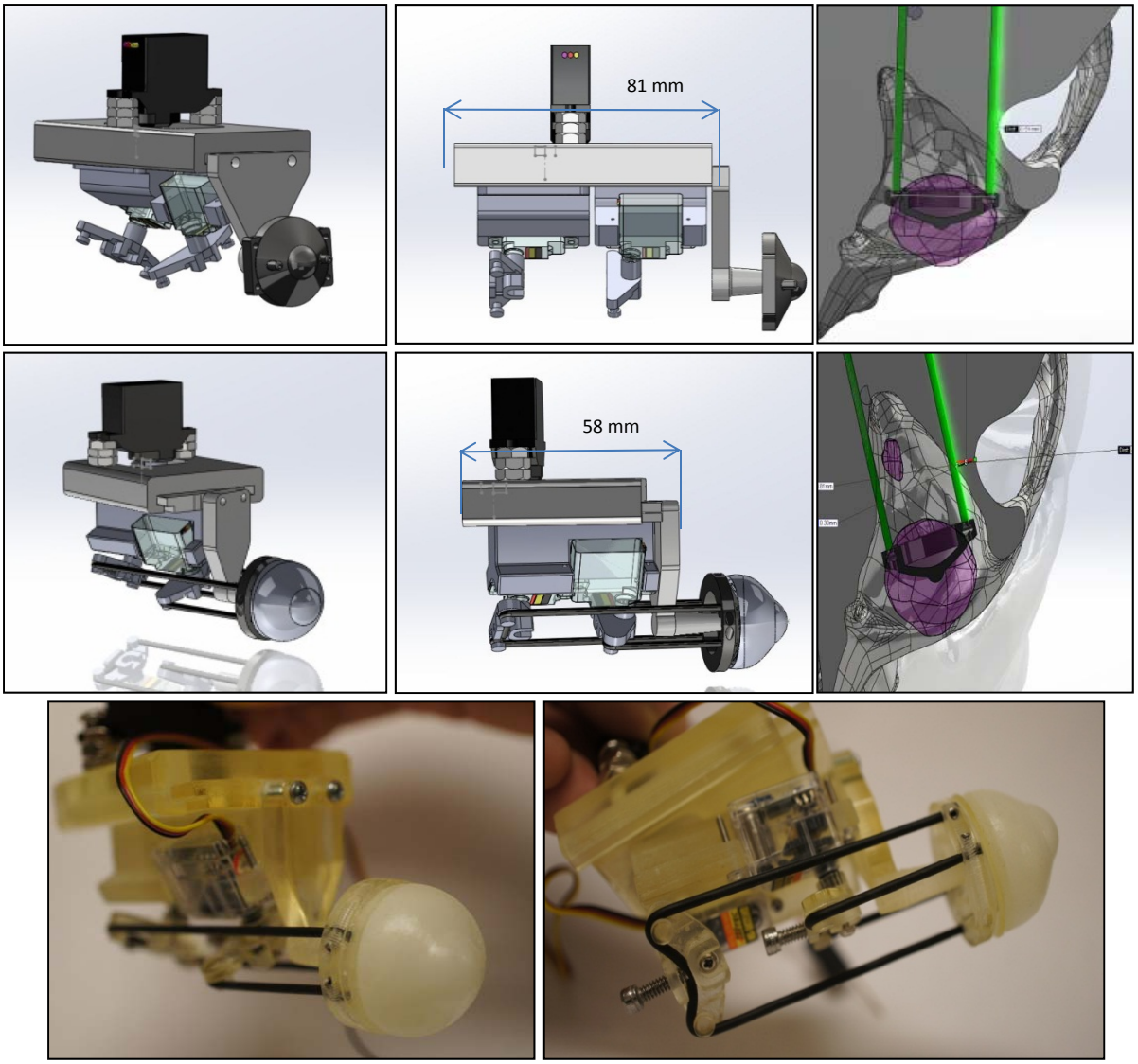

Figure 45: comparison of initial and modified orientations of eye motion mechanisms, preserving orbital wall thickness and reducing overall mechanism size. Assembled, compact motion module.

In Q6, the final main actuated component of the eye motion system, the blinking mechanism was prototyped, so that the mannequin-mounted version of the system could provide a sense of presence and indication of level of consciousness, and help to provide indications of eye trauma; blinking would be prevented, for example, during a retrobulbar hemorrhage scenario.

The eyelid is made of silicone soft layers (see section 2.3.5.a.iii for eye/face module design), mounted to an orbital rim structure. A silicone/mesh protrusion of the eyelid, corresponding roughly with the levator and Muller's muscles, passes through a gap created in the upper part of the orbital rim of the portal. This protrusion will links with a retraction mechanism, part of the eye motion assembly. Shown below is Q6 iteration of the design of the bony components of the system, with protrusion slots.

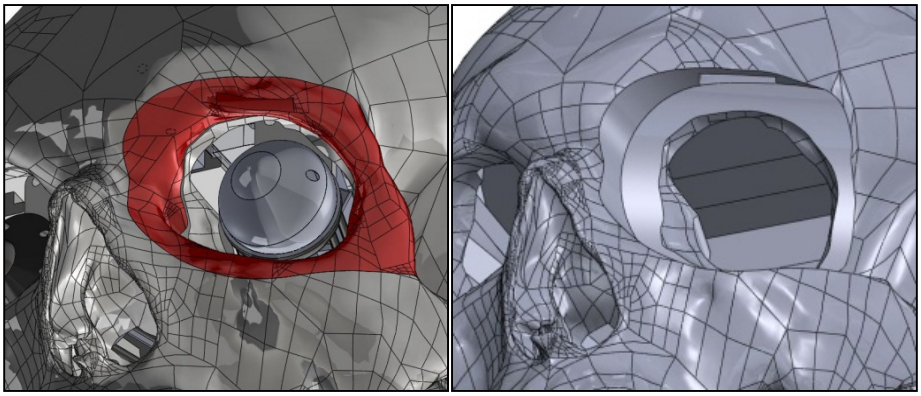

Figure 46: Orbital rim installed in skull, with slot for "levator muscle" protrusion of eye lid; orbital rim removed with slot for access to blinking mechanism behind forehead.

The blinking mechanism is a servo-actuated crank-slider, with an end-hook which will mate with the eye lid protrusion. A crank-slider linkage is necessary to orient the pulling direction of the eyelid and to avoid collision with the internal wall in the skull.

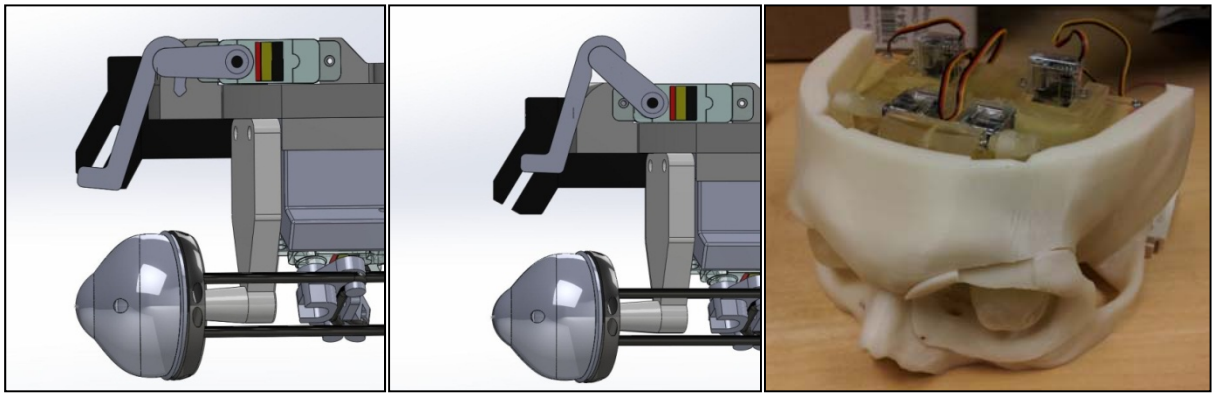

Figure 47: Blink motion eyelid retraction mechanism. Skull segment with motion mechanism for testing of assembly and fit. Also shown is partially seated bony orbital rim which will support the trauma portal soft tissue.

Also in Q6, the contralateral portion of the system was designed. A reflection of the mechanism across the sagittal plane results in collision between the servo control arms of the posterior servo. Instead, keeping the same servo mounting frame and rotating its placement prevents collisions and reduces part count. This can be seen in the detail of Figure 48.

The slide mechanisms for proptosis were lengthened, their anterior ends modified to support the angled orientation of the mechanism, and the main frame that supports the assembly widened with mounting features for attachment to the skull. To further unify the design, the same, smaller servos used for eye motion were used for the proptosis motion. This design decision simplifies the bill of materials, also reduces mechanism size and simplifies software control of the system.

Two additional servos are shown, used for the blinking mechanism.

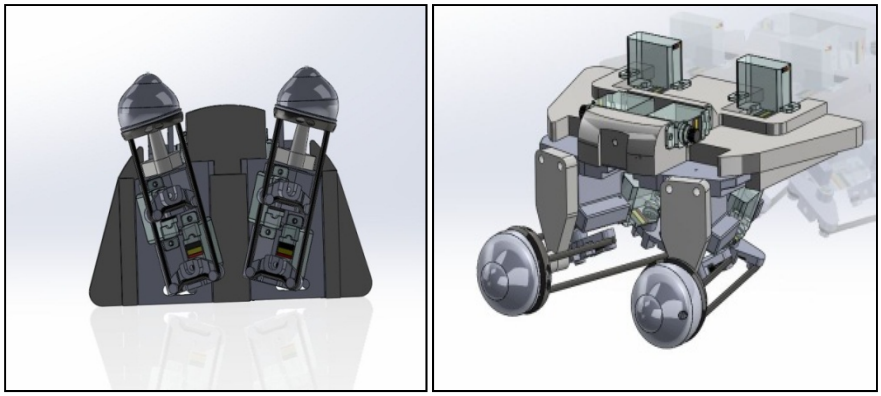

Figure 48: Bilateral eye motion mechanism with servo configuration maintained left/right vs. reflected..

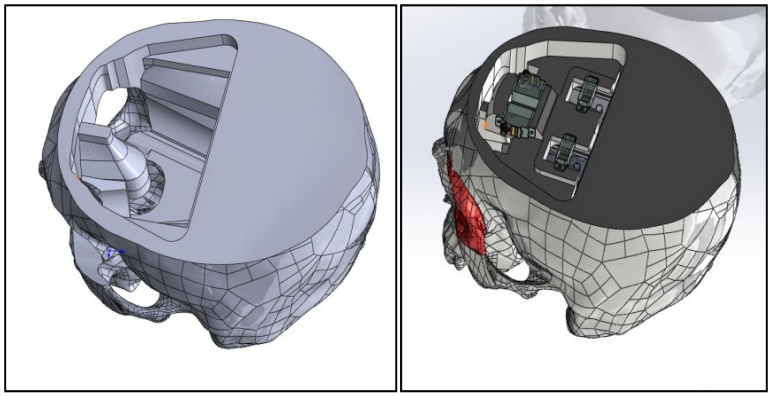

Figure 49: Partitioning of skull; skull component with motion cavity shown; assembled skull design with mechanism.

The bilateral assembly was connected to our drive circuitry for testing and debugging of the code, mainly to ensure that all of the independent and linked motions behave correctly – blinking of both eyes occurring in the same direction (the servos are arranged opposite to each other, so inverse command signals must be sent to them for the output shafts to generate the same blinking motions).

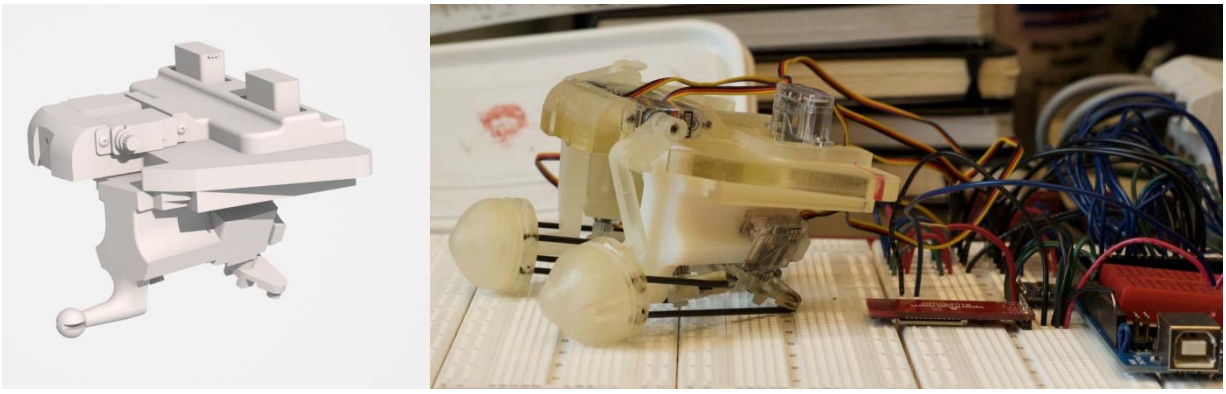

Figure 50: CAD rendering of bilateral version of eye motion mechanisms and initial testing of servo drives of pitch/yaw and propotosis actions.

2.3.5.a.i. Eye motion kinematics

Because the position of the elastic cables would physically interfere with rigid components of the system if the servos were oriented at 90 degrees to each other, the servos are rotated 50 degrees away from parallel, or +/- 25 degrees away from the vertical y-axis shown in Figure 51. In this configuration, rotation of the globe requires motions of both servos.

The eye mechanism can rotate in both the yaw (α) and pitch (β) directions, under the control of the two independent servos, with rotations θ_1 and θ_2.

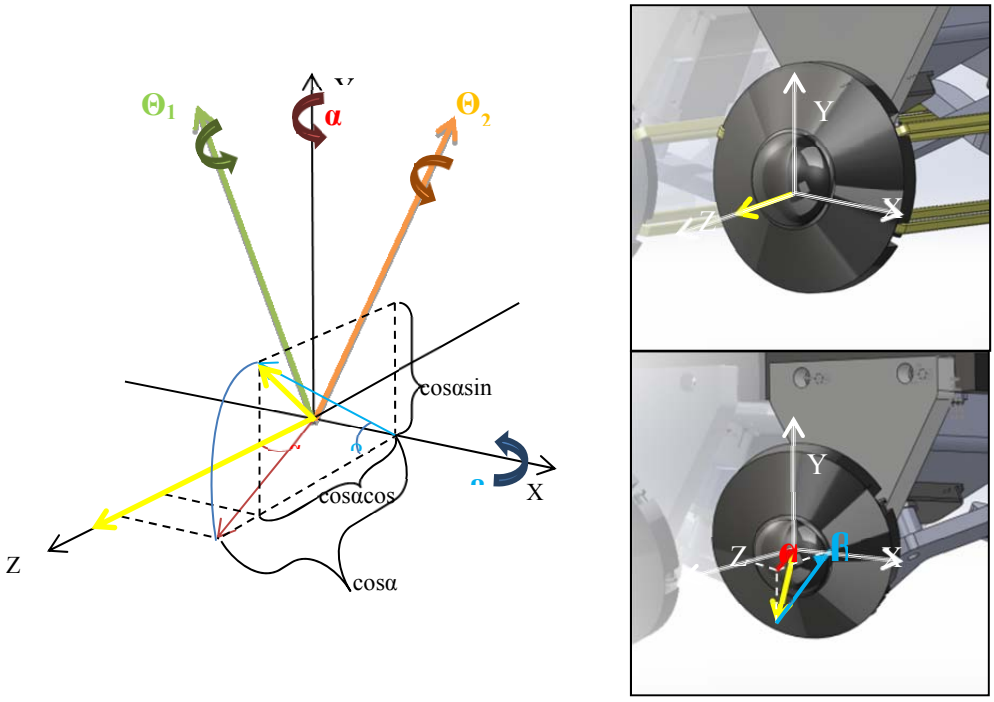

Figure 51: Eye motion polar coordinate system. Globe motion control is defined about the X and Y axes, while the servos rotate at offset axes, with motions θ_1 and θ_2.

To make the calculations more general, the servo offset angle is defined as γ and the command positions sent to the servos for a given eye are determined by:

$$\theta_1 = \tan^{-1}\left[\frac{(\sin\alpha\cos\gamma + \cos\alpha\sin\beta\sin\gamma)}{\cos\alpha\cos\beta}\right]$$

and

$$\theta_2 = \tan^{-1}\left[\frac{(\sin\alpha\cos\gamma - \cos\alpha\sin\beta\sin\gamma)}{\cos\alpha\cos\beta}\right]$$

These equations were implemented in the motion controller for testing the eye motion mechanism. A basic point-and-click interface was written to control, eye orientation, proptosis position and motion speed.

Using an Arduino Duemilanove microcontroller and a graphical user interface written in Processing, motion control of the mechanism was achieved. This formed the basis of a later, more comprehensive controller, described below. Examples of control entry and corresponding eye mechanism positions are shown.

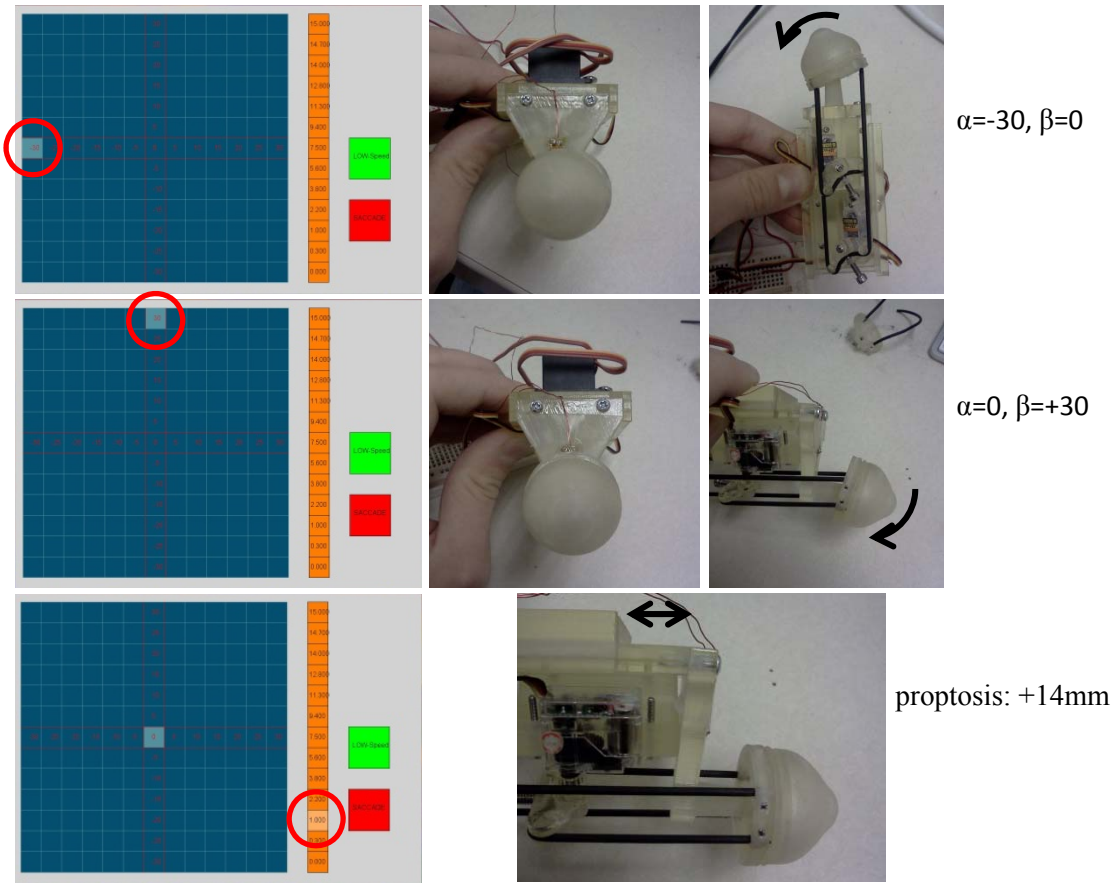

Figure 52: Processing control panel for pitch/yaw/proptosis showing motions of mechanism corresponding with graphically entered target positions.

During Q7, we described a move from the Arduino 2009 platform for interfacing with the eye/head/neck control systems to the Arduino Mega 2560. The alternate board supports 40 more digital I/O lines and 10 additional analog input channels. Based on the restrictions of the central microprocessor and our needs for controlling multiple functions, we replaced a stock interface program available for the Arduino with one of our own, which optimizes the available I/O channels for our use. The board was configured to run 8 different latching valves, 12 servos (primarily eye mechanism motion), I2C communications to the digital-to-analog modules for use with the electronic regulators we acquired earlier, one or two stepper motors, two quadrature encoders, and unassigned I/O for 10 PWM or digital I/O lines (e.g. pump control, single acting valves), three serial communication ports, and all 16 analog input lines.

To test this system and provide control for the existing hardware elements, we prepared the GUI currently being used with the eye motion platform described above and the latching valves on the air muscle test bed developed earlier (see section 2.3.5.a.v).

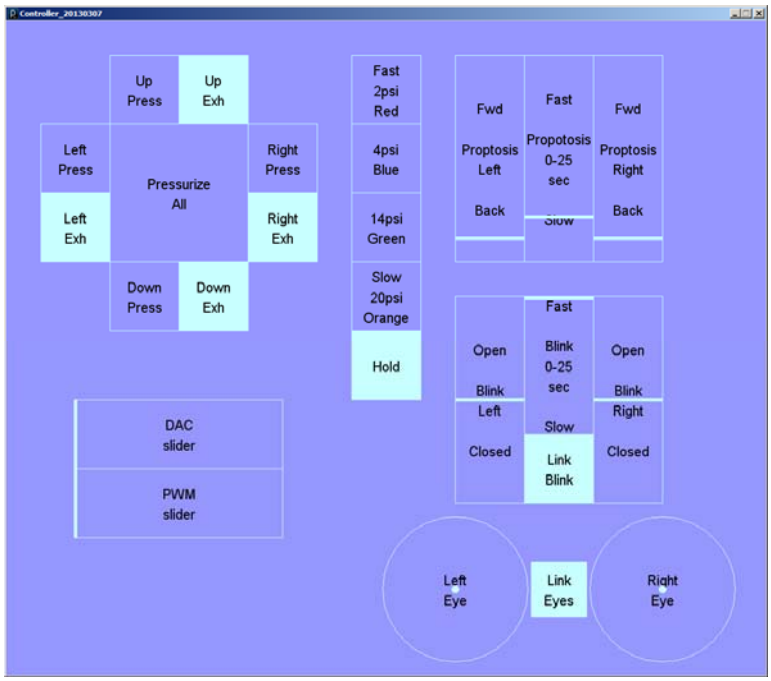

Figure 53:Comprehensive development graphical user interface, including pneumatic controls (upper left), proptosis position and speed for left and right eye (upper right), blinking servo position and speed and whether left/right eyes are linked (middle right), and independent or linked eye orientation control

The control circuitry was unified as well, shifting from an initial version with discrete transistors (see Figure 54) to a smaller number of ICs. A Bluetooth module was added to the circuit, which would allow the Instructor Tablet computer associated with the mannequin (Laerdal SimMan Essential, see mannequin acquisition and modification sections below) to control the new components wirelessly. When connected to the mannequin's power supply, we achieved a state where the new components require no external wired connections.

Testing of the valves in late Q7 showed that the 12V mannequin supply, when run through the earlier discrete transistor circuit or the new version, did not produce sufficiently high voltage at the 12V-rated valve inputs. Voltage drops across the transistors result in insufficient voltage at the valves, so we have observed that some of the valves are not reliably actuated. To solve this issue, we ordered, installed and tested a DC/DC converter, which boosted the 12V supply from the mannequin to 15V output of the converter. This comes at the cost of a higher current draw from the mannequin, so we were limited to running two valves at a time at most (mannequin current limit is 1A). Since the valves would generally be activated one or two at a time during normal operation, this is not expected to be issue – only during initialization of the system would numerous valves be activated in short order, but this can be done sequentially rather than all in parallel, and since the time to pulse the valves to set their state is under 100ms, this did not present problems.

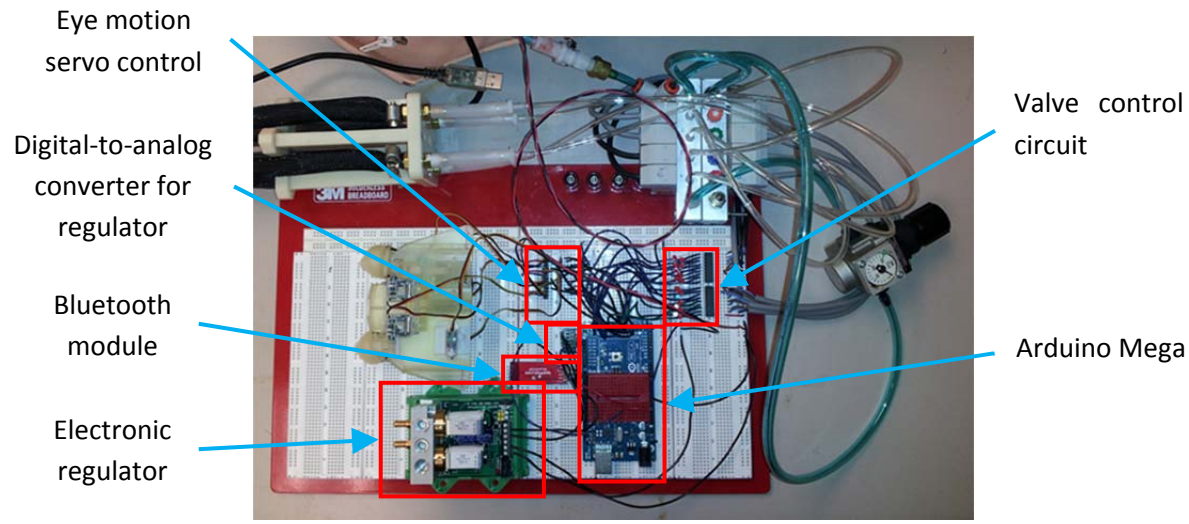

Figure 54: Protoboard for eye servo and neck pneumatic valve control

2.3.5.a.ii. Pupil contraction

Demonstrating responsiveness to light or to level of consciousness or to certain pathology, pupil contraction/dilation was felt to be an important element for the eye modules, especially in scenarios where the patient would be conscious. In Year 1, we reviewed and tested a variety of technologies to generate such motion, via mechanisms that could fit within a portion of the space inside the globe. For the suite of eye modules envisioned, surgeons would not explore or intervene inside the sclera, so the posterior chamber can be substantially used for actuation or sensing elements.

The first test pupil used ferrofluids in the presence of an electromagnetic field. We attempted to create a small, closed reservoir of ferrofluid, which would expand and contract when the magnetic field strength of the electromagnet was varied. We found that the drive current passing through the electromagnet and size of the wire coil required to generate a useful response were both too large to be practical for installation within the space of the eye globe. In addition, creation of a varying magnetic field in the vicinity of the magnetic position tracking system would create an unacceptable and unpredictable distortion of the position measurements.

Next we examined the use of Nitinol shape memory alloy (SMA) actuation, which does not create a significant magnetic field during use, and has a very small volume to actuation force ratio. The SMA was coupled to a series of filaments that pulled the inner margin of a silicone iris inwards, with the outer margin anchored and providing a restoring force. The contractile filament concept was found to be reasonably successful, though was found to be complicated to assemble. The main challenge was that when SMA is actuated, it contracts by less than 5% of its rest length; to achieve a reduction in pupil diameter from 8mm to 4mm (smaller than the normal human range of pupil sizes) a 2mm contraction of the SMA would be required, necessitating a total length of the SMA of over 40mm, larger than the diameter of the eye globe (typically about 25mm).

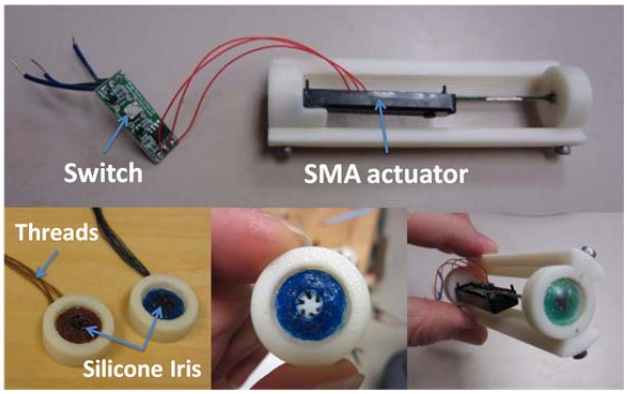

Figure 55: Examples of test platforms for evaluating tensile filament actuation of elastic iris using shape memory alloy actuators.

A further approach, to keep the actuator size approximately equal to that of the iris, we created molding techniques to make a toroidal “balloon”, which could be inflated or evacuated with air or fluid pressure. With the outer margin of the torus restrained, the inner diameter is reduced when the torus is inflated. The example shown below makes use of plain, unpigmented silicone however any color could be used for cosmetic purposes.

Figure 56: Sequence of inflation of toroidal "iris" to cause contraction of pupil.

We also prototyped interleaved iris “petals”, somewhat analogous to a camera aperture. With the 3D fabrication system acquired for this program, we were able to create complex flexural joints to allow for a natural contractile motion with a relatively circular pupil perimeter. A pair of filaments wraps around all of the petals, and when tightened, through the action of a small motor, causes the petals to converge towards the midpoint of the pupil. We conducted experiments to look at the effects of a motor in operation near the magnetic position trackers. Provided that motors are mounted towards the posterior portion of the head, we found that they do not generate noticeable distortion in instrument positioning. The flexure assembly was designed to fit within the volume of the eye globe, and continues to remain under consideration for use in future eye modules.

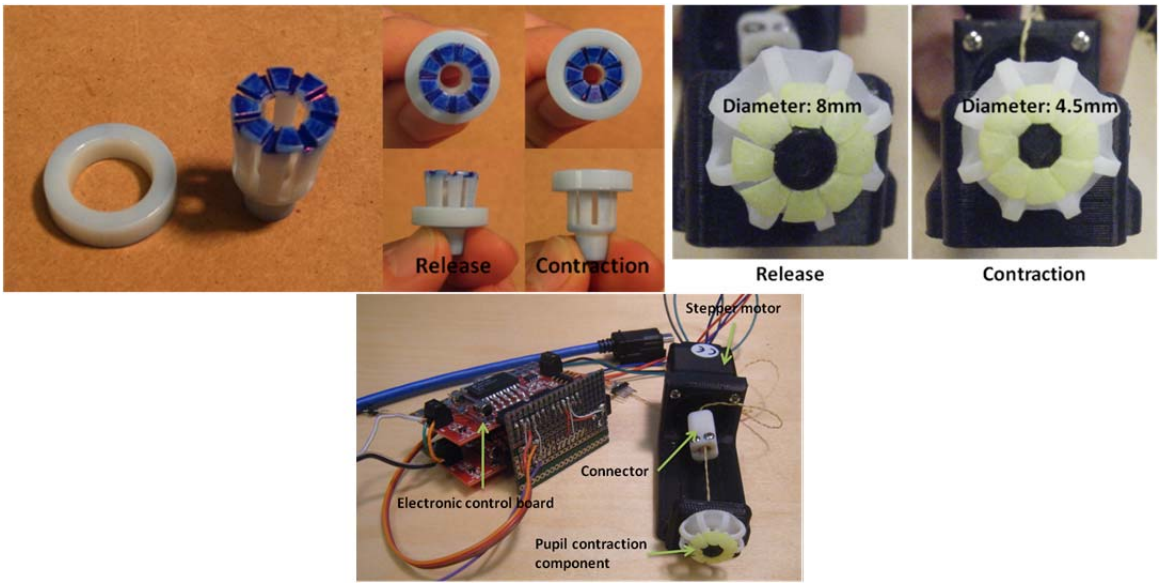

Figure 57: Two iterations of contracting petal concept for pupil contraction mechanism with testbed motor driven system. Transmission makes use of twist-actuator, shortening the tensile cable as it is twisted by the stepper motor.

Lastly, we contacted the E-Ink company (E-Ink Corp., Billerica, MA), which makes electroactive displays that would have very good visibility under daylight or other conditions, would have low power consumption and very small volume. Unfortunately their response was that the non-recurring engineering costs could only be justified if the annual minimum order quantity is in the 100,000+ range.

2.3.5.a.iii. Periorbital tissue modules

Year 2 saw significant advances over the original proof-of-concept and Year 1 versions of the updated eyelid modules, which included a simple tarsal plate structure. Much experimentation was done to explore the potential range of anatomical features that could be included in the anatomical modules, a subset of which were implemented in the versions presented at the USUHS courses, and all of which remain available for future implementation in potential commercial versions of the system or its subsystems.

During Q5, we began to add silastic tubing into the margin of the eyelid model to provide the anatomy for performing canalicular repair, for more advanced eye lid laceration scenarios that the initial full-thickness marginal laceration. Dr. Mazzoli provided advice and detail on the relative sizes of the canaliculi and the punctum, the small opening that drains tears from the eye.

In addition, we began to generate CT-derived skin surface models to generate new eye lid structures, vs. our earlier Phase I system that used the life-cast original. Shown below are surfaced CT data, CAD models of elements of the mold, partially molded lid structures, with the first mold lid removed prior to installation of the second lid with the cavity for the tarsal plate, and the front and back views of the new lid structures.

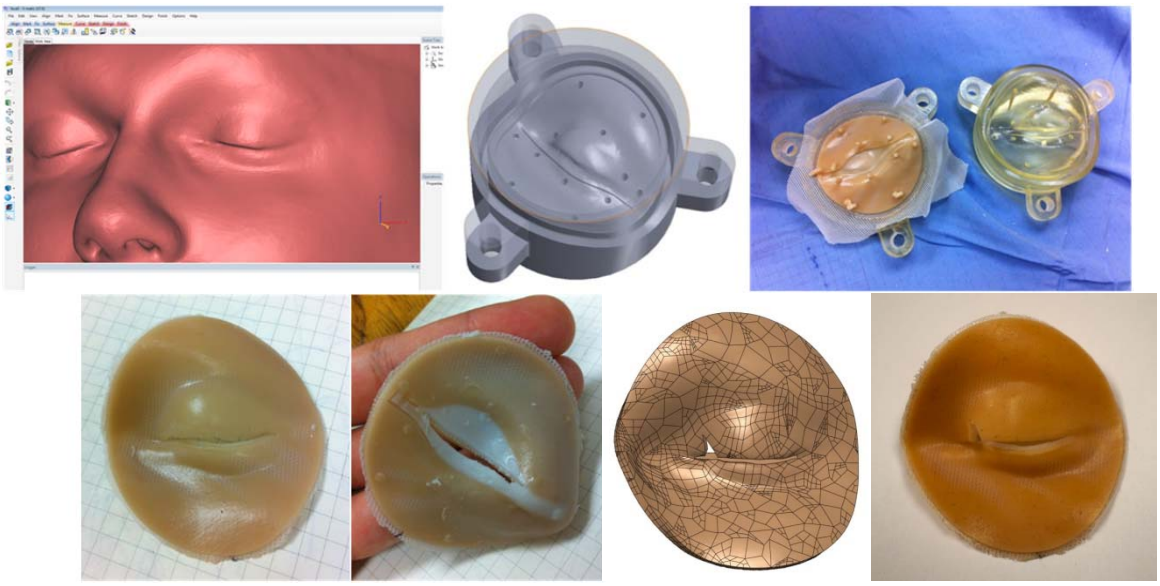

Figure 58: Eyelid based on CT-derived data: (top row) Mimics software view of anatomy, CAD model of mold, partially completed eye lid, prior to over-molding of tarsal plate. (bottom row) Front and back views of overmolded portal structure, CAD model with laceration, physical test model with defined laceration molded-in.

We tested a series of models in which the "laceration" would be designed directly into the 3D printed molds, so that differences between trauma modules due to artistic variation or between instructors creating their own lacerations would not occur.

Using the components that were produced at that time, we also performed tests to determine how to create molded eye lids with multiple layers that would be compatible with the blinking mechanism described in the earlier sections. The initial part of the test was to create incisions in the lids and attach threads to examine the likely motion during retraction. These tests suggest that an approach to the soft tissue components is to incise the skin layer, seat the molded soft tissue into a second mold with the lid in a hyper extended position and mold in additional silicone to create the redundant tissue that Dr. Mazzoli described for us in earlier conversations. This redundant tissue rolls over during the eye lid opening process, creating the fold of the eye lid. Using the 3D models extracted from the CT scans using Mimics and 3-matic an inner layer was designed that extends through a cutout above the upper eyelid and an extruded feature extending upward from the tarsal plate. Initial testing of a modified module demonstrating blinking under servo control is described in 2.3.9.b.

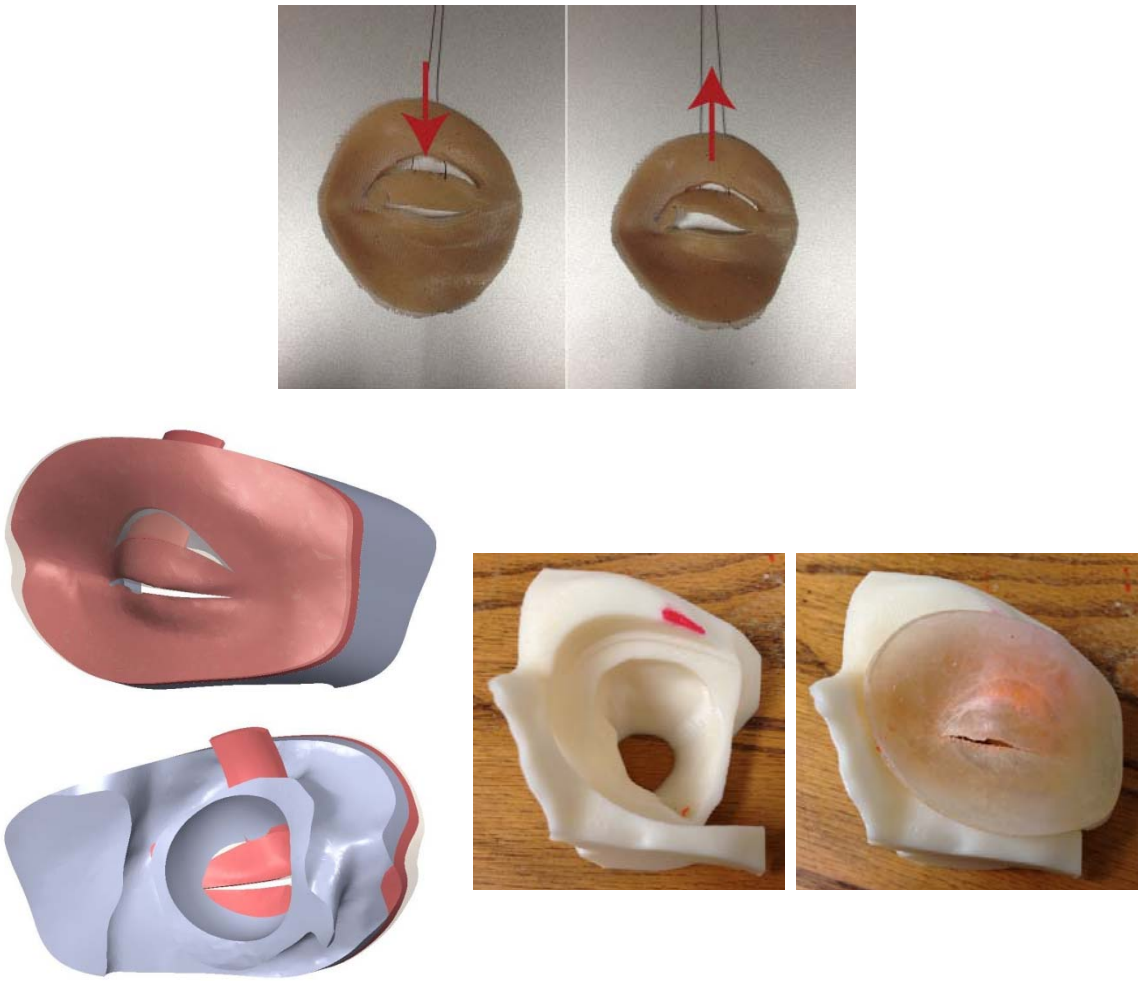

Figure 59: Blinking soft tissue test object; design for eye lid with levator muscle structure; test version installed in skull section, with orbital rim and assembled soft tissue layers.

During Q7, work on moving the lacrimal duct structures forward, necessary to complete development of an eye module for lacerated lid with canalicular repair.

The lacrimal assembly in this iteration consists of the canalicular ducts and the nasolacrimal sac/duct. With the ducts running through the margin of the upper and lower eyelids, the module mold includes alignment slots for the canalicular/tarsal assembly. The ducts consist of silastic tubing of an appropriate diameter, bonded and sealed with silicone glue. The assembly is then attached to the tarsal plate using nylon string. The whole assembly is then seated in the revised mold using the new alignment slots. Sprues, normally a by-product of the molding process that is discarded, are preserved to serve as alignments pegs. The mold revision ensures proper placement of the assembly in the mold prior to injection. The entire assembly is then encapsulated by silicone during the casting of the portal, resulting in a lifelike, multilayered object.

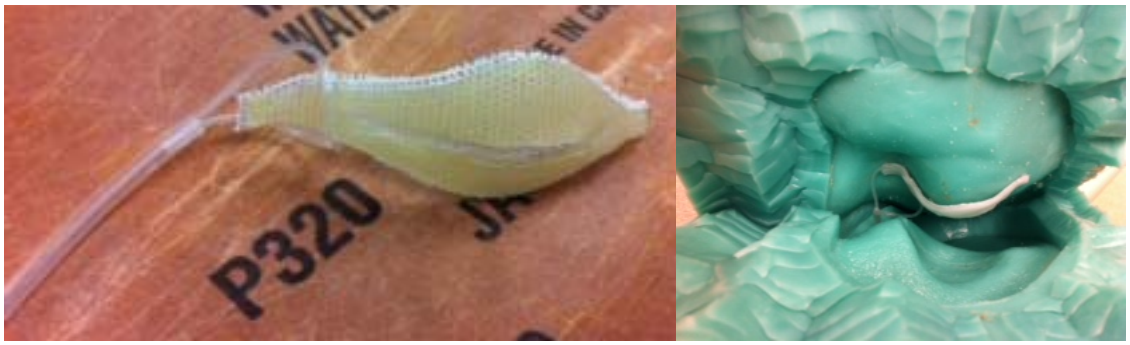

Figure 60:(Left) eye tarsal plate, with attached lacrimal, nasolacrimal duct tubing, reinforcing mesh (as per previous versions of the portal) (Right) Mold for eyelid portal, with tarsal plate, ducts in place for over-molding with softer durometer silicone for eyelid/skin structures. Sprues from tarsal plate molding process hold the plate and duct structure in place for overmolding process.

During Q8 we implemented and improved upon the canalicular structures. The overall size and position of the silastic tube was modified to more accurately reflect the anatomical structures. Small grooves, similar to the ones present in an actual lateral canthal ligament, have been replicated in the module and securely hold the canaliculus in place.

In Year 3, after review by the SMEs, it was determined that it would be extremely difficult and not useful to excise the canaliculus from the surrounding tissue in an actual surgery, and that there is no reason for the simulator to be able to do this. Instead, the canaliculus is contained within the muscle and tissue that makes up the medial canthal tendon. Therefore, the simulated canaliculus need only be a channel that can be located by identifying its white colored surface and can be intubated. When lubricated with a small amount of silicone oil, the part pictured below fulfills this requirement.

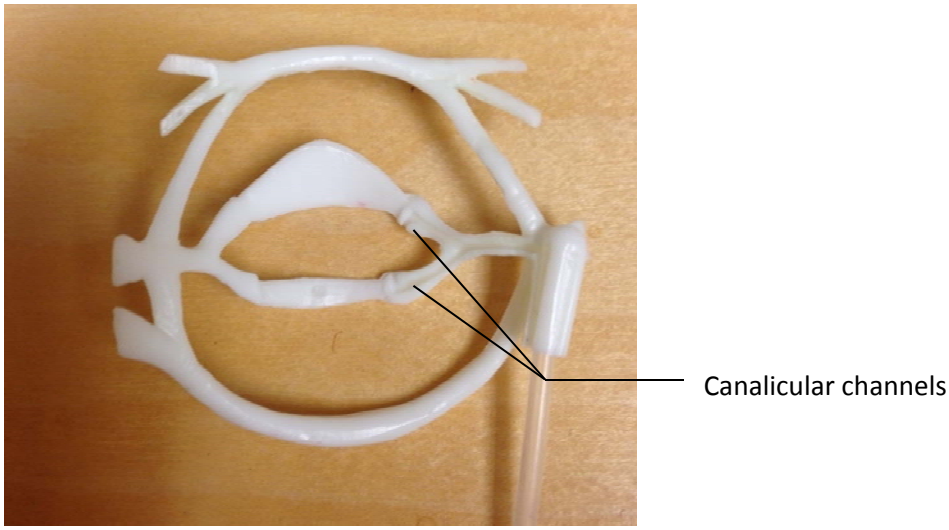

Figure 61, Canalicular channels

In Year 2 we made a substantial redesign for the tarsal plate part for use in a second-generation module that we showed to our SME at the 2013 USUHS Ocular Training Course. Unlike the previous generation

tarsal plate part, a one-piece, flat band that resembles a simplified version of the anatomical structure, the second-generation tarsal plate more closely resembles the real anatomy. It includes a well-defined medial canthal ligament which contains the aforementioned canalicular grooves in the superior and inferious crus, an anatomically accurate lateral canthal ligament, Whitnal's ligament, Lockwood's ligament, and the upper and lower tarsal plates.

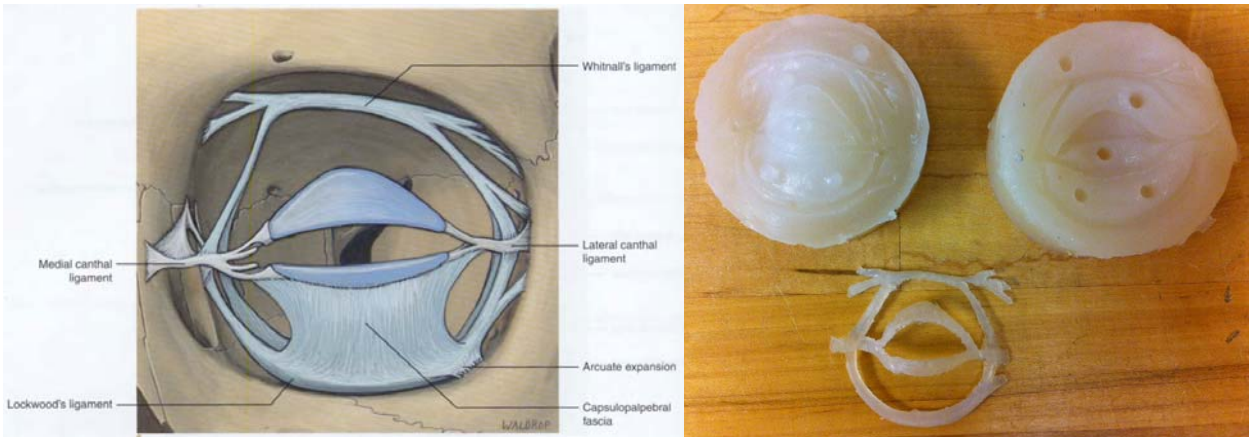

Figure 62: (Left) Textbook anatomy of tarsal plates, periorbital ligaments used as reference for advanced module design. (Right) Molds and cast version of new anatomy, fabricated in stiffer silicone than surrounding eyelid tissue.

All of these structures are cast as a single part. The part aids in providing a realistic surgical experience, strengthens the overall structure by providing more surface area for the module to bond with, and provides a robust framework for the attachment of the canalicular tubes. Furthermore, the lateral canthal ligament and Lockwood's ligament have been outfitted with wires to serve as cut detectors during the proptosis procedure. During this procedure, a surgeon is required to cut through the lateral canthal ligaments, bisecting it until they reach the Lockwood's ligament. They then bisect the Lockwood's ligament until pressure on the orbit is released. The embedded wires indicate whether these incisions have been properly executed. The electronics for this detection circuit are deliberately simple; the wires through the ligaments tie a digital input channel on the Arduino microcontroller (or other later system) to ground (also providing electrical safety as there is little current passing through the wires at any time). When the wires are cut, the ground connection is lost and a pull-up resistor internal to the microcontroller raises the measured voltage, signaling the incision.

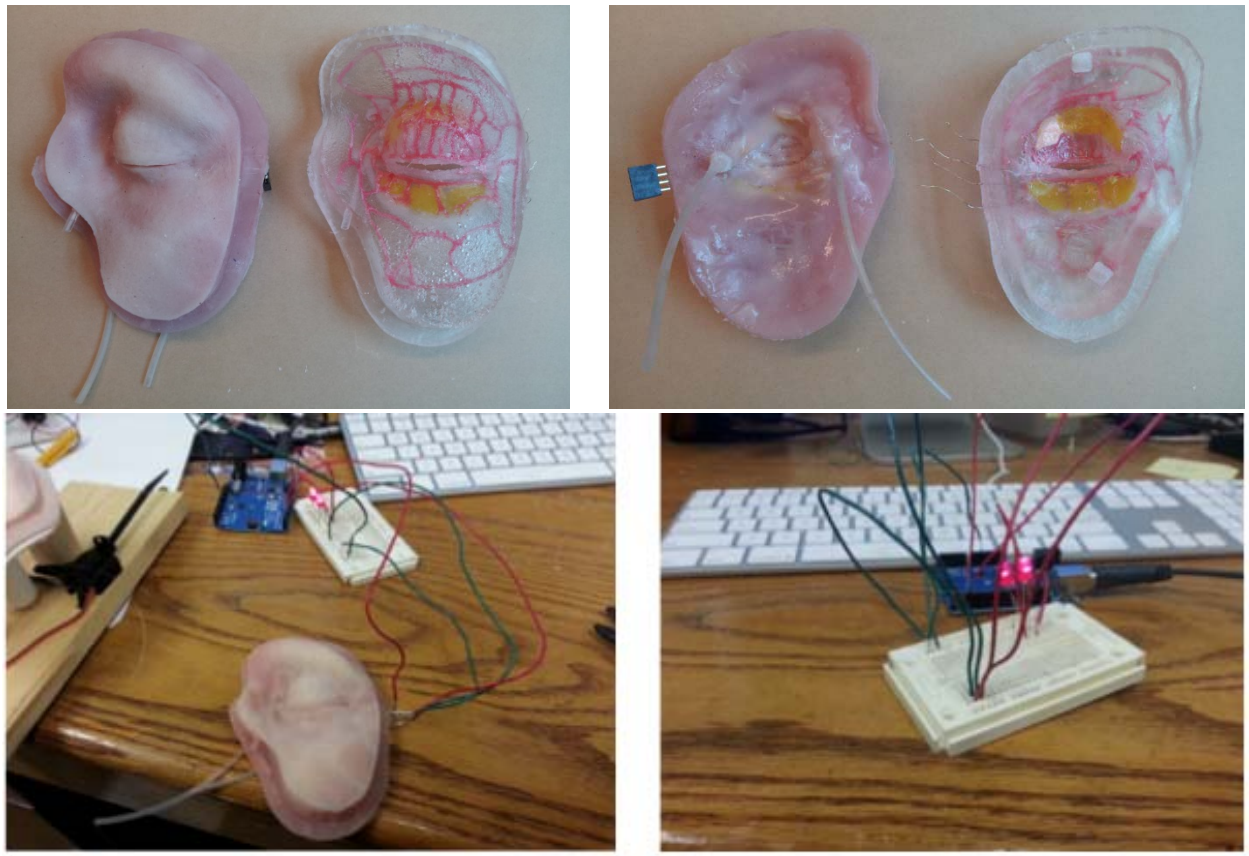

Figure 63: (upper row) Front and rear views of new-version trauma module (uninjured version). Soft, pigmented silicone and hard, clear version for illustration. Internal structures include tarsal plate with ligaments, periorbital fat deposits, arterial vasculature, canaliculi and naso-lacrimal duct. Canthal ligaments have fine wire embedded in them (visible in rear-view, bare wires and attached to temporary connector), arterial system has inlet and outlet ports for blood simulant flow and external pressure sensing. (lower row) Module connected to microprocessor showing illuminated LEDs that indicate un-cut anatomy.

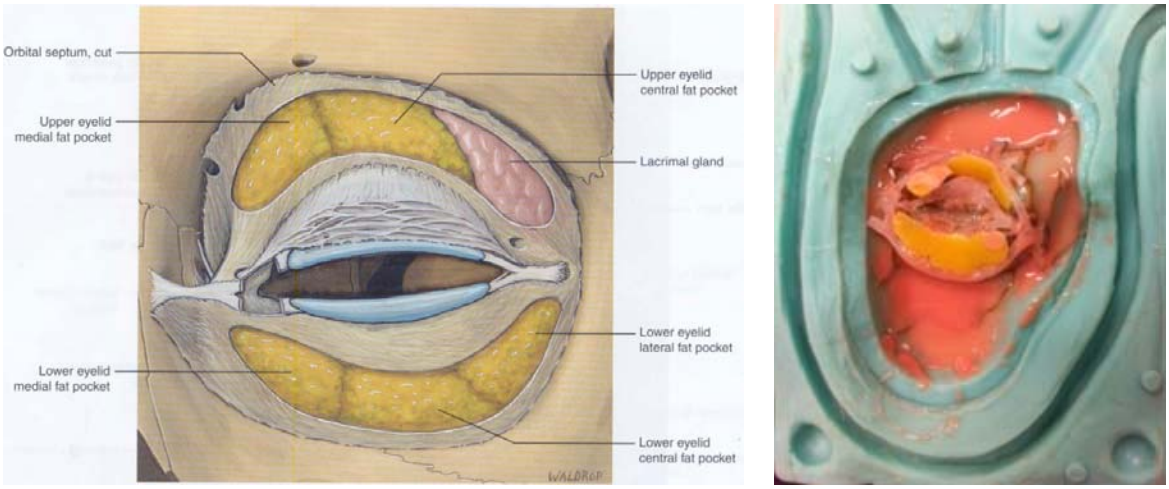

Figure 64: (Left) Textbook anatomy showing fat deposits, lacrimal gland. (Right) Intermediate step in advanced module casting, showing placement of periorbital fat deposits.

The module was further augmented by the inclusion of a layer of periorbital fat and a lacrimal gland (Figure 64). The fat adds to the overall realism of the module, creating a more lifelike feel. Additionally, the fat could be used to simulate a subconjuctival prolapse. It is possible to view the fat deposits as well as the lacrimal gland by inverting the eyelid with a forceps. These structures add a level of realism that with previously unavailable.

We further augmented the module through the inclusion of a functional arterial system (Figure 65). An analog of the authentic orbital arterial system was designed and created for the purpose of providing the option of a lifelike bleeding scenario. The arteries can be filled with blood simulant fed from an IV bag or active pump system. Pressure of the arterial system, monitored by an external pressure sensor, drops when an artery is cut, and hemorrhage of the simulant occurs. This data can be incorporated into the model. We can also detect when a hemorrhage is stopped by the user, opening up the possibility for additional future scenarios.

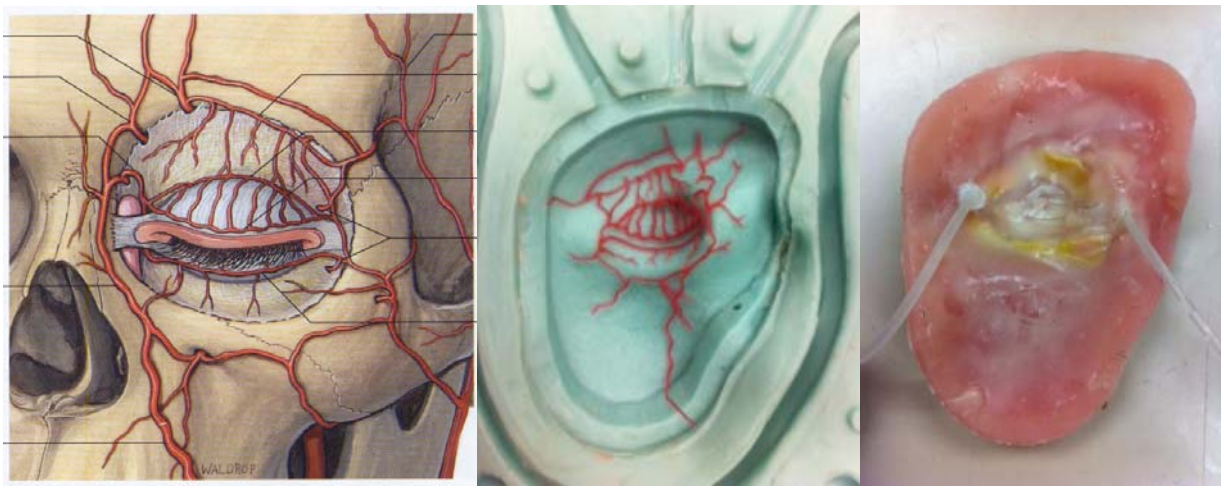

Figure 65:(Left) Textbook anatomy showing arterial network. (Center) Inlay of wax vessels to preserve vessel lumens – wax is melted/dissolved out after silicone cures to produce empty vessel lumens. (Right) fully assembled advanced module, with inlet and outlet taps for bleeding from eyelid laceration module.

In Q9, the skin layer of the trauma module was modified to include previously lacking landmarks normally associated with the eyelid, notably: the bulge in the lower eyelid caused by the “bunching” of skin when the eye is open; a prominent fold in the upper eyelid; the Meibomian glands; and the lacrimal caruncle – the crease of skin at the medial angle where the eyelid terminates. These are prominent geographic landmarks of the eyelid which were missing from our model. Due to the extensive modification of component parts of the module, it was necessary to make a new module mold in which to over-mold the assembly. This provided us with an opportunity to fix these oversights. Accordingly, we increased the under-eye thickness for more lifelike appearance; added a skin fold to upper eyelid; added lacrimal caruncle for added realism; and added decorative Meibomian gland pores to the eyelid margins.

Underlying the revised skin layer, the modules contain a parts cradle made of Shore 0030 silicone, a tarsus with sacrificial wax canaliculus and mesh substrate made of Shore 20A silicone, a periorbital fat

layer made of Shore 0010 silicone, a conjunctiva layer made of Shore 10A silicone and an eye globe made of Shore 20A silicone. The tarsus, canaliculus, and periorbital fat layers were installed in the cradle using RTV silicone glue. These parts were then over-molded at 80psi with Shore 20A silicone pigmented to resemble skin. The resulting part was then placed in an oven to allow the wax part to melt out. The evacuated canaliculus was then reamed out with a flexible plastic tube to ensure all wax had been removed. The conjuctival layer (Figure 67, see also 692.3.5.a.iv) was then attached to the back of the eyelids with silicone glue. A circular cut was made in the conjunctiva which corresponds to the outside edge of the cornea. The conjunctiva was then glued to the eye globe, allowing the globe to move freely, while still being firmly attached to the module. The final steps would involve painting, creating a laceration, and applying moulage and hair.

Figure 66: Module cradle; cradle mold; cradle cover

During the assembly and construction of the first module, it became apparent that replacing silicone RTV glue with 2 part silicone of the same type as the outer skin would decrease the chances of failure. The silicone in its liquid stage flows readily, filling in all the gaps between the cradle and the tarsus.

Including the conjunctival layer, improved eye globe, and a tarsus with integrated canaliculus/lacrimal duct, we produced three such modules.

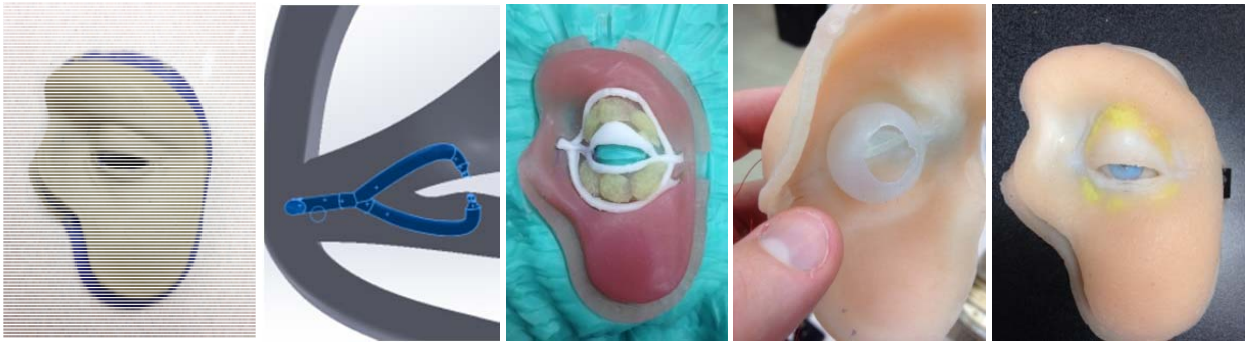

Figure 67: Revised external skin surface model with additional anatomical landmarks and features; CAD model of sacrificial wax canaliculus; assembly of soft, subcutaneous tissues, fat deposits, tarsal plate and tendons; partially installed conjunctiva; overmolded skin layer with installed globe.

MEEI's Dr. Freitag, one of our SMEs had mentioned that real skin is pliant and elastic, yet still firm. After repeatedly grasping and pulling the skin of the module, she concluded that while this module's skin was soft, it was not elastic enough. She explained that human skin would "give" more than the simulated skin did. In order to achieve this elasticity, we determined that the skin should be a multi-layer structure, consisting of a thin, firm outer layer sitting atop a very elastic, pliant layer. This more closely mimics the anatomic structure of skin, which is composed of a tougher epidermis and a more pliant dermis/subcutaneous layer.

A test sample was constructed, comprised of a thin layer of Shore 20A silicone, followed by a thicker layer of Shore 0010A silicone with Smooth-On Slacker tactile mutator. The test sample exhibited the characteristics that our consulting physician described. When grasping the skin with forceps and pulling, the skin appears to separate from the underlying mass and deforms. Upon releasing the skin, it returns to its original shape. Applying this technique to all future iterations of the modules adds only one additional step.

We also corrected the routing of the lacrimal duct hose connector that mates with the port in the skull that leads to the nasal airway. Instead of routing the lacrimal duct out the back of the module, the duct is now routed internally. The duct terminates in the nasal passage of the simulator, which more closely reflects the anatomical structures.

Figure 68: Mold insert for revised canalicular routing in tarsal plate, prior to removal of flashing; mold for replication of revised design.

After overmolding several version 2 tarsal plates in the cradle, we determined that the part should be decreased in thickness. Both version 1 and version 2 produced an unacceptably thick eyelid that detracted from the user experience. Version 3 is identical to version 2 except that the thicknesses of the superior and inferior tarsus have been decreased from .075" to .06". The results are favorable and more closely reflect the anatomical structures; the design retains the possibility of decreasing the thickness further should this be recommended in the future.

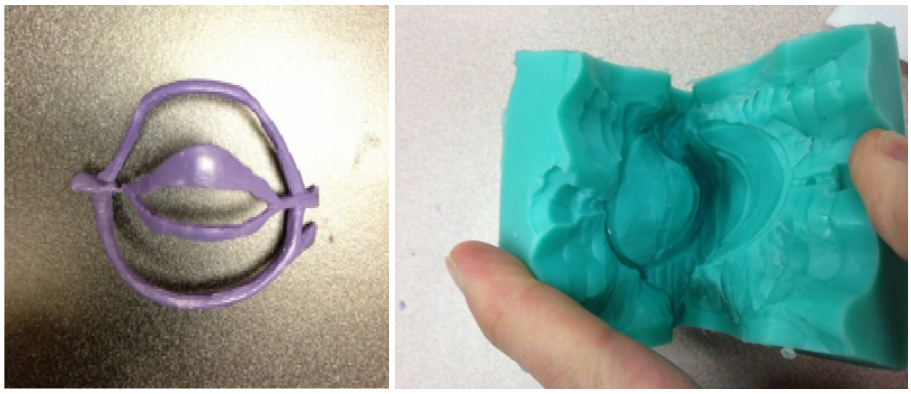

Figure 69: Tarsal plate wax positive; corresponding mold for version 3

Late in the program, the design of the canaliculi was once again refined, following a meeting with representatives of FCI Ophthalmics (a potential licensee of the technology) to achieve a more realistic match with normal anatomy. These soft tissue structures do not appear in the CT imagery we used for the basis of our model, and anatomy texts generally do not have complete sets of views of the canaliculi and lacrimal sac from which 3D anatomy can easily be determined. The image from Grey's anatomy is typical, leaving out the depth dimension. The CAD model used to create the facial mold shows the inward pointing section of the canaliculi that mates with the lacrimal sac, which remains with the skull.

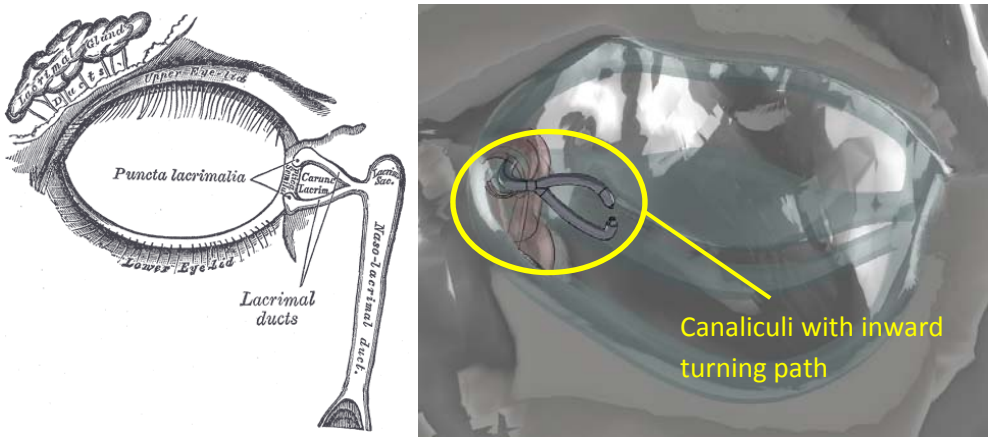

Figure 70: (Left) Front view of anatomy from Grey's Anatomy. (Right) View from slightly above plane of eye globe, showing canaliculi merging, then turning inwards into the head before meeting the lacrimal sac.

These developments of anatomical components of the periorbital tissue were absorbed into the later revision of the modules that encompasses the entire face, which is described in later sections.

2.3.5.a.iv. Eye globe tissue modules

Given the change from the original static eye globes to mobile versions and the simplicity of the original eyelid models, development and improvement of the anatomical components of the eye extended from Year 2 through completion of the project, and are envisioned to continue to evolve as the system is revised pursuant to future research and commercialization efforts.

The early (Year 1) spherical globe models were replaced with partial globes that include the anterior segment and the part of the globe forward of the equator, and a conical seat behind that mates with the motion system and fluidic supplies for aqueous humor and blood simulants necessary for lacerated globe and retrobulbar hemorrhage scenarios.

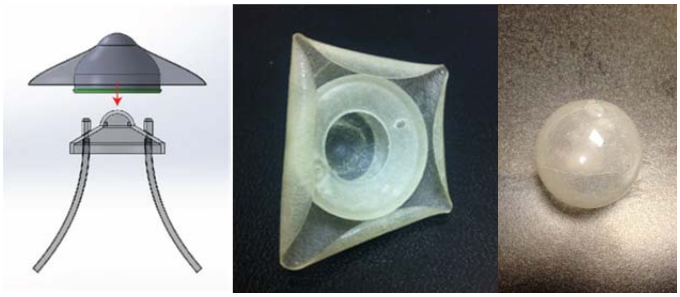

Figure 71: Year 2 status of concept design for globe segment model with initial conjunctiva; glove molded conjunctiva (hollow, silicone sphere).

During Q6, we explored a two part assembly design: one for the eye lid and orbital rim, one for the globe. This approach would permit mixing and matching of different kinds of trauma modules, from simple lid laceration with no globe involvement, to lid avulsion and lacerated orbit. The globe component would be compatible with the symptoms of retrobulbar hemorrhage – proptosis and hemorrhagic chemosis. Shown below is the bony orbital rim described above overlying a multi-layer flexible conjunctiva structure. The blue layer would form part of the globe module, bonded to the globe at the margin of the cornea, extending to the seat in which the orbital rim is mounted. This would be semi-transparent, so simulated blood would be visible. The red layer would be mounted to the skull and seal the fluid space between red and blue, separate from the mechanical and electrical spaces within the skull. The tubes and ports that connect to the globe would provide an inlet for simulated blood to enter this space. Removal of the eye lid and globe portals would provide access to the fluid space for ease of cleaning and inspection. This concept was superceded by later developments, but remains an option for future work.

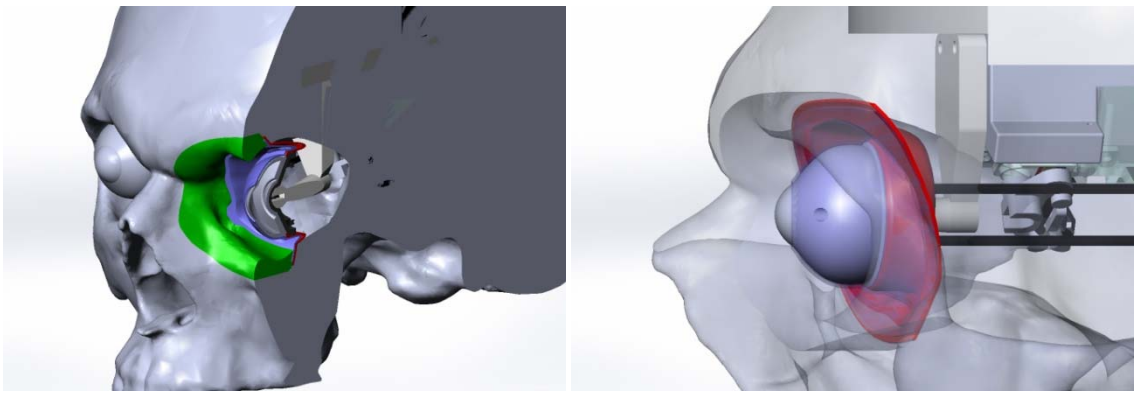

Figure 72: Concepts for flexible conjunctiva layers and sealing surface to protect mechanisms from fluid contact.

At the end of Year 2, we developed a method for fabricating a conjunctival layer that, like the true anatomy, seals the external environment of the trauma module from the interior by connecting the limbus of the globe (the mating zone between the cornea and the sclera) to the interior surface of the tarsus with a continuous layer of thin silicone tissue. The conjunctiva layer is formed by brushing silicone onto a spherical mold in multiple layers, removing the hollow sphere from the mold and the inverting half of it so that a two layer structure that conforms to the outer surface of the eye globe is created. A circular opening cut into the sphere aligns with the cornea and an almond-shaped opening opposite the circular cut corresponds with the opening of the eye lids and provide alignment features to support bonding of this structure to the inside of the eyelid module and the outside of the globe. This is described in more detail below and in the context of the full-face modules described in section 2.3.5.a.vi.

During Year 3**,** a new technique for the creation of the eye globe was developed. The previous technique for making the eye globe involved injecting a 3D printed mold with silicone. The resulting globe had noticeable parting lines that detracted from the realism of the simulator (see Figure 2). Similarly, the iris was cast from a 3D printed mold and lacked realism. Borrowing from the successful technique used in creating the conjunctiva, the new eye globe is made brushing successive thin layers onto a model of the eye globe. The model consists of a 3D printed hemispherical globe, with 2 recessed inserts. The first insert in the shape of the lens is inserted into the globe model. A deliberate gap, which is later filled in with silicone, supports the lens. The top of the lens insert provides a surface to which the iris can be mounted. The iris is created by brushing tinted silicone onto the back of the cornea insert, attaching it to the lens insert and allowing it to cure. The iris is the painted using silicone pigment to resemble a human iris, and then is again placed between the iris insert and lens insert. A layer of white tinted silicone is then brushed onto the globe model. While that is curing, the lens inset assembly is then inserted into the globe model. After curing, a layer of clear silicone is bushed over the entire assembly, capturing the iris in a by a narrow band around its circumference. Once cured, the silicone part is lifted off the model and the inserts are removed from the back, resulting in a smooth, hollow hemisphere of silicone with a precise air gap between the cornea and iris and a shelf to hold the lens. A base is then fabricated using the same technique. Silicone is brushed onto the base model and while still uncured, the globe part is placed on top of it. The entire assembly cures as one seamless part. Excess silicone around the base is trimmed as the final step. The result is a hollow silicone eye “globe”, with two puncture-able orifices for fluid access. A clear solution (like the PVA gel identified in Year 1) can be injected through the orifice filling the globe. This version of the globe was replicated and presented to cornea specialists at the 2014 USUHS Ocular Trauma Course for review and testing. They found that the cornea could be lacerated to create realistic wounds, and subsequently sutured to create a fluid-tight seal, similar to that of the real cornea (Figure 73).

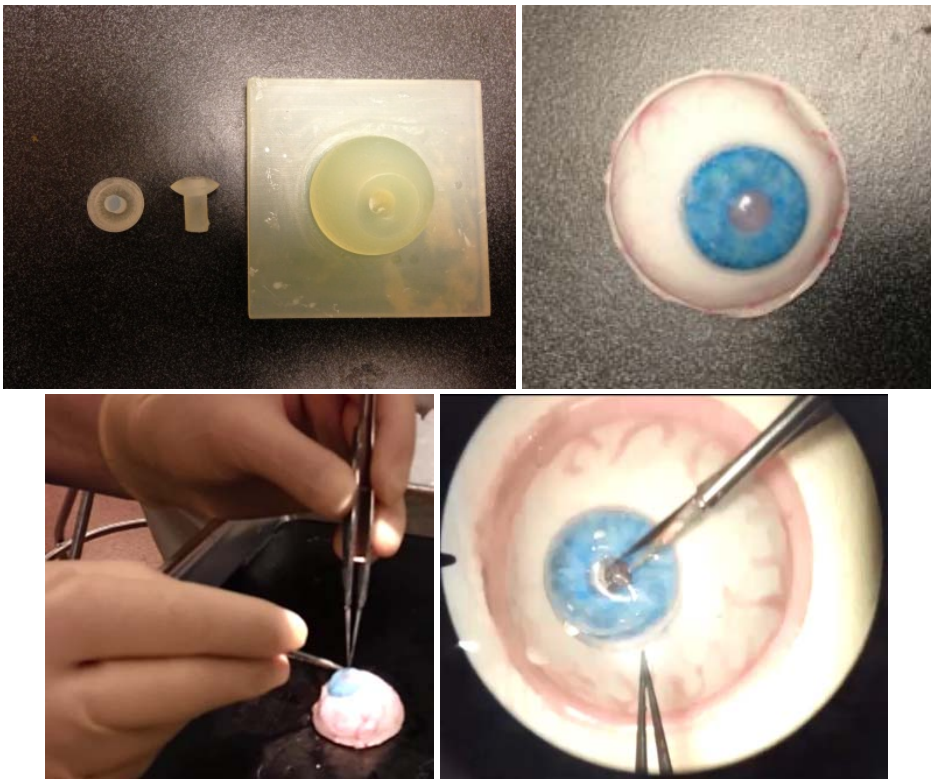

Figure 73: Globe mold with inserts for lens and cornea spaces; finished globe; view of cornea specialist suturing laceration; view of simulated cornea repair through (standard, non-AR) operating microscope.

In Year 4, a new method for creating the eye globe and conjunctiva was developed. The methods described above were time consuming and labor intensive and had a high rate of variability in the product. Rapid prototyped molds were developed that could cast a bi-cameral globe and conjunctiva in a single injection. The mold was made in 6 parts and was created first using the Object 260V 3D printer, and later by a Dimension Elite FDM 3D printer. Molds created using the Objet can prevent thin silicone structures from curing fully, leaving some gelatinous regions, due to the presence of miniscule amounts of support material which can cause cure inhibition. No suitable solvent was found to remove the support material. Alternative molds were printed using the FDM style printer. These molds do not inhibit silicone. The surfaces were polished to a high gloss in order to achieve clear, smooth castings. Especially careful design of the FDM parts allows us to have very tight control over the structure of the eye globes. The new corneas are 0.5mm in thickness at the center and gradually thicken to 1mm at the edge. The conjunctiva maintains a uniform 0.5mm thickness throughout. The sclera has a similarly controlled thickness. The result is an easily reproducible, accurate, bi-cameral globe with a conjunctiva bonded at the limbus (Figure 74). The lens, iris, and backing plate are fabricated separately and are assembled using silicone epoxy. The resulting assembly can be filled with two different materials—saline solution in the corneal chamber and PVA slime (or other viscus material) in the scleral chamber – a further improvement that matches real anatomy.

Figure 74: Year 4 eye globe mold, disassembled (left); Year 4 eye-globe and conjunctiva, detail (middle); eye globe and conjunctiva (right)

2.3.5.a.v. Neck motion system

At MMVR 2012 in the TATRC exhibit area, RDECOM had on display a remotely controlled lower limb hemorrhage simulator (prototype of the KForce (Fairfax, VA) Trauma FX MATT system), which included animatronic elements that allowed the legs to flail, making placement of tourniquets realistically difficult. Similarly, for the conscious patient in need of airway management (intubation, surgical airway), the obstructed airway, the gag reflex on intubation or the pain of making the incisions for cricothyroidotomy are likely to result in conscious head motion and make the process of performing the procedure more difficult.

During Q4, we began the early stages of adapting a neck motion mechanism technique that was partially developed for our COMETS trauma mannequin, to allow for both passive motion of the head and neck over the normal range of motion, and generate active motions to jerk the head from side to side. Figure 75 shows a preliminary design for a McKibben (air) muscle system, allowing for motion in pitch, yaw and roll.

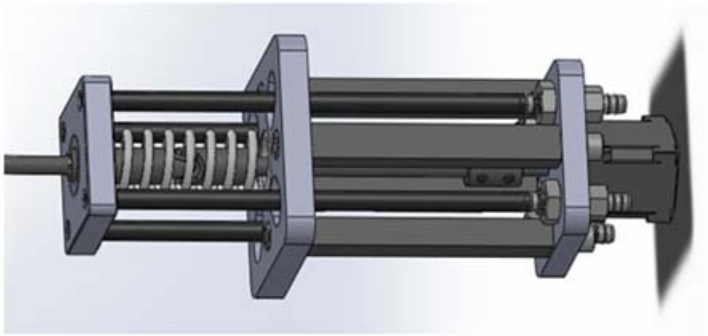

Figure 75: design for test platform for generating neck motions (pitch, pan, roll) using McKibben muscles.

Early in Q5, we performed initial testing of single elements of the pneumatic (McKibben) muscles that would generate neck motion and neck compliance and a solenoid valve controller for simultaneous control of all of the muscles. We also contacted Dr. Yong-Lae Park at the Harvard Wyss Institute (Harvard Biorobotics Laboratory) for advice on optimizing the air muscle design and developed a controller to test the motion capabilities of the current system.

Dr. Park's advice led to selection of an alternate, looser weave braid material that allows for a larger expansion limit of the muscle and thus a larger contraction. In addition, a closer fit between the internal diameter of the braid and the external diameter of the inner pneumatic tube prevents a buckling phenomenon that we observed in our early testing.

Figure 76 shows the initial solenoid valve assembly, a modular system that we employed previously and a basic user interface.

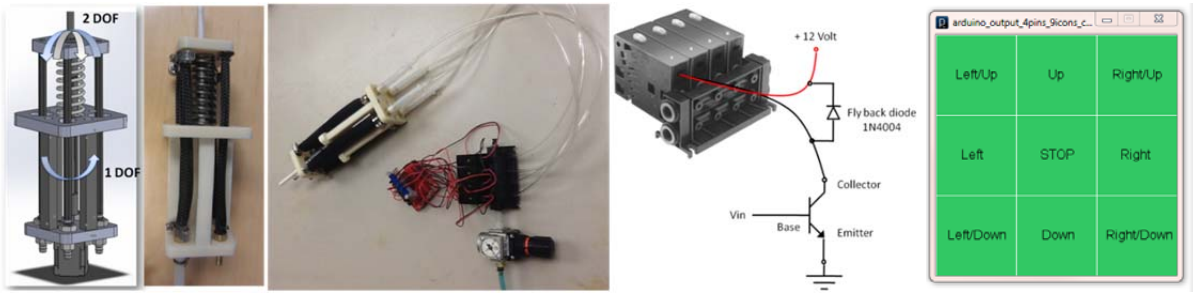

Figure 76: Neck motion test-bed design, initial structure fabrication, test system with enhanced muscle mesh, electrical control system, GUI for 8-direction motion control.

In Q6, we upgraded the pneumatic valving system to make use of one 3-way latching valve for each air muscle (supplies pressure or exhausts the air muscle), supplied from a common manifold. The air muscles exhaust into a common second manifold, which in turn is exhausted to atmospheric pressure through a series of relief valves, so that air the muscles are exhausted quickly or slowly depending on which relief valve is activated.

As described above in the context of the eye motion controller, earlier tests made use of an Arduino 2009 microcontroller. With four latching input valves and four latching exhaust valves in the pneumatic design, requiring two digital control lines each for a total of 16 digital outputs, we acquired an Arduino Mega microcontroller, which has 54 digital input/output connections. The neck motion control software was modified to make full use of the Mega's capabilities, and additional capabilities added for interfacing with the mannequin.

With this more capable system, we extended the basic function tests performed earlier to perform the same tests using the mannequin's power and pneumatic supplies, crucial in creating the mannequin-integrated system that was one of our primary goals.

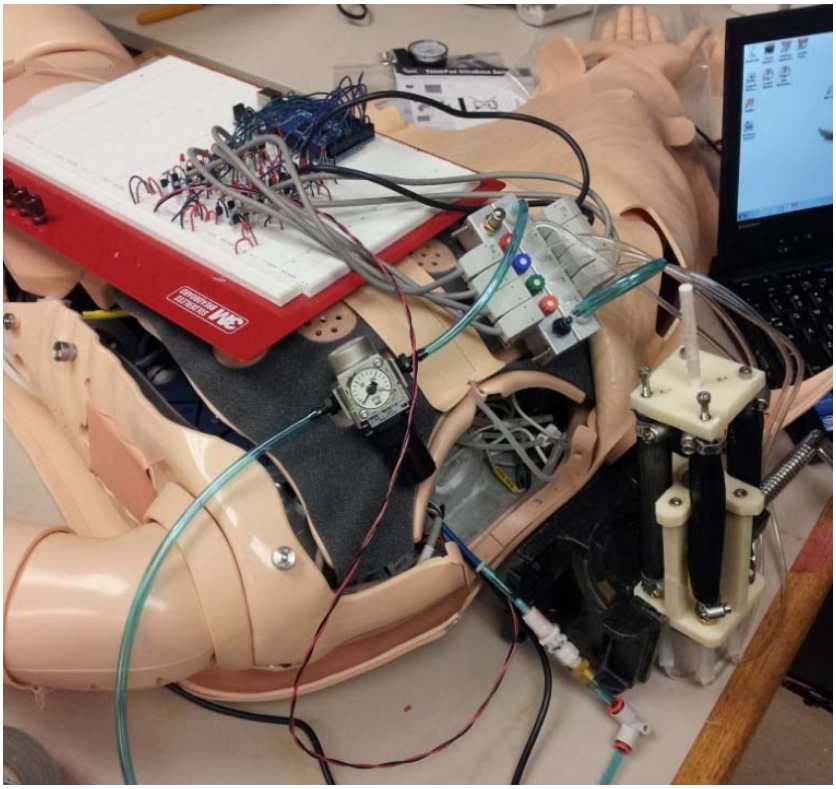

Figure 77: Pneumatic control system with fully enabled latching valves for four air muscles and four exhaust back-pressure valves. Arduino Mega and control circuitry in prototype form on mannequin's chest, valves and manifolds on right shoulder, pressure regulator on left shoulder, test platform for air muscles adjacent to neck-region.

We conducted investigations into optimizing the McKibben muscles for low-pressure supply air from the mannequin (rated at approximately 1 atmosphere by Laerdal), by sourcing thinner-wall elastic tubing for the muscles' internal bladders and changing the fitting diameters to minimize pinching that distorts the muscle end geometry. Additional details are described in section 2.3.9.a.

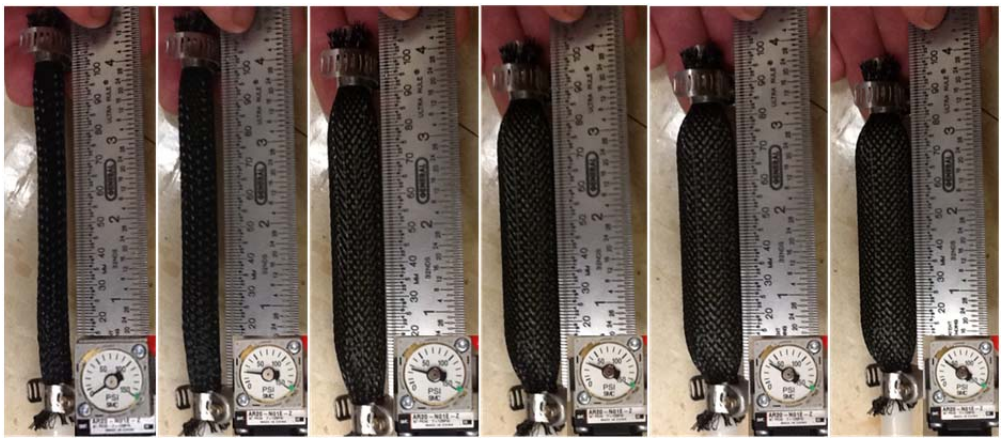

Figure 78: Air muscle images from Q5 showing pinching by hose clamps at muscle ends. Alternate design under development.

2.3.5.a.vi. CT-derived face, head cowl and airway development

The preceding description of soft-tissue component design and fabrication techniques was based primarily on the use of the original, life-cast version of the head form, useful for development and the teaching opportunity of the USUHS Ocular Trauma Course. This limited anatomy did not support development of trauma modules for the right eye or the remainder of the face and the neck, necessary for the facial trauma and cricothyroidotomy module installation. During the later months of Year 3, we completed extraction of the facial contours and soft tissue structures from the CT anatomy used to create the skeletal features described in this and earlier reports (not human use). This included the contours of the full airway, including oral, nasal, pharyngeal and laryngeal spaces. We created CAD models of all of these structures and partitioned them into relevant sections: a full-face module that replaces the single-eye module; a cowl that includes the top and back of the head skin, ears and neck; nasal airway; oral/pharyngeal/laryngeal airway. Certain soft tissue structures, especially in the neck, were difficult to segment from the CT anatomy, so anatomical references and advice of experts in these areas was called on to fill data gaps. This was also true of the mandible/maxilla due to extensive image artifacts in the original CT scans that generated image artifacts. Figure 79 shows preliminary models of the face, nasal airway and cowl, while the final version of these components is shown in Figure 80.

Figure 79: Soft tissue models derived from CT rather than life-cast sources. These models will serve as the basis for all future development of the system

In Year 4 a new skin was developed for the CT derived skull described above and neck in section 2.3.9.a. The skin takes the form of a front mask comprising the forehead, eyes, nose mouth, chin, and laryngeal area, and a cowl, comprising the skin of the back of the head, ears, and neck. The cowl is resident on the simulator and is not designed to be removable. It mates to the contours of the back of the skull and is fixed rigidly in place to a baseplate. The face mask is attached to the cowl via a zipper. The zipper attachment is secured to the face and head skin using a silicone epoxy. Early prototypes were held in place with suture, however this was labor intensive and has generally poorer results. Repeated use of the zipper mechanism at the 2015 Ocular Trauma Course shows it to be a durable and reliable solution.

The face mask is designed to be a consumable part, but it can be reused a number of times before being replaced. Unlike the previous head, the new head allows the use of both eyes. Additionally, the head

features an insert for performing cricothyroidotomies. This insert can be replaced an unlimited number of times without adversely affecting the face mask, and because of its smaller size and the simplicity of its fabrication, would be relatively inexpensive.

Figure 80: (clockwise) new face and cowl installed; new face and cowl partially disassembled; eye/eyelid detail; cowl disassembled.

The fabrication technique used in the new head design has evolved on similar lines to the new eye globes described in section 2.3.5.a.iv. The modular mold for the face mask was created using the Dimension FDM printer. This allowed for very high pressure injection of parts. Due to the complexity of the eyelid structures and the need for repeatable, high quality results, it was decided that the tarsus and canaliculous should be overmolded onto a freshly cast face part. The mold can be configured to allow the face (including the eyelid skin) to be cast in one step. Once cured, a modular insert can be removed, and a different module inserted. This module contains the features needed to cast the tarsus. The tarsal module also allows for the insertion of a sacrificial canalicular structure similar to the one described in section 2.3.5.a.iii. Nylon mesh is also installed prior to casting. Once installed, the tarsus is injected at

high pressure. The eye globes with attached conjunctiva (described above) are permanently affixed to the face. The eye globes attach to the eye-motion mechanism by three hose barbs. The result is a seamless, perfectly bonded tarsus attached to the back of the eyelid. This process simplifies and dramatically improves the quality of the result as compared to earlier techniques. This method greatly reduces the complexity of the fabrication process and is similar to the way in which the parts would be reproduced in industry.

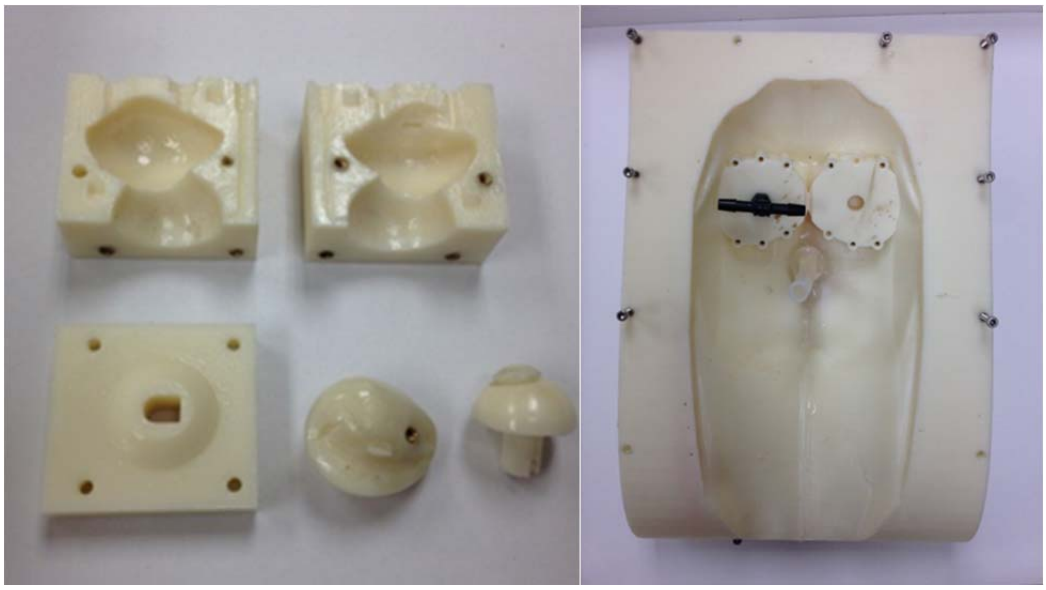

Figure 81: Rapid prototyped molds for face (left) and eye globe/conjunctiva (right)

A face was created in Year 4 to work in conjunction with the maxillofacial fractures described above. The simulated facial injuries created are intended to be are too extensive to allow for intubation nasally or orally, and are intended to steer the user towards determining that a cricothroidotomy is required (Figure 82).

In the final months of the program, a mounting frame was constructed to allow the same head/neck structure used for the mannequin-integrated version of the system to be mounted to the standalone simulator. It was demonstrated at IMSH 2015 in the TATRC Corral and can be seen in Figure 80 and Figure 82.

Figure 82: Severe facial trauma face

As we continued to solicit the input of our SMEs during the final stages of development, we recognized the need to provide a backing plate with appropriate eye attachment points so that the SMEs could evaluate a sample facemask without the entire system being present. To that end, we designed a hard plastic backing plate for the facemask. The backing plate allows a user to perform a simulated eyelid repair on a facemask as they would in the simulator. The backing plate (shown below) inspired Dr. Colyer from USUHS to envision a stand-alone version of the ocular trauma simulator that consists only of a facemask and backing plate for use in a classroom setting. The lack of instrument tracking and stand would severely limit the functionality of the simulator but could be a practical solution for budget constrained schools/training programs.

Figure 83: Stand-alone facemask, assembled (left); disassembled (right).

2.3.5.b. Start developing augmented reality training guidance system for enhanced eye trauma simulator.

While not originally scheduled for commencement until a few months into the program, efforts towards creating AR components began nearly from the beginning of the program.

2.3.5.b.i. Hardware Development

An early development was repurposing one of the Model 800 6DOF sensors for use in providing position/orientation data for a virtual reality head mounted display (VR HMD), as a concept example to consider how such a system could be employed.

Figure 84: commercial VR glasses with mounting frame for magnetic position tracker and model 800 sensor from proof-of-principle simulator (larger sensor appropriate for this use vs. attachment to surgical instruments).

Early discussions with Dr. Mazzoli identified some of the surgical microscopes typically in use by Army ophthalmologists stationed in Kandahar, and contact was made with Scan Optics Pty Ltd (Adelaide, Australia). This firm uses Olympus optics that are modified with additional optical and structural features, a path that we have paralleled. Scan Optics was able to provide us with structural CAD models of the microscope head that they modify, which we are using in our more recent design processes.

Early efforts to develop our own binocular microscope with integrated displays lead to one of the projects of one of our graduate student interns, who initially created a functional microscope using binoculars and inexpensive, repurposed optics (Figure 85).

The second phase of this work involved the acquisition of a standard, trinocular microscope head (Amscope ZM245NT, Irvine, CA), which was partially disassembled and additional beam splitters and lenses were installed to investigate whether a small LCD display such as that on an iPod could be used to present useful data through the microscope eyepiece view (Figure 85). At the time, our understanding of microscope optics was developing, and the display was over-magnified, showing very large, distinct pixels through the view rather than an image of useful resolution.

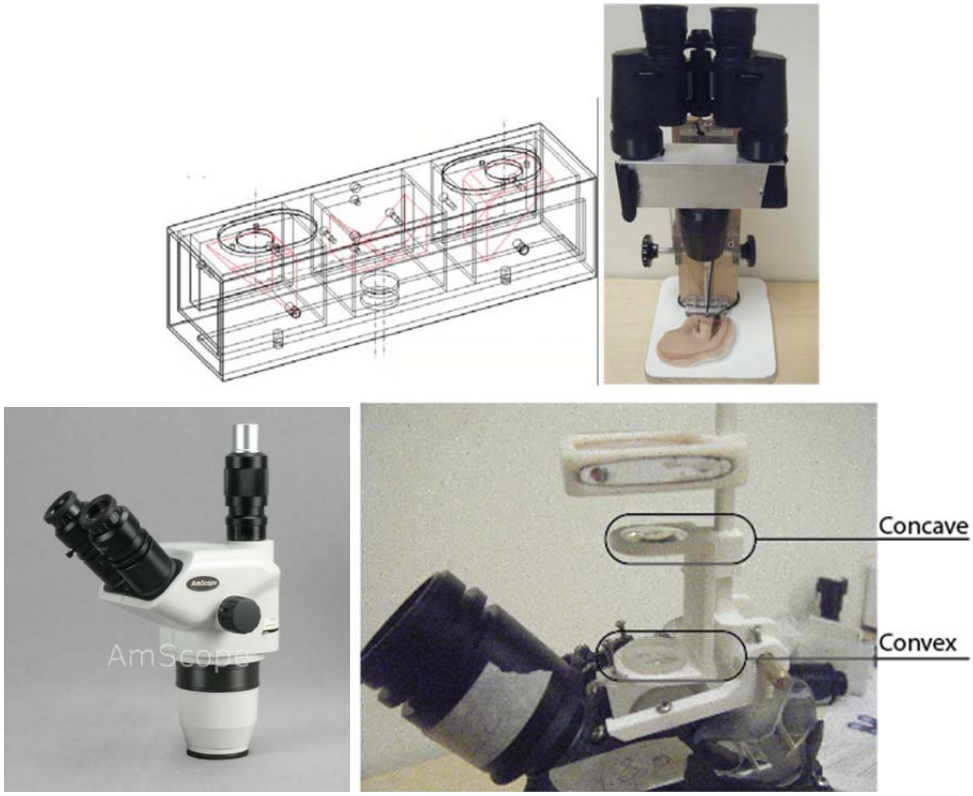

Figure 85: Evolution of augmented reality microscope optics. Schematic of binocular prism array; assembled low-cost test platform; commercial trinocular microscope head; initial modification to eyepiece prism array to include display, optics, beamsplitter.

Subsequent to these developments, during Q4, detailed investigation into optical design, including use of the thin-lens approximation using principal ray analysis through a compound lens arrangement, lead to the next design, which used a 25.5mm width LCD display borrowed from a separate project for evaluation purposes. We made use of the parametric sketching tools available in the Solidworks (DS Solidworks Corp, Waltham, MA) CAD package, which allows the definition of geometric constraints and physical dimensions. This served as a graphical calculation tool that we used to determine lens and mirror location, given LCD size, desired output image size and commercially available lens focal lengths and diameters (Figure 86). Figure 87 shows a test-bed arrangement of lenses and beam splitters, resulting in the two images shown alongside. They show the raw view through the microscope (a Laerdal mannequin eye, showing reflected LEDs from microscope ring light), and combined image of eye with an overlaid large blue iris/black pupil image. This demonstrated successful demagnification of the LCD display, so that the full resolution of the LCD is available for information display.

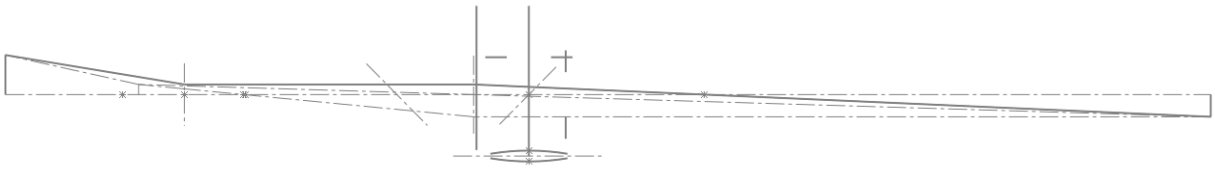

Figure 86: Thin lens approximation implemented in graphical calculator using sketching and constraint tools of Solidworks CAD program. Principle rays pass through lens focal points, creating real and virtual images. LCD module at left; concave lens straightens converging light; concave lens focuses rays to eyepiece lens location at right. Also shown is microscope objective lens (bottom) and beam splitter (diagonal at center) This schematic is equivalent to the test system shown below, with all reflecting elements removed to create an axially aligned system (reflections do not affect the refraction and image size elements of the model.

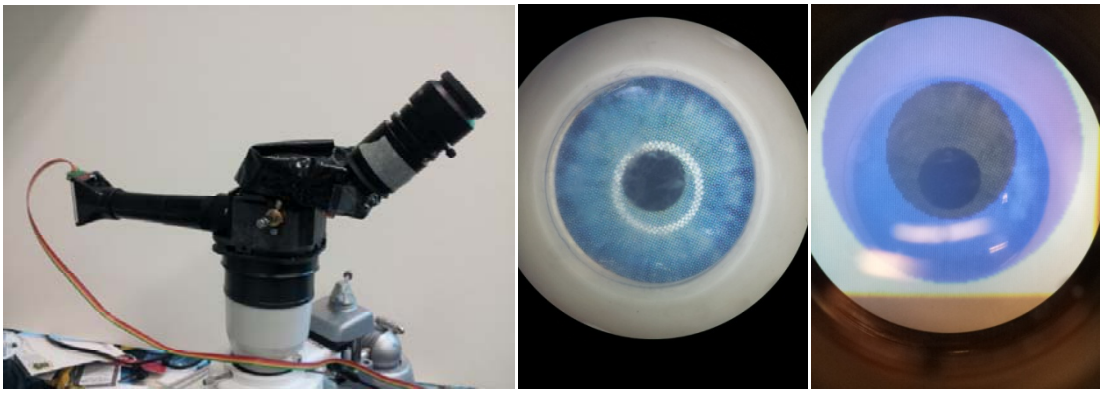

Figure 87: (left) initial prototype of optics testbed based on thin lens calculation method. (center) Plain image through microscope. (right) Overlaid image from LCD combined with center image.

During year 2 we further developed the augmented reality surgical microscope system, combining a high brightness LCD monitor and optics into a commercial stereo microscope, to fuse the image of the surgical field through the microscope with graphical overlays generated by the LCD. Using a more complex, 3D graphical design tool (Figure 88) that was derived from the earlier version, we created a design for a relatively compact, complete AR microscope system (Figure 89). Further progress on this element of the work is described in sections 2.3.7.c and 2.3.12.b.

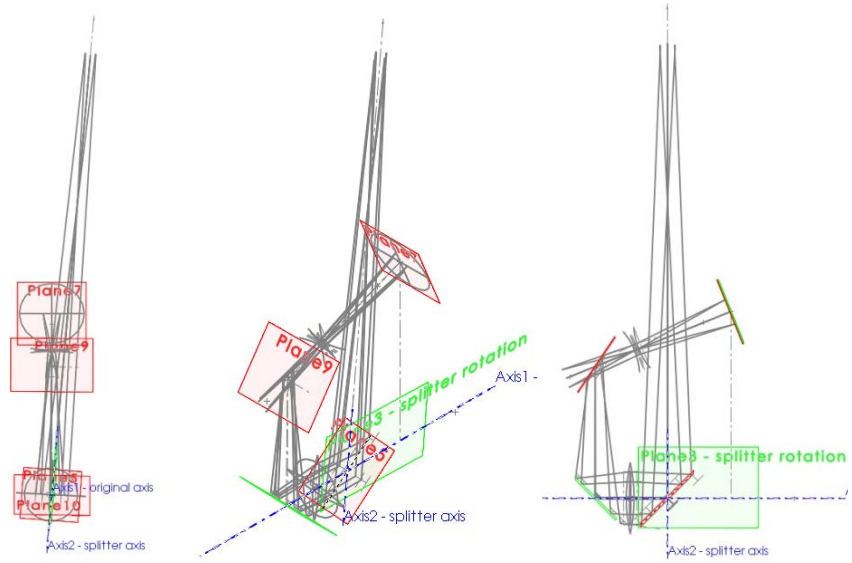

Figure 88: Front, isometric and side views of new 3D optical path calculator.

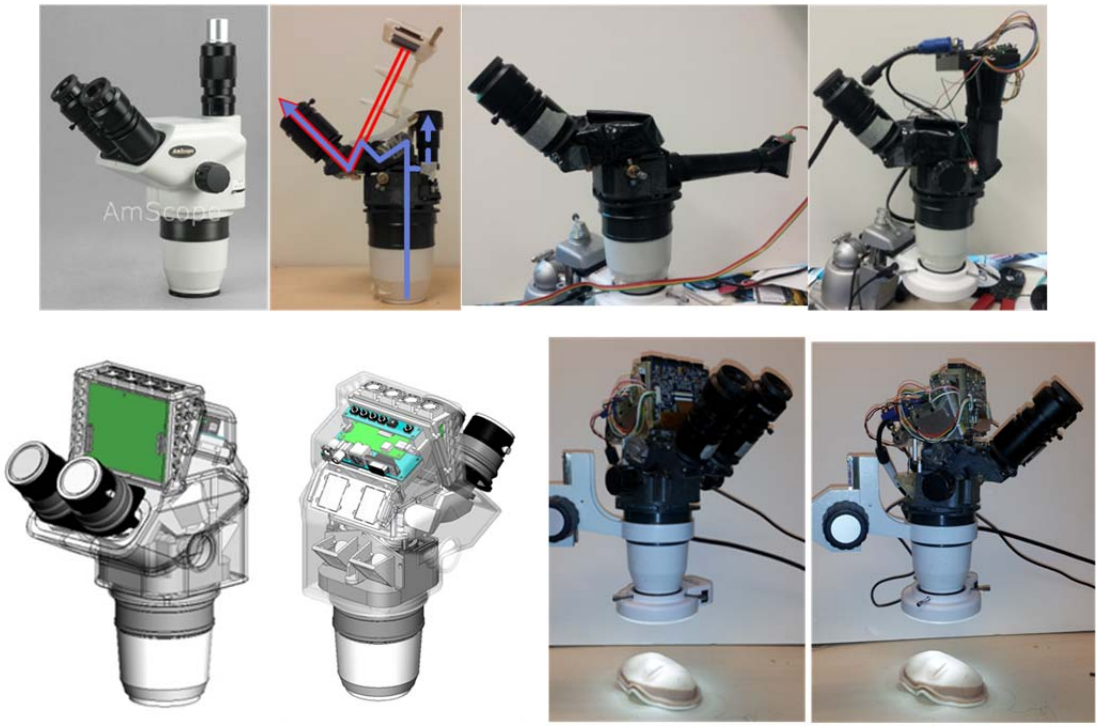

Figure 89: Sequential development of AR microscope during year 2. COTS trinocular microscope head. Early external display test. Initial inline test of small LCD display. Integration of high brightness LCD during Q5. CAD models of microscope with more compactly integrated display and optics. Internal structure of AR microscope awaiting external shell fabrication.

Early in the program we acquired and began testing the Microsoft (Redmond, WA) Kinect system, to examine its capabilities and applicability for tracking gestures. As shown below, we can recognize the head form and the user's hand in the depth map, however the minimum distance range of the system

(intended for body tracking for video game interactions) is somewhat larger than would be desirable – the Kinect would need to be mounted at considerable height above the mannequin.

In addition to the Kinect, we acquired a nano-projector video projector (Qumi Q5, Vivitek Corp.), with high brightness and resolution. This system was tested to investigate color schemes compatible with the flesh-tones of the mannequin face and the utility of projecting content onto and around the head. In addition, we tested the Kinect by coupling its imaging capabilities with virtual buttons projected around the face successfully.

A little-known property of the Kinect is that it can be used through mirrors – the projected infrared field and the field of view of the IR camera can be reflected. We took advantage of this property by adding a first surface mirror into the structural frame, positioned so that the Kinect field and that of the projector overlap the face of the head form and the area around it. This allowed us to reduce the necessary height of the system above the face by at least 40%. As shown in Figure 91, we installed the web camera to overlap the same area so that we could effectively capture surgical instrument and hand motions of relevance.

Further development of the AR systems is described in section 2.3.7.

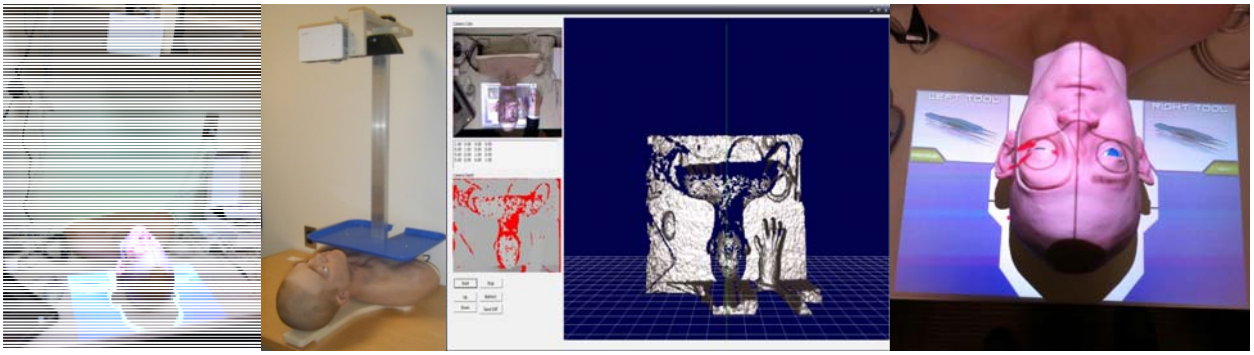

Figure 90: (left) Kinect representation of head form with visual image, depth map and rendering. (right) test pattern projected onto head-form face with addition of interaction zones for instruments (equivalent to tray location), graphical representation of bleeding from zone of left eye.

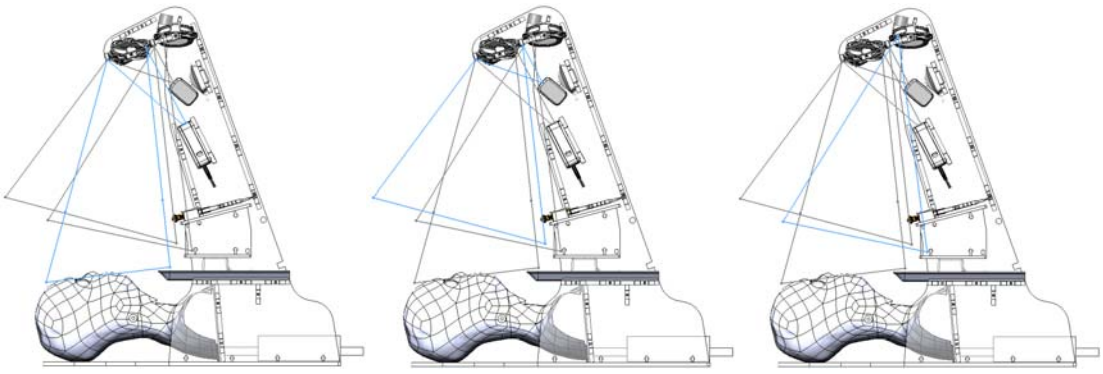

Figure 91: Fields of view of projection/imaging components. In blue are: (left) video projection, (center) Kinect motion tracking, (right) web-cam. A first-surface mirror mounted near the top of the system allows for reduced overall height; minimum focal distance for Kinect and projector would otherwise add 12" or more vertically.

2.3.5.b.ii. Content & Architecture Development

The content elements developed for the Phase I simulator (improved proof-of-concept system based on initial feedback), including user tracking, data collection, results and teaching content presentation, served as the basis for the broader development of the content presented through the AR components (as well as normal video displays and potentially tablets or other portable just-in-time content presentation platforms). In support of this effort, we developed our content materials with consideration of SCORM compliance where relevant/possible, and platform independence using templates such at HTML5 and cascading stylesheets to manage the details of presentation on diverse display technologies. A typical rendering of an early node in a scenario's content is shown below (dynamically generated based on the size, nature of browser).

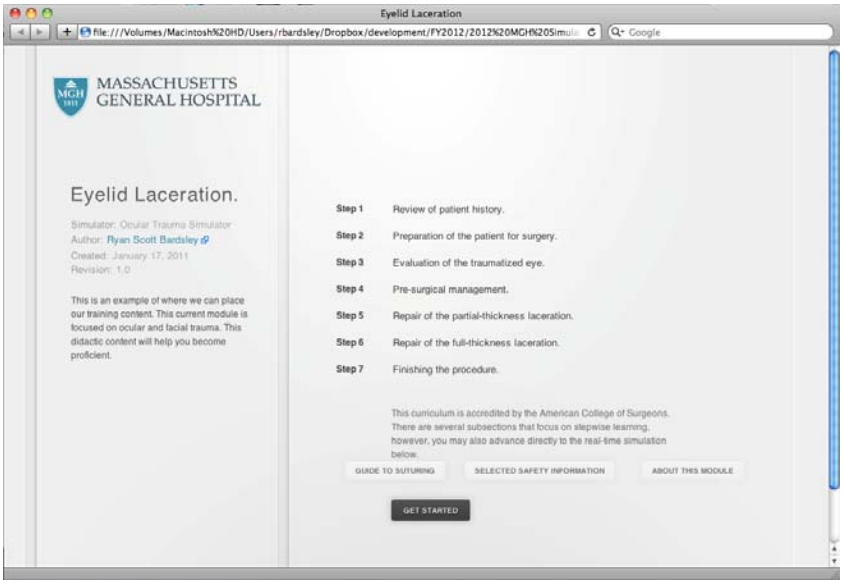

Figure 92: Rendered version of scenario content using standard web browser.

Content prepared in a common, modular format and the interactivity enabled by the multiple sensor, user interface and display options available in our system, enable a rich capability to present materials to users in forms appropriate to their skill levels and training and to their prior training sessions on the simulator. The modular format provides for standardized templates that instructors can use to generate new content, and tailor how it is presented based on the common interface to all of the sensor and display capabilities of the simulator.

As described earlier as an element of the Phase I system (section 2.3.2.b.vi), the surgical gesture detection system that we developed is intended to identify, almost in real-time, the meaningful elements of surgical gestures, to detect whether a trainee is following the expert-defined sequence of elements of a procedure. When event-level data is analyzed, this substantially reduces the computational burden of real-time measurement and evaluation, as compared with continuous path analysis at all times. It enables identification of instances where more detailed analysis of the instrument path(s) is necessary, as it is expected to be for some elements of a scenario.

To develop the system, we identified a hierarchical taxonomy to describe relationships between raw and derived data (e.g. position, velocity), events (e.g. threshold or ROI crossings), and in year 1 began to create tools to perform the automated segmentation. Early results and progress in this area were described in more detail in one of our IMIASH 2012 papers [Ottensmeyer et al., 2012], attached in section 7.4 of the Appendix, Attached Publications.

During Q4, we collected performance data at the USUHS trials, providing baseline data to begin to compare experts and novices. The sample images in Figure 93, from different subjects performing different parts of the scenario, are illustrative of the different phases of the analysis and show differences between experts and novices.

The first plots depict the raw, unprocessed tool path data for two USUHS participants, over a two minute segment of an eyelid laceration repair simulation. The top pair of figures depicts data from an advanced plastics specialist, while the bottom two figures are generated by a first or second year resident. Each different trace color represents a different tool used. The upper figure pair clearly presents a more compact and less dispersed set of movements in contrast to the lower figure pair. This behavior appears to be consistent across surgical specialties; our earlier research in laparoscopy simulation showed very similar gross characteristics [Stylopoulos et al, 2004].

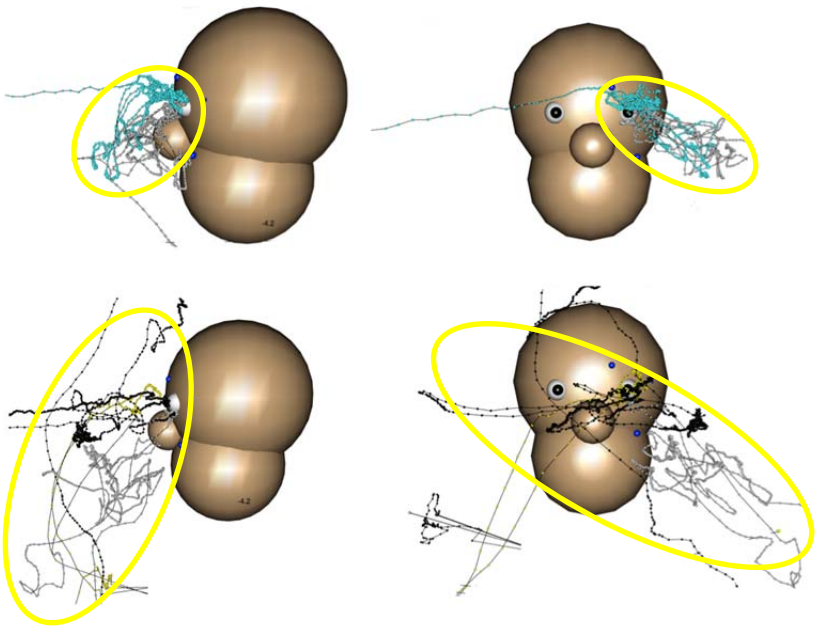

Figure 93: Raw instrument trajectory data over 2 minutes of lid laceration repair. (Top) Advanced plastics specialist using 0.5mm Castroviejo suturing forceps (grey) and Barraquer needle holder (teal), with compact motion envelope. (Bottom) Early year resident using 0.2mm Castroviejo forceps (black), 0.5mm Castroviejo forceps (grey) and Vannas scissors. Blue points above and below "patient's" left eye are calibration points for registration of physical model to position tracker.

Figure 94 shows automated ROI crossing information (color coded bands – green is near eye, blue is near instrument tray) and instrument manipulation (scissor actions – raw scissor motion data in second plot) to identify cutting actions near to the eye, combined with manual event recordings (black

triangles), representative of completion of a series of knot tying, through the removal of excess suture material by cutting. This trace represents 18 minutes of events, dramatically reducing the amount of data that needs to be presented to represent performance, and converting the raw data into surgically meaningful information.

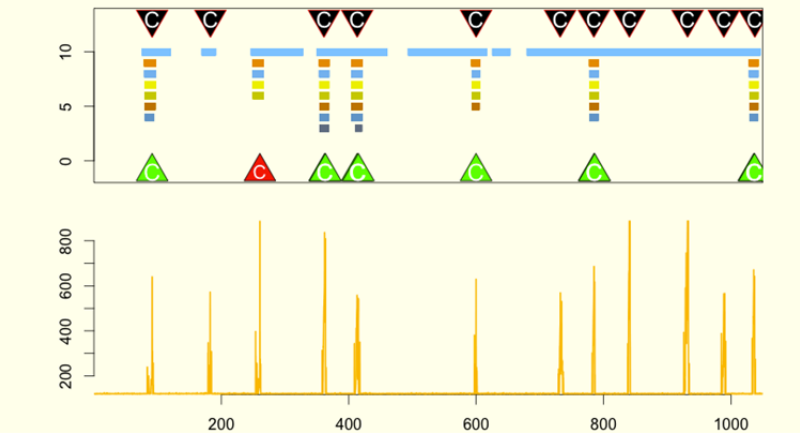

Figure 94: Upper plot - automatically and manually detected events: color bars show entry, residence time and departure from geometric Regions of Interest; green triangles show scissor actions within RoIs close to eye lids; red triangle shows two cuts in rapid succession; for comparison, black triangles record manual entries of any cutting action;. Lower plot – raw data for scissor closure action.

During Q5 we made progress in the gesture-driven sequencing of the instructional and feedback materials presented to participants. Rather than requiring that a user interact primarily with keyboard or mouse to advance the scenario, the various sensing elements provide the system with state and gesture information. For example, when setting up the system, it detects whether the proper instrument is connected, provides instructions for how to do so (training the user in how to use the system), and advances automatically when that step is complete. Later in the scenario, the system updates the instructional display tracking the placement of sutures, for example, advancing when it detects cutting corresponding with the trimming of sutures and replacement of the scissors in the instrument tray (Figure 95).

Figure 95: Examples of gesture driven scenario content. Simulator preparation instructions driven by correct sensor/instrument attachment. In-scenario feedback on completion of series of sutures.

2.3.5.b.iii. Developer interface improvements

In Q5, the developer interface, used for data collection and export of the data to the analysis tools continued to evolve. Features added were horizontal scrolling through the full data set and indications of the location of the current view is relative to the entire scenario, zoom functions, display of the details of manually entered event keystrokes, ability to change the rate of playback, from 4x normal to 1/64x normal speed, and selection tools to export only desired subsets of the acquired data.

The display of the virtual scene, showing graphical models of the instruments and the mannequin head were decluttered, showing only connected instruments rather than the whole available suite.

We added management tools for the AVI video files that correspond with the collected instrument data. We created a new software library that can access AVI streams in input and output, choose the proper compressor in order to save the AVI stream in the best format to optimize hard drive space consumption and the CPU overhead.

2.3.5.b.iv. Quantitative scoring and data analysis

In Q5, the list of quantitative overall performance metrics included:

- Total Activity within ROI
- Total Duration within ROI
- Longest Run within ROI
- Total Transitions between ROIs
- ROI Containment
- Adaptive ROIs measures

as well as the beginning of a method for examining hand tremor.

Additional details on the AR system are covered in the section 2.3.7.c.

2.3.6. "Month 8" - Design of mandibular/maxillary trauma modules, upper airway model for use of airway devices, new cricothyroidotomy portal.

2.3.6.a. Mandible, maxilla and facial fracture modules

During Q6, discussion with Dr. Troulis concerned the types of facial fractures that would be most relevant in the context of facial trauma and complications that would necessitate surgical cricothyroidotomy. She recommended that bilateral mandibular fracture can allow the lower jaw to collapse, blocking the oral airway. We also discussed typical responses to jaw fracture, including wiring of the lower to the upper jaw to stabilize the bones, which in turn helps to reduce or stop ongoing oral hemorrhage.

During Year 3, based on these recommendations and statistics showing frequency of different fracture zones, we designed the jaw and facial components of the full skull of the head form, including a series of disconnectable components to simulate fractures. The components would need to have realistic behavior when palpated through the skin, and have the capability of being reconfigured to present alternate fractures without complete removal and replacement of the jaw or face.

For the jaw, three levels of separation are available: the fully healthy mandible, when all components are linked together; fractures to the angle and the body, which have 33% and 20% frequency among all jaw fractures, and a version in which a bone segment has been lost from the jaw.

Figure 96: Preliminary segmentation of mandible to support alternate fracture patterns within single jaw element. Lower teeth not shown – to be mounted separately together with oral soft tissues.

Similar considerations were used to define the facial fractures: an outer "mask" was separated from the rest of the skull and subdivided. Two face bone masks were designed, one completely healthy and another with a zygomatic complex fracture (tripod fracture – 40%) and with a LeFort I (15%), which is a completely separation of the palate from the rest of the skull. These fractures as well as the ones realized for the mandible are the most common.

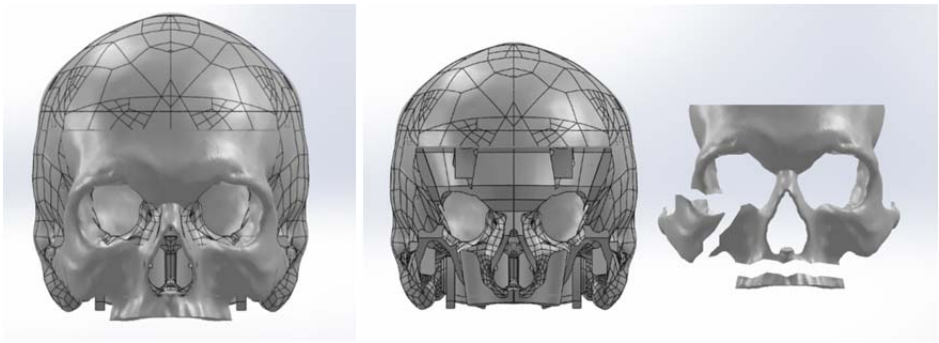

Figure 97: Preliminary segmentation of maxilla and face to support alternate fracture patterns within single skull element. Upper teeth not shown – to be mounted separately together with oral soft tissues.

At the end of the year, the details of the linking mechanisms between the bone segments were completed.

Substantial work on this topic was undertaken during Year 4. The designs for facial fracture components that were shown at the 24 June 2014 IPR meeting, with adjustability to customize fixed vs. fractured bone elements, were fabricated. Mandibular, mid-face and zygomatic fracture components are available. These were not designed for surgical repair scenarios, but rather to provide realism to facial trauma scenarios for first responders, so that mobile bone segments are palpable underneath the skin surface. Future funding that has been awarded from CIMIT, which will commence after the conclusion of this program, will include further developments for surgical repair of facial fractures.

As described, the skull of the system was divided into a series of bone segments that can individually be locked in place, or allowed to "float", representing facial fractures. The floating segments are held loosely in place with elastic links embedded between mandible segments and between maxillary/mid-face components representing Le Fort fractures. The variety of bone segments available allows for a wide range of potential fracture patterns to be presented to the first responder, including those that will complicate airway management. Further, for injuries that may result in complete loss of bone segments, individual jaw segments can be removed.

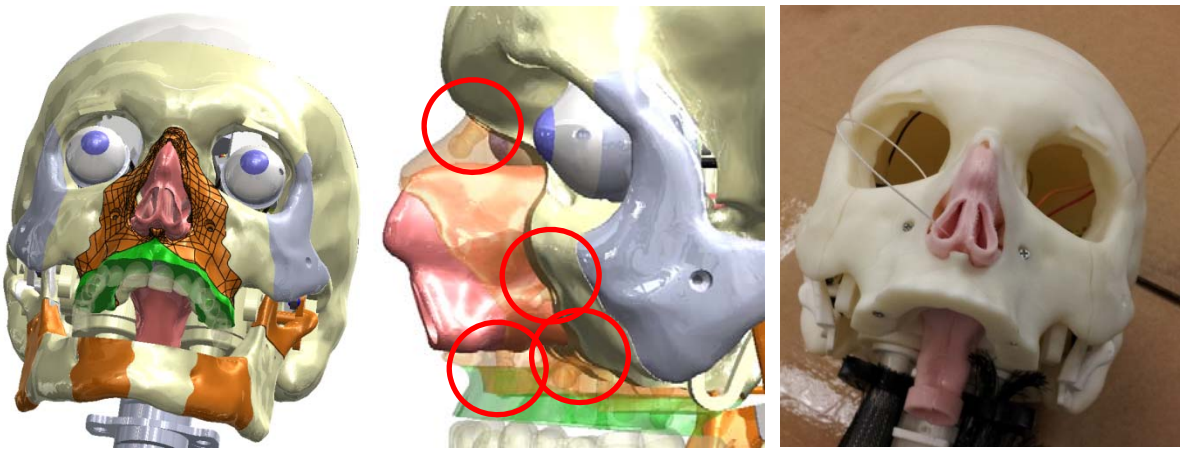

Figure 98: (Left) Model showing separable bone components. (Middle) Locations of elastic links between main skull and Le Fort fracture segments. Screw hole for locking zygomatic fracture component is visible in the grey segment. (Right) Fracturable skull with nasal airway segment showing stent passing through lacrimal sac and naso-lacrimal duct, and screws holding Le Fort fracture components in place in locked configuration.

As the CT data set available had significant artifact in the mandibular and maxillary regions due to the presence of metal fillings, we adapted a free, publicly available model of human teeth and created our own adapter structure to mount them to the known structures. In addition, soft tissues were sculpted, based on the existing tissue and bone contours. The sculpted positive, for creation of molds for these components, is shown in Figure 99, including highly detailed models of the teeth and gums. Corresponding elements for the oral airway are described in section 2.3.6.d.

Figure 99: Clay mold for gum and inner oral cavity, showing segments of teeth 3D printed from downloaded models and skull and mandible sections based on our CT-derived models

2.3.6.b. Jaw motion and head yaw motion mechanisms.

During Year 3, we investigated normal human jaw motion to ensure that for an uninjured jaw, the available range of motion is correct, so that intubation or similar procedures would be possible. According to Posselt's Diagram [Koolstra, 2002], the movement of the jaw can be described as pure rotation for the first 10° and a rotation-translation for the next 20°. To achieve this motion, a spherical pin slides in a curved track that allows the jaw to both slide and pivot. An open frame captures a second pin on the jaw to limit the range of motion to the normal human range (Figure 100).

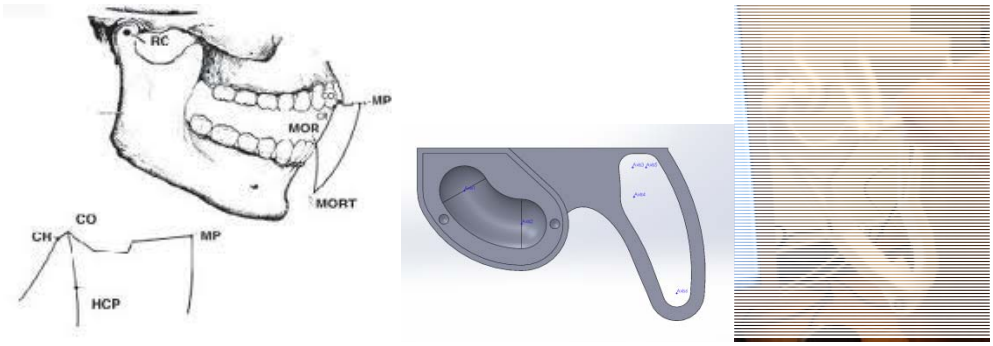

Figure 100: Posselt diagram showing the range of motion of the human jaw; design of motion restriction frame; initial mechanical prototype of jaw structure.

To generate motion controlled by the system itself, a servo and transmission system was designed and constructed. A single, continuous rotation servo drives a belt and slip clutch that allows the jaw to be opened and closed to the mechanical limits without needing precise position control of the servo; a limit switch detects when the jaw is fully closed (Figure 101). The elasticity of the facial/oral silicone components aids in providing restoring force to the open jaw to return it to a nearly closed state.

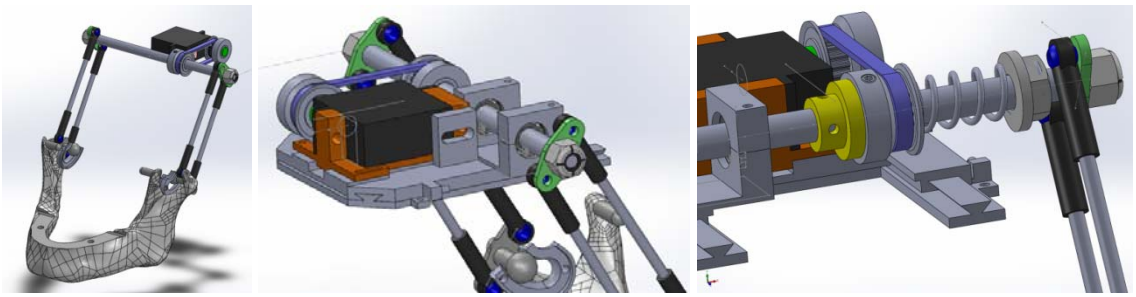

Figure 101: Jaw mechanism showing pivot action acting through parallel links, leaving the oral space and access to the pharynx open; slider carriage which supports the forward/back motion of the jaw coupled with the angular open/close action; clutch mechanism to allow for manual back-driving of the jaw regardless of the position set by the mechanism.

In addition to jaw motion and the pneumatic control of the pitch and roll action of the neck, the head needs to be able to rotate about the neck axis (left/right "no" action). A stepper-motor and bevel gear mechanism was designed to mate with a central flexible shaft that runs along the length of the neck. The shaft is anchored at the base of the neck, and the motor causes the top of the neck to rotate with respect to the shaft. A pair of limit switches was included to detect when the head reaches the left or right limits of motion and a potentiometer mounted to the flexible shaft detects relative motion between the shaft and the skull.

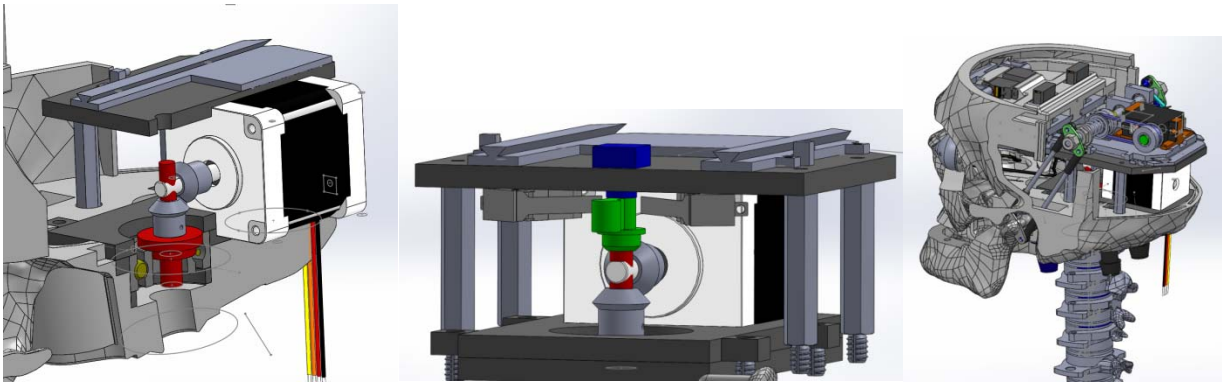

Figure 102: Head motion stepper motor and bevel gear linking motor shaft (model shaft is longer than real shaft) and upper fitting of flexible shaft (red); positioning of limit switches and potentiometer relative to flexible shaft axis; partial cut-away view of jaw motion and head motion mechanisms, also showing servos for blinking and proptosis motion.

Simplified versions of the main components of these motion elements were fabricated and assembled to test the concepts, verify whether the actuators selected were strong enough, and tune the slip-clutch stiffness to allow for motor controlled jaw motion with manual back-drivability in the mechanism (Figure 103). The final version is shown below in Figure 152 and was integrated into the head-neck form that is compatible with both the stand-alone system and mannequin mounting.

Figure 103: Test assembly of jaw (omitting fracture elements), head base with air muscle mounting sites and flexible shaft seat, full mechanism mounted for testing.

2.3.6.c. Cricothyroidotomy sensing system

Cricothyroidotomy is a standard technique for establishing an airway when the mouth and nose are too heavily obstructed or if the upper airway is swollen to the point of closing the airway. The technique involves making an incision through the skin covering the larynx, followed by cutting through the cricothyroid membrane and finally insertion of a breathing tube through the openings in the skin.

Ideally, the simulator should (a) respond appropriately to any intervention that would be successful on a real casualty, and (b) detect when a trainee makes an error and provide the capability for identifying how that error was made to enable corrective instructions to be given. To support this, we prototyped a series of incision detection and localization sensors.

The first series created low resistance path in a grid or serpentine pattern embedded in a silicone matrix. The conductor links a ground-terminal in the sensing electronic circuit and a digital input terminal with a pull-up resistor enabled on our data acquisition system. During the pre-incision state, the connection to ground through the sensor provides a low voltage signal to the digital input terminal. When cut, the digital input loses continuity to ground, and the pull-up resistor raises the input value observed by the digital input to the high state. The images show the low resistance of the assembled system, consisting of a sandwich of silicone layers enclosing a serpentine pattern of conductive silver ink. For small deformations, this system worked well, however larger deformations, such as those that would be generated by grasping and lifting the tissue to position it for cutting caused the silver ink to fracture, breaking contact along the path even after stretching is removed.

Figure 104: measuring resistance of serpentine conductive ink trace embedded within silicone. Silicone stretches as normal skin, but conductivity is lost as ink trace is fractured.

The next iteration examined conductive textile threads (typically cotton thread with metal filaments woven into the twist) and very fine steel wool, extracting fibers from the wool to arrange within the silicone. Such materials did not break upon stretching, however cutting through the silicone/steel wool/fiber was very distinctive, producing unrealistic tactile feedback.

Figure 105: Conductive thread and unwoven fiber; fibers embedded in silicone for testing.

We explored the use of carbon-black impregnated rubber materials, including a one-part thermo-setting RTV rubber and conductor-coated sponge neoprene. The conductive RTV was found to have highly inconsistent conductivity between the conductive rubber bulk of the material and the electrical contacts of the data acquisition system. The conductor-coated neoprene was embedded within silicone to protect the conductive layer from external abrasion and inadvertent contact. Initially it provided the desired conductive path, however after a variable, but short time period, resistance rose until the material behaved as an insulator, which was interpreted by the system as a user cutting through the conductive path and completing an incision. We believe that the silicone setting process allows liquid precursors to soak into the conductive layer, causing it to swell and driving the conductive particles apart from each other. Without a continuous path for electricity to flow, conductivity is lost.

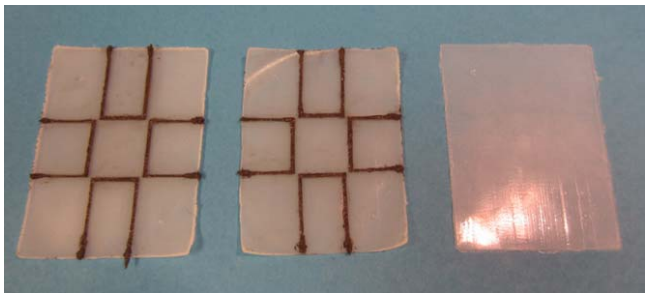

Figure 106:Test sample for evaluating conductive RTV silicone impregnated with conductive particles.

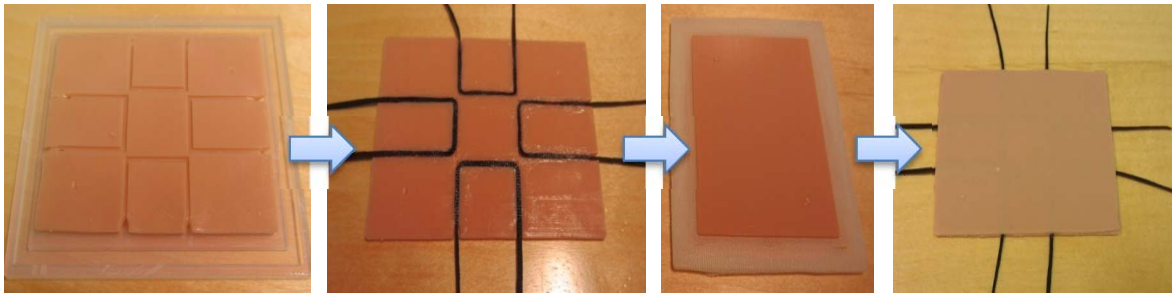

Figure 107: Test sample for laying strips of surface-conductive neoprene into silicone skin analog.

During Q4, additional study of conductive polymers, sheets and other materials allowed us to identify a conductive adhesive tape from 3M, which has a random array of conductive fibers embedded in a polymer tape with a pressure sensitive adhesive on both sides. We experimented with a series of different arrangements of the tape as substitutes for the earlier conductive materials, and showed promising results. The tape allows for relatively reliable contact to the data acquisition wiring, and is much easier to install into an anatomical assembly of simulated skin (epidermis, dermis, hypodermis) and subcutaneous fat. Figure 108 shows the functional layers (including a small reservoir of blood simulant for effect when incising), a demonstration of the system as applied to a commercial airway, and a microprocessor board sensing the location of the incision made in the layered assembly. The thin tape parts easily when cut with a scalpel, so that the silicone and other layers of the structure generate the majority of the tactile feedback experienced by the trainee.

In Q5, we continued development of the cricothyroidotomy primary incision detection sensor. The analog system is similar in concept to resistive touch-screen technology. Three conductive layers are insulated from each other. The upper and middle “drive” layers can have voltage gradients applied across them in orthogonal directions – one in the x and one in the y direction – or can be placed in a high impedance state so that no current passes through it. The lowest, the detection layer, is connected to an analog input channel. When the conductive metal blade of a scalpel cuts through the 3-layers, the blade creates a path from both drive layers to the detection layer. Rapidly alternating which of the drive layers is active allows the detection layer to feed an analog voltage that is proportional to the distance across the drive layer to the microcontroller. In this manner, a nearly continuous output of cut position coordinates can be fed to the controller. The drive circuitry is shown in Figure 109.

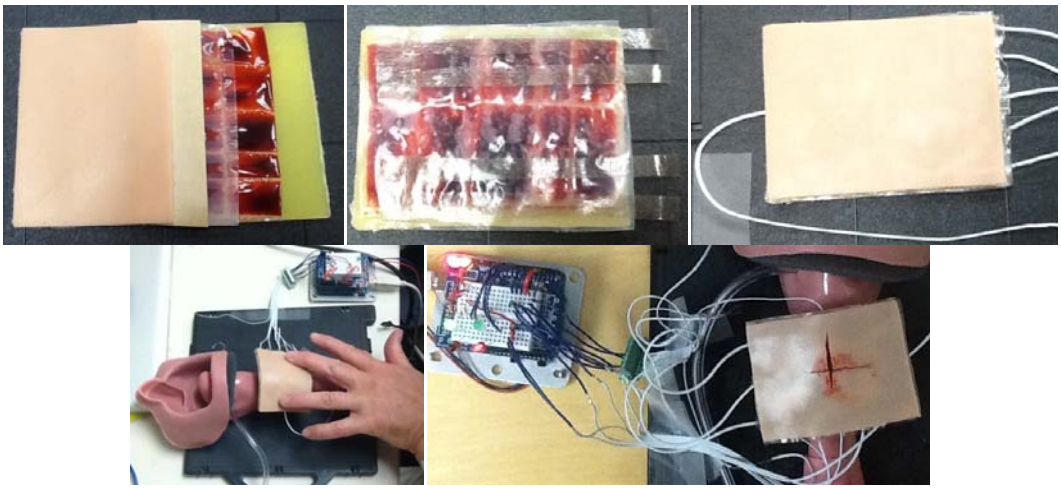

Figure 108: (top) test layers of cricothyroidotomy portal concept – skin, sensor layer, blood simulant reservoir, subcutaneous fat; partially assembled test block, with conductive tape strips aligned perpendicular to correct cutting direction; assembled cut sensor. (bottom) Example placement of sensor/cric block on commercial airway model; microcontroller testing shows illuminated LEDs following cutting through sensor elements.

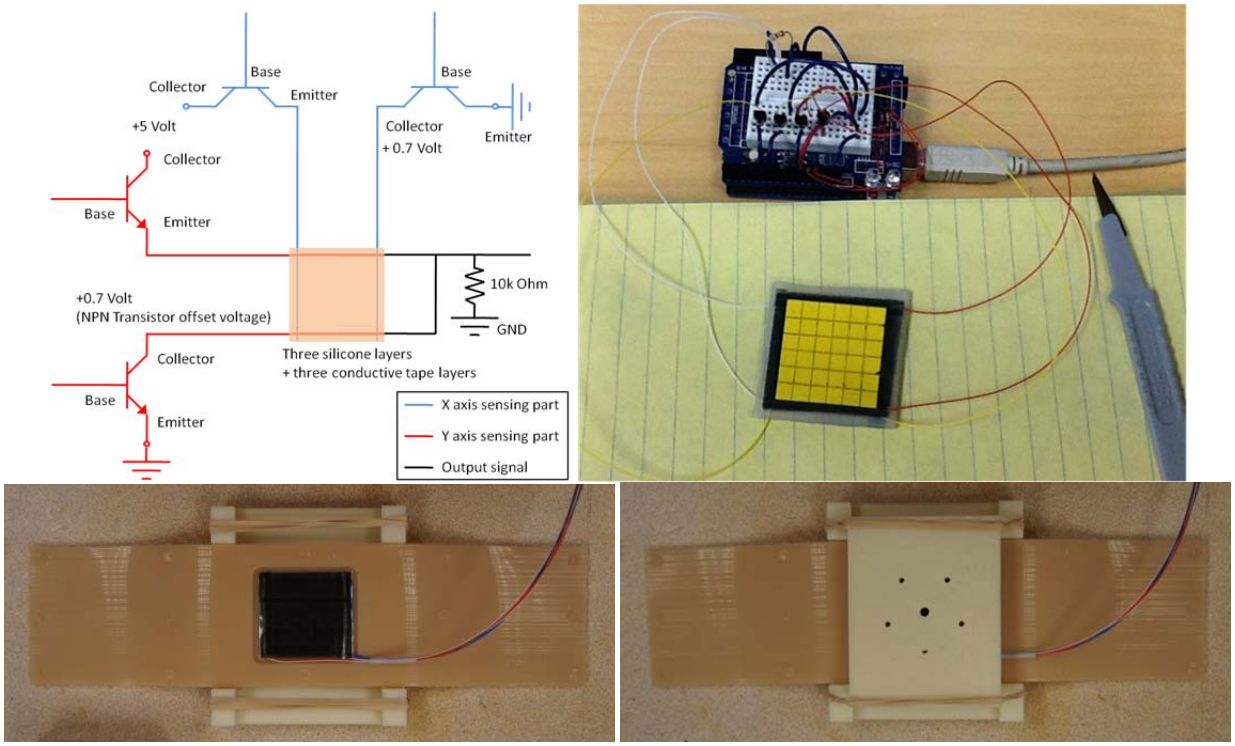

Figure 109: Drive circuit and sensor body for cricothyroidotomy incision sensor. Sensor in place on neck "skin" and over-molding assembly to encapsulate the sensor.

A concept for a simplified version that uses only two conductive layers and employs commercially available neoprene rubber with conductive surfaces (previously used in the original yes/no concept) was explored, however high and variable contact resistance between the thin surface layers and the incising blade made this solution unsuitable.

In order to establish the relationship between the resistance value and distance, we performed the calibration test as shown in below. The resistance value has linear relationship with the distance between the electric wires at the edge of the sensor and incision point. This test was performed by piercing the sensor at regular points along the length and width of the sensor. An extended cut does not display as linear a response, however it is sufficient to indicate the direction and length of an incision.

The cricothyroidotomy sensor was installed on a Laerdal mannequin head that was used for development purposes, and shown as part of the demo presentation to TATRC personnel at MHSRS/ATACCC 2012. The sensing system was included in an invention disclosure that was submitted during year 2. In a reconfigured shape, it is compatible with the airway model that was developed after year 2, described in the following section.

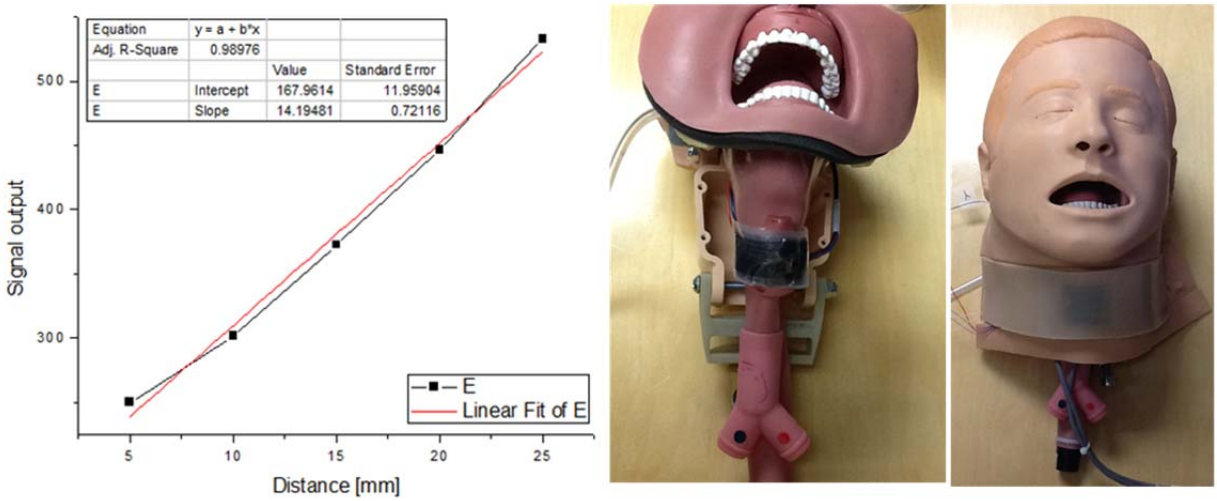

Figure 110: Cricothyroidotomy primary incision sensor calibration curves; sensor in place over commercial larynx; sensor integrated into replacement neck skin band over commercial mannequin head/neck (Laerdal SimMan Essential)

2.3.6.d. Airway model

As described in section 2.3.5.a, we segmented the airway features of the CT data, with good results for the naso- through laryngopharynx and nasal cavities (Figure 111). Due to the presence of dental filling-related artifact in the CT images, we scaled an imported model of teeth and created sculpted models of the soft tissues of the mouth.

Using the CT-derived anatomical modules as a basis, simplified versions of the soft tissues of the nasal passages (reduced complexity of nasal turbinates to ensure a large enough path for nasal intubation) were fabricated. Due to the complexity of the nasal cavities, they were cast in left and right halves which were bonded together and installed into the skull. The combined component includes passages that are aligned with and connect to the naso-lacrimal duct and the lacrimal sac in the rigid structure of the skull, so that stent-based repair of the canaliculi can be performed with standard instruments that extend from the puncta in the eyelids out through the nostrils (Figure 113).

Full models of the teeth and soft tissues of the mouth including tongue, and the upper airway including larynx and upper trachea have been fabricated and are included in the new version of the head. These are compatible with nasal and oral intubation and cricothyroidotomy (Figure 112, Figure 113).

Figure 112 shows sculpted positives for creation of molds, including highly detailed models of an airway that includes the epiglottis and vocal folds, for use as landmarks when intubation is performed on the system and a detailed tongue. The structures are compatible with future implementation of addition of internal bladders to generate tissue swelling.

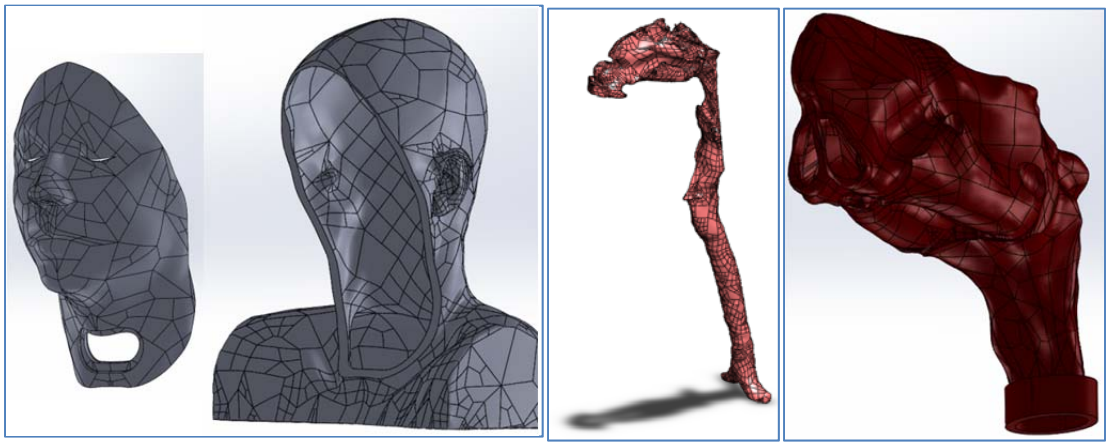

Figure 111: CT derived skin surfaces with substantially uniform offset, reduced thickness in the facial regions close to skull surface. “Negative space” of airway including nasal, pharyngeal and tracheal regions. Detail of simplified airway with continuous passages through left and right nostrils.

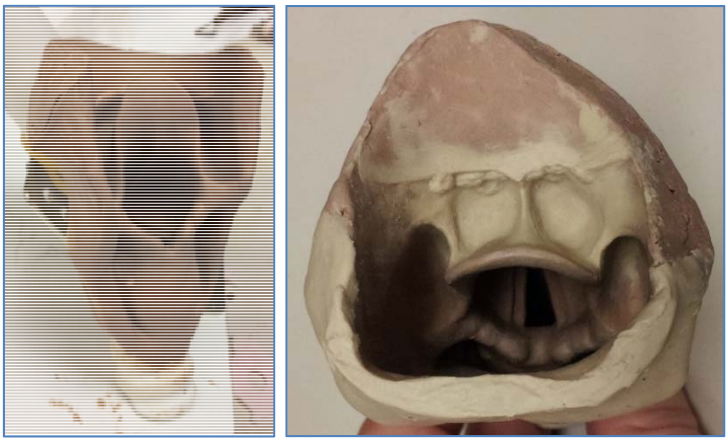

Figure 112: Sculpted details of larynx with epiglottis, vocal folds; gum and inner soft tissues; tongue and initial cast rubber iteration.

Figure 113: Demonstration of continuous passage through lower canaliculus, naso-lacrimal duct and out through nose. Partially and fully assembled airway including nasal, oral and laryngeal structures.

2.3.6.e. Hemorrhage, CSF/aqueous humor fluid supply system

In parallel with the physical modeling, we developed early schematic plans of the internal systems to control elements such as bleeding, CSF leakage through ears or nose and channeling fluid to the eye globes to generate a slow flow of simulated aqueous humor out of lacerations in the cornea. Early iterations of the system conceived of the inclusion of vascular access to carotid, jugular or other vessels, however the emphasis on developing components for use in the Ocular Trauma course lowered the priority in favor of other simulator components.

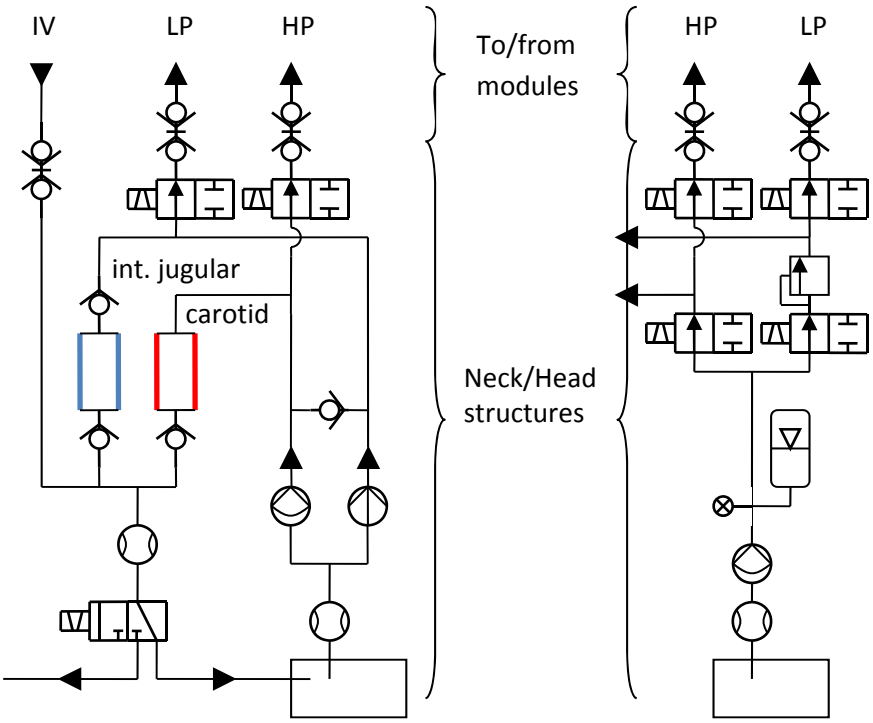

Figure 114: Section of fluid schematic concept for control of blood simulant. (left) Dual pump method for generating arterial and venous pressures independently. (right) Single pump method with accumulator and regulator.

In Year 2, a hemorrhage control sensing system was explored. A network of soft, collapsible tubing "vessels" links external openings in the relevant anatomy and to a common pressure sensor internally. Fluid flowing unimpeded out through the network from a common source would register low pressures at the sensor; measured pressure increases as hemostasis is achieved across the set of available bleeding sites as net resistance to flow is increased. If fully implemented, the network of simulated vasculature would span the entire head and neck region. Instead of placing multiple pressure sensors about a series of target zones for intervention where a medic would apply pressure to stop bleeding, we studied detection of the signatures of pressure changes as different sections of a network were occluded. Using a single, inline, pressure transducer we could detect (and ultimately generate responses to treatment) in an intervention independent manner.

This system would be of use in generating advanced trauma scenarios for first responders; when linked to a full-body mannequin, there would be no access to the instrument tracking features of the simulator. Detection of the appropriate (and inappropriate) application of direct pressure to control bleeding would be a measurable means of scoring performance. As with the instrument tracking, regions of interest in terms of pressure thresholds, timing and duration of application of pressure and correct site of application can all be defined and integrated into the software architecture as "gestures".

Figure 115 illustrates typical results from a test implementation of the sensor/tubing network system. A Deltran DPT-100 pressure transducer (Utah Medical Products, Midvale, UT), a low cost, relatively rugged device for clinical use was used. Based on a Wheatstone bridge, it is capable of monitoring pressure

from -30 mmHg to 300 mmHg. For the tests, the sensor was coupled to an industry-standard instrument amplifier (INA125P, Texas Instruments, Dallas, TX) which provides a series of reliable voltage sources and single resistor gain setting, the output of which was sampled by our Arduino board for data collection and analysis (Figure 116). For the range of sensor outputs measured, the gain resistance was 15Ω. In monitoring the pressure signal from the inline transducer, changes in pressure of the overall system as well as spikes that correspond with treatment were observed. The raw pressure signal (blue) from the sensor can be analyzed to extract the signatures (red) from applying or releasing direct pressure on the hemorrhaging vessel. Combined the average systemic pressure and the change signatures, detection of hemorrhage control can be implemented.

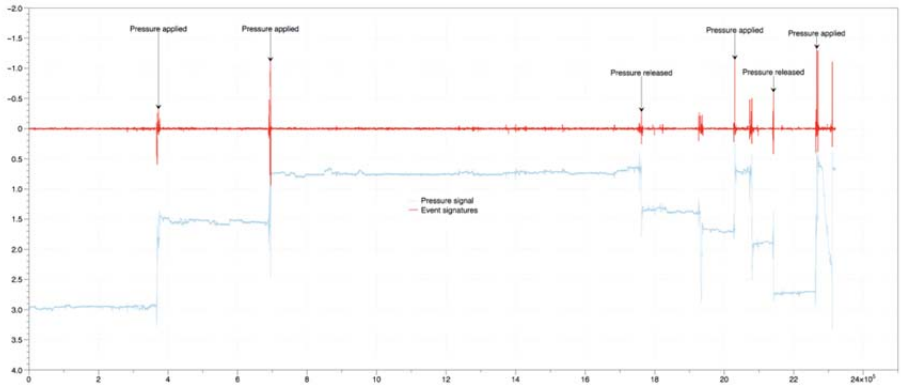

Figure 115: Raw hemorrhage back-pressure measured by restricting flow through one or more branches of the vasculature (blue). Derivative of pressure (dP/dt) for use to flag when significant changes occur, e.g. start or end of hemorrhage control (red).

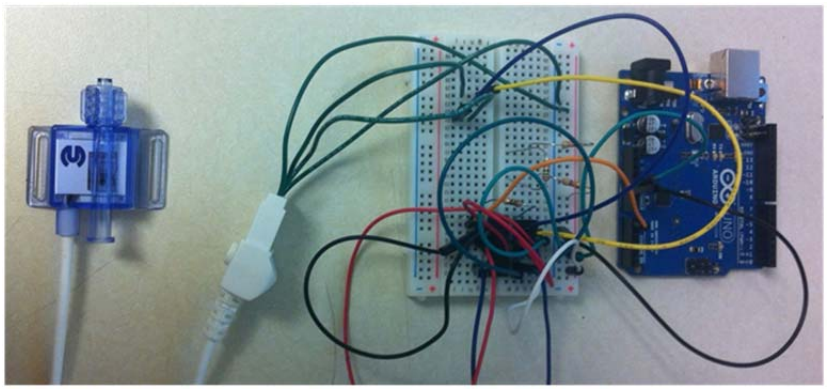

Figure 116: Test assembly for hemorrhage control pressure sensing. Clinical pressure sensor, signal amplifier chip, microcontroller kit for data acquisition.

The hemostasis sensing method developed in year 2 serves as the means for determining whether fluid flow is manually controlled. During Year 3, we developed a fluid control manifold system to channel high and low pressure blood simulant and low pressure clear fluid, simulating aqueous humor for the globe modules and cerebrospinal fluid to channels terminating in the nasal airway and the ears. The system borrows a design paradigm that we employed in our earlier COMETS trauma mannequin system [Bardsley et al., 2014], using two plates to form the manifold, with ports and fluidic components on one

side, and the flow channels formed into the other (Figure 117). Faster and with the capability for finer features than the CNC aluminum version developed for COMETS, we used the Objet 3D printer to fabricate these components, with the added benefit that flow can be visualized through plates fabricated in a transparent plastic. Detailed design of this element with mounting frame features to mount it within the space in the upper skull is shown in Figure 118. The control circuitry for the valve array has been assembled in prototype form and control software has been expanded to accommodate the additional valves. An initial implementation assigned one digital output channel per valve from the Arduino Mega; the final version employs a series of port expanders that use I2C commands from the Arduino using only two wires (plus power and ground) to the expander, which can be mounted in the same space as the valve assembly, minimizing bus wiring between the microcontroller, which would ideally be mounted within the chest cavity of the mannequin (together with access to the mannequins blood supply and a reservoir for clear fluid), and the valve array in the head.

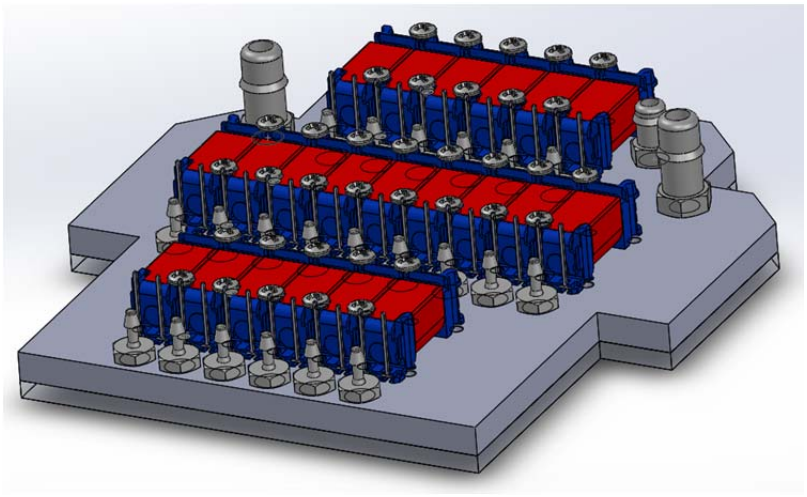

Figure 117: Three-source fluid manifold and control system. Three banks of miniature valves source high and low pressure blood simulant and low pressure clear fluid from remote pressurized reservoirs in the mannequin body. The upper six valves provide control of clear fluid as a CSF/aqueous humor simulant to each ear, both eyes, the nasal airway and one site to be determined/reserved. The low pressure bank supplies blood simulant to the ears, nasal airway, post-conjunctival space for each eye and multiple bleeding sites in the facial module. The front bank of valves supplies high pressure (arterial) flow to bleeding sites on the facial module.

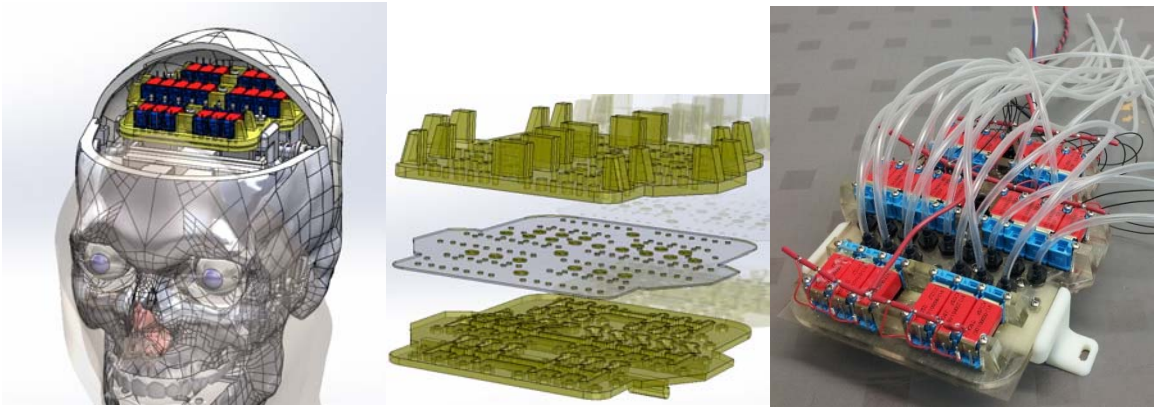

Figure 118: (Left) models of the manifold assembly in place on the head, (middle) two part manifold with gasket structure, and (right) assembled valve array, awaiting installation in the head.

In addition to the mounting and channel components, we explored directly 3D printing the gasket using TangoPlus soft rubber material. In previous projects, we used silicone sealant to attach manifold sections together, which tended to force silicone into the flow channels and make disassembly for repair extremely difficult. The use of a transparent plastic (Fullcure 720) for the manifold parts also facilitated checking to ensure that the parts were sufficiently clamped together – leaks of red blood simulant could easily be seen during testing.

2.3.7. "Month 10" –

2.3.7.a. User testing of enhanced eye trauma simulator at USUHS or Madigan Army Medical Center.

We received approvals from our IRB and ORP HRPO for a second, and later a third data collection exercise and participation in the 2013 (and 2014) USUHS Ocular Trauma course. In addition, we supported preparation of the Simulator Validation Program (SVP) proposal by Dr. Marcus Colyer and colleagues at USUHS, which called for use of this simulator as representative of a non-tissue alternative to training on animal tissues.

During Q8, as with the first year's testing, we made 25 lid laceration modules available for the students and faculty to use, all of which were used over the two-day wet-lab sessions of the course. As with Year 1, student availability was limited due to the primary requirements for their participation in the animal and lecture sessions. A software error resulted in the omission of residents PGY year from the database, however we verified that at least ten PGY2 and PGY3 residents used the simulator. The rest of the modules were used by faculty, of whom three were oculoplastics specialists.

All participants filled out a survey form which was requested by Dr. Marcus Colyer, course director, to provide feedback on participant impressions about the simulator. This survey presented Likert scale-type questions, asking for agreement/disagreement or relative opinions and, on the following topics:

- User interface and teaching content
    - Teaching content was clear and understandable
    - Interface guidance was helpful in learning the technique
    - There was too much detail in the teaching content
- Eyelid laceration module
    - Tarsal plate hardness was too hard/too soft
    - Eyelid hardness was too hard/too soft
    - Resistance to needle puncture was too much/too little
    - Friction of passing the needle through the tissue was too much/too little
    - Friction of passing suture through the tissue
- Simulator stand and instruments
    - Structure of the stand interfered with interaction with the surgical field
    - Cables and connectors interfered with performing the procedure

- Cable management bracelets and attachments interfered with performing the procedure
- Instruments were easy to take from and return to the rack
- Sutures were easy to access
- Lights were in a suitable position
- Lighting brightness was too dim/too bright

For each section, and open ended comment/suggestion section was included.

We performed preliminary analysis on the data compiling the results for the scored questions.

For the interface and teaching content, the experts and novices showed the same overall preferences. The majority agreed or strongly agreed that the content was clear and understandable and that it was helpful. Both groups however, disagreed that there was too much detail in the content. We interpreted this to mean that there was insufficient detail and that more should be added. Among the comments, were requests for additional detail generally, more specific instructions regarding details of the knots and suture techniques to be used in the different phases of the procedure as well as acceptable alternative methods, and information on suture depth and tissues to approximate.

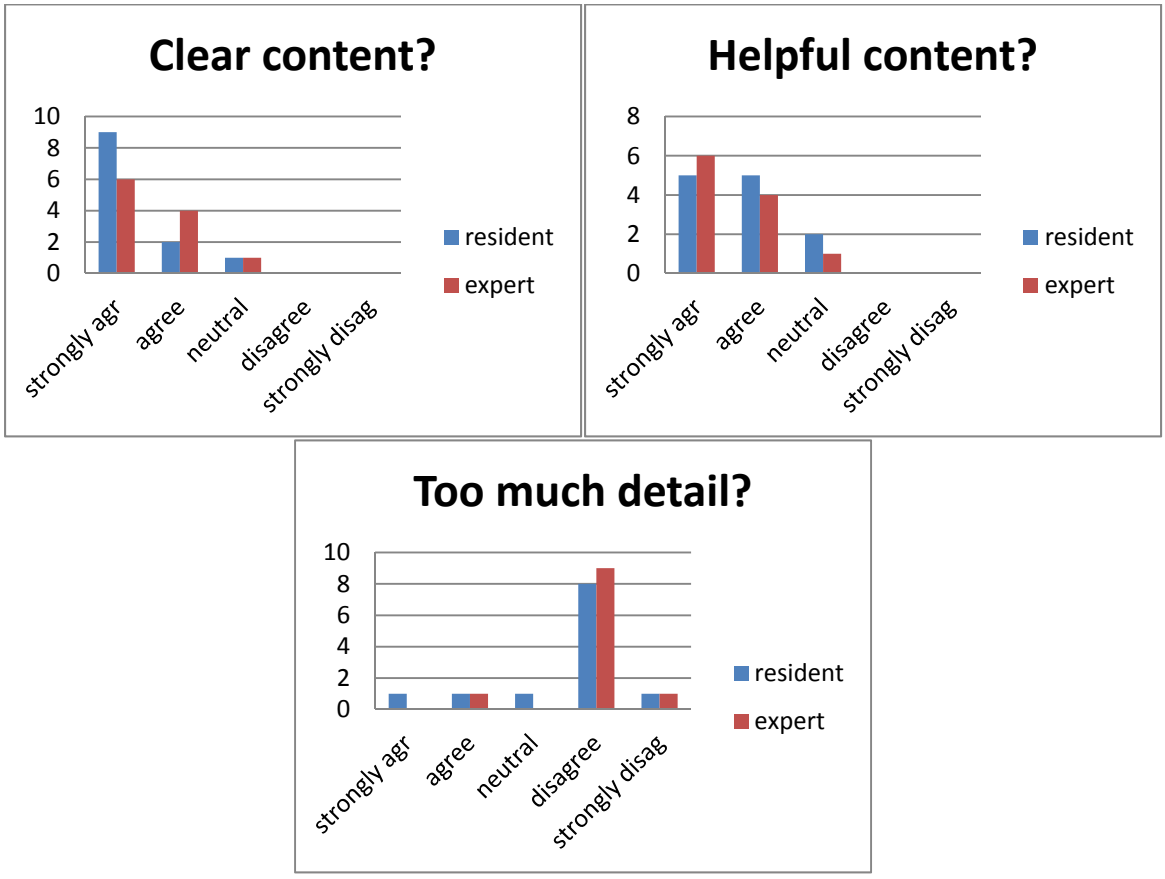

Figure 119: Simulator content responses between residents and experts

For the eyelid laceration module itself, experts and novices tended to have similar responses as well. Tarsal plate hardness was judged almost evenly split between about right or too soft; eyelid hardness was about right or too hard for most respondents; puncture resistance was about right for the majority of experts and residents; needle friction was about right for the majority, and suture friction was either about right or too much, evenly divided between experts and residents. Comments were fewer, however there were requests for additional and more obvious anatomical landmarks. These would be included through changes in pigment added to the later versions of the modules and alterations in the mold to include features such as the Meibomian gland pore, which were present, but not particularly deep.

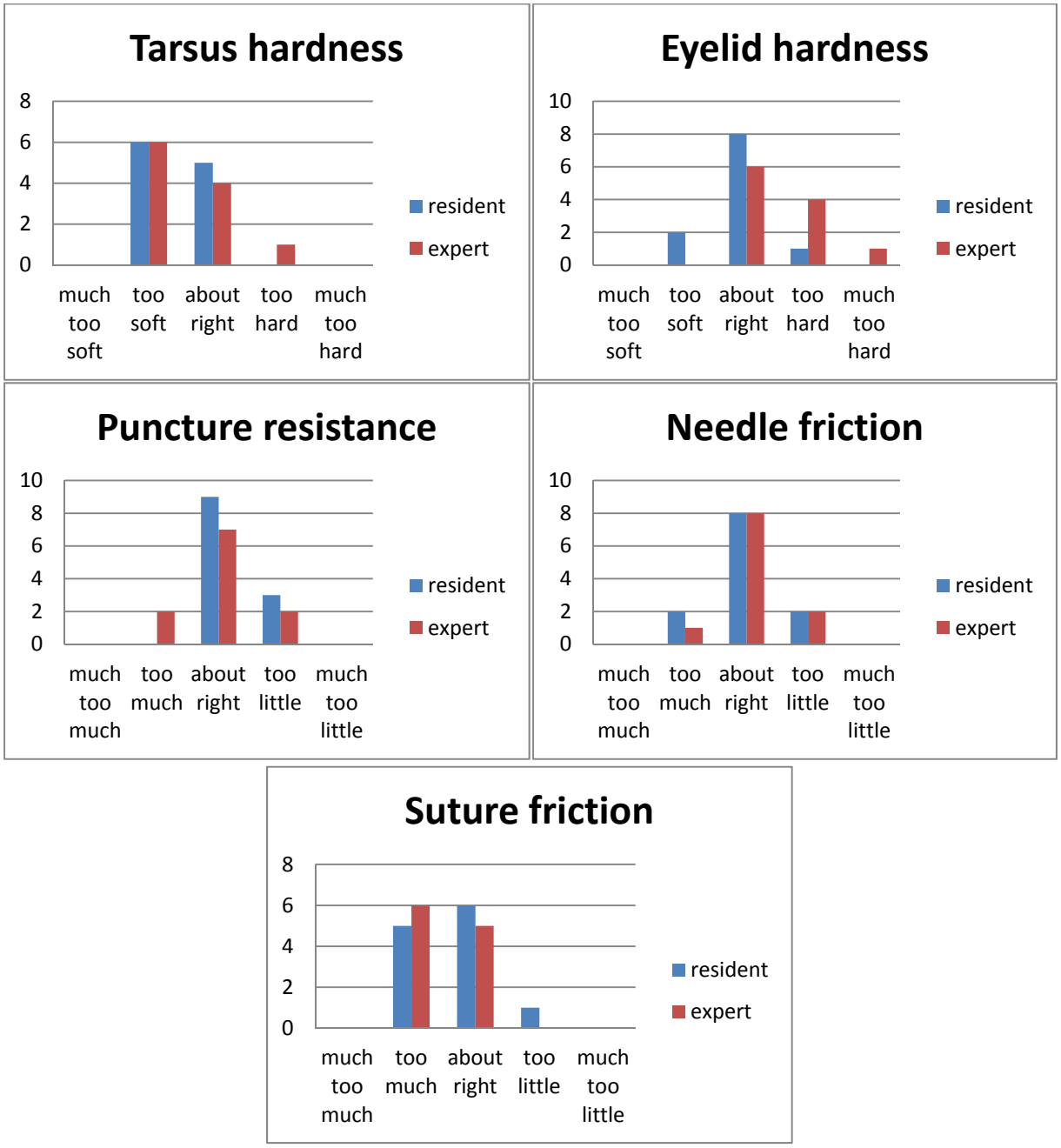

Figure 120: Lid laceration module physical characteristics responses

For the simulator stand and instruments, responses were more broadly distributed in certain cases. The median response was that the stand did not interfere, however there were some who felt that it interfered somewhat (possible that the agree/disagree statement was misunderstood and inverted). Cables and connectors clearly were troubling for some, but not for others. The cable management bracelets were roughly evenly distributed between those who were neutral, disagreed or strongly disagreed that they interfered with the task. The instrument access using the tray and the connection mechanism were found to be easy to use by nearly all participants. The lighting system was found to be about right by most, although too dim for some users. The majority of the comments concerned the cabling attached to the instruments, with some requests for wireless instruments (which is not possible given current magnetic tracker state of the art technology and requirements on the size and mass of the component that would be attached to the instruments), others suggesting alternate cable management approaches.

Discussions with Dr. Colyer following the course lead to an invitation to participate in the 2014 course.

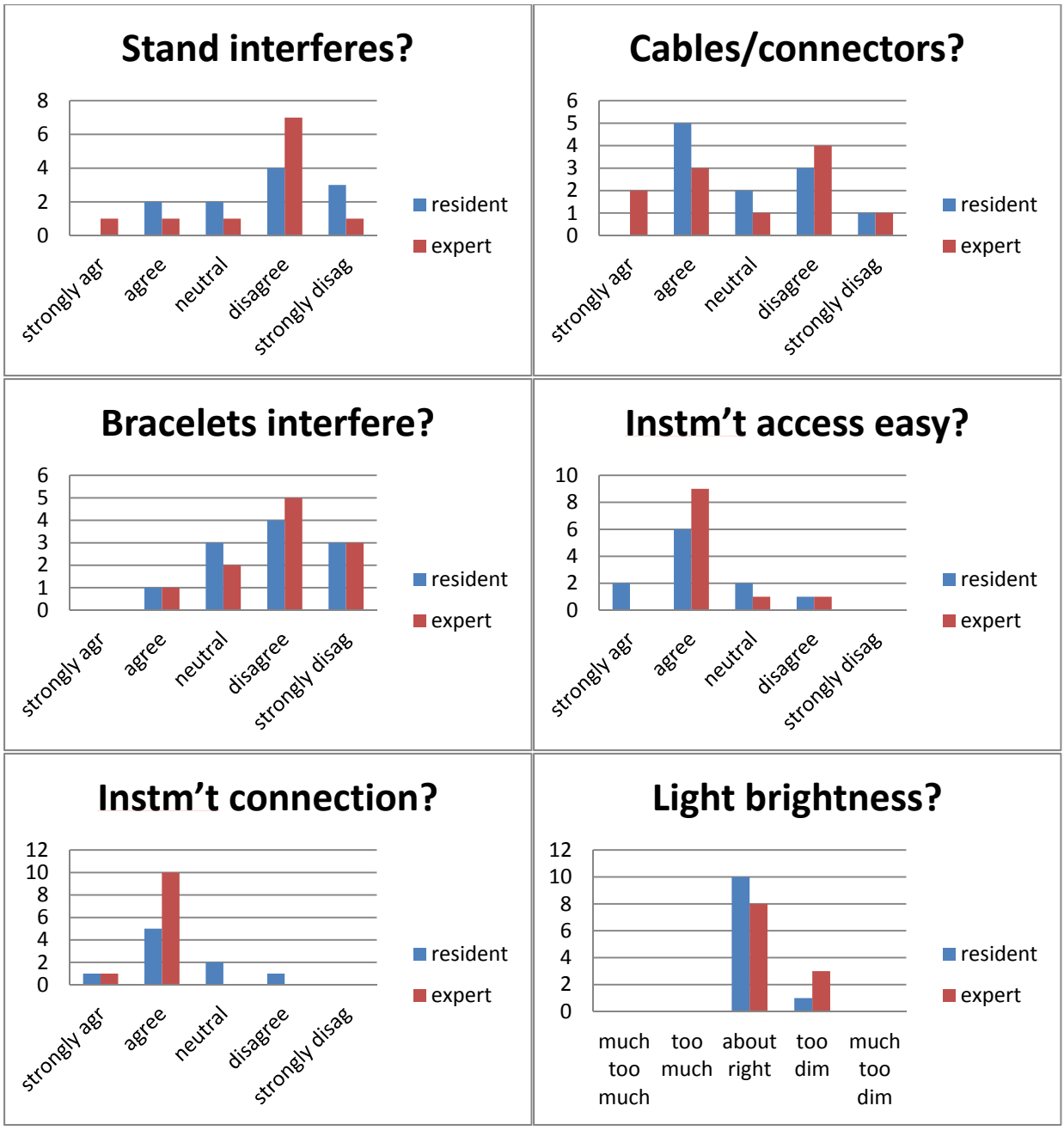

Figure 121: Standalone simulator characteristics responses.

2.3.7.b. Pass upgraded proof-of-concept simulator specifications onto commercial partner.

All of the developments regarding contact with potential commercial partners over the entire program were described in section 2.3.3.b.

2.3.7.c. Continue working on augmented reality guidance system for enhanced eye trauma simulator.

2.3.7.c.i. Augmented Reality Microscope

In year 2, the AR microscope reached a functionally complete state, with the optics for both left and right eye implemented, measurement of the zoom level made available by linking a precision potentiometer to the microscope zoom shaft, creation of power circuitry for the LCD, backlight and surgical light source, creation of software tools to display stereoscopic views and mounting of an Ascension position tracking sensor to the microscope to track its location relative to the mannequin head. The software architecture was modified to display a model of the microscope within the virtual environment of the data acquisition interface, and the same position tracking information is used to define the stereoscopic imagery shown to the user through the microscope. Test patterns were displayable through the microscope. Software tools were used to align the graphical overlays of left and right eyes with each other and with the real object, and improvements to the hardware were made to rotate the horizontally aligned images from the LCD to the angled optical path through the microscope (divergence of 10 degrees between eyes requires 5 degree rotation of LCD image either in software or through mirror positioning – software rotation results in poorer image quality using current LCD).

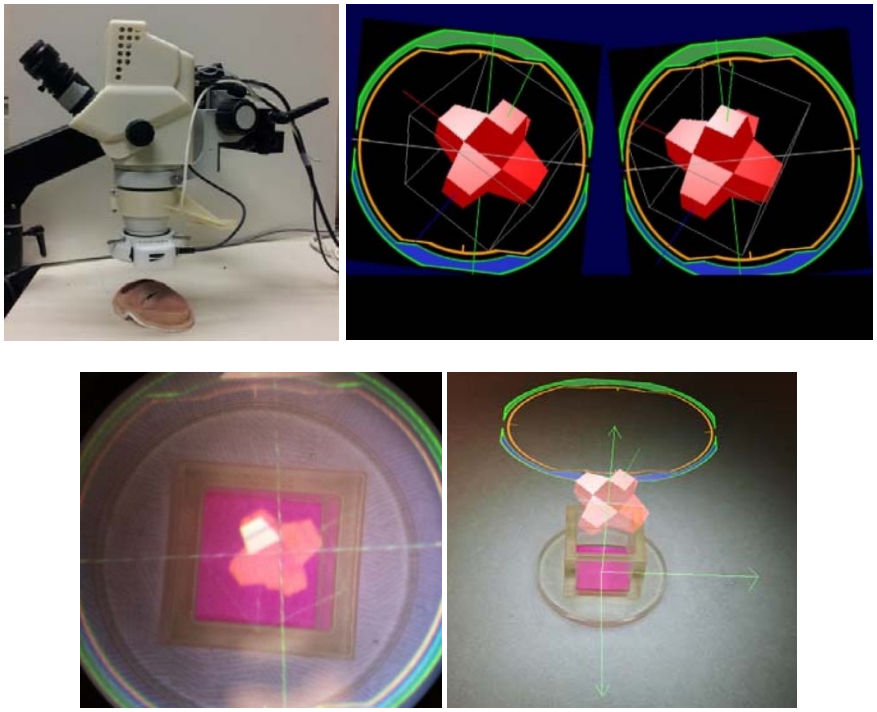

Figure 122: Year 2 AR microscope with enclosure, internal LCD, ring light (at bottom), position sensor mounted to right of lower cowling. Test patterns generated by software. Monocular view of test pattern fused with optical image of test object. Representation of the virtual test object in relation to a real test object.

Following the earlier work, the software architecture was modified to display a model of the microscope within the virtual environment of the data acquisition interface, and the same position tracking information is used to define the stereoscopic imagery shown to the user through the microscope. As the microscope is translated or rotated, the overlaid view changes to match. Test patterns were

displayed; the next steps in this area include implementing views of the virtual environment for overlay onto the view of the real objects.

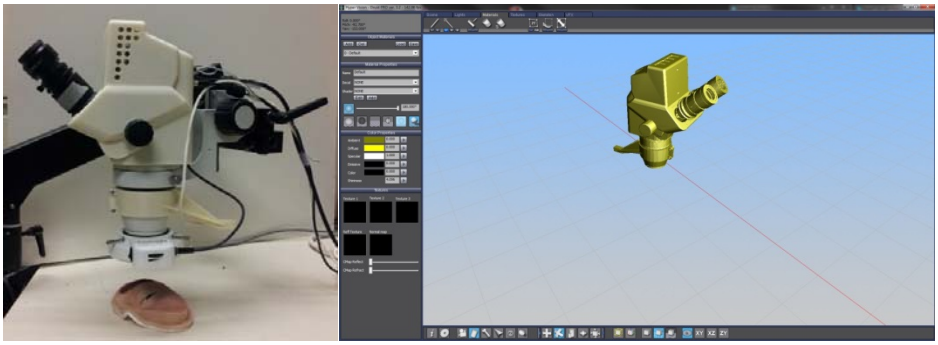

Figure 123: AR microscope with enclosure, internal LCD, ring light (at bottom), position sensor mounted to right of lower cowling. Graphical model of microscope in virtual environment for calculation of relevant display to be presented on LCD and viewed through eyepieces.

It can be seen in Figure 122 that the graphical images are rotated with respect to each other (note colored rings around target object). This was necessary because the optical paths of the eye pieces diverge from each other by 10 degrees. To make the LCD image appear aligned through the eyepieces, the LCD image needed to be rotated by 5 degrees each in the opposite directions. Control panel elements were added to our primary data acquisition interface to adjust this rotation as well as offset, skew and scale the output images.

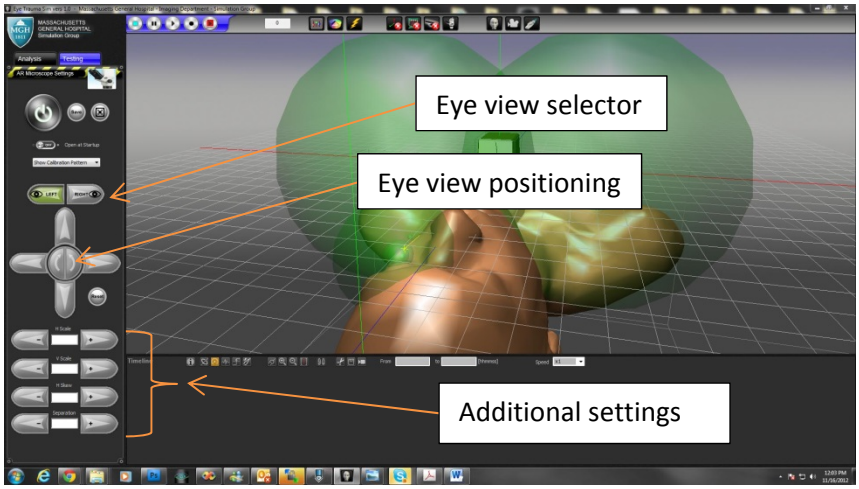

Figure 124: Control panel for microscope view positioning and alignment.

We observed that while this adjustment aligns the images, the pixels grids viewed through the eyepieces remained at angles with respect to each other. Image quality would be improved further if the pixel grids were aligned, which required modification of the optical path set up between display and eye piece lenses.

The earlier 2D graphical tool described above assumed that the path from display, through lenses and mirrors to the eyepiece lay on a plane. Relaxing that assumption and allowing a 3D path permited the generation of a path with chirality (rotation). The 3D calculation tool set the LCD images to be aligned with the pixel array and the output optical axis aligned with the eyepiece. Four points defined on the LCD plane were projected through the series of lenses and mirrors to their image positions. The rotation of lines connecting pairs of image points shows the rotation of the image. By adjusting mirror locations and angles, the LCD image could be rotated optically (rather than graphically), resulting in the desired alignment. Once the mirror angles were calculated, the mirror holding components in the microscope were modified to match, 3D printed and installed, replacing the earlier versions.

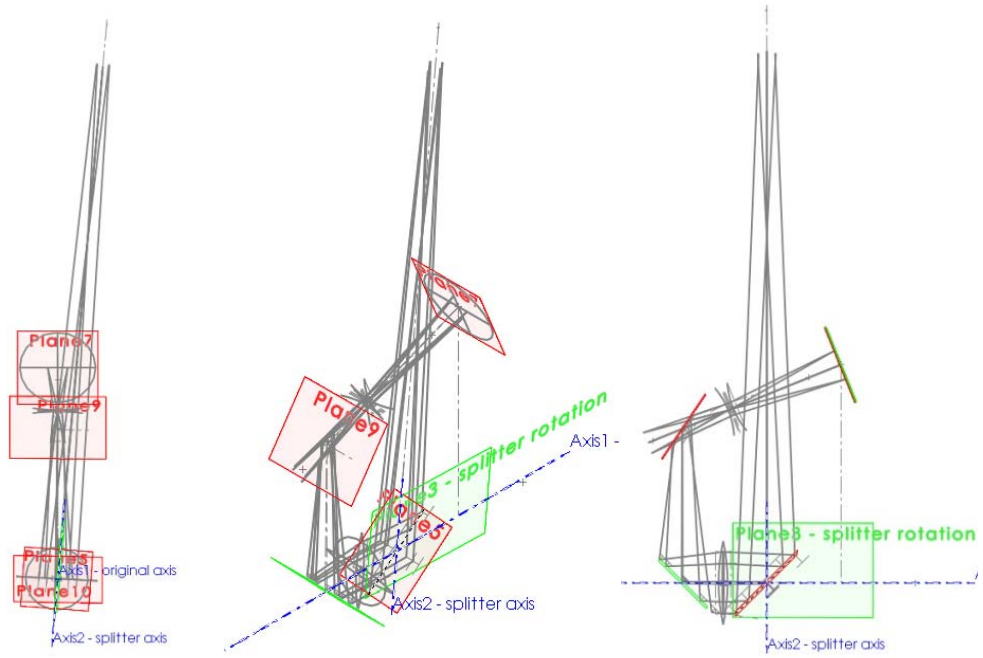

Figure 125: Front, isometric and side views of new 3D optical path calculator.

During Year 3, enhancements and improvements to the AR microscope and the augmented reality display systems of the simulator continued.

As described in further detail in section 2.3.8, we added a modular touch-screen display, in addition to the microscope display and that of the microprojector (used to project content, dynamic graphical alterations to the face of the mannequin). This required extending the 3D engine software to support multiple rendering ports, reducing the overhead required to manage the microscope display.

2.3.7.c.ii. AV Recording and Compression

After the implementation of the different components required for the video acquisition, in Q5 all these software components were combined in order to create the architecture to manage the video acquisition (webcam interface, with a manual decoding YUV filter implementation) a codec manager (for video compression into the desired video format) and the AVI manager (already implemented in the previous months.

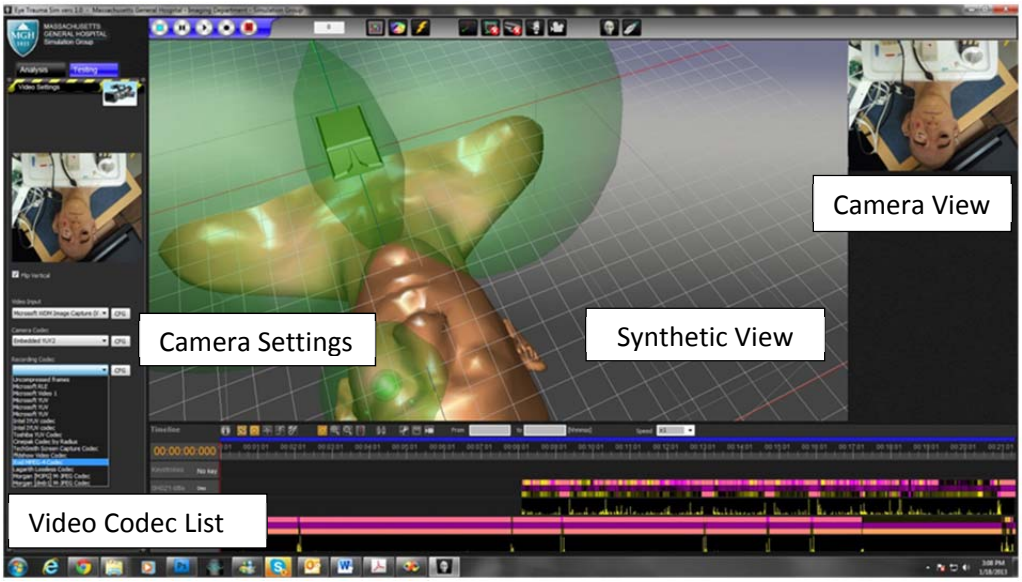

Figure 126: Updated data acquisition interface including new video capture elements. Available CODEC list and camera settings at left. Instrument tracking data streams shown in colored bars at bottom

In year 2, we observed that image artifacts (patches of saturated image) appeared in the video captured from user testing. While this did not prevent use of the video for development purposes, it was distracting for anyone reviewing the video. In Year 3 (Q9), the YUV filter implementation was improved to eliminate the artifacts.

Synchronization between the instrument tracking data and the video so that the synthetic view playback corresponded with the video playback was completed, enabling scrolling through recorded data from a scenario and selection of sub-elements for more detailed review and analysis.

2.3.7.c.iii. Hand/Instrument Motion Tracking

Our Year 1 tests of the Kinect system, suggested that the tracking resolution was insufficient, in part because the minimum working distance between the Kinect and the surgical field was too large. A novel hand/finger tracking device called Leap Motion (Leap Motion, Inc., San Francisco, CA) had recently appeared on the market, and early release of development systems were made available to developers with interesting applications, as determined by review of abstracts submitted to the company. In Q6, we obtained one Leap system and began to evaluate its capabilities. It appeared based on product literature, that it could detect up to 10 finger tips within its working space, a space approximately 24” on a side, and that it was much better suited for hand/finger tracking than the Kinect.

Figure 127: Photo of Leap unit, with mini-USB connector. Product photo from Leap web site; demo application available with device shows only line segments for finger tips, not rendered hands.

In Q7, we studied the possible uses of the Leap Motion finger/hand tracking system, through modification of the example programs included with the SDK, such as the Sample_VS2008 project, which demonstrated access to the raw data coming from the sensor. The device performed similarly to videos displayed on the vendor website, as which we confirmed for ourselves through use of the example programs and software demos that it is possible to download from Internet. The sensor provided multiple finger positions and orientations (each tracked finger in five degrees of freedom) and the code generated extra data (timestamp, number of fingers, frame ID). Mounted under a monitor positioned to the side of the simulation platform, the Leap could track surgical instruments (possibly out of range of the tracking system) or surgeon's gloved fingers and provide indications on the screen – sharp instruments and gloved fingers being incompatible with various touch screen technologies.

While initial experience showed that it performed similarly to the vendor's product videos, in Year 3 we revisited the use of the Kinect, which had since been redesigned to include a near-field mode. We studied the Microsoft Kinect SDK in order to replace the older and less powerful framework developed from third parties to integrate the Microsoft Kinect functionalities into the system. The new version was found to be fast and very stable, allowing more control of the device. Using the Microsoft Kinect SDK, we tested the Kinect for PC and the Kinect for X-Box versions in order to choose the best one for the project. In addition, on both Kinects, an optional optical element intended to shorten the working distance of the Kinect by 40% so that users with small rooms can still interact with the Kinect (Nyko Zoom, Nyko Technologies, Los Angeles, CA) was mounted, but without success – the optical distortions introduced were found to be unacceptable. Our final design iteration for the Kinect is to use the Kinect for PC with Near Mode activated.

Also in Year 3 we evaluated the use of the Natural Point TrackIR 5, an infrared optical tracking system developed for the gaming market, but used extensively for gaze tracking and device tracking work. Our findings were that the system's sensor noise was unacceptable for instrument tracking, and the need to use a set of retroreflective markers or IR emitting LEDs in a pre-determined configuration make the system unsuitable for our current uses. In the future, tracking of head motion as a proxy for gaze or area of attention may be useful, however this is likely to be outside the current scope of work.

2.3.7.c.iv. Event Driven Gesture Analysis

During Q6, we met with several of our subject matter experts to continue our framing of the educational goals of the upper eyelid laceration repair module. While very difficult to depict graphically, our state diagram of the entire procedure grew extensively. Based on input from the SMEs, we mapped the entire procedure from start to finish, including many actions beyond the scope of the system. The purpose of this exercise was to understand what context the user was being placed in when using the simulator. States of the procedure such as requesting an x-ray of the patient would be carried out in software as a series of interactive steps in the GUI rather than an interaction with the simulator mannequin.

Several areas of the training module, when mapped, started to illustrate repetitive functions. We captured these repetitive functions (actions, gestures, thresholds, etc.) and used them to drive our software development processes. For example, our ability to detect a specific sequence of events associated with placing the needle through the eyelid and retrieving it through the other side formed a basic building block in our suturing gesture recognition system. If the system detected a second pattern of this type, we would know that the user had taken two bites to pass the suture through the location in the wound. Should these events be followed by a knot tying gesture, we would then be able to warn the user that it was advisable to leave the sutures untied until all of the sutures have been placed and the lid margin approximated. This capability is necessary both for real-time, in-context surgical guidance for novices as well as forming the foundation of our gesture recognition framework.

As of Q6, the description hierarchy tree had 10 levels of description:

- Curriculum: 1 entry (eye trauma course)
- Module: 1 entry (marginal lid laceration)
- Styles: 1 entry (“textbook” sequence – later entries to include surgeon-specific techniques)
- Steps: 5 entries for current style (e.g. examination, suturing tarsal plate, incision closure) – different numbers of Steps will apply to alternate Styles
- Tasks: 52 defined across all Steps, with varying numbers for each Step – marginal suture through tarsal plate
- Gestures: may be simple (review X-ray) or compound, with

further divisions (e.g. 2-1-1 suture gesture)

- Sub0-Gesture: optional –structure for capturing needle passages without knot tying
- Sub1-Gesture: high level components of gestures, e.g. single bite suture, 2-throw knot, 1-throw knot, cut suture
- Sub2-Gesture: mid level gesture component, e.g. tissue grasping, needle bites, repetitions of throws, suture grasping, knot tensioning
- Event: sensor-driven events that comprise the Sub2-Gestures: instrument jaw opening/closing, applied force level threshold transitions, passage across region of interest boundaries, focused path analysis

Sample elements of the hierarchy are depicted in the sidebar above.

The relatively simple early approach we developed to drive progression through the scenario content (e.g. instrument attachment/detachment, RoI threshold crossing) was expanded in year 2 with a richer set of algorithms in order to recognize the different gestures performed by the surgeon during the procedure. This was based on a more extensive set of elemental states, listed in Table 1. This list was extended with an initial set of error conditions for triggering warnings from audio cues to video instructions on correct technique.

Table 1: Elemental states detected by gesture algorithm in year 2.

ID	Routine Description
-2	Stop state machine
-1	restart state machine
0	NULL
1	Scissor is cutting inside a specified ROI
2	true if a forceps is connected
3	true if no forceps are connected
4	True if a needle holder is connected
5	True if no needle older are connected
6	True if an instrument is inside a specific ROI
7	True if a scissor enter inside a specific ROI, cut and after goes out
8	Record data for scoring
9	Plot scoring results
10	True if the spear is connected
11	True if the spear enter in a specific ROI and remains there for at least 3 seconds
12	True if the forceps enters into a specific ROI and remains there for at least 3 seconds
13	True if a double pass suture is performed (first pass)
14	True if a double pass suture is performed (second Pass)
15	True if 2-1-1 is performed (not complete)

ID	WARNING CHECKING

100	Check for too hard forceps grasping (A)
101	Check for too hard forceps grasping (B)
130	Check for single pass suture instead of a double one (A)
131	Check for single pass suture instead of a double one (B)

We investigated extending the scripting language that was based on Boolean values by including a numerical parameter for certain routines, in order to create different settings (e.g. trim length of sutures) for reuse of the same algorithm for different types of users.

A series of schematics of the state machine structure implemented in code is shown below, with the various links between states defined by the test functions that determine which threshold has been crossed.

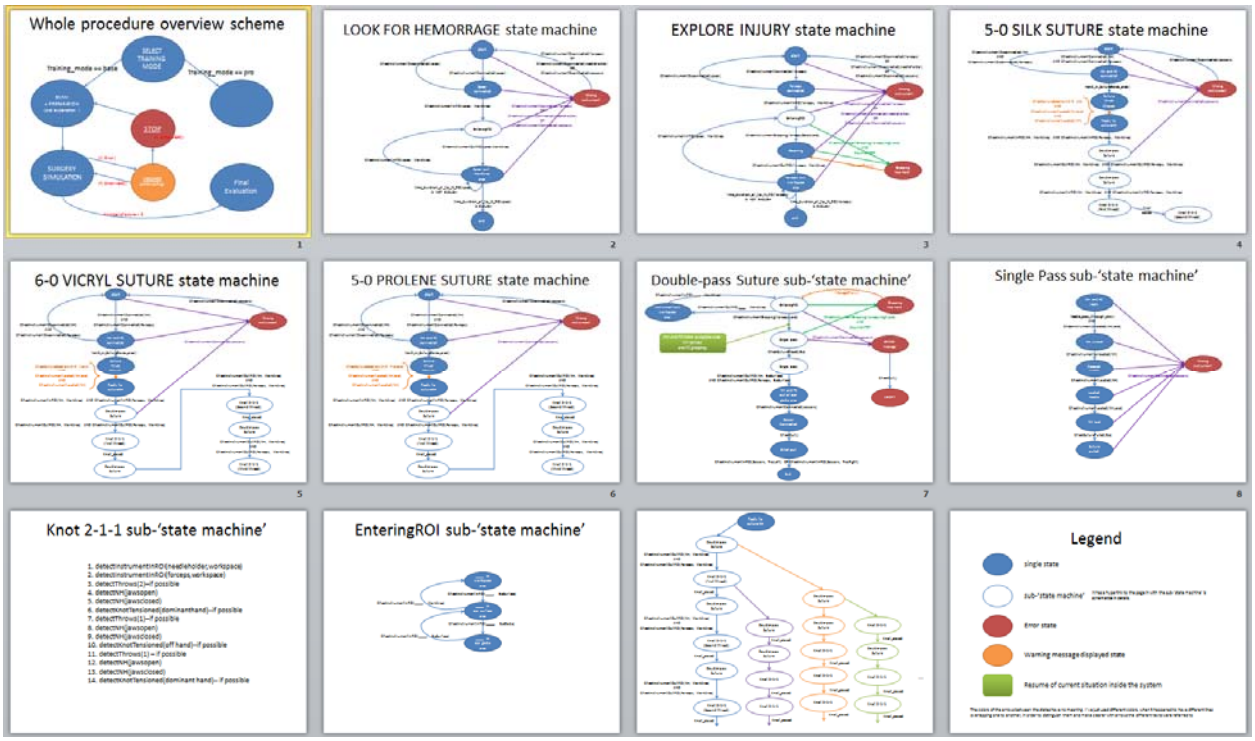

Figure 128: schematics of elements of state connections for different levels of gesture recognition hierarchy

In addition, the XML-based scripting language used to manage simulation content was extended to allow control of graphical user interface elements (buttons, sliders) and addition of comments to improve readability. The entire gesture recognition software core was exported to an external DLL to permit reuse of the code for future/alternative surgical simulators. It included elements to manage simulation content slides and the event handler signaling transitions between content elements, both to the correct next step in a procedure and to warning/error states that trigger presentation of additional teaching materials. The architecture was modified to split content management and gesture recognition/segmentation into two independent processes. For the 2013 USUHS session, a subset of the full content was enabled, with tools to allow the instructor to drive content display/progression.

Throughout Year 3, the gesture recognition system, including algorithms and the (scenario) developer interface continued to evolve and improve.

The earliest new element was implementation of the ability to perform the analysis process on pre-recorded data, rather than only on live streams of incoming position/sensor data. The timeline display of data was expanded to include additional lines identifying various classes of events, with flags entered where the relevant events are detected.

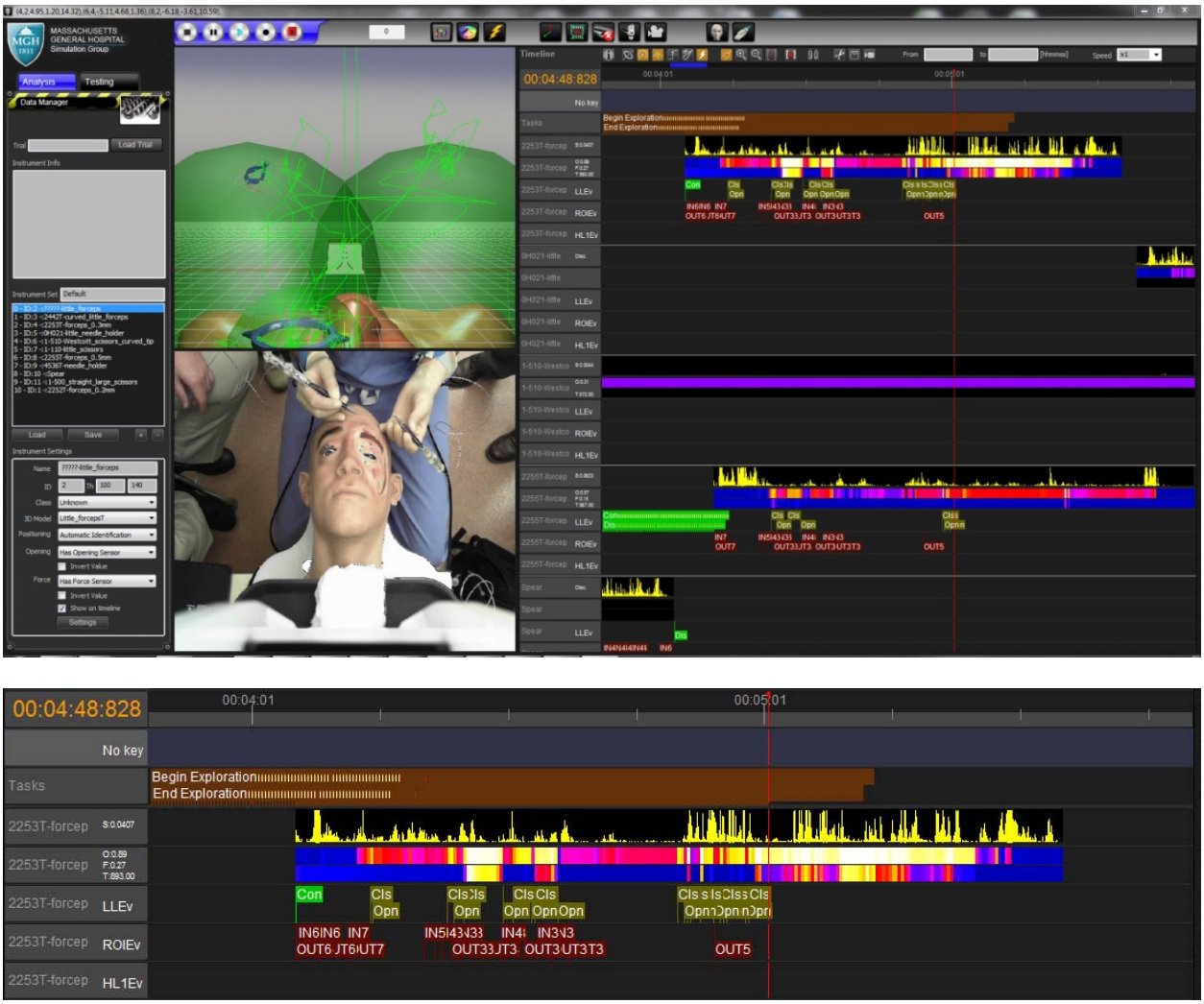

Figure 129: Q9 (Year 3) user interface and detail of event timeline.

On the timeline the events were separated in order to facilitate the analysis and comparison between automatic and manual gesture entries. The different tracks present on the timeline are:

- Tasks – representing the subdivision of the entire procedure in different sections (Cleaning, Exploration, Suturing). Each section is segmented based on the findings of the algorithm, based on which surgical instruments are connected and the movements of those instruments across

the different ROIs. The instruments are considered by category (e.g. alternate forceps have the same category, different scissors)

- LLEv – (Low Level Events) identifying all the elementary events such as instruments connections and disconnections, opening, closing. This category of events forms the bricks used to create higher levels of events.
- ROIEv – (ROI Events) representing all events regarding the transitions between different ROIs. This category of events is still considered among low level events but is on a separate track because they occur very often and can create problems in the analysis of the other LLEv.
- HL1Ev – High Level Events of 1st class are all those events that can be detected as combinations of LLEv and maybe integrating other information available from the surgical instruments. This category of events is also logically connected with the Task track.

All events visualized on the timeline have different colors; for certain type of events that usually require a beginning and ending of an action, the labels appear at different heights in order to facilitate visualization of the beginning and ending of those actions.

Under this structure, the decomposition for the eyelid laceration procedure is shown in Table 2, forming a subset of the 10-level hierarchy described above, with every level of the hierarchy is created as combination of events of the previous levels. Each entry of the table was implemented as single algorithm and each algorithm determines the setting of the appropriate state variable or adds a new event into the events list. Warning management was implemented as single level structure where the unique layer was made up of a set of LLE and each event was associated with a specific recovery action or set of actions. Every section (task) was subdivided, having a constant structure with a beginning, execution and end.

Table 2: Year 3 Task decomposition for eyelid laceration repair scenario

Eyelid Laceration Repairing Gesture Engine						
	Procedure Analysis Engine				Warning Analysis Engine	Recovery Actions
Proc	Tasks	SubTasks	High Level Events	Low Level Events	Warning Events	
Eyelid laceration repairing Procedure	Cleaning	Begin Cleaning	Instrument Set Connected	Spear Connection	Improper instruments disconnection	Message Audio/Video
		Cleaning	Spear moving inside the Eye ROI	Spear Tray ROI Out	Timeout to begin the cleaning	Message Audio/Video/Content
				Spear Eye ROI In	timeout to end the cleaning	Message Audio/Video
		End Cleaning	Spear back in the tray	Spear Tray ROI IN	Proper Instrument set	Message Audio/Video/Content
			Spear Disconnection	Spear Disconnection		
	Exploration	Begin Exploration	Instrument Set Connected	Connect FC1	Improper Instrument disconnection	Message Audio/Video
				Connect FC2	Proper Instrument set	Message Audio/Video
			FC1 OR FC2 Out of the Tray ROI	FC1 Tray ROI OUT	Timeout to begin the Exploration	Message Audio/Video/Content
				FC2 Tray ROI OUT	Timeout to end the Exploration	Message Audio/Video
		Exploration	FC1 working in Eye ROI	FC1 Eye ROI IN	Too hard grasping	Message Audio/Video/Content
				FC1 Grasping	Grasping out of the proper workspace	Message Audio/Video/Content
				FC1 Releasing		
			FC2 working in Eye ROI	FC2 Eye ROI IN		
				FC2 Grasping		
				FC2 Releasing		
		End Exploration	FC2 back into the Tray	FC2 Tray ROI IN		
			FC1 Back into the tray	FC1 Tray ROI IN		
	Suturing	Beginning suturing	Instrument Set Connected	FC Connection	Improper Instrument disconnection	Message Audio/Video
				NH Connection	Proper Instrument set	Message Audio/Video
				SC Connection	Timeout to begin the Suturing	Message Audio/Video/Content
			FC or NH in Eye ROI	FC Tray ROI OUT	Timeout to end the Suturing	Message Audio/Video
				NH Tray ROI OUT	Too hard grasping	Message Audio/Video/Content
				SC Tray ROI Out	Grasping out of the proper workspace	Message Audio/Video/Content
		Placing Stitches	Inserting needle	NH Loaded	Cutting out of the proper workspace	Message Audio/Video/Content
				FC Grasping	dangerous needle pulling	Message Audio/Video/Content
				FC Tip Globe ROI IN		
				NH Tip Globe ROI IN		
			Pulling needle	NH Unloaded		
				NH Loaded		
				NH Tip Globe ROI OUT		
			tying knot	FC Globe ROI OUT		
				FC Grasping		
				FC Releasing		
				FC-NH Pulling (needs to be defined)		
			Cutting thread	SC cutting into the eye ROI		
		End Suturing	FC Back to Tray	FC Tray ROI IN		
			Scissor Back to Tray	SC Tray ROI IN		
			NH Back to tray	NH Tray ROI IN		

During Year 3, we initiated a process to begin validation of the gesture recognition algorithm, through recruitment of expert opthalmologists and interaction with Dr. Paul Latkany of the Vision Center for Excellence. The software was installed on a laptop sent to Dr. Latkany to allow him and his colleagues to examine the data. The user interface was altered to add a control that hides the event tracks in order to avoid influencing the analysts during the manual gesture entry. Following a series of meetings and conference calls where the different teams (SimGroup and Latkany's team) agreed on the modality for the validation of the event drive gesture segmentation and task recognition, a series changes was made to the software. As first step, a table of all possible events was created, showing all the correlations between the different low level events combinations and the corresponding high level ones. The package sent to the analysts included the table of events at the different levels (low level, high level 1, subtasks and tasks). Latkany's team would perform manual gesture recognition, entering a keystroke each time a specific event on the table occurs during the playback of previously recorded sessions (user trials at the USUHS Ocular Trauma Courses). The manual entries on a subset of the recorded sessions were to be compared with the events generated by the automatic system. Manual entry would be performed only for the high level events, as the reliability of the low level ones is very close to the ideal – the quantitative identification of instrument connection, geometric position, etc. do not have sufficient statistical noise to be relevant. High level events, however, derive from combinations of low level events (patterns of LLE) which may vary or include errors. Validation would verify the reliability of the selected patterns, namely the logic expressions that will trigger the generation of a HLE. Once manual entry is completed, we will be able to perform a comparison between the two sets of events and calculate the reliability of the event driven gesture segmentation and task recognition. Due to scheduling difficulties, completion of this work was not achieved by the end of the program.

In parallel with this effort, the analysis engine reached the stage of development that allowed the application of metrics exclusively to motions related to the phases of a procedure, excluding those that are not relevant (e.g. simulator-related events such as connecting instruments, which would be extraneous to a real procedure). For example, in the section below, manual entry indicates the start and end of the cleaning phase, while the automatic system further selects only the green section of data for consideration.

Figure 130: partitioning of data into relevant zones

Further, detectable error states have been implemented in the warnings section of the analysis engine (Table 3).

Table 3: Gesture detection system warning engine events - extendable list.

Tasks	Warning Analysis Engine
Cleaning	Improper instrument disconnection
	Timeout for beginning of cleaning
	Timeout for end of cleaning
	Improper instrument set selection
Exploration	Improper instrument disconnection
	Improper instrument set selection
	Timeout for beginning of exploration
	Timeout for end of exploration
	Grasping tissue with excess force
	Grasping while outside of proper workspace
Suturing	Improper instrument disconnection
	Improper instrument set selection
	Timeout for beginning of suturing
	Timeout for end of suturing
	Grasping tissue with excess force
	Grasping while outside of proper workspace
	Cutting suture while outside proper workspace
	Excess distance of needle motion (dangerous needle pulling)

2.3.7.c.v. Simulation Content Frame Structure

Extending the content frames described earlier, during Q7, the scripting language (XML-based) developed to manage the simulation content was extended, introducing new functionalities and extending the syntax. Included in the updated structure describing of the content and functionality for a given node in the procedure were user interface slider button positioning and extensions to the types of buttons present in the simulation flow.

To support good coding practice and simplify development for future users, the capability to add comments in the frame structure was added. Further replacement of the system condition index (numbers between the <system_Cond> tags – see code extract below) with a set of mnemonic labels was implemented.

```
// first slide with menu selection
 <Section>
  <ID>1</ID>
 <Slide>Contents\Simulations\MMVR\Slides\2013MMVROCFGUI.001.jpg</Slide>
  <Audio>none</Audio>
  <Light>0</Light> // no light on the mannequin
  <Events>
   <Button1>0,1,0.0000,0.4870</Button1>   // NO Button on the left side of the screen
   <Button2>3,23,0.8339,0.4870</Button2>  // Next Button on the right side of the screen
   <Button3>0,0,0.4169,0.9000</Button3>
   <Time>0,2</Time>
   <system_Cond>-1,0</system_Cond>
   <system_Cond>0,0</system_Cond>
```

```
    <system_Cond>0,0</system_Cond>
    <system_Cond>0,0</system_Cond>
    <system_Cond>0,0</system_Cond>
    <Warning_Cond>0,0</Warning_Cond>
    <Warning_Cond>0,0</Warning_Cond>
    <Warning_Cond>0,0</Warning_Cond>
   </Events>
  </Section>
```

The architecture was further modified by separating the slide content management and the gesture segmentation. These two last components now run independently. Some of the Gesture recognition routines were improved to increase accuracy and tolerance in detection of incorrect movements in the workspace.

2.3.7.c.vi. Content Development for Scenarios

Towards the end of Year 2, the didactic content for the eyelid laceration module was fully-developed to incorporate the complete set of steps involved from a clinical point of view. These steps were established after reviewing existing training materials as well as from several meetings with our subject matter experts. While comprehensive and available for use on the simulator, for the Ocular Trauma courses, we provided a subset consistent with Dr. Mazzoli's teaching requirements at the 2013 course, allowing a user to be guided by an instructor and immediately begin suturing.

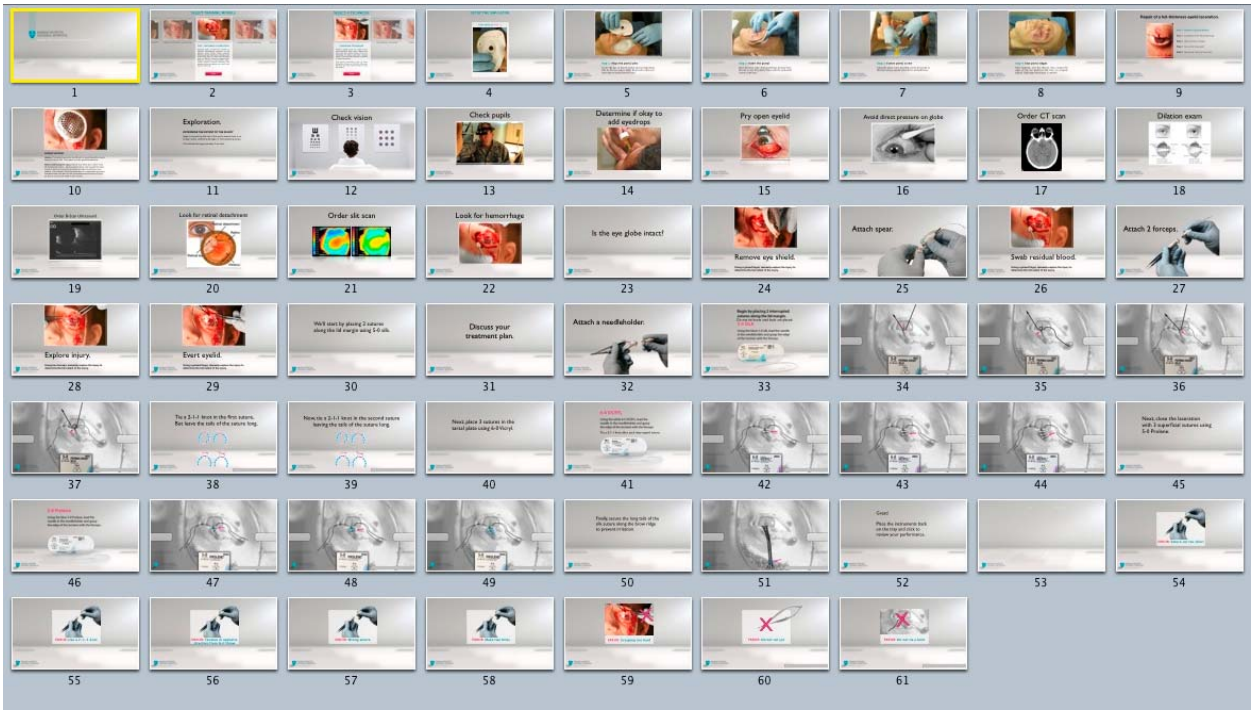

Figure 131: full sequence of available content and sequential guidance slides for lid laceration scenario.

Of the 61 screens of content, such as that pictured below, we set to "hidden" those steps that would typically be involved in patient prep or early diagnosis.

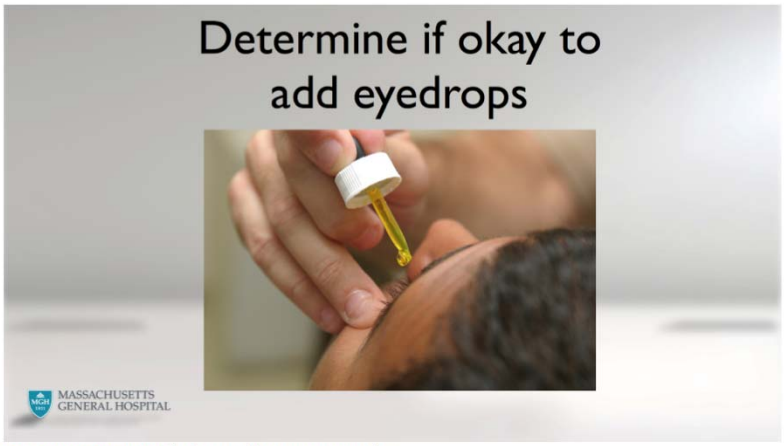

[PLAY AUDIO FILE] Click next button on right.

Figure 132: Pre-scenario preparation informational slide, available for full content use (hidden for 2013 Ocular Trauma Course use)

To better integrate with our underlying learning architecture, the eyelid laceration didactic content was organized as an individual module. As the system is designed to support multiple scenarios, providing an architecture that supports future content is important. The user begins by selecting the module he/she wants to train on and clicks the *start* button in the center of the screen. Additional modules would be found by navigating to the left or right of the central area on the screen.

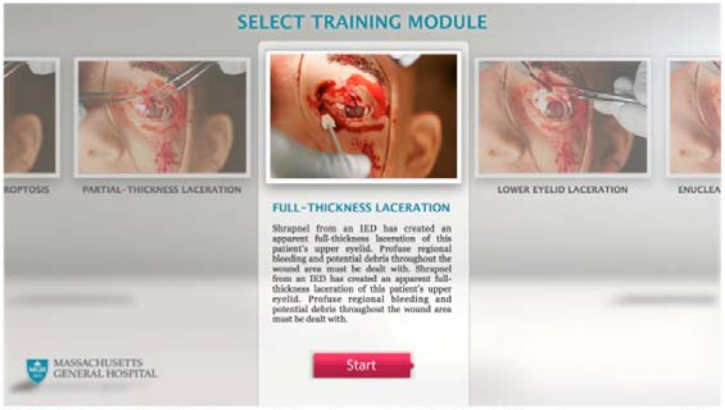

[PLAY AUDIO FILE] Ability to scroll through modules horizontally using arrows on left and right. Click start to continue.

Figure 133: Scenario selection interface screen

Once a module is selected, the user is then presented with the ability to practice a specific technique to suturing the injured eyelid. We found that each surgeon and subject matter expert we consulted had strong opinions about the "right" way to provide guidance to the novice trainee. As they all referenced a "textbook" way of suturing as an underlying foundation to their personal approach, we began by implementing that basic version.

Figure 134: Selection among different techniques for given procedure

Our design allows a novice to learn the nominal approach to suturing a laceration of the upper eyelid. Once completed, the user is then able to practice the individual techniques advocated by different surgeons. As they progress through the scenario, video and audio commentary can accompany a custom-tailored set of didactic content in the interface to illustrate to the novice where they are deviating from the textbook procedure.

2.3.8. "Month 11" - Completion of prototype stand-alone ocular and craniofacial trauma training module, control software supporting sensing and response functionality.

During Year 3, the hardware of the standalone system reached a near final stage, with the addition of a mounting frame that allows for the attachment and reconfiguration of a touch-screen interface (to replace the prior laptop-based system), and a four degree of freedom microscope mounting system for positioning the AR microscope relative to the eye module.

The microscope mount is designed as a closed loop, 5-bar linkage, with a pair of thumb screws to either side of the microscope head that each lock two degrees of freedom of the linkage. The linkage allows for repositioning of the microscope head in the horizontal plane above the mannequin head and moderate rotation of the microscope (in addition to that available by rotating the microscope within the ring-mount). The ring-mount provides adjustment of the vertical (focus) position of the microscope. As with the touch-screen mount, the microscope mount is modular, allowing for quick installation and removal without modification of the rest of the system, to facilitate rapid transition between oculoplastics and eye globe surgery scenarios (Figure 135).

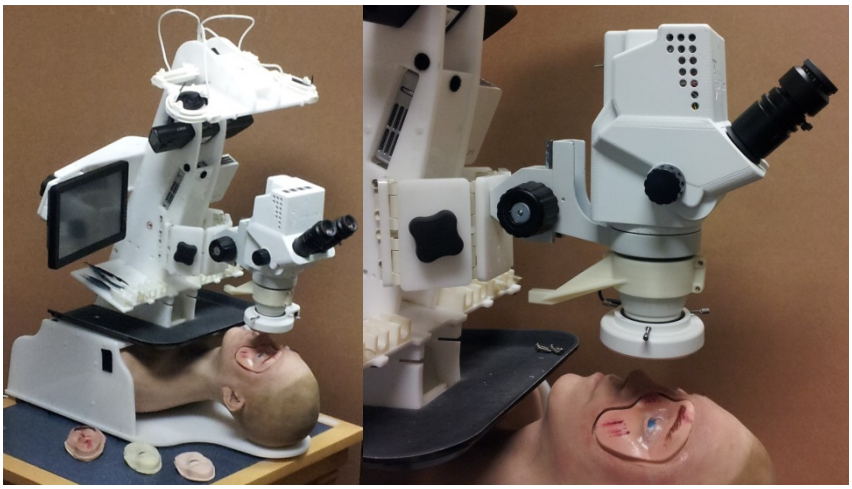

Figure 135: Standalone system with modular touch-screen and AR microscope components mounted. The head form remains to be replaced by the new skeleton and full-face versions of the head and trauma modules. In the left image, note the revised instrument tray, which now does not include the suture boxes (as recommended by experts at USUHS) and the somewhat extended utility tray, which now extends closer to the mannequin's chin than the original version did.

The touch-screen mount is modular and can be installed either to the right or left of the stand to accommodate users performing procedures on the left or right of the mannequin, using only two large thumb screws (Figure 136).

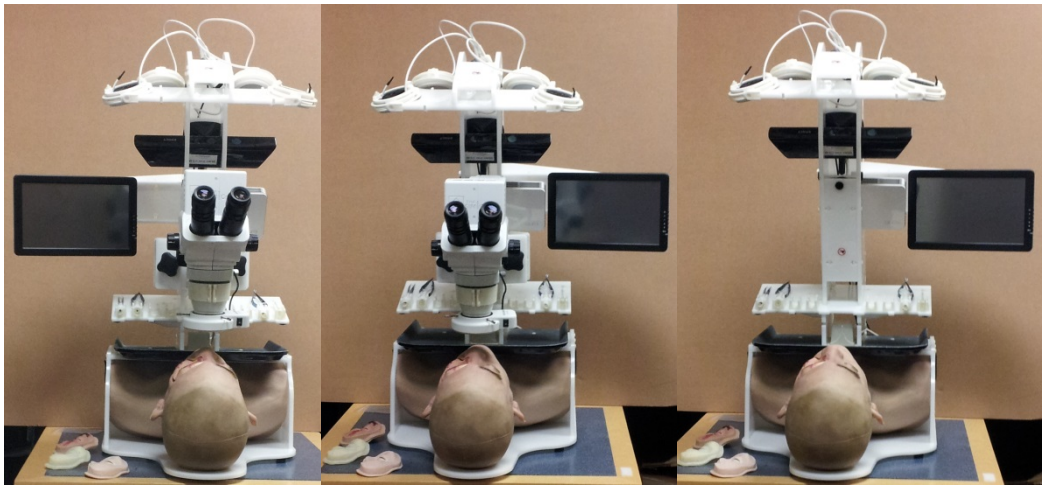

Figure 136: Images demonstrating modularity of the display components; Left or right positioning of the touch-screen, attachment or removal of the AR microscope.

Following revisions and improvements after each of three demonstrations/uses at the annual USUHS Ocular Trauma course, the system design and software have reached a stable, useable form. The standalone platform includes the modular components to support the AR microscope. During testing of the system, it was found that the weight of the microscope tended to make the system prone to tipping towards the user with small amounts of force, so a revision to the microscope mount, with an extension

towards the rear of the system and steel bar counterweights, was designed and installed in the final months of the program (Figure 137).

The new version of the head and neck now replace the original head form, attached to the frame using a new adaptor platform. The location of the eyes of the new head have been closely aligned with those of the old mannequin, relative to the magnetic tracking system emitter, minimizing any changes to the interface software that depend on the location of the Regions of Interest around the eyes. The newly acquired additional instruments described at the June 2014 IPR meeting were installed into the standard instrument holder structure, and a final revision to the mini-circuit board for the holders which simplifies adjustment of gains, offsets and instrument ID detection was designed and awaits assembly into the full suite of instruments.

This system was shown at IMSH 2015 in the "TATRC Corral".

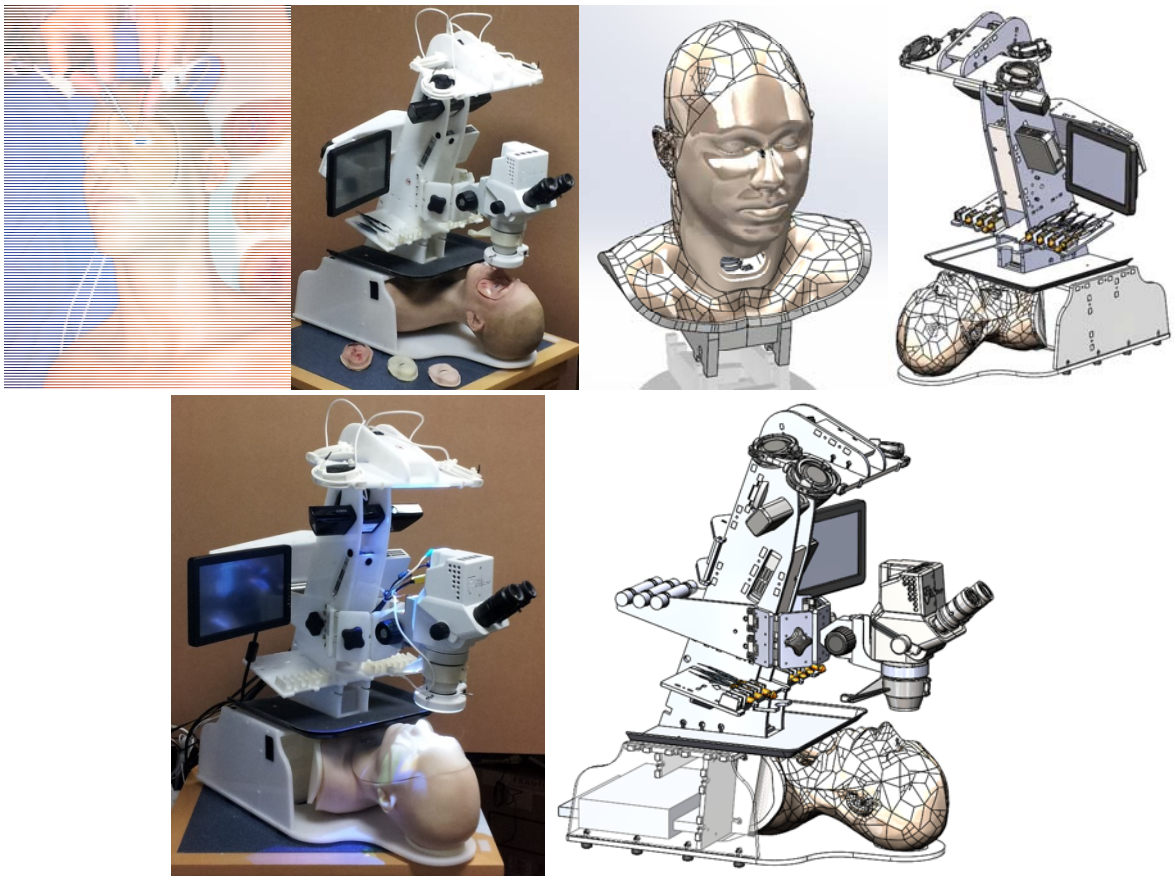

Figure 137:Original head form and standalone structure; New head form with adapter mounting structure to attach directly to the standalone frame. Assembled frame with new head. System with counterweights for AR microscope.

In addition to the structure, alternate facial modules, supporting training for retrobulbar hemorrhage and facial fracture were prepared. The first facial model shown in Figure 138 is the default, healthy

tissue version, which can be modified by manually lacerating the lids. The face including forehead, tissues forward of the ears and the neck below the larynx forms one full module that is attached to the cowl, which covers the sides and back of the head, and the neck past the base of the neck, using a fine tooth zipper system. The cricothyroidotomy site has been left as a separate component for ease of replacement. In the final iteration, we chose to create unified eye/face trauma modules, rather than a series of distinct components to be assembled on site with gaps and margins at multiple sites about the face. The gap between cowl and eye module of the old version of the head form could never be minimized to the point of being unremarkable, and was present directly in the field of view of the trainee.

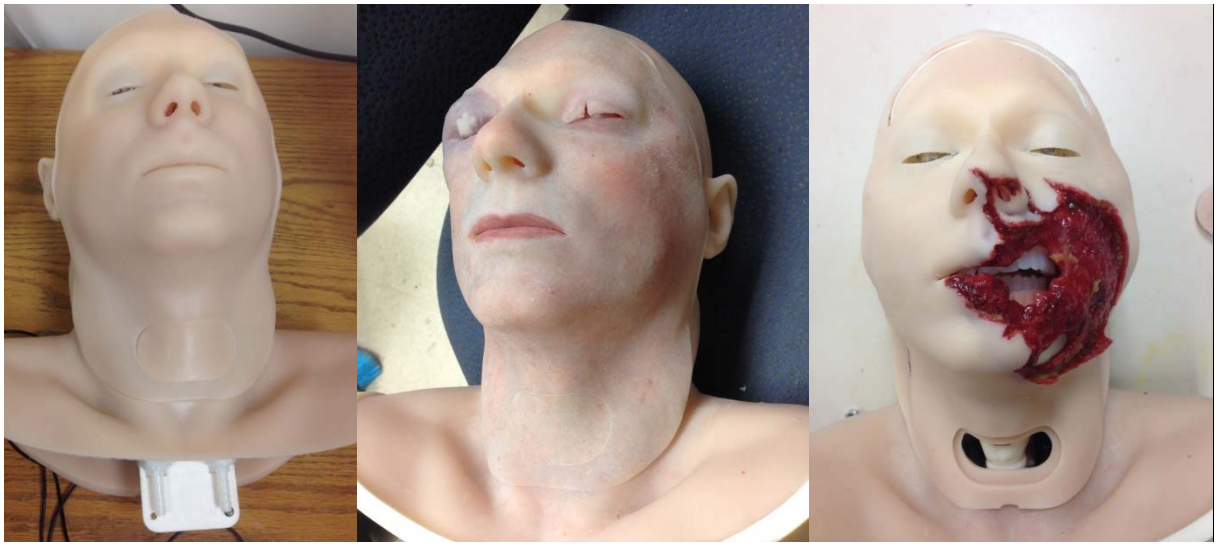

Figure 138: Base healthy face attached to cowl. Face module with swollen periocular tissue. Face module with massive trauma and exposed oral cavity.

2.3.9. "Month 12" - Testing of fit, function of sensors, actuators, replaceable components.

The following sections review testing of a variety of the animatronic components of the system

2.3.9.a. Air muscle and neck motion testing and additional neck design

Following early experiments to characterize our air muscle designs, described above, during Q5, we completed the test rig to allow testing of motion in all directions and reevaluate the capabilities of the new muscles (Figure 139). This system appears to be sufficient to generate neck motions that would be used in the mannequin-integrated version of the head (Phase III) to simulate a struggling/gagging casualty, a feature that does not appear to be present in the commercial market.

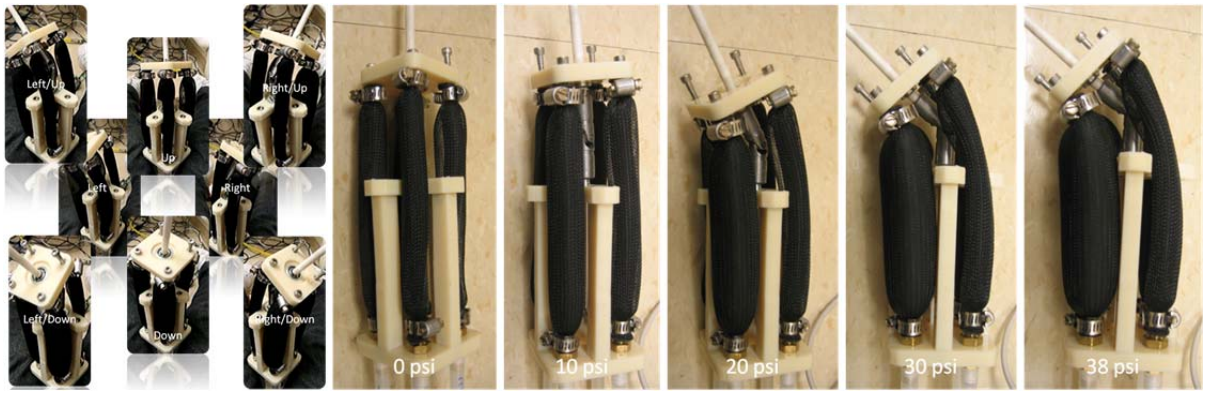

Figure 139: Motion control of neck using combinations of single or adjacent air muscles. Activation of single air muscle to illustrate range of motion. Base of "neck" at the bottom, "head" would be at the top.

In Q8 we continued this work in designing a more anatomically correct neck structure that integrated the neck pitching motions with head yaw. The mannequin-integrated version of the system incorporates the active motions, while the stand-alone version retains the linkages to allow the surgeon to passively move the head with the same, normal range of neck motion, but without the actuation components, thereby minimizing metallic elements that can distort the surgical instrument tracking system.

Using the anatomical models that were segmented during Year 1 and concepts developed during our earlier COMETS autonomous casualty simulation mannequin project, we created a flexible neck structure using a series of vertebral bodies and disks, each of which accommodates a fraction of the full flexing range of motion of the human neck.

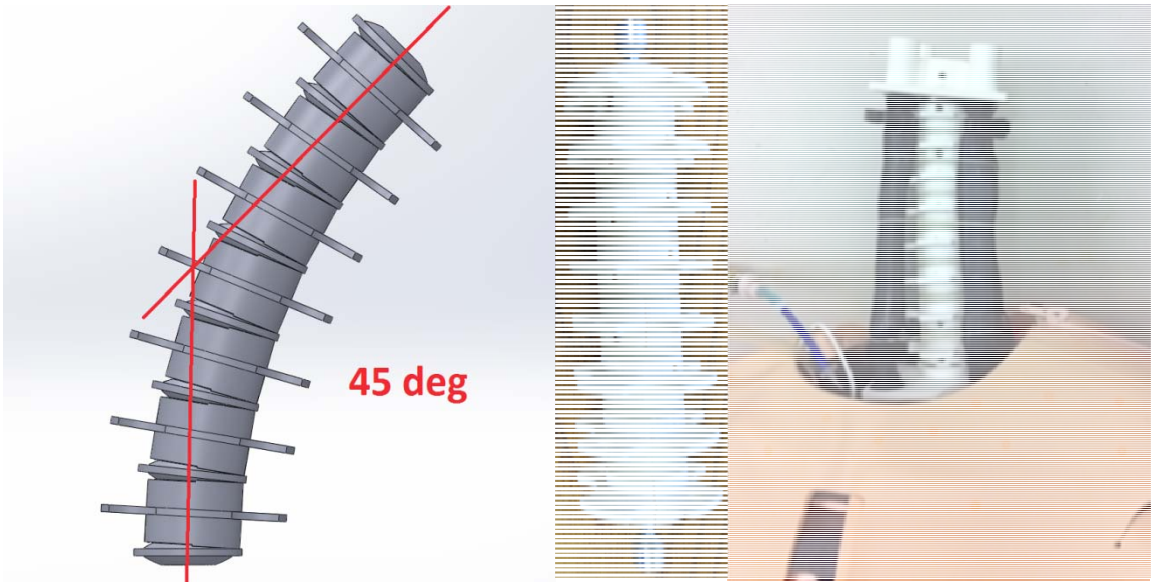

Figure 140: Anatomically inspired neck structure CAD model, physical implementation, and mounting to trauma mannequin.

The vertebral bodies have flanges extending away from their cores that mate with the McKibben muscles, so that they rotate with respect to each other when the head turns. A central flexible transmission shaft provides tensile strength and links the base of the neck to a head rotation motor that will be mounted in the head. Human neck range of motion is different in flexion/extension and lateral abduction, so the vertebral bodies were designed such that their surface contours allow for more motion before one body collides with the next at the front and back of the body than the left/right direction.

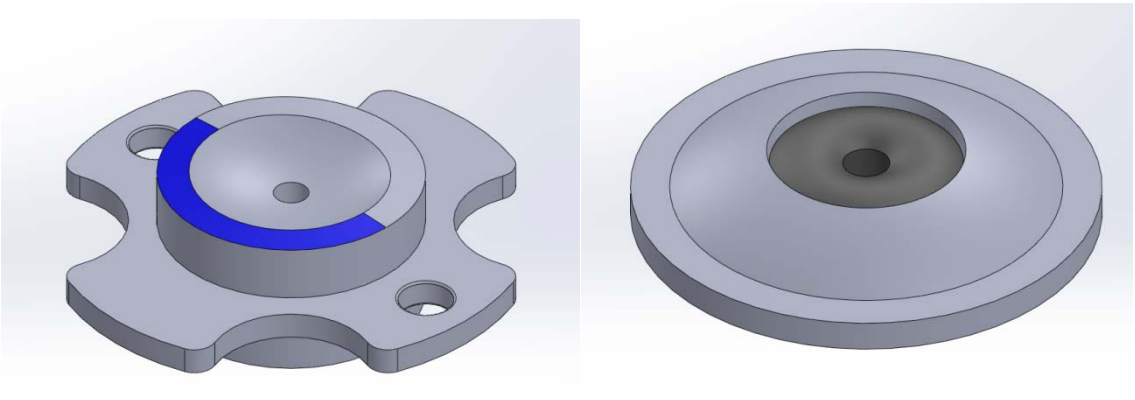

Figure 141: Vertebral body and disk designs

In the course of designing the neck mechanism, we reviewed the McKibben muscle design. The earlier work and inquiry showed that sparse mesh permits larger overall deformation. Thinner bladder walls, for a given material stiffness allow for greater deformation for a given supply pressure, as does a softer material for a given thickness. We identified both thinner wall silicone tubing and lower durometer tubing and redesigned the muscles to accommodate the new material. In addition, we found that the original tube fittings used as attachment points, which were smaller in diameter than the silicone and mesh tubing diameters resulted in pinching at the muscle ends, reducing the available amount of muscle contraction. Related to that, standard hose clamps that had been used were prone to pinch and puncture the silicone tubing walls. We replaced the fittings and hose clamps with larger diameter fittings and plastic snap-grip hose clamps without the hard, sharp edges.

With these design changes, we reexamined McKibben muscle performance, comparing the thin and two grades of soft rubber to determine the best available of materials sourced from industrial supply houses. The thin wall silicone was found to have the best performance of the materials tested.

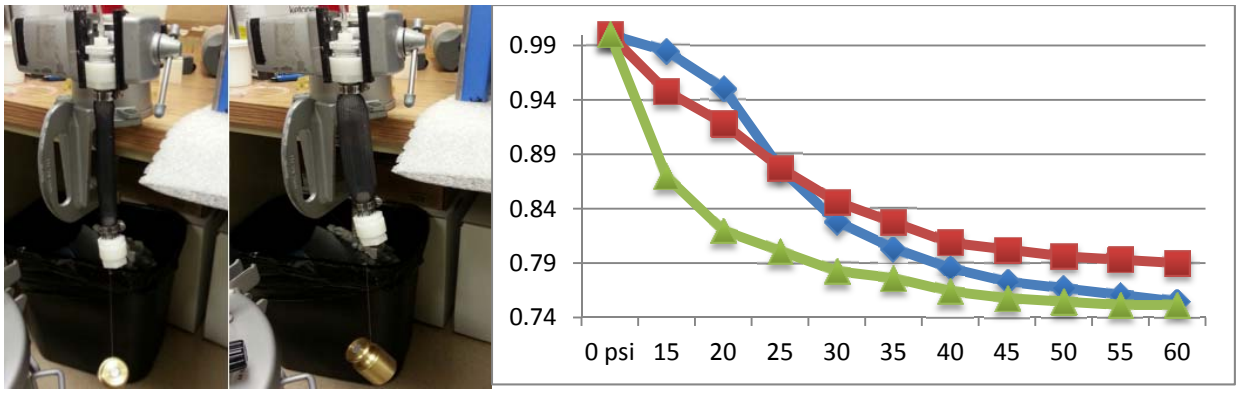

Figure 142: Retesting McKibben muscles with new materials, fittings. 500g load results shown: relative contraction for black latex (blue), amber latex (red) and thin wall silicone tubing (green)

A mating platform (shown extending below cowl in Figure 138) was designed to attach the neck design to the Laerdal SimMan Essential mannequin that we acquired in Q6. Using the pneumatic control system described above, we tested the range of neck motion. While the neck assembly was capable of the full human range of motion, when coupled to the air muscles, the available contraction appeared to reduce the actual range delivered. In addition while the neck flexes quite far when the muscles contract, the platform shown (representing the mounting structure of the skull) may pitch by a lesser amount. The mannequin therefore moves less under its own control than can be generated by manual manipulation of the head/neck by a trainee. In future work, we will endeavor to increase the controllable motion, however for the purposes of creating a system that can present autonomous motion that will indicate consciousness and present a simulation of a casualty resisting treatment (e.g. intubation/cricrothyroidotomy), this system satisfies the basic goals.

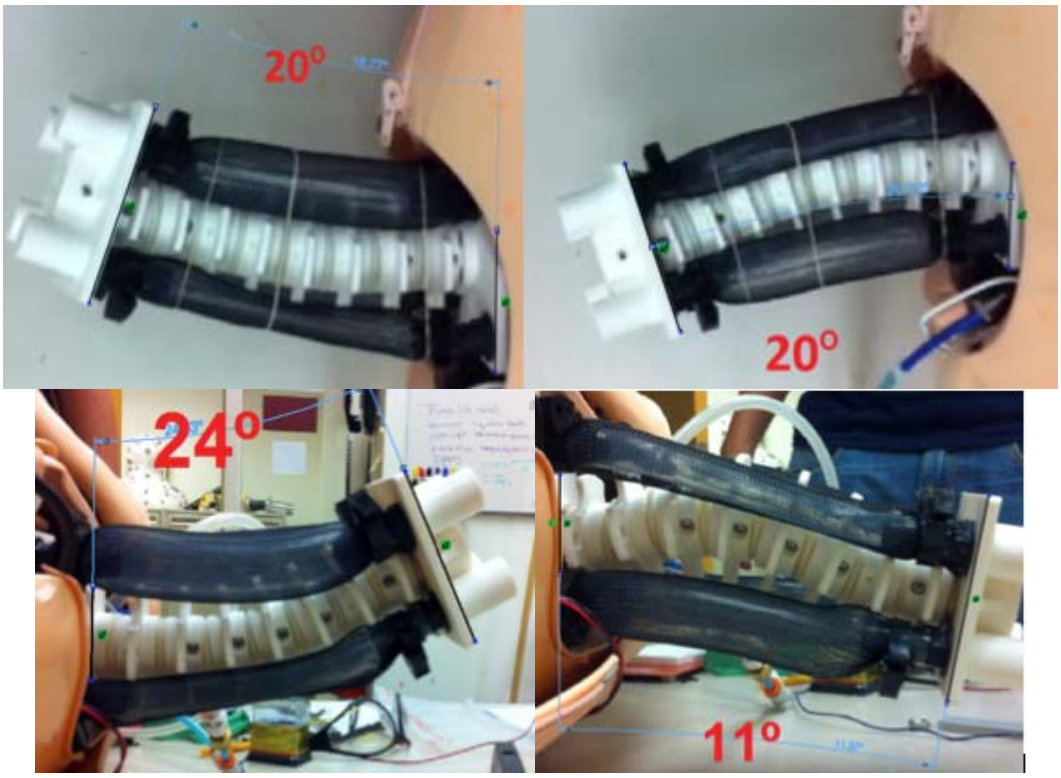

Figure 143:Initial range of motion of neck actuation system

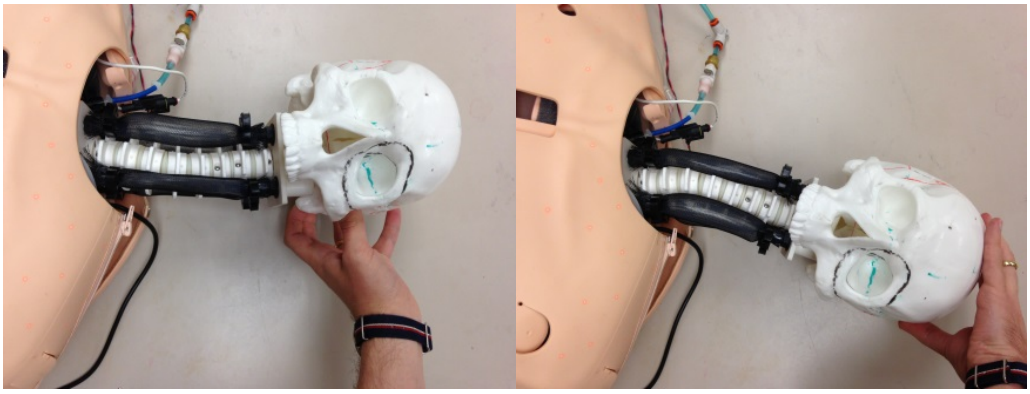

Figure 144: Manual manipulation of neck with attached skull model

The current range of rotational motion of the head with respect to the neck is +/- 55 degrees, similar to that of the human head relative to the upper segments of the cervical spine. Early testing performed without the cowl and face installed suggests that the existing motor may not be able to provide sufficient torque to drive the system through this full range, however an alternative design is available should the full range be desirable later (e.g. for commercial partner development). The jaw motion is similarly nearly the full range of angles (30 degrees), with the final value to be determined once the facial component is installed.

In Year 3, we examined the detailed placement of the anchor points for the air muscles; while there is limited real estate for the upper ends of the muscles, the neck opening of the mannequin allows for both wide and narrow positioning. In principle, a wider stance should provide for a higher activation torque when flexing the neck, while a narrower stance, with the muscle closer to the axis of the neck, should result in a larger range of motion. Findings were mixed, with the expected results occurring in the back and left directions, the reverse to the right, and no noticeable effect towards the front. As such, the narrow footprint configuration will be used, to conserve space for other elements within the neck.

During Year 3, we extended this work to add anatomical features of the spinous processes, with fracture elements included. These are designed to be palpable landmarks and indicative of potential spinal injury. A palpation test object was created and reviewed by our local SMEs to provide feedback on whether the choices of skin and muscle substitute materials allowed for a realistic tactile sensation.

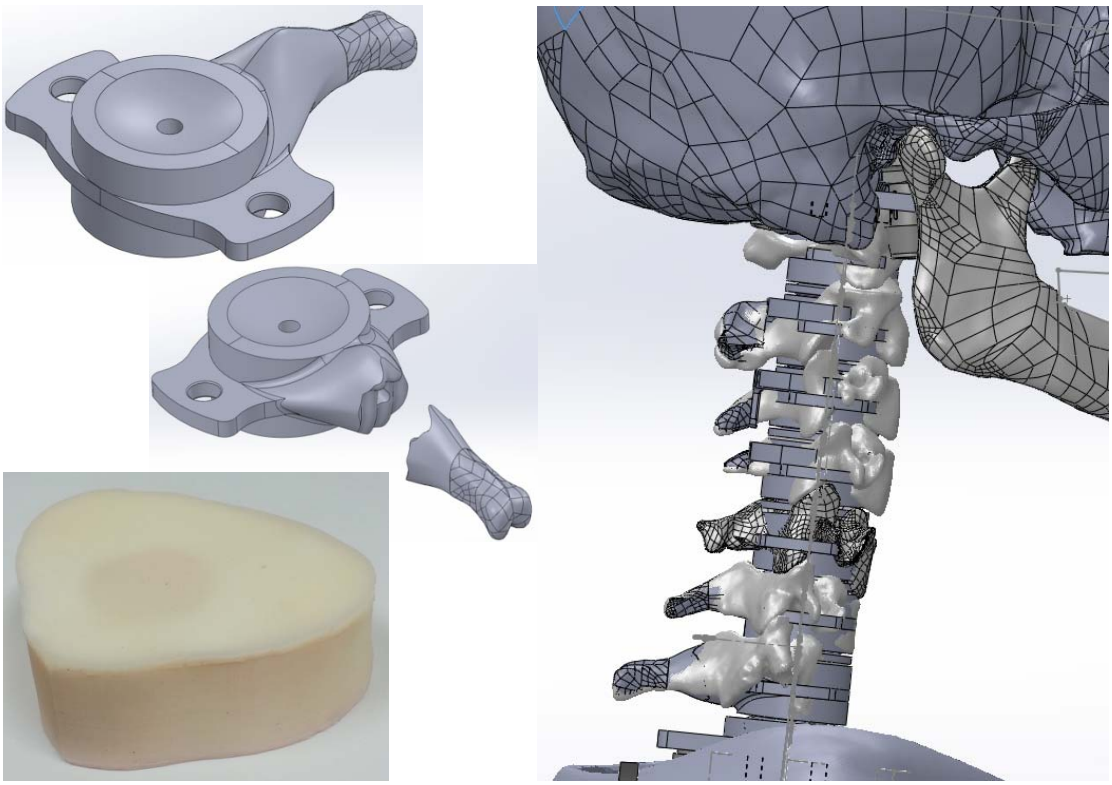

Figure 145: Neck element design with addition of anatomical features to the common core. Palpation test module, including neck surface contour based on CT anatomy with embedded vertebral body and fractured spinous process.

2.3.9.b. Blink actuation testing

In Q7, much progress was made on the blinking mechanism. Based on developments described above, a prototype blinking portal was created which demonstrated an effective solution using embedded nylon string in the tarsal plate which can then be actuated by a servo. The string can be physically attached to the substrate in future iterations. This solution is consistent with the earlier developments of the servo-driven blink mechanism.

Testing revealed that changes to the portal were necessary, consisting of incising relief flaps into the silicone. These flaps allow the silicone to bend more freely and control the way in which it deforms. In production, these flaps will be incorporated into the mold design. This feature addresses one of Dr. Mazzoli's principal suggestions regarding the eyelids, namely that redundant tissue should be present, permitting more realistic manipulation and proper creasing when the eyelid blinks.

Figure 146: Servo control of module eyelid blinking

2.3.10. "Month 14" - Design of modifications to trauma mannequin for integration of ocular and craniofacial simulator structure module.

This program conceived that the eye/face trauma simulator would be integrated into a full-body medical simulation mannequin, ideally a commercial system, or into our prior COMETS autonomous training system mannequin as necessary. During year 1, we conducted a series of examinations of a cross section of commercial mannequins including:

- Laerdal SimMan at the Harvard Center for Medical Simulation
- Gaumard Hal at the Harvard CMS
- A prototype of the CAE-Healthcare Caesar mannequin, while on display at the MGH Learning Laboratory facility, which is the core of MGH's simulation-based training efforts
- A CAE/METI iStan mannequin at the Tufts University School of Medicine-Clinical Skills and Simulation Center
- A CAE/METI METIMan, which was briefly on loan to us specifically for examination

- A Laerdal Nursing Kelly system used by one of our team (Bardsley) for an unrelated project

In addition, one of our team (Ottensmeyer) had a parallel project to modify the head of a Laerdal ALS simulator to add functionality, allowing us to closely examine the structure, especially the airway components, of this mannequin head/neck module.

Based on the analysis, we initially considered acquiring a Laerdal Kelly mannequin for test integration. This lower cost, lower fidelity mannequin than planned for the final system would allow us to "walk before we run" and allow for additional space within the physical structure of the mannequin for necessary actuator, reservoir, power and other systems. Efforts towards development of the standalone system, however, took early priority, so we later moved directly to a higher fidelity system.

During Q5 we discussed the availability of CAE Healthcare's Caesar mannequin, which was not expected to be available for purchase during our original timeline. At the MHSRS 2012 conference, one of the mannequins was on display and the sales staff conveyed that they were available for distribution. Examination of the system, however, suggested that integration of a new head onto the mannequin would be more difficult than the options we had been examining with Laerdal. In addition, the Laerdal system that had sufficient capabilities for our purposes costs approximately half as much as Caesar. In addition, an equivalent of Laerdal's SDK was not available for Caesar. As a result, we submitted a purchase requisition for a Laerdal SimMan Essential, which arrived during Q6.

In Q6, the early work involved opening the mannequin to identify power and air pressure supplies, test its normal functionality under control of the Laerdal software, and begin a detailed look into the SDK. Laerdal provided technical details of the mannequin's structure, pneumatic supply and electrical and communications capabilities.

We combined the CAD models of the main internal structural plate from Laerdal with a 3D laser scan of the outer surfaces of the mannequin shoulders, using a long focal distance photo of the mannequin to aid in aligning the head/neck anatomy with the original mannequin head. This is serving as the basis for our structural design of the connection and mounting of our head to the mannequin's body.

As described earlier, we designed for use of the mannequin's air and power supply to drive the mechanisms for the head and neck.

Immediately inside the mannequin's left shoulder are a series of electrical connectors, one of which is dedicated for head control. It includes terminals for 12V supply and a serial communications port that commands the standard mannequin head. We added our own connector in place of the original to access power and detect the pulse-control signals of the mannequin, so that the hemorrhage system could be synchronized with the mannequin's pulse. This was used to power the Arduino Mega and the series of pneumatic latching valves described in section 2.3.5.a.v. As described earlier, in addition to the control of the valves, the Arduino's software was expanded to control up to 12 servos (including the eight designed into the blinking/eye motion/proptosis mechanism), two electronically controlled pressure regulators, up to 10 PWM-controlled devices (e.g. fluid or air pumps) or other digitally

controlled devices (e.g. additional valves for hemorrhage), up to two stepper motors (head rotation), measurement of 16 analog sensors.

The pneumatic supply provided pressure that varied from a peak of approximately 1 atmosphere and fell by approximately 25% before the mannequin's compressor turned on to recharge the internal reservoir. This pressure drop is related to the mannequin's own breathing mechanism, which consumes air during each breath (small internal bladders push the main chest plate outwards), allowing the system pressure to fall since there is no regulated internal reservoir. Our testing of the neck mechanism under this air supply showed that with the fall of system pressure, actuated air muscles lost force cyclically as the mannequin compressor cycled, with slowly changing neck position as pressure fell, and a return to the set position when the compressor ran. For the prototype, this ongoing variation in neck position was considered to be a useful indication of consciousness.

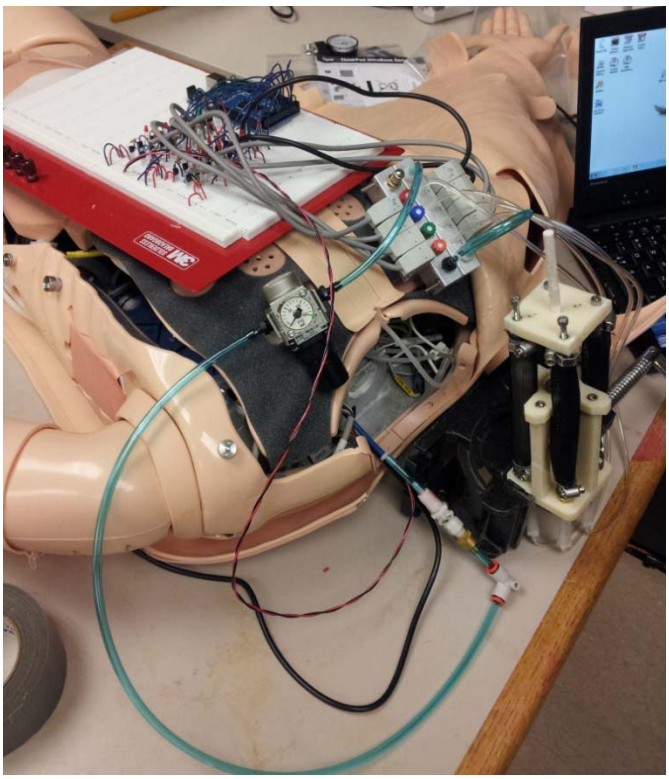

Figure 147: Early test of air muscle system integrated with mannequin air and power supply. Blue tubing is connected in place of stock head air connector, twisted pair (black/red) wires supply mannequin power to the solenoid valve control circuitry and the Arduino Mega microcontroller.

During Q7, we isolated one of the problems that appeared during discrete component testing: while the air muscle valves are specified for use with 12V control signals, and the mannequin's supply voltage is also 12V, the transistors that switch the valves on and off have their own voltage drops in series with the valves. As a result, the voltage available to the valves is reduced below 12V, by an amount that makes valve activation unreliable. Two solutions were identified: replace the 12V valves with their 6V equivalents, or use a voltage converter which boosts the 12V supply up to 15V (at the cost of drawing more current from the batteries), so after the transistor voltage drop, the valves would still have enough

driving force to reliably activate. A suitable voltage converter was ordered, received and tested to confirm that it functioned as planned.

During Q8, in conjunction with the neck mechanism developments described above, we used the CAD models provided by Laerdal for the main frame of the mannequin to create a mounting frame that mates the neck to the mannequin main body. The attached neck is shown in Figure 143 and Figure 144.

The upper end of the neck is anchored to the neck and bends on it using an integrated vertebral disk structure. The lower end is fastened to a custom mounting plate that mates with the Laerdal mannequin frame. This plate can be replaced with alternate structures to make the system physically compatible with other mannequin bodies.

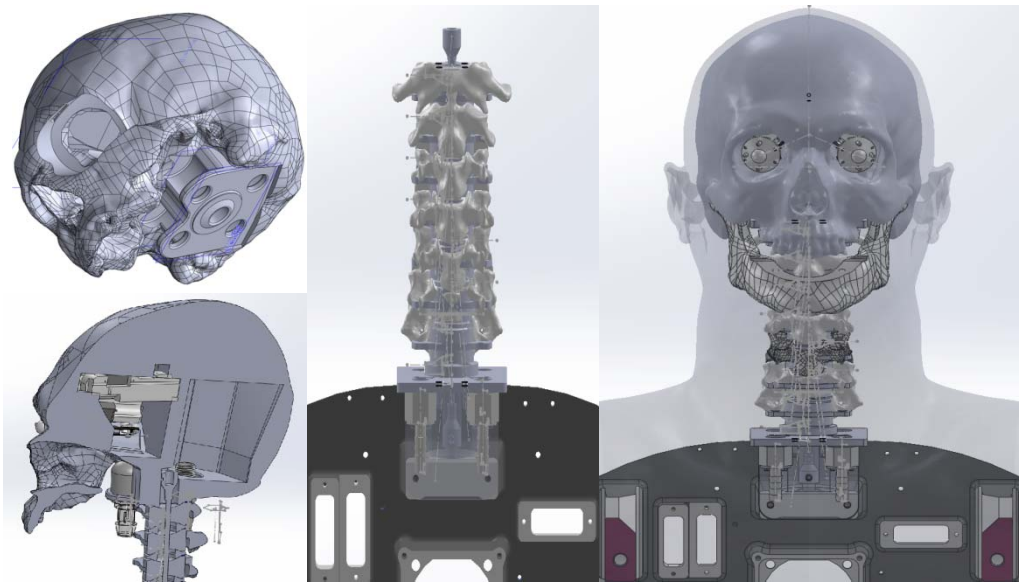

Figure 148: Skull attachment design features for the neck, accommodating anchor sites for the ends of the McKibben muscles; neck system design as mounted to Laerdal structural frame, with CT anatomy spine overlaid; CD model including skull to verify proper scaling and size of neck components.

Based on our findings, we determined that with the exception of removal of the mannequin's stock head and disconnection of power and fluid lines, no further physical modifications to the mannequin were necessary to accommodate our system. The spaces in the abdomen and the chest were sufficient to fit the additional valves, electronics and fluid reservoirs necessary for integration of the head/neck into the Laerdal body.

Figure 149: Disassembly and examination of Laerdal SimMan Essential mannequin in support of designing interface components to mate the new head/neck to the commercial body. Aligned CAD models in use for design of attachments between new head/neck and stock mannequin.

2.3.11. “Month 16” - Revision of physiology model software.

The selection of a mannequin platform substantially drove the approach to physiological integration between the eye/face trauma system and the mannequin. The Laerdal SimMan Essential standard control interface at the time of acquisition provided detailed controls for all of the available physiological parameters and mannequin actuators. As such, it has no independent physiological model driving its behavior; the instructor/simulator technician actively controls, for example, changes in blood pressure (which may be set for step or ramp changes), but blood loss or trainee intervention do not directly affect mannequin physiology. This was distinct from the more expensive CAE/METI systems, for example, which had an underlying physiological model.

In Year 1, in advance of receipt of the physical mannequin, we obtained access to the Laerdal application programmer’s interface software tools, which Laerdal provides to developers so that they can develop control and feedback tools for their advanced mannequins (e.g. SimMan). Discussions with Laerdal’s Jim Azukas showed that their lower cost systems, some of which were compatible with their new SimPad technology, would not have an API available in the near term, so use of such mannequins may have permitted integration with power and fluidic systems, but control and physiological modeling would have to have been implemented separate from, rather than integrated with the mannequin’s own systems.

At that time, we also examined open source physiology models, such as Hummod [Hester et al., 2011] in the context of preparing a proposal for the JPC-1 "Developer Tools for Medical Education Public Physiology Research Platform" program announcement, and discussed physiological interactions primarily related to eye trauma/surgery with our SMEs Mazzoli and Freitag. In relation to performing eye surgery, they identified only one characteristic physiological effect (beyond those related to blood loss or airway obstruction), namely the oculocardiac reflex. This reflex is triggered upon compression of the eyeball or traction applied to intraocular muscles, and results in a decrease in pulse rate. Given the direct control of the Laerdal mannequin that was selected, this could be implemented by either presenting the operator with the magnitude of force applied to the globe (the scope of this simulator did not extend to inclusion of intraocular muscles) and relying on the operator to adjust heart rate, or a semi-automatic system, in which elevation of globe force would generate a command to decrease mannequin heart rate.

This work began substantially during Q7. In the first two months of the quarter, we examined the Laerdal SDK in detail, starting with familiarization with the programming language (C#) and with the layout of the VS (Visual Studio) C# project. To avoid potentially damaging the mannequin, when necessary we performed preliminary testing of code using the Laerdal virtual mannequin system, which presents a system that responds to code written using the SDK the same way the real SimMan would.

The initial focus was the LaerdalSimulatorAPI.dll dynamically linked library. The goal of the work was to implement an appropriate approach to use the functions and methods provided by the dynamic library, in order to use them in a new C++ application. As the source code and documentation of the DLL was not provided, extrapolation of the content of the DLL was necessary. To help with that we used the "Object Browser" VS functionality and the free .NET decompiler and assembly browser "JetBrains dotPeek 1.0" [6].

Early approaches aimed at minimizing the number of additional files needed while retaining as much simplicity as possible in the conversion the functionality available in the C#-based SDK, to functions compatible with our C++-based simulator were unsuccessful. A subsequent approach treating each component of the C# SDK separately, creating a large library of files to form a bridge between the two languages was attempted by one of our interns next.

2.3.11.a. Developing the Wrapper for LaerdalSimulator.dll

The DLL wrapper works as a bridge, linking the C# DLL with the C++ client application. In order to create the link, every member (classes, delegates, interfaces and enums) of the C# DLL, had to be re-declared inside the wrapper.

To create the wrapper we used an approach based on creating a different C++ file for every class implemented in the original DLL, and another single C++ file which contains enumerators and interface classes. Because of that, the wrapper project consists in the following files:

[6] Download and documentation available at www.jetbrains.com/decompiler

- **ExceptionData_Wrapper.h**, which contains the declaration of the class ExceptionData_Wrapper and its methods/constructors/destructors
- **ExceptionData_Wrapper.cpp** which contains the implementation of the methods of the class ExceptionData_Wrapper
- **ManikinException_Wrapper.h** which contains the declaration of the class ManikinException_Wrapper and its methods/constructors/destructors
- **ManikinException_Wrapper.cpp** which contains the implementation of the methods of the class ManikinException_Wrapper
- **ManikinFactory_Wrapper.h** which contains the declaration of the class ManikinFactory_Wrapper and its methods/constructors/destructors
- **ManikinFactory_Wrapper.cpp** which contains the implementation of the methods of the class ManikinFactory_Wrapper
- **LaerdalSimulatorAPI_Wrapper.h** which contains the declaration of interface classes, delegates and enumerators.
- **LaerdalSimulatorAPI_Wrapper.cpp** which contains the declaration of the enums (*as they are declare already in the .h file maybe I would delete them from here*) and would contain (*still to be done*) the implementation for some get/set methods for the interfaces.
- **LaerdalSimulatorAPI.h** header file of the original DLL created by me (*need some changes)*.

To test the wrapper our CS intern created a small Dialog application that showed the client a window and performed a series of functions based on activation of dialog buttons.

The first test performed was on the class ExceptionData_Wrapper. It contained a series of properties (data) that could be read and written. This simple test did not need require the protection of linking to the virtual mannequin and was performed directly on the physical mannequin. The testing procedure comprised the following steps:

- calling the **set** method of the property declared inside the wrapper. This is linked to the **set** method of the C# DLL, so whenever a new value is passed to the wrapper **set** function, the same value would be passed to the property of the LaerdalSimulator.dll.
- calling the **get** method declared inside the wrapper. Because of the linkage, this would read the value of the property contained in the C# DLL
- if the two value are the same, the linkage is verified

The test demonstrated that a link was built, a first step towards establishing communication between our application and the mannequin. Unknown to us at that time was that there was a mismatch in firmware versions between the SDK and the purchased mannequin that slowed further progress until we found and resolved this issue.

In Year 3, we evaluated LLEAP, a new version of the SimMan SDK that became available. As it was still under pre-release development, we determined that we would continue to use the older SDK and consider a shift to the newer technology in future work.

Over the remainder of the year, we developed our final solution for linking our software with the mannequin to allow the control and querying of various physiological parameters. We established access the heart rate and the pulse-oximeter functionalities, which are representative of all of the other accessible parameters of the mannequin. As the SimMan Essential has no internal physiology model, control of its parameters by our system is equivalent to control of the same parameters from the instructor's laptop, essentially completing the conceptual component of integration of our system with the controls of the mannequin.

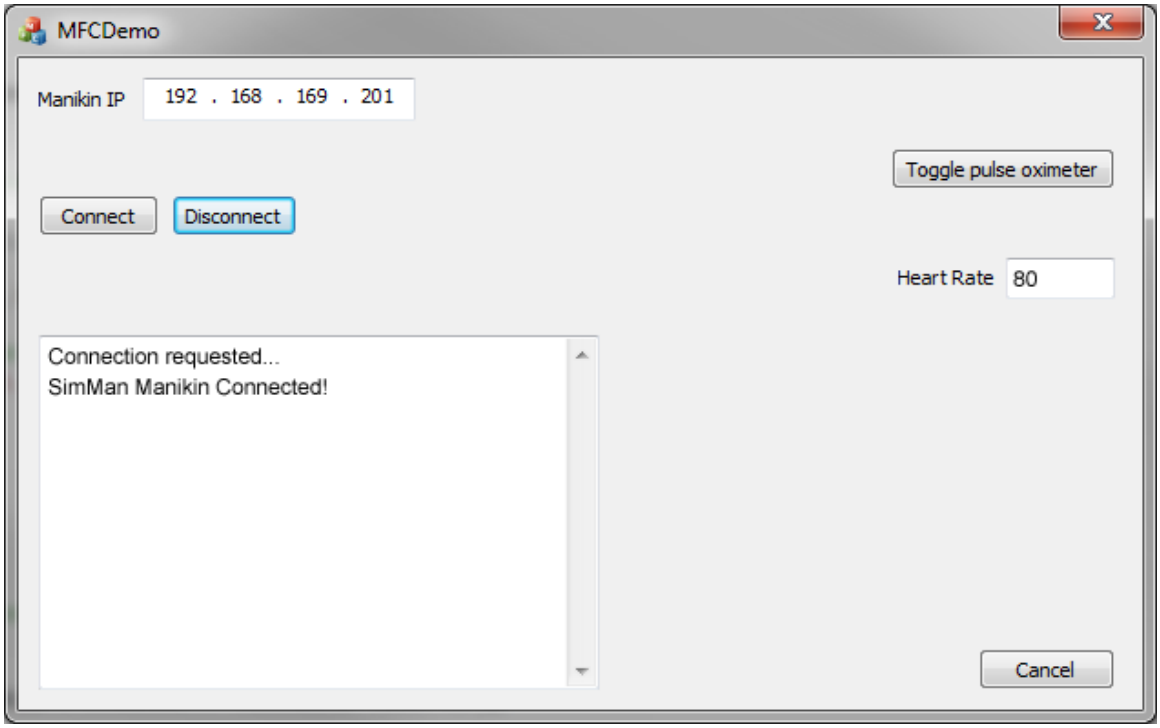

Figure 150: Sample interface showing connection between software and mannequin, a text box where the mannequin's heart rate can be sampled (from the instructor laptop) and set (overriding instructor laptop settings), and the pulse-oximeter sensor can be turned on and off. The full suite of SDK-linked physiology parameters is accessible using the same technique.

We made additional progress in interfacing with the physiology of the mannequin. We can control all parameters that can be externally overridden, and read the mannequin's physiology for the remaining parameters that are set internally. The window below shows the WiFi connection parameters, samples of the mannequin's parameters, and control over both binary (on/off) controls and analog values (e.g. heart rate). The actual application of these parameters will be internal to the simulator and its interface.

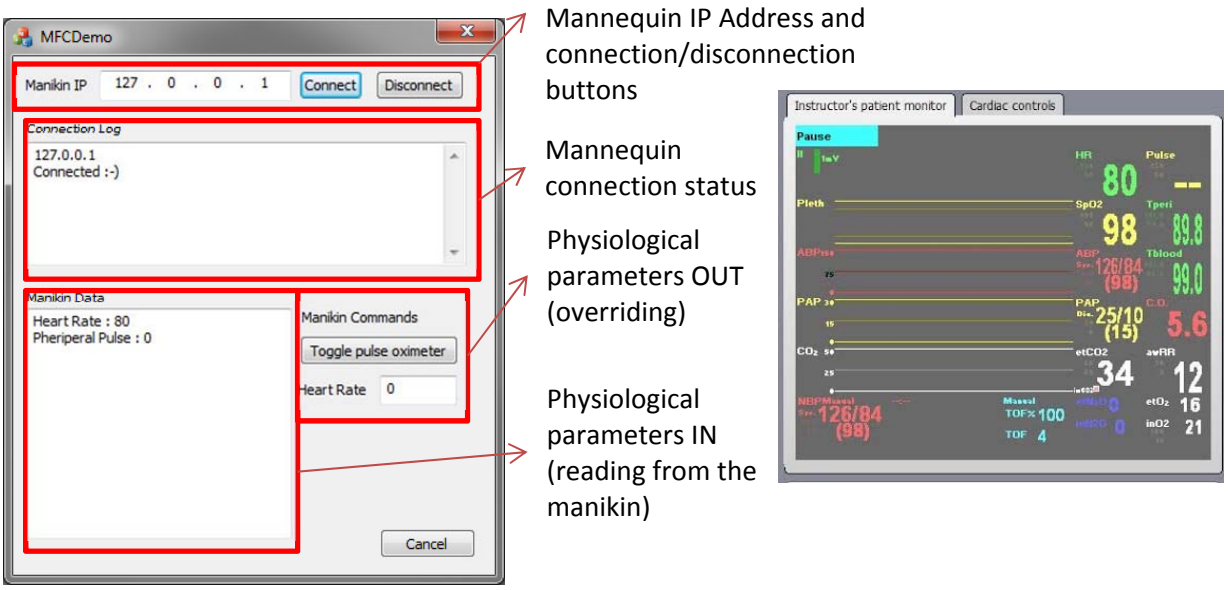

Figure 151: (Left) Parameter control interface panel (Right) Display from Laerdal mannequin showing Heart Rate matching set value from control interface panel (80bpm)

2.3.12. "Month 18" –

2.3.12.a. Completion of prototype integrated ocular and craniofacial trauma system with mannequin.

During Year 3, we completed mounting of the head form to the mannequin's body, primarily for fit testing and to confirm clearances between Laerdal and OCF components. All of the functionality of the system had been previously established. Examples of such instances show the OCF head and the stock component laid next to each other, with the OCF head attached to the mannequin's body, and the final version with the swollen periocular tissue face module attached. The "cowl" fits within the standard opening of the mannequin neck.

Figure 152: Head/neck with Year 3 partial facial module overlaid, attached to Laerdal SimMan Essential. Original SimMan head shown for references. Final version of head/neck form mounted to mannequin with swollen periocular tissue face module attached.

2.3.12.b. Completion of augmented reality system supporting stand-alone simulator.

The system that was created through this project provides for a wide variety of modes for interacting with the artificial anatomy, beginning with conventional video display and touch screen control, and extending through position-tracked instruments that trigger events when they cross into geometric or actuation/force spaces, instrument-free hand-tracking and interaction with virtual buttons and virtual moulage projected onto the scene, to the video-augmented binocular surgical microscope. Computer controlled lighting is automatically brightened to direct attention towards the face, or dimmed to cue recognition that relevant content is being displayed on-screen. Content development was focused primarily on the needs of the trainees at the USUHS Ocular Trauma course learning basic eyelid laceration repair, but "hooks" into all of the functionality of the system are available for implementation of additional scenarios, from directly viewed oculoplastics to microscope mediated corneo-scleral procedures, and anatomical components were developed to address nearly all of the originally planned procedures.

Figure 153: Standalone system with full suite of AR components installed: Kinect operating through mirror to enable hand tracking; projector displaying virtual buttons for non-contact interaction (illumination projected on table-top and face); AR microscope with position tracking to enable synchronized motion of microscope and imagery overlaid on direct view of facial anatomy.

2.3.13. "Month 20" - User testing of combined system.

This phase of testing was performed primarily in the context of receiving ongoing feedback on the system elements from the SMEs on partially assembled components; we were unable to schedule a

dedicated field test of the head-form mounted to the mannequin together with the demonstration/use needs of the system for Ocular Trauma Course.

The SMEs (Mazzoli and Freitag, primarily, as well as the faculty at the USUHS Course who used the standalone simulator) found the increasing realism of the system to be improvements that would support better training of their trainees.

The mobility of the head and neck structure was acceptable for the needs of the ophthalmologist. Additional feedback from the first responder community will be sought in future efforts.

2.3.14. “Month 23” - Completion of revisions based on user testing.

Final identified revisions and elements for completion that implemented as the end of the final extension period drew to a close included:

- Addition of the final port-expander chips to the controller of the fluid and pneumatic valve manifolds
- Creation of the instrument holders for the additional instruments requested for the 2015 USUHS course (described in section 2.3.4.c)
- Completion of the counterweight system to support the AR microscope, for demonstration at IMSH 2015
- Completion of the mounting frame to connect the mannequin-compatible version of the head/neck to the base of the standalone simulator
- Adjustment of microscope optics to verify proper rotation of the graphical images in each eyepiece
- Fabrication of final face modules for demonstration at IMSH 2015

2.3.15. “Month 24” - Final report submission.

This report represents the product of this final milestone.

3. Key Research Accomplishments

- Creation of advanced simulator for eye trauma based on proof-of-principle demo system
    - Design and fabrication of interchangeable, hot-swappable, auto-identifying, precisely registered suite of sensorized ophthalmological instruments that can be extended to additional surgical procedures
    - Development of basic data acquisition and global scoring system into dynamically adaptable platform with capacity for multiple position tracking technologies (magnetic, optical, other) and definition of surgically relevant regions of interest
    - Construction of modular structural framework to provide mounting of and registration between mannequin head, instrument tracking system, projection display, Kinect motion tracker and AR microscope, novel instrument/rack interface for one-handed instrument connector interchange
    - Development of binocular operating microscope with augmented reality capability: graphical overlays registered and dynamically updated to track real anatomy
    - Creation of software tools to support multiple modes of AR within common simulation platform: projected interfaces controls with hand/instrument tracking, generation of stereoscopic imagery and alignment tools for head-down AR interaction through microscope
    - Multiple generations of anatomical improvements from single layer left eyelid and simplified globe to full-facial trauma modules supporting: simple lid laceration; canalicular involvement/intervention; retrobulbar hemorrhage indications/intervention, palpation of facial fracture; realistic airway features; globe with anterior and partial posterior chambers, transparent lens, anatomically thin and operable cornea and sclera

    - Preparation of software implementation for validation of gesture/task detection by expert observers, provision of the software to collaborators

- Development of surgical gesture sequence recognition algorithm for online, real time tracking of performance
    - Conceptualizing the hierarchical structure of surgical procedures from high level tasks to elementary events that can reliably be detected through tracking of instrument motions, information on instrument connectivity and force/position data from strain gages or other sensor inputs
    - Developing state space structure to map possible transitions between states generated by individual surgical gestures, sequences of gestures and sequences of sequences
    - Recognition of reduced computational load of analysis of surgical motions, sub-tasks, tasks, procedures through the implementation of the event-driven surgical gesture recognition
    - Creation of streaming/video data acquisition, storage and review software tools to enable expert review of observed behaviors in support of identifying scenario-specific

gesture sequences, verification of automated gesture recognition and validation of trainee/expert performance differences
    - Improvements/expansion of software code and gesture recognition architecture to allow for post-hoc analysis of recorded data; addition of manually entered and automatically generated event flags to be displayed on timeline playback system; implementation of latest task decomposition and warning engine creation

- Development of fabrication techniques for realistic anatomical model creation and development of novel sensing/actuation systems for an animatronic surgical head/neck structure
    - Segmentation of full head, neck, upper torso high resolution CT data set to provide reference 3D models of bone, skin surface, muscle zones for this effort and ongoing/future developments of this and related simulators
    - Evaluation of alternate fabrication methods for lid laceration module for improved efficiency, quality
    - Development of sequential/interchangeable mold structures for creating bespoke facial modules that support full-featured through simplified module fabrication, reusing common mold components
    - Addition of tarsal plate structure, prototype auxiliary features including eye lashes, brows, grey line, Meibomian gland external pores as available options
    - Improvement of eye globe modules, to include improved resolution, transparent cornea, pigmented iris, improved geometry sclera. Evaluation of alternate vitreous humor simulant materials
    - Ongoing improvements to anatomical landmarks/features, fabrication, materials selection for periorbital skin, eye lids, canaliculi, conjunctiva.
    - Design and fabrication of jaw motion and head left/right motion systems
    - Design and fabrication of neck structure with anatomical features (spinous processes)
    - Design of fluid control manifold system for distribution of high and low pressure blood simulant, low pressure clear fluid for CSF, aqueous humor
    - Design of fractured jaw and maxilla/face components allowing for mobile bone segments to be palpated under mannequin skin
    - Mechanical platform combining pitch/yaw/proptosis/blinking action for establishing sense of “presence” and demonstrating relevant signs of injury
    - Creation of unified tarsal plate/ligament structures for improved realism, addition of vessels and canaliculi into eyelid models, sensing wires into canthal ligaments for detection of cantholysis

- Integration of head/neck structures with commercial mannequin system
    - Evaluated multiple commercial mannequin systems for ease of compatibility with replacement of stock head/neck with alternate eye/face-trauma specific replacement
    - Creation of software architecture to link mannequin SDK to eye/face-trauma specific controls with capability for scenario-specific interventions to influence behavior of overall mannequin operation, sample physiological parameters set by instructor tablet,

overwrite physiological parameters from simulator software, enable/disable features of the mannequin control system
    - Designed & fabricated mounting structure for neck that can be modified easily for compatibility with other mannequin types/vendors
    - Evaluated and developed air muscle actuation of animatronic neck including range of motion based on mannequin compressed air
    - Established methods for linking simulator software with mannequin software to sample physiological parameters set by instructor tablet, overwrite physiological parameters from simulator software, enable/disable features of the mannequin control system
    - Developed microcontroller-based interface between head/neck controller and solenoid/servo/sensor elements within the head/neck

- Conduct data collection exercises/basic validation with surgeons, fellows, residents
    - Prepared, amended human subjects research protocol to support initial and ongoing data collection in cooperation with annual USUHS Ocular Trauma course
    - Collection of ~50 data sets for lid laceration repair from attending physicians, fellows and PGY2-PGY4 residents
    - Preliminary analysis of data towards identifying important geometric, instrument action thresholds
    - Support of Simulator Validation Program study at USUHS comparing simulator training for lid laceration repair with animal tissue-based prior gold-standard
    - Collection of survey data for feedback on simulator, results showing areas for improvement of physical structure, anatomical models and presentation of content

4. Reportable Outcomes

Conference slides, abstracts, posters and the patent application documentation are available on request.

4.1.1. Conference papers and oral presentations

Ottensmeyer MP, Ahn B, Moore JC, Munteanu E, Iorino S, De Novi G, Bardsley R, Shah R, Neumann P, Langston D. Ocular and Craniofacial Trauma Treatment Training System: Overview & Eyelid Laceration Module. Workshop Proceedings of the 8th International Conference on Intelligent Environments. J.A. Botía et al. (Eds.) IOS Press, 2012. pp 319-330.

De Novi G, Bardsley R, Shah R, Ottensmeyer MP, Moore JC, Ahn B. Event-driven Surgical Gesture Segmentation and Task Recognition for Ocular Trauma Simulation. Workshop Proceedings of the 8th International Conference on Intelligent Environments. J.A. Botía et al. (Eds.) IOS Press, 2012. pp 341-352.

4.1.2. Conference and workshop abstracts and posters

Ottensmeyer MP, De Novi G, Bardsley RS, Moore JC, Ahn B, Iorino S, Munteanu E, Troulis MJ, Mazzoli RA, Dawson SL. Ocular and Craniofacial Trauma Treatment Training System: Lid & globe laceration module work in progress & program overview / Poster presentation, Medicine Meets Virtual Reality, Newport Beach, CA, 9-11 Feb 2012

Ahn B, Moore JC, Munteanu E, Iorino S, Bardsley RS, De Novi G, Dawson SL, Troulis MJ, Ottensmeyer MP. Ocular and Craniofacial Trauma Treatment Training System: Trauma module animatronics and structure, simulator interface / Poster presentation, 65th Annual SAC Poster Session, Boston, MA,18-19 Apr 2012

De Novi G, Bardsley RS, Shah R, Ottensmeyer MP. Event-driven Surgical Gesture Segmentation and Task Recognition for Ocular Trauma Simulation / Poster presentation, 65th Annual MGH SAC Poster Session, Boston, MA, 18-19 Apr 2012

Ahn B, Moore JC, Munteanu E, Ottensmeyer MP. Eye Motion and Pupil Contraction Modular Systems for Eye Trauma Treatment Training Simulator / Poster presentation, MGH ORCD Poster Celebration, Boston, MA, 24 May 2012

De Novi G, Bardsley RS, Shah R, Ottensmeyer MP. Event-driven Surgical Gesture Segmentation and Task Recognition for Ocular Trauma Simulation / Poster presentation, MGH ORCD Poster Celebration, Boston, MA, 24 May 2012

Ottensmeyer MP, De Novi G, Ahn B, Bardsley RS, Moore JC, Shah R, Munteanu E, Iorino S, Dawson SL. Development of an Ocular-Facial Trauma Treatment Training Simulator / Poster presentation, Military Health System Research Symposium, Ft. Lauderdale, FL, 13-16 Aug 2012

Ahn B, Moore JC, Zivieri S, De Novi G, Bardsley RS, Ottensmeyer MP. Ocular and Craniofacial Trauma Simulator Development: AR Surgical Microscope, CT-Derived Physical Anatomy, Sensor & Actuator Systems / Poster presentation, MGH 66th Annual SAC Poster Session, Boston, MA 20-21 Mar 2013

De Novi G, Bardsley RS, Festi M, Ottensmeyer MP. Ocular and Craniofacial Trauma Simulator: Event Driven Gesture Recognition, Contextual Feedback Interface and User Trial Result / Poster presentation, MGH 66th Annual SAC Poster Session, Boston, MA 20-21 Mar 2013

Ottensmeyer MP, De Novi G, Loan G, Pifferi F, Festi M. Development of an Ocular-Facial Trauma Treatment Training Simulator / Poster presentation, oral presentation, Military Health System Research Symposium, Ft. Lauderdale, FL, 11-15 Aug 2013

Ottensmeyer MP, De Novi G. Conversion of stereo surgical microscope for augmented reality application in an eye trauma simulator / Poster presentation, Medicine Meets Virtual Reality, Manhattan Beach, CA, 19-22 Feb 2014

De Novi G, Loan G, Ottensmeyer MP. Ocular and Craniofacial Trauma Simulator: Event Driven Gesture Recognition, Contextual Feedback Interface and User Trial Result / Poster presentation, International Meeting on Simulation in Healthcare, San Francisco, CA, 25-29 Jan 2014

De Novi G, Loan GJ, Gallerani M, Pifferi F, Ottensmeyer MP. Ocular and craniofacial trauma treatment training simulator: hardware advances and user feedback / Poster presentation, Military Health System Research Symposium, Ft. Lauderdale, FL, 18-24 August 2014

De Novi G, Loan GJ, Ottensmeyer MP. Progress on Ocular and Facial Trauma Training Simulator / Poster presentation, MGH 68th Annual SAC Poster Session, Boston, MA 1-2 Apr 2015

4.1.3. Invited Presentations

TATRC display area demonstration of prototype simulator / MMVR19, Medicine Meets Virtual Reality, Newport Beach, CA, 9-11 Feb 2012

Eye trauma simulation – review and novel system development / Oral presentation / 5th Military Vision Symposium on Ocular and Vision Injury, Boston, MA, 18 Sep 2012

Simulation – grand concepts & eye trauma example / Oral presentation / Vision Center of Excellence Roadmap Meeting, 2012, Boston, MA, 17-19 Oct 2012

Ottensmeyer MP. Ocular Trauma Training Simulator: Work in progress – system, gesture tracking, user trial. / Oral presentation / MMVR 2013, San Diego, CA, 21 Feb 2013

Ottensmeyer MP, De Novi G, Bardsley RS. Ocular and Craniofacial Trauma Treatment Training System: Program overview & work in progress / TATRC display area demonstration and poster / MMVR20, Medicine Meets Virtual Reality, San Diego, CA, 21 Feb 2013

4.1.4. Student Theses

Master's thesis, Stefano Iorino, Politecnico De Milano, Facolta' Del Design, Italy: "TrackSim: UN SIMULATORE DI INTERVENTI CHIRURGICI PER TRAUMI OCULARI E CRANIOFACCIALI" ("TrackSim: A simulator for eye trauma and craniofacial surgery"), 2012.

Master's thesis, Evgheni Munteanu, Universita' Di Bologna, Facolta' De Ingegneria, Italy: "Progetto di un Sistema de elaborazione di segnali biomedicali per applicazioni di chirurgia ocular" ("A Biomedical Signal Processing System for Ocular Surgery"), 2012.

Master's thesis, Simone Zivieri, Universita' Degli Studi Di Modena E Reggio Emilia, Ingegneria "Enzo Ferrari", Italy: "EYE-MECH: Integrated Design of a Robotic Eye for Application in Surgical Simulators", 2013.

Master's thesis, Martina Festi, Universita' Degli Studi De Bologna, Facolta' De Ingegneria, Italy: "EYE-TRAUMA Project: Event Driven Control Software for Gesture Recognition in Medical Simulation", 2013.

Master's thesis, Federico Pifferi, Universita' Degli Studi Di Modena E Reggio Emilia, Ingegneria "Enzo Ferrari", Italy: "Virtual and Physical Prototyping of the Neck of a Humanoid Robot for Surgical Simulators", 2013.

Master's thesis, Marcello Gallerani, Universita' Degli Studi Di Modena E Reggio Emilia, Ingegneria "Enzo Ferrari", Italy: "Integrated Design and Prototyping of a Robotic Head for Ocular and Craniofacial Trauma Simulators", 2014.

4.1.5. Invention disclosures and patent applications

MGH Invention Disclosure, "Ocular Trauma Treatment Training Systems". Case number 22084, logged 02/25/2013.

MGH Invention Disclosure, "Training Simulator for Ocular Trauma and Other Domains Using Event-Based Surgical Gesture Detection and Multiple Instrument and Hand Motion Tracking Systems". Case number 22275, logged 06/11/2013.

4.1.6. Patent Applications

United States Provisional Patent Application, "Augmented Reality Microscope". Serial number 61/766,987, filed 02/20/2013, serial number 61/860,397, filed 07/31/2013, serial number 61/861,179, filed 08/01/2013.

United States Patent Application, "Trauma Training Simulator With Event-Based Gesture Detection and Instrument-Motion Tracking". Ottensmeyer MP, De Novi G, Loan GJ, Bardsley RS, Moore JC. Serial number 20150037775, filed 06/30/2014.

4.1.7. Licenses

Negotiations ongoing towards option to license technology by Simulation Systems, LLC pending further progress on STTR proposal submission.

4.1.8. Training experiences:

Post-doctoral research fellowship: Gianluca De Novi, Ph.D. (U. Bologna) Robotics. Developing software architecture and implementation of simulator interface. Hired as permanent employee, currently Lead Software Architect for MGH Simulation Group.

Post-doctoral research fellowship: Bummo Ahn, Ph.D. (KAIST, South Korea) Mechanical engineering. Developing mechatronic systems for simulator, instrument motion sensing, intervention sensing. Returned to South Korea, currently Senior Researcher, Korea Institute of Industrial Technology.

Internship: Stefano Iorino, master's candidate, Design and Engineering, Faculty of Design Politecnico di Milano, Milan, Italy. 6-month term working on system structural design, instrument connection system, lighting system, AR microscope prototype optics.

Internship: Evgheni Munteanu, master's candidate, Mechatronics, Department of Electronics Informatics and Systems, Faculty of Engineering, University of Bologna, Bologna, Italy. 4-month term working on developing USB-based interfaces for surgical instrument motion tracking, control of simulator lighting system.

Internship: Simone Zivieri, master's candidate, mechanical engineering, University of Modena and Reggio Emilia. 6-month work term learning mechanical design, CAD, control of servomechanisms, calibrating elastic response of transmission; working on the eye motion mechatronics. Graduated cum laude.

Internship: Martina Festi, master's candidate, computer science, University of Bologna. 6-month work term learning to use C# libraries, bridging methods between C# and C++, as applied to interfacing simulator to Laerdal mannequin SDK, assembly language coding as applied to simulator data acquisition microcontroller. Graduation expected towards end of 2013.

Internship: Federico Pifferi, master's candidate, mechanical engineering, University of Modena and Regio Emilia, 6-month work term learning CAD, mechanical design, control of pneumatic actuators, design of pneumatic actuators. Working on design of animatronic neck of mannequin.

Internship: Marcello Gallerani, master's candidate, mechanical engineering, University of Modena and Regio Emilia, 6-month work term, learning CAD, mechanical design, control of servos, stepper motors. Working on design of animatronic jaw, head motion of mannequin.

4.1.9. Funding applications

Participated in preparation of pre-proposal and invited full proposal in response to W81XWH-12-JPC1-DTME-PRP, "Developer Tools for Medical Education Public Physiology Research Platform". Proposal entitled ""iBody": a Unified Public Physiology Research Engine - Open Infrastructure Enabling an Integrated Continuum of Virtual and Physical Simulation Technology Platforms" under co-PIs James A. Gordon, M.D. and John Parrish, M.D.

Selected as subawardee/contractor for “Feasibility and Implementation of Ocular Injury Simulator Surgical Systems in Training Military Ophthalmologists”, proposal for Medical Simulator Validation Program intramural solicitation (SVP), Marcus Colyer, M.D., P.I. Provided access to simulator and production of consumable trauma modules, materials and travel expenses to be reimbursed for 2013, 2014 and 2015 USUHS Ocular Trauma Course events.

Proposal awarded: “Eye/Face Trauma Simulation Enhancements”, Mark P. Ottensmeyer, Ph.D., P.I. Subaward of USAMRMC W81XWH-14-2-0008 (Joint Warfighter Medical Research Program), extending work previously supported by CIMIT. Proposal to develop mid-facial fracture module, adapt simulator to be compatible with CIMIT modular mannequin system under development.

Proposal awarded: “Advanced Modular Manikin”, James A. Gordon, M.D., P.I. USAMRMC W81XWH-14-C-0100. Program to develop platform technology for a modular manikin systems, adapting ocular-craniofacial simulator for use as one possible head module for this system.

Work in progress on NIH PA-15-270 STTR proposal with Simulation Systems, LLC. Planned research and development will address verification and validation of simulator data collection and measurement of trainee performance vs. expert performance.

5. Conclusion

This report presents the full scope of the progress made to create a novel eye and face trauma simulator for use by trainee surgeons and those new or returning to eye trauma practice as well as first responders facing eye trauma and likely coincident facial trauma in the field.

The system that we developed is a prototype that presents a solution to a variety of gaps in the available training methods in this domain.

Firstly, at the outset of the program, there were no available commercial systems that provided simulated training experiences in responding to ocular/periocular eye trauma. There were VR-based systems that focused on procedures such as cataract and retinal surgery and simple part task trainers for globe surgery (the above, plus strabismus, enucleation, etc.), but no simulation-based systems for eye/periocular trauma and oculoplastics. With the drive towards eliminating animal-based training and the challenge of learning procedures on patients in need of surgery done correctly the first time, the need for a simulator to fill this gap was clear and this system provides such a solution.

Next, there is a growing need for quantitative evaluation capabilities in training to verify that a trainee has met meaningful criteria for successful learning, and these criteria should be more fine-grained than a global score based on gross features such as overall path length or elapsed time. Identifying specific areas for improvement can help to focus training so that it can be made more efficient, which is important in the era of limited resident hours and growing recognition of the costs of training in an OR environment. To further enhance the learning experience, having an automated system that captures the experience of the senior physician “looking over the shoulder” of the trainee to provide context-relevant corrections and additional teaching material would be an improvement over inanimate system and would leverage the skills of a single expert across multiple trainees. Again, this simulator presents a solution that approaches these challenges.

Lastly, our original motivation was to address needs that span the spectrum of care providers. In particular we aimed to create something that would support the needs of the first responders, who had, at the outset, very few options to provide a realistic experience of eye trauma, compared with the relatively robust general medical simulator marketplace. At the same time, we aimed to create a system that would enable transmission and preservation of the skills of physicians with combat-trauma response skills to the next generations of physicians, in an environment where certain basic skills were being deemphasized in civilian training and/or are increasingly limited to a smaller number of regional centers. Creating a system that included components that could be integrated both with a benchtop/”wet-lab” simulator and with full-body mannequins was a challenge that attempted to reach both audiences with relevant features while reusing/repurposing as many of the common features as possible.

As distilled in the Key Research Accomplishments, we were successful in constructing a system that provides capabilities addressing each of the gaps. The final CT-derived anatomical features provided a

diversity of options to provide training experiences for both the surgeons and the first responders, through presentation of lacerations through multiple tissue layers for repair or palpable indications of facial fracture or integrated moulage prompting responses such as cricothyroidotomy. The suite of sensors, distributed across surgical instruments and the anatomical components themselves (e.g. force sensing eye globe supports, cut sensors for detecting cricothyroidotomy incision length and orientation) similarly allow detection both of correct but also incorrect response to the given scenario, and helps to avoid "gaming" the system. The animatronic components of eye/lid/head motion and features intended to generate blood simulant/fluid flow support increased realism to help to immerse the trainee in the scenario and reinforce the learning experience. The software architecture integrates the sensing capabilities, 3D model based information about the locations of instruments and sensors and knowledge derived from experts to identify how a trainee is performing an intervention and present context-relevant information to enhance the learning experience.

The system represents a platform technology that is going on to support further developments in the ocular/facial trauma domain. We were part of the Massachusetts General Hospital team that pursued one of the phase 1 Advanced Modular Manikin research and development efforts, in which we adapted and expanded upon the head/neck structure and the electronic interface to make it compatible with our designs and prototype of the AMM. The full-face modules are under consideration as part-task trainers on their own to support lower cost training or skills refreshing for canalicular stenting and lid/globe laceration repair (omitting the sensing/software elements). The Event-Driven Surgical Gesture Recognition approach is a generic tool that can be applied just as well to other domains of instrument-mediated medicine (minimally invasive/robotic surgery, microsurgery, etc.), and we are exploring where we will be able to apply the technique in future work. We are investigating further funding opportunities with a commercial partner to expand the verification/validation work in support of a transition to a commercial version of the system. And lastly, we were successful in applying for funding to enhance the system with additional features including a more advance surgical fracture repair feature set (i.e. stabilizing the bone fragments with plates and screws) and an enucleation module for injuries so severe that salvage of the globe would not be possible.

Perhaps most importantly, we were successful in creating a prototype that had utility for training not just after completion but also in the course of development. We are incredibly grateful for the support and expertise of Drs. Richard Stutzman and Marcus Colyer, course directors of the USUHS Ocular Trauma Course, and the opportunity to provide the system for use in training by the course faculty for the students, so that the students had the opportunity to learn techniques on simulated human anatomy (vs. animal). Because of the unplanned, extended period of performance, we had the opportunity to observe and learn from the interactions of the faculty and students with the system and make more improvements to it than might have been possible under the original calendar.

The last of the preceding successes hints at some of the areas in which this research effort fell short of measuring up to our original aspirations. The commencement of the program came in the shadow of a funding gap that saw most of the originally proposed team temporarily leaving MGH, resulting in a

slower than desired start to the program as original team members returned in some cases from geographic relocation and new personnel were recruited, and a lag in the calendar. That lag led to mismatch between some of our early goals for user testing and the best scheduled opportunities to conduct that testing. With the benefit of hindsight, the linear, sequential structure of the milestones that was proposed was at odds with the nature of the research effort, which is rarely a linear effort as new technologies and ideas emerge that could not be predicted in the original proposal. We greatly appreciate the flexibility that was shown by our sponsors in granting no-cost extensions that helped to accommodate the divergence between plan and execution and enabled the aforementioned additional opportunities to work with the end user faculty members and students.

This project also illustrated the importance of excellent project planning, management and tracking skills as part of a team in parallel with the R&D expertise. With respect to the emphases of the project, we were very successful in addressing the slice of the simulator that responded to the training needs for a lid laceration scenario, but less so regarding the other surgical tasks (canalicular repair, retrobulbar hemorrhage and cricothyroidotomy) and the manikin integration element – physical components were developed that support additional work towards complete scenarios, but did not reach the same level as that of the lid laceration. The need to maintain balance between all of the elements of the plan is one of the lessons learned for future work. Also related to the management element, the PI had significant challenges in meeting the reporting requirements of the program, initially as a result of the happy addition of twin infants during Year 3, but later as a result of over-commitment across a number of research programs; proposals for other research that were prepared since this program began specifically called out for additional personnel to aid in meeting such requirements in the future.

In the third PMI category of (Plus, Minus) and Interesting, as a primarily research oriented effort, the simulator that was developed incorporated a much higher density of features that would likely be desirable in a commercial product. Combining the position tracking, AR projection, AR microscope, dual use capability of the head/neck form as both the bench-top and mannequin-integrated, etc. could result in a product that would be overly complex and expensive. That point is well taken; the direction towards which we expect the system will evolve would be to select the most relevant subset of features for particular applications, and with the benefit of the modularity that we built into the prototype, relatively quickly adapt the design and capabilities of a new system for those more specific applications. We followed this path in the adaptation of the head/neck design for compatibility with the AMM project, which retained the animatronic and anatomical features, while dispensing with the instrument tracking/gesture recognition elements. Such down-selection restores the focus that will be necessary for commercial successful spin-off elements of this project.

In terms of overall impact of this program, it is already clear that the simulator will not be orphaned following submission of this final report. As described, the results obtained to date have supported a successful grant proposal to extend the capabilities of the system, which will open additional

opportunities: the enucleation component under development bears similarity to the requirements for strabismus surgery, which is of interest to physicians at Boston Children's Hospital, with whom we have had preliminary discussions. The intellectual property developed was deemed by our institution to be of sufficient value to warrant conversion of the patent application, with the expectation that the costs will be recouped through future licensing opportunities. And last, but not lease, in addition to the series of data collection and Simulator Validation Program efforts in which we participated during the extended period of performance, the system continued/continues to be used at the USUHS Ocular Trauma courses in 2015 and planned for 2016.

6. Acknowledgement

We profusely thank the USAMRAA, our COR and contracting office for their support and forbearance. The course directors, faculty and students of the USUHS Ocular Trauma Course have our greatest appreciation, respect, and thanks for their service. Our local subject matter experts and their colleagues were instrumental in guiding our engineering, software and artistic efforts towards creation of a useful and well used device, and they have our thanks. Lastly, we recognize the vision and support of the original inspiration and biggest champion of this project, Dr. Robert A. Mazzoli (with apologies for including a candid action shot!)

7. Appendices

7.1. List of all Personnel Receiving Pay

Mark P. Ottensmeyer, Ph.D. (PI)
Steven L. Dawson, M.D. (SME)
Maria J. Troulis, D.D.S. (SME)
Ryan S. Bardsley (systems designer)
John Cho Moore (industrial designer)
Gianluca De Novi, Ph.D. (software architect)
Gregory J. Loan (clinical engineer)
Bummo Ahn (post-doctoral research fellow)
Rajesh Shah (biomedical engineer)

David Brennan (imaging technician)
Daniel Langston (contractor)

7.2. References

Bardsley RS, Ottensmeyer MP, Samosky JT, Dawson SL. Methods and apparatus for providing realistic medical training. US Patent 8,647,124, published 02/11/2014

Big Blue Saw. "Construction techniques: Tab and Slot with T-nut construction". https://www.bigbluesaw.com/articles-list/big-blue-saw-designing-for-waterjet/construction-techniques-tab-and-slot-with-t-nut-construction.html. Copyright 2015

De Novi G, Bardsley R, Shah R, Ottensmeyer MP, Moore JC, Ahn B. Event-driven Surgical Gesture Segmentation and Task Recognition for Ocular Trauma Simulation. Workshop Proceedings of the 8th International Conference on Intelligent Environments. J.A. Botía et al. (Eds.) IOS Press, 2012. pp 341-352.

Hester R, Brown A, Husband L, Iliescu R, Pruett WA, Summers RL, Coleman T. HumMod: A modeling environment for the simulation of integrative human physiology. Frontiers in Physiology 2011; 2:12

Koolstra JH. Dynamics of the human masticatory system. Critical Reviews in Oral Biology & Medicine 2002; 13(4):366-76

Luboz V, Wu X, Krissian K, Westin CF, Kikinis R, Cotin S, Dawson S. A segmentation and reconstruction technique for 3D vascular structures. In Eighth International Conference on Medical Image Computing and Computer-Assisted Intervention (MICCAI'05), Lecture Notes in Computer Science 3749. Palm Springs, CA, USA, 2005;43-50

Ottensmeyer MP, Ahn B, Moore JC, Munteanu E, Iorino S, De Novi G, Bardsley R, Shah R, Neumann P, Langston D. Ocular and Craniofacial Trauma Treatment Training System: Overview & Eyelid Laceration

Module. Workshop Proceedings of the 8th International Conference on Intelligent Environments. J.A. Botía et al. (Eds.) IOS Press, 2012. pp 319-330.

Ritter EM, Bowyer MW. Simulation for trauma and combat casualty care. Minimally Invasive Therapy 2005; 14(4-5):224-234

Stylopoulos N, Cotin S, Maithel SK, Ottensmeyer M, Jackson PG, Bardsley RS, Neumann PF, Rattner DW, Dawson SL. Computer-enhanced laparoscopic training system (CELTS). Surgical Endoscopy 2004; 18:782-789

7.3. Bibliography of Publications

7.3.1. Conference papers and oral presentations

Ottensmeyer MP, Ahn B, Moore JC, Munteanu E, Iorino S, De Novi G, Bardsley R, Shah R, Neumann P, Langston D. Ocular and Craniofacial Trauma Treatment Training System: Overview & Eyelid Laceration Module. Workshop Proceedings of the 8th International Conference on Intelligent Environments. J.A. Botía et al. (Eds.) IOS Press, 2012. pp 319-330.

De Novi G, Bardsley R, Shah R, Ottensmeyer MP, Moore JC, Ahn B. Event-driven Surgical Gesture Segmentation and Task Recognition for Ocular Trauma Simulation. Workshop Proceedings of the 8th International Conference on Intelligent Environments. J.A. Botía et al. (Eds.) IOS Press, 2012. pp 341-352.

7.3.2. Conference and workshop abstracts and posters

Ottensmeyer MP, De Novi G, Bardsley RS, Moore JC, Ahn B, Iorino S, Munteanu E, Troulis MJ, Mazzoli RA, Dawson SL. Ocular and Craniofacial Trauma Treatment Training System: Lid & globe laceration module work in progress & program overview / Poster presentation, Medicine Meets Virtual Reality, Newport Beach, CA, 9-11 Feb 2012

Ahn B, Moore JC, Munteanu E, Iorino S, Bardsley RS, De Novi G, Dawson SL, Troulis MJ, Ottensmeyer MP. Ocular and Craniofacial Trauma Treatment Training System: Trauma module animatronics and structure, simulator interface / Poster presentation, 65th Annual SAC Poster Session, Boston, MA,18-19 Apr 2012

De Novi G, Bardsley RS, Shah R, Ottensmeyer MP. Event-driven Surgical Gesture Segmentation and Task Recognition for Ocular Trauma Simulation / Poster presentation, 65th Annual MGH SAC Poster Session, Boston, MA, 18-19 Apr 2012

Ahn B, Moore JC, Munteanu E, Ottensmeyer MP. Eye Motion and Pupil Contraction Modular Systems for Eye Trauma Treatment Training Simulator / Poster presentation, MGH ORCD Poster Celebration, Boston, MA, 24 May 2012

De Novi G, Bardsley RS, Shah R, Ottensmeyer MP. Event-driven Surgical Gesture Segmentation and Task Recognition for Ocular Trauma Simulation / Poster presentation, MGH ORCD Poster Celebration, Boston, MA, 24 May 2012

Ottensmeyer MP, De Novi G, Ahn B, Bardsley RS, Moore JC, Shah R, Munteanu E, Iorino S, Dawson SL. Development of an Ocular-Facial Trauma Treatment Training Simulator / Poster presentation, Military Health System Research Symposium, Ft. Lauderdale, FL, 13-16 Aug 2012

Ahn B, Moore JC, Zivieri S, De Novi G, Bardsley RS, Ottensmeyer MP. Ocular and Craniofacial Trauma Simulator Development: AR Surgical Microscope, CT-Derived Physical Anatomy, Sensor & Actuator Systems / Poster presentation, MGH 66th Annual SAC Poster Session, Boston, MA 20-21 Mar 2013

De Novi G, Bardsley RS, Festi M, Ottensmeyer MP. Ocular and Craniofacial Trauma Simulator: Event Driven Gesture Recognition, Contextual Feedback Interface and User Trial Result / Poster presentation, MGH 66th Annual SAC Poster Session, Boston, MA 20-21 Mar 2013

Ottensmeyer MP, De Novi G, Loan G, Pifferi F, Festi M. Development of an Ocular-Facial Trauma Treatment Training Simulator / Poster presentation, oral presentation, Military Health System Research Symposium, Ft. Lauderdale, FL, 11-15 Aug 2013

Ottensmeyer MP, De Novi G. Conversion of stereo surgical microscope for augmented reality application in an eye trauma simulator / Poster presentation, Medicine Meets Virtual Reality, Manhattan Beach, CA, 19-22 Feb 2014

De Novi G, Loan G, Ottensmeyer MP. Ocular and Craniofacial Trauma Simulator: Event Driven Gesture Recognition, Contextual Feedback Interface and User Trial Result / Poster presentation, International Meeting on Simulation in Healthcare, San Francisco, CA, 25-29 Jan 2014

De Novi G, Loan GJ, Gallerani M, Pifferi F, Ottensmeyer MP. Ocular and craniofacial trauma treatment training simulator: hardware advances and user feedback / Poster presentation, Military Health System Research Symposium, Ft. Lauderdale, FL, 18-24 August 2014

De Novi G, Loan GJ, Ottensmeyer MP. Progress on Ocular and Facial Trauma Training Simulator / Poster presentation, MGH 68th Annual SAC Poster Session, Boston, MA 1-2 Apr 2015

7.3.3. Invited Presentations

TATRC display area demonstration of prototype simulator / MMVR19, Medicine Meets Virtual Reality, Newport Beach, CA, 9-11 Feb 2012

Eye trauma simulation – review and novel system development / Oral presentation / 5th Military Vision Symposium on Ocular and Vision Injury, Boston, MA, 18 Sep 2012

Simulation – grand concepts & eye trauma example / Oral presentation / Vision Center of Excellence Roadmap Meeting, 2012, Boston, MA, 17-19 Oct 2012

Ottensmeyer MP. Ocular Trauma Training Simulator: Work in progress – system, gesture tracking, user trial. / Oral presentation / MMVR 2013, San Diego, CA, 21 Feb 2013

Ottensmeyer MP, De Novi G, Bardsley RS. Ocular and Craniofacial Trauma Treatment Training System: Program overview & work in progress / TATRC display area demonstration and poster / MMVR20, Medicine Meets Virtual Reality, San Diego, CA, 21 Feb 2013

7.3.4. Student Theses

Master's thesis, Stefano Iorino, Politecnico De Milano, Facolta' Del Design, Italy: "TrackSim: UN SIMULATORE DI INTERVENTI CHIRURGICI PER TRAUMI OCULARI E CRANIOFACCIALI" ("TrackSim: A simulator for eye trauma and craniofacial surgery"), 2012.

Master's thesis, Evgheni Munteanu, Universita' Di Bologna, Facolta' De Ingegneria, Italy: "Progetto di un Sistema de elaborazione di segnali biomedicali per applicazioni di chirurgia ocular" ("A Biomedical Signal Processing System for Ocular Surgery"), 2012.

Master's thesis, Simone Zivieri, Universita' Degli Studi Di Modena E Reggio Emilia, Ingegneria "Enzo Ferrari", Italy: "EYE-MECH: Integrated Design of a Robotic Eye for Application in Surgical Simulators", 2013.

Master's thesis, Martina Festi, Universita' Degli Studi De Bologna, Facolta' De Ingegneria, Italy: "EYE-TRAUMA Project: Event Driven Control Software for Gesture Recognition in Medical Simulation", 2013.

Master's thesis, Federico Pifferi, Universita' Degli Studi Di Modena E Reggio Emilia, Ingegneria "Enzo Ferrari", Italy: "Virtual and Physical Prototyping of the Neck of a Humanoid Robot for Surgical Simulators", 2013.

Master's thesis, Marcello Gallerani, Universita' Degli Studi Di Modena E Reggio Emilia, Ingegneria "Enzo Ferrari", Italy: "Integrated Design and Prototyping of a Robotic Head for Ocular and Craniofacial Trauma Simulators", 2014.

7.3.5. Patent Applications

United States Provisional Patent Application, "Augmented Reality Microscope". Serial number 61/766,987, filed 02/20/2013, serial number 61/860,397, filed 07/31/2013, serial number 61/861,179, filed 08/01/2013.

United States Patent Application, "Trauma Training Simulator With Event-Based Gesture Detection and Instrument-Motion Tracking". Ottensmeyer MP, De Novi G, Loan GJ, Bardsley RS, Moore JC. Serial number 20150037775, filed 06/30/2014.

7.3.6. Sponsor Presentations

Development of an Ocular and Craniofacial Trauma Treatment Training System / JPC-1/TATRC CCTI In-Progress Review presentation, Ft. Detrick MD, 19 June 2013

7.4. Attached Publications

Workshop Proceedings of the 8th International Conference on Intelligent Environments
J.A. Botía et al. (Eds.)
IOS Press, 2012

doi:10.3233/978-1-61499-080-2-319

Ocular and Craniofacial Trauma Treatment Training System: Overview & Eyelid Laceration Module

Mark P. OTTENSMEYER[a,b,1], Bummo AHN[a,b], John CHO MOORE[a], Evgheni MUNTEANU[a], Stefano IORINO[a], Gianluca DE NOVI[a,b], Ryan BARDSLEY[a], Rajesh SHAH[a], Paul NEUMANN[c], Dan LANGSTON[d]
[a] *Simulation Group, Department of Imaging, Massachusetts General Hospital*
[b] *Harvard Medical School*
[c] *NinePoint Medical*
[d] *Dan Langston Studio*

Abstract. Eye trauma in combat-related injuries can be devastating. Body armor improvements increase survivability from many injuries, however the face remains relatively unprotected, especially from IED blast and fragments. The number of physicians with significant eye trauma expertise is limited due to lack of teaching opportunities and evolution of surgical techniques away from microsuturing. To provide a non-animal, non-cadaver training system, a hybrid physical/virtual eye trauma simulation system for surgical technique learning and evaluation is being developed. It includes a silicone/polymer head with replaceable eye trauma modules with realistic anatomy. Position/orientation and grasp force/position of surgical instruments are measured, and real time scoring and feedback methods are under development. These elements are integrated with teaching materials presented on-screen and during training scenarios via augmented reality projection. The initial efforts focus on a lacerated eye lid scenario. Developments towards additional trauma modules with animatronic features are discussed.

Keywords. Eye trauma, surgical gesture measurement, augmented reality

1. Introduction

1.1. Motivation

Craniofacial and ocular injuries have been elements of up to 29% of all battlefield injuries suffered by US, UK and allied forces in recent conflicts in Iraq and Afghanistan. While improvements in armor systems have reduced fatality due to injuries to the torso, the face and head remain relatively vulnerable and casualties present with more injuries to the eyes and face than proportional relative to body surface area. Emphasis on the use of eye protection reduced the prevalence of eye injuries from Operation Desert Storm in 1991 (13%) to Operations Iraqi Freedom and Enduring Freedom in 2001-2005 (6%)[1]. Strict compliance with eye protection usage can reduce eye injuries to 0.5% in some cases [2], however this is typically not

[1] Corresponding Author.

achieved, and rates vary [3]. The eye is sensitive to blast injuries and without proper eye protection, many small fragments that might not penetrate skin, are likely to do damage to the eye and surrounding tissues.

At the same time as soldiers are surviving formerly fatal injuries, but with disfiguring and disabling eye/face wounds, the skills required to address them are not as broadly available as they once were. Microsuturing has been superseded by sutureless methods for certain procedures, so the relevant skills are not as frequently used. Trauma cases are typically referred to trauma centers, so fewer ophthalmologists have exposure to relevant cases, and the uniqueness of each trauma case makes the learning process a lengthy one. In addition, there are financial disincentives to specialize in trauma vs. other ophthalmology specialties, involving reimbursement levels for re-operations for a given case.

Alternative training modes include use of cadaver tissues [4], animal eyes and tissues [5], and simulated anatomy [6]. Cadaver and animal eye tissue typically has different mechanical behavior from live tissue. Further, there is a strong push for military medical training to reduce or eliminate the use of tissue for training purposes. With both tissue training and the use of simulated anatomy, there is a need for senior oversight and guidance, which is an expensive use of a skilled surgeon's time which needs to be balanced against time spent in the OR.

There is a need, therefore, to provide more and better opportunities for self-directed, repeated and repeatable, diverse and relevant synthetic training options. In support of this, we are developing an eye and facial trauma simulation system, integrating not only a physical mannequin, but the enhancements provided by multiple modes of content and guidance presentation, multiple modes of sensing, and the capability for presenting a variety of trauma cases using the same base platform.

1.2. Previous Research

Existing eye surgery simulation systems tend towards opposite ends of the virtual vs. fully-physical spectrum. In the virtual space, there are a variety of simulators focused on non-trauma scenarios, including cataract surgery [7][8]. A recent entrant to the virtual arena is [9]. Primary drawbacks of fully virtual systems is that they either dispense with tactile and force feedback components, in a domain where careful control of applied forces is crucial, or when force feedback is included, it relies on typical commercial haptic interfaces, which are difficult to integrate within the tight confines around the eye. Further, multiple instruments are used during the course of a typical procedure (multiple forceps, needle holders, scissors, accessories such as surgical sponges), which must be "faked" if a common interface handle is used, or detachable connectors designed to allow swapping of instruments.

In the domain of the fully physical are a number of commercial products [6][10]. These have varying levels of accuracy, typically matched closely to the needs for training particular procedures. With careful choice of materials used in fabrication, they can provide accurate tissue behavior, however the automatic performance measurement possibilities of the virtual are unavailable. Performance evaluation depends on the oversight of proctors and senior physicians, and when used in a self-directed fashion, there would be minimal opportunity for immediate feedback or advice on improvement.

One notable effort to combine approaches is that of [11], in which an *ex vivo* human or animal eye was supported in a cup mounted on a force sensor, to evaluate loads applied to the eye. Sensing of instrument motions was not performed.

The general focus of our research group is to combine the most useful features of the physical with the complementary features of the virtual when developing medical training simulators: physical realism, so force feedback is obtained passively from physical objects, combined with tracking and responsiveness capabilities of the virtual – measurement of instrument trajectories, sensing of interventions and automatic provision of real-time feedback, evaluation and guidance.

One example of this work was a collapsed lung response simulator [12][13], which tracked trajectories of "chest tubes" and "chest darts", causing the physical mannequin to respond appropriately to insertion, automatically detecting success or failure and providing immediate feedback to the trainee. Similarly, we developed an early laparoscopy interface which quantitatively measured physical instrument motions while performing basic training exercises, yielding performance scores relative to an aggregate of expert performance results [14] and most recently, a full-body trauma victim mannequin for use in training for severe extremity hemorrhage, which housed an autonomous control unit inside the body of a physical mannequin [15].

1.3. Eye lid anatomy

The system currently focuses on learning techniques relevant to the repair of eye lid lacerations. The eye lid (Figure 1) is made up of the layers of skin, the orbicularis oculi muscle, the orbital septum (not shown), tarsal plate and the palpebral conjunctiva. The muscle layer extends close to the margin of the lid and is a visible dividing line between the inner and outer layers of the lid, known as the grey line. Towards the inner corner of the eye (medial canthus) are the lacrimal ducts, which drain tears away from the eye and into the nasal sinus. Additional features are the eyelashes, growing out in front of the grey line, and the openings of the meibomian glands, behind the grey line.

For the purposes of the initial simulation, we consider lacerations through the margin of the lid, in regions away from the lacrimal ducts, so the users will be primarily be concerned with alignment and approximation of the tarsal plate, skin surface and the margin of the eyelid.

In future versions, we will be including lacrimal ducts, which require more advanced techniques to repair, and the lateral canthal tendons, which are dissected as part of a procedure to relieve pressure from bleeding in the eye socket often due to blunt trauma. Similarly, while the current globe is in a fixed position, future versions will have both passive and active mobility, as described below.

1.4. Eye globe anatomy

Future versions of the simulator will focus on repair of injuries to the anterior anatomy of the eye globe, primarily partial and full-thickness lacerations through the cornea and sclera (white). The major structures of the anterior hemisphere of the eye (Figure 1) are the clear cornea, the anterior chamber, filled with watery aqueous humor, the iris, which contracts and dilates under the control of the ciliary muscle, the lens and capsule, the sclera (white), which is the structural wall of the eye, the choroid layer inside the sclera, and taking up most of the volume of the eye, the jelly-like vitreous humor.

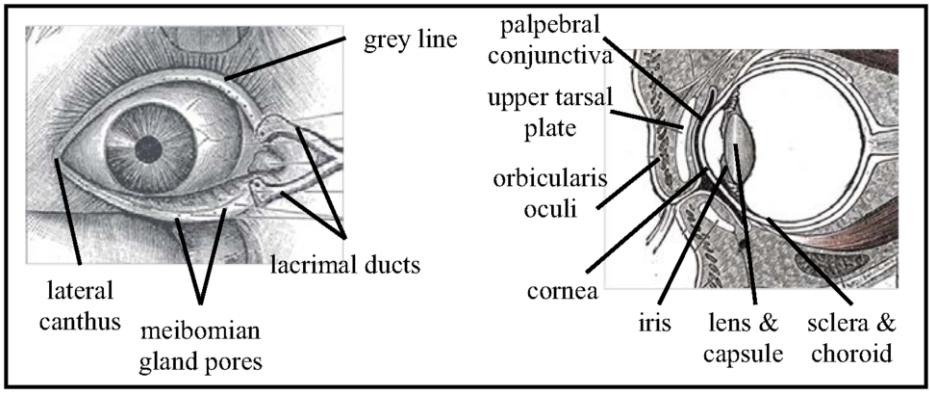

Figure 1: (left) External eye showing lacrimal ducts. (right) Cross section of the eye lid and globe. Adapted from http://en.wikipedia.org/wiki/File:Gray888.png, http://en.wikipedia.org/wiki/File:Gray896.png, http://en.wikipedia.org/wiki/File:Gray1205.png

2. System Overview

Out system is a stand-alone eye/face trauma simulator with augmented reality teaching/evaluation content. It consists of a mannequin head/neck with a replaceable eyelid and eye globe module. Titanium ophthalmic surgical instruments are tracked in six degrees of freedom (DOF) and grasping action and grasping force are measured. In the current version, the AR (augmented reality) hardware is comprised of a Microsoft Kinect and a pico-projector. A lighting system, stand, tray, electronics for the surgical instruments, and a host PC computer complete the system (Figure 2).

The physical components of the system are integrated as part of a learning system, which will keep track of user identity and performance, present teaching content relevant to particular training scenarios, monitor performance of surgical exercises during the particular scenario, and present feedback during and after the scenario, including performance scores.

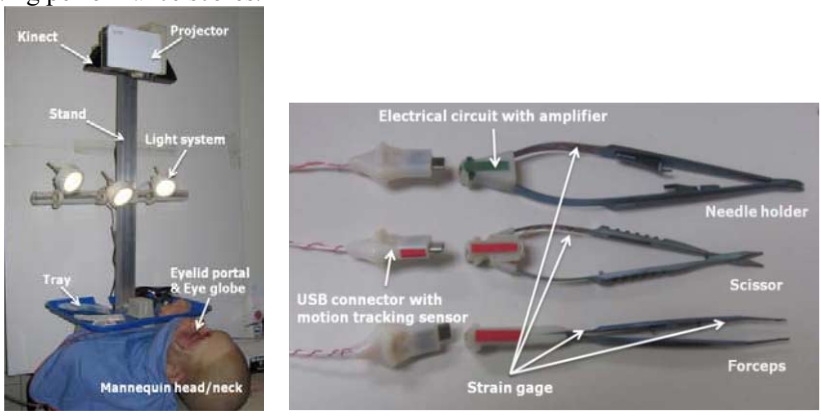

Figure 2: Stand-alone ocular and craniofacial trauma treatment training system: (left) Mannequin head/neck with eyelid portal and eye globe, and hardware architecture for augmented reality (AR) (right) Surgical instruments, hot-swappable connectors and signal conditioning circuitry.

2.1. Anatomical Modeling and Fabrication

At present, the major anatomical components of the system are the mannequin head/neck, multiple copies of a module including the tissue of the eyelids, brow, and upper cheek, and the eye globe itself. We will briefly describe the fabrication techniques for each of these.

2.1.1. Head form – skin and core

With the participation of a volunteer, adult male, we created a life cast (Figure 3) using standard techniques and materials (skin safe silicone, plaster wrap) to create the external impression. This mold was removed from the model and used to cast a clay first copy of the model's head. This clay positive was then textured and retouched by hand and molded again to create the final mold for the head. A plastic positive was cast from the mold and laser scanned, so that a graphical/CAD model with identical dimensions would be available for the simulation. A second positive, made of molding clay, was shaved down to approximate the shape of the underlying skull based on standard thicknesses of soft tissue over the skull. In the eye region, a cavity was created, offsetting the surface, so that replaceable modules fitting within this space could be subsequently fabricated. Finally, the external impression and the internal core were reassembled, with an additional insert occupying the space of the eye portal. A silicone skin, with the correct external and internal contours and eye portal space was cast. The CAD model was used to create a rapid prototyped core for use in mounting the replaceable components and the initial mounting of the tracking system field emitter.

Figure 3: Molding sequence for prototype head-form. Life casting. Clay duplicate. Plastic positive with 3D scanning fiducial marks. Silicone production mold. Plaster core with 3D scanning fiducial marks, air holes for skin casting. Final molded silicone skin, with pigmentation and replaceable trauma modules.

2.1.2. Ocular adnexa

The opening in the skin layer surrounds the trauma module inserts, which include the eyelids and surrounding tissues, both cast in silicone. The eyelids are complex structures that include multiple tissue layers and a variety of complex external

anatomical features, however, most significant for our first trauma scenario are the skin and a stiffer, underlying structure called the tarsal plate (Figure 4).

The tarsal plate was designed by first laser scanning the positive plastic casting of the eye portal. The scanned 3D model was then imported into SolidWorks CAD software and the surface model of the eyelid was thickened to create the mold for the tarsal plate. The mold was then printed on an Objet Eden 260V 3D printer (Objet Ltd., USA), capable of printing smooth and clear surfaced parts. During fabrication, a piece of nylon mesh is sandwiched between two tarsal plate mold parts and silicone is injected into the mold. The mesh helps to limit the tendency for punctures and cuts in the silicone to propagate. The part is removed from the mold and placed in the portal mold where silicone is again injected to create the eyelid with tarsal plate.

Figure 4: Molding of eye portal - production mold, early single material eyelid models; eye lids with "tarsal plates" (back and front after suturing during data collection scenario).

2.1.3. Eye globe

The current version of the globe (Figure 5) is similarly fabricated in various grades of silicone. A nylon mesh is wrapped around a two-piece inner mold core. An external core is aligned and attached to the inner, and white pigmented silicone is injected, forming the sclera (white of the eye). A stem at the back of the eye allows for removal of the inner core. Following removal, a molded, clear silicone lens, pigmented iris and clear cornea are bonded in place in the anterior segment of the eye globe, and a sealing plug to fill the stem at the posterior pole of the globe. The plug includes an access hole, filled with silicone adhesive, which is self-sealing after puncture. A syringe is used to evacuate air from the globe and replace it with a material representing the vitreous humor, a jelly-like material that fills the human eye behind the lens. We have employed a number of different materials for this purpose – polyvinyl acetate/borax "slime", egg white and Astroglide lubricant, all of which exhibit a "stringiness" when an instrument contacts the material and is withdrawn, similar to the vitreous humor.

Figure 5: Eye globe fabrication sequence and modeling, example of "stringiness" of materials similar to vitreous humor

2.2. Surgical Instruments, Tracking System and Sensors

2.2.1. Surgical Instruments

In the repair of lid (and later, globe) lacerations, a variety of surgical instruments are necessary. For our simulator, we provide the user with Castroviejo suturing forceps, a Castroviejo curved needle holder and curved Westcott tenotomy scissors (Figure 2 (right)). Additional instruments are available for future procedures, including finer tipped tools for corneo-scleral injuries. During scenarios, information on the instruments' spatial positions, open/close position and tip force, and surgeon's hand motion is required to grade the surgical techniques of users. To detect the instrument motion, we use miniature, magnetic position tracking sensors (Model 180 6DOF sensor, Ascension Technology, USA) and a tracking system (3D Guidance trakSTAR, Ascension Technology, USA). To be compatible with the magnetic tracking system, all of the instruments are fabricated from titanium. The instruments are enhanced with strain gages (CEA-06-062UW-350, Micro-Measurements, USA), which are placed at appropriate sites based on finite element analysis (SolidWorks 2012), to detect the open/close position of the instrument jaws and to measure the force applied between the jaws of the forceps to the tissue (Figure 6). To convert the gage output signals into useful data for our system, we developed miniature circuit boards (actual size 10mm x 16mm) with a microcontroller (Microchip PIC18F2450) and electrical components that are attached to each instrument. This is achieved using housings fabricated using the 3D printer. The microcontroller supports USB communication and has a 10-bit analog to digital converter with 10 different inputs. The board currently communicates with the PC using the USB bus. For each instrument, there are three analog output signals: one is the tool identification signal; the other two are the opening and force states of the tool. The tracking sensors are expensive and are tethered to their interface electronics, so to minimize cost and the number of cables that the surgeon must contend with, we developed interchangeable connectors between the instruments and DAQ/interface board, which also hold and align the tracking sensor with the instruments. Figure 7 shows the pad and component layout of the DAQ/interface board. To the left are three micro-USB connectors that mate with the instrument mini boards. Top and bottom are headers which allow connection to additional boards. To the right are (top to bottom), power supply, USB connection, and a chip programming interface connector. This board can also be used for future motor/pump control and additional sensor DAQ.

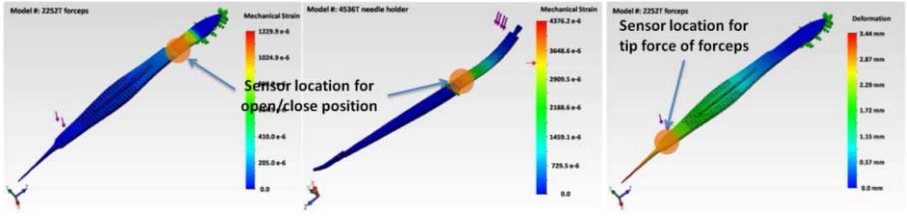

Figure 6: Finite element analysis results for half-model of each instrument: (left) the maximum strain sites at the rear of the instruments are the best place to detect the open/close position of instruments. (right) To measure the tip force we attached the strain gage to the flat inner surface as close as possible to the tip.

2.2.2. AR hardware

To detect hand motions around and display graphical overlays onto the mannequin head, we are using the Microsoft Kinect motion tracking system and a "pico" projector

(Vivitek Qumi). We also developed a portable framing system to ensure precise and reliable registration between the display and tracking systems. The projector and Kinect can be adjusted and locked into the best position. The head of the mannequin can extend over the edge of the table for access similar to a patient's head extending past the end of an operating table. The mannequin is rigidly fixed to the stand, avoiding vibration. A tray provides a site for a single-handed instrument exchange fixture. The lighting system was implemented on the simulator stand to approximate the intensity of surgical lamps and to minimize shadows. All of the parts can be disassembled for ease of transportation; off-site data collection tests are planned.

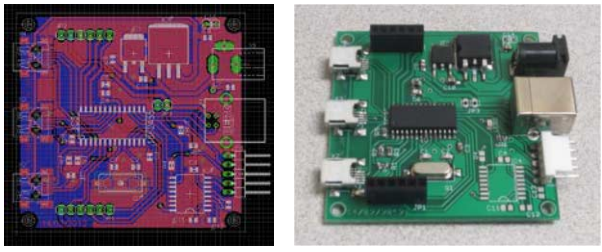

Figure 7: DAQ/interface board showing top-side component positions and board layout. To the left are three micro-USB connectors that mate with the instrument mini-boards. Top and bottom are headers which connect to additional boards. To the right are (top to bottom), power supply, USB connection, and a chip programming interface connector (for installing the firmware on the microcontroller).

2.2.3. Modular eye motion and pupil contraction systems

Future trauma scenarios will require additional functionality in the replaceable lid/globe modules, so we are developing eye motion and pupil contraction components. These motions are intended for first-responder scenarios, in which they can provide clues during diagnosis of the casualty in an emergency incident. As space is limited within a simulator's head, and noise from some types of motors may be distracting to the user, we are considering the use of shape memory alloy (SMA) wire actuation.

In one prototype, the eye motion component consists of two SMA linear actuators (MigaOne-15, MIGA Motor Company), a driver and motion limit detection circuit, a pivoting eye motion plate, ball-and-socket links, connectors, and supporters as shown in Figure 8 (left). The circular plate rotates in two degrees of freedom (pitch and yaw).

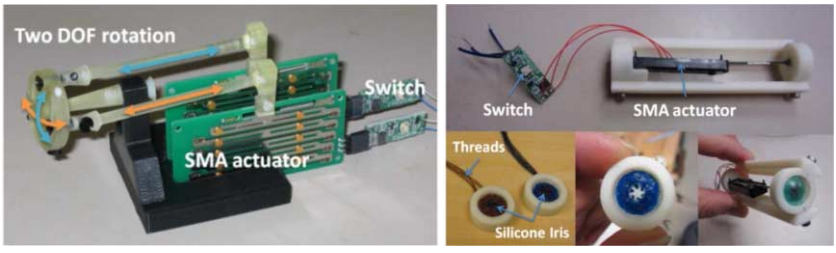

Figure 8: (left) 2DOF rotation eye motion and (right) pupil contraction components using SMA actuators.

In order to develop the pupil contraction component, we observed the range of motion of pupil contraction and dilation, and designed a contracting iris mechanism. Figure 8 (right) shows a silicone iris, supporting parts, fibers linking the iris to the actuator, and an SMA linear actuator (NanoMuscle NM706-Super, MIGA Motor Company). We sutured the inner margin of the silicone iris using thread, which passes through an array of holes. When the SMA actuator contracts, the fibers pull the inner

iris margin towards the center of the pupil. When the actuator is shut off, the elastic iris returns to its normally dilated position.

2.3. Content and learning architecture

Our initial developments towards a content presentation and learning architecture is geared towards junior surgeons with limited prior oculoplastics and globe surgery experience, and more senior physicians who may not have frequent trauma patient exposure. We aim to tailor the system to military surgeons, who would benefit from pre-deployment ocular and periocular surgical planning and technique refresher courses.

The planned architecture will allow access to background content and teaching materials on multiple platforms. Smart-phones, personal computers and similar devices would be appropriate at this stage. The user's interaction will begin with a typical login, in which the system recognizes the identity and level of expertise of the user. This will be followed by content access, logged by the system to allow bypass of such background when access to the simulator is available. In the current context, this would include relevant anatomy, suturing technique, operative strategy and surgical tips.

As mentioned, our first scenario is marginal lid laceration, although the current module design also supports non-marginal injury presentation. Injuries are generated by manually cutting through the skin and tarsal plate structures of the module in the location desired by the trainer/course proctor. At the outset of a simulator session, patient history, lab tests, pre-op imaging work and similar information will be presented to the user. Once these items have been reviewed, the simulator is initialized, the user takes hold of selected instruments, and the trauma module is unveiled.

The user, with instrument and hand-tracking enabled, will perform an examination of the injury, verify the absence of foreign bodies and additional injuries (in the initial scenario), and begin to conduct the repair. Tracking and sensor data are recorded to disk for post-processing at present, however we are developing online gesture recognition techniques to allow intra-operative feedback, such as suggestions when a non-standard technique appears to be used.

During the scenario, the user will be able to use two or three instruments simultaneously (surgeons often palm one instrument and pick up an additional one in the same hand before returning it to the tray – cutting of excess suture is one typical example, in which forceps or a needle holder are not put down first), and the tracking system will be able to identify which instrument is in use at a given time. For procedures requiring four or more instruments, the user will hot-swap the connector on the end of an instrument no longer in use, to the newly necessary device. The connector/DAQ system automatically detects its identity.

Following scenario completion, performance statistics will be presented to the user. At present, we can calculate task completion time and path length, as well as timing and sequence of instrument usage. We are developing techniques to identify distinct surgical gestures (e.g. knot tying, suture cutting, tissue grasping), so that finer grained, more useful feedback can be determined and presented to the user.

2.4. Data Acquisition and Event-based Gesture Segmentation Software

At present, software developments have primarily focused on data acquisition and instrument interface tools. The application has the flexibility to use multiple user interface input devices (e.g. mouse, SpaceNavigator, trackball). It records position

tracking streams from up to eight different magnetic position tracking sensors, from up to two strain gages on each instrument, and the identity of each instrument. In addition, Kinect outputs, representing hand motions (vs. instrument motions) are being integrated into the system; hand tracking can be used to detect actions like picking up a specific type of suture. All of these data are recorded as separate streams and saved in XML format. Simultaneously, a 3D rendering of the instruments and head form is displayed to the user (Figure 9). The system is easily expandable to track more instruments, the AR loupes when available, and head motion relative to the base once a flexible neck is implemented. The 3D rendering is important as it enables navigation around the scene, useful during the post processing playback as we manually observe task performance and work towards an automated gesture recognition algorithm.

Thresholding functions are built into the DAQ software, allowing preliminary segmentation using features such as closing and opening of scissors (indicating cutting), and the simultaneous closure of forceps jaws and the increase of measured force, suggesting that tissue has been grasped (vs. closing in free-space). Similarly, the entry into or exit from pre-determined regions of interest (RoI's) are recognized as meaningful state transitions. We refer to this as "event-based surgical gesture recognition," and propose that the subsequent recognition of sequences of events will be useful for identifying differences in performance between users. This process will be described in detail in a separate paper.

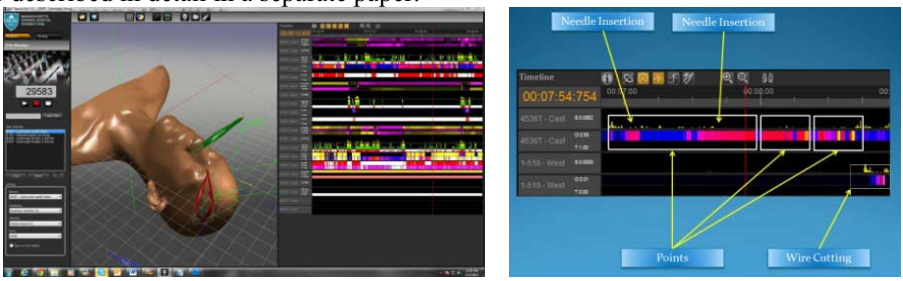

Figure 9: (left) Developer's interface showing data streams and graphical display of instrument positions. (right) Data stream examples showing discrete events to be segmented using software under development.

3. Data Acquisition Trials

Three of our subject matter expert oculoplastics surgeons have performed marginal laceration repair on our modules, in each case repairing cuts in nearly identical locations and of identical geometry (perpendicular, full-thickness upper lid laceration at lid mid-line, with extension of the laceration parallel to lid margin). They were asked to perform the repair, aligning and connecting the tarsal plate and overlying tissues, while making only commentary that would typically be employed in the OR (rather than in a teaching case, in which additional discussion would be necessary). Following the repair exercise, they performed a series of 15 partial tasks, including a variety of knot tying and suturing techniques, to help us collect data in support of detecting the discrete events within the extended full scenario testing.

In all of these tasks, instrument tracking was recorded, as was video-taping of the operative field, and an external observer's synchronized, manual event detection (time-stamped key presses). Analysis of these data is underway; the analysis techniques are described in an accompanying paper [16]. The results will be used to automate gesture

recognition during external user data collection trials in the next few months (these studies will be covered under appropriate human subjects research approvals from our IRB and that of the funding sponsor). Those tests will include both junior and senior surgeons, and we expect to find distinguishing characteristics between them that will allow us to provide meaningful and timely scoring and recommendation to future users.

4. Results

At present, we have a functional system that is in use by our subject matter experts for initial testing purposes. It is capable of:

- Real-time on-screen display of surgical motions with animated instruments
- Display of all trajectory, force, grasp position values in real time
- Detection of thresholds to identify grasp/release

We have identified, through the experts' usage experience, a series of improvements to the eye lid structure (addition of tarsal plate to original, single layer lid, corrections to the material properties of the tarsal plate and skin silicone selection). Similarly, the instrument connectors and cable management have improved, with additional sensor attachment stability, strengthened mating between the connector housing and the instruments, and modifications to the Velcro attachments we use to attach sensor wires to the user's wrists (and out of the way of the instruments).

Most importantly, initial data collections are allowing us to proceed towards the development of gesture segmentation algorithms and scoring methods.

Informal feedback from our surgeon experts suggest that we are close to acceptably realistic tissue stiffness, both around the lid region and around the rest of the head form. Similarly, they approve of the globe geometry, layer thicknesses, cornea and lens clarity, and properties of the vitreous humor.

5. Future work

We are progressing towards a complete system on a number of different fronts.

The eyelid anatomy continues to evolve as we implement additional realism. Meibomian gland pores, adjustments to layer thickness, and the addition of the lacrimal ducts and canthal ligaments are under development, as are methods for including conjunctival and muscle layers.

Revisions to the signal acquisition and conditioning circuitry are under way – the current "mini-boards" exhibit some heating in the circuit that is noticeable to the user and may be affecting the gain and/or offset of the force and grasp position signals.

The pupil contraction and ocular motion components are being integrated into a modified version of the existing globe anatomy, and additional sensors to detect the patency of repairs to corneo-scleral lacerations will be added to the system. These sensors will also be useful to aid in the detection of canthotomy/cantholysis treatment in response to simulated retrobulbar hemorrhage.

Beyond improvements to the current system, the head form will be reconfigured to accept multiple eye portals (left and right, and different trauma states), as well as facial hemorrhage and fracture modules, and airway components, which will support the detection of artificial airway devices and surgical cricothyroidotomy.

6. Acknowledgements

We would like to express our grateful appreciation of our Subject Matter Experts: Dr. Robert Mazzoli, Dr. Suzanne Freitag, M.D., Dr. Daniel Lefebvre, Dr. Justin Kanoff, Dr. Maria Troulis, and Dr. Steven L. Dawson.

This material is based upon work supported by the U.S. Army Medical Research Acquisition Activity under Contract No. W81XWH-11-C-0095. The U.S. Army Medical Research Acquisition Activity, 820 Chandler Street, Fort Detrick MD 21702-5014 is the awarding and administering acquisition office.

Any opinions, findings and conclusions or recommendations expressed in this material are those of the author(s) and do not necessarily reflect the views of the U.S. Army Medical Research Acquisition Activity.

7. References

[1] J. Breeze, K. McVeigh, J.J. Lee, A.M. Monaghan, A.J. Gibbons, Management of maxillofacial wounds sustained by British service personnel in Afghanistan. *Int. J. Oral Maxillofac. Surg. 2011*;40:483–486.

[2] J. Breeze J, Horsfall I, Hepper A, J. Clasper, Face, neck, and eye protection: adapting body armour to counter the changing patterns of injuries on the battlefield. **Br J Oral Maxillofac Surg. 2011** Dec;49(8):602-6. Epub 2010 Oct 30.

[3] R.A. Mazzoli, Don't Shoot Your Eye Out. *Naval Operational Medical Lessons Learned Newsletter*, Sept. 2008.

[4] EM Helveston, Coffey AC. Surgical practice kit. Ophthalmic suture simulator. *Arch Ophthalmol. 1986* Jun;104(6):923-4.

[5] R. Leuschke, A. Bhandari, B. Sires, B. Hannaford, Low cost eye surgery simulator with skill assessment component, *Stud Health Technol Inform*. 2007; 125:286-91.

[6] A. Yeh, B.T. Chan-Kai, A.K. Lauer, Basic training module for vitreoretinal surgery and the Casey Eye Institute Vitrectomy Indices Tool for Skills Assessment. *Clin Ophthalmol. 2011*;5:1249-56. Epub 2011 Sep 1.

[7] D.J. Solverson, R.A. Mazzoli, W.R. Raymond, M.L. Nelson, E.A. Hansen, M.F. Torres, Bhandari A, Hartranft CD. Virtual reality simulation in acquiring and differentiating basic ophthalmic microsurgical skills. *Simul Healthc*. 2009 Summer;4(2):98-103.

[8] E. Dumortier, J. Dequidt, S. Cotin, C. Duriez, J. Allard, J. Rouland, Computer-Based Training System for Cataract Surgery. *Proc. Third International ICST Conference on Electronic Healthcare for the 21st Century*, 2010.

[9] Millersville Review Staff. Saving Soldiers' Sight. *Review: Millersville University Magazine*. 2011:126(1):2-7

[10] D.D. Carda, D. Van, T.W. Johan, 2012 Model human eye. United States. Eye Care and Cure Pte. Ltd (Singapore, SG). US Patent No.: 8137111,

[11] R. Leuschke, A. Bhandari, B. Sires, B. Hannaford, Low cost eye surgery simulator with skill assessment component. *Stud Health Technol Inform*. 2007;125:286-91.

[12] S.L. Dawson, M.P. Ottensmeyer, S.M. Cotin, P.F. Neumann, Medical procedure training system. Application #: 10/488,415. Publication #: US 2004/0234933 A1. Filing date: Mar 2, 2004.

[13] E.M. Ritter, M.W. Bowyer, Simulation for trauma and combat casualty care. *Minimally Invasive Therapy*. 2005; 14:4-5; 224–234.

[14] N. Stylopoulos, S. Cotin, S.K. Maithel, M. Ottensmeyer, P.G. Jackson, R.S. Bardsley, P.F. Neumann, D.W. Rattner, S.L. Dawson, Computer-enhanced laparoscopic training system (CELTS): bridging the gap. *Surg Endosc*. 2004 May;18(5):782-9.

[15] R.S. Bardsley, M.P. Ottensmeyer, J.T. Samosky, S.L. Dawson. Methods and Apparatus for Autonomous Casualty Simulation. Application #: 12/067,260. Publication # US 2008/0227073 A1. Filing Date: Sep 28, 2006.

[16] G. De Novi, R. Bardsley, R. Shah, M.P. Ottensmeyer, J.C. Moore, B. Ahn. Event-driven Surgical Gesture Segmentation and Task Recognition for Ocular Trauma Simulation. *Proc. IMIASH 2012 - 1st International Workshop on Intelligent Multimodal Interfaces Applied in Skills Transfer, Healthcare and Rehabilitation, Guanajuato, Mexico.* Accepted for publication.

Workshop Proceedings of the 8th International Conference on Intelligent Environments
J.A. Botía et al. (Eds.)
IOS Press, 2012

doi:10.3233/978-1-61499-080-2-341

Event-driven Surgical Gesture Segmentation and Task Recognition for Ocular Trauma Simulation

Gianluca DE NOVI[a,b,1], Ryan BARDSLEY[a], Rajesh SHAH[a],
Mark P. OTTENSMEYER[a,b], John Cho MOORE[a], Bummo AHN[a,b]
[a]*Simulation Group, Dept. of Imaging, Massachusetts General Hospital*
[b]*Harvard Medical School*

Abstract. This paper describes a novel approach for segmenting surgical gestures in an eye trauma treatment simulator, based on the analysis of system and environmental events, generated in order to track user performance. Subdivision of surgical procedures into tasks & sub-tasks allows for application of more accurate metrics (optimized per task), which may more appropriately evaluate user performance. This approach may also be applied in other surgical contexts. For the specific case of eye trauma treatment this system can generate different classes of events that, when combined, may drive a state machine with the capability of subdividing the macro operation(s). The results of this process may be utilized to develop informative feedback to the user in the form of performance metrics and training guidance.

Keywords. Surgical gesture recognition, surgical simulation, surgical training, evaluation metrics.

Introduction

One of the most important aspects of surgical training tools is providing accurate and appropriate evaluation of user performance. This evaluation is a non-trivial process with many facets and approaches [1][2][3][4]. In the context of surgical gesture[2], performance is commonly evaluated through the analysis of movements and trajectories obtained from tracking the path of the surgical instruments, and their associated geometrical (spatial), and temporal features (e.g. smoothness, speed, and compactness) [4]. One method to improve this evaluation process is to reduce the overall surgical procedure into a set of tasks and to apply specific, task-oriented, evaluation metrics to each task [1]. Another important rationale for conducting this reductive process is that it permits selective exclusion of unrelated or extraneous actions (e.g. environment interactions) from potentially computation-intensive analyses. One of the issues related with the task evaluation approach is that the entire procedure must be subdivided into

[1] Corresponding author.

[2] A surgical gesture is the execution of a specific action, performed by moving and/or acting on the surgical tools.

tasks, subtasks and gestures automatically – computationally analyzing the movement data to identify each gesture, subtask, or task (gesture-subtask-task segmentation) [6][9]. A significant body of work has been devoted to this last topic. For example, research has been conducted based on evaluating the human body movements to analyze surgical gestures using human anatomy-driven hidden Markov models (HMM) [7]. While the most common approaches are movement-based, gesture segmentation does not necessarily need to be driven by analysis of the surgeon's (or surgical instruments) movements. The movement signal *is* necessary in order to identify the level of expertise of the surgeon. Efficient movements made by an experienced surgeon are typically more accurate and localized within the surgical field than dispersive and less compact movements made by novices [9].

This paper describes a new approach for surgical gesture segmentation and task recognition that can be performed by analyzing the *events* generated by the system (surgical instruments and environment) instead of the surgeon's (or surgical instruments) *movements*. The key motivation for focusing attention on the events generated by the system is that the events may contribute significant intermediate representations of information. This serves to discretize the movement recognition and analysis process, thereby reducing the complexity of segmentation. We define *events* as actions that can change the state of a state machine, e.g. opening and closing of a specific instrument, grasping with forceps, or entering/exiting from a specific region-of-interest. Assuming a well-structured system, it is possible to track the appropriate number and class of events. From this point, it may be possible to identify specific patterns of events/states that clearly correlate with specific gestures, subtasks and tasks of a surgical procedure.

The focus of this paper is the application of this event-driven approach in an ocular trauma simulator. However, this event-driven approach may be extended to a wider range of surgical procedures.

1. Background

In 2003, our group developed a laparoscopic skills trainer based on the SAGES Fundamentals of Laparoscopic Surgery (FLS) task curriculum. Using a modified commercial tracking system, the Computer-Enhanced Laparoscopic Skills Training Simulator (CELTS) allowed trainees to use actual laparoscopic instruments to perform FLS tasks on physical "task boards" including a silicone suture pad and peg-boards. The CELTS system resulted in the formation of several fundamental design concepts that we have leveraged in our current ocular and craniofacial trauma simulator. CELTS implements a full-color, real-time video display, rather than virtual rendering, to provide the surgical field of view. In combination with natural gravitation effects and standard laparoscopic instruments, CELTS provided trainees with a realistic approximation of procedural elements. The specialized tracking system permitted recording of translation and rotation with additional software-based task metrics. Using this system, our group demonstrated that appropriate performance metrics could be defined and a standardized scoring system could be designed [9].

The metrics generated by CELTS involved post-processing of the entire motion trajectory of the surgeon's gestures, which illustrated distinct differences in performance between experts and novices. However, finer-grained details used to provide real-time feedback and automated generation of suggestions for improvement,

could not be extracted using those metrics alone. To address this issue, we propose a method of event-based task segmentation that will enable immediate evaluation and improved feedback.

2. Methods

The methodology utilized for surgical gesture segmentation and task recognition is driven by specific patterns of events generated by the system. By this process, motion path analysis[3] is deferred to a conditional, later tier of analysis. The analysis of a list of discrete events is considerably less computationally expensive, than the continuous analysis on a moving window of data sampled at high rates from one or more surgical instruments paths. This may unambiguously indicate user actions and in cases where it does not, additional path analysis can be conducted on a focused subset of the streamed data. The same approach may be applied both to the subtask and task levels of analysis. As in other methodologies, the first step to perform is to determine the structure of a data frame of measured parameters at each time point. In our case, the parameters measured for each surgical instrument were: time stamp; instrument identity; raw sensor position and orientation; jaw closure; and jaw grasping force. Second order data extends the data frame by deriving instrument tip position, tip velocity, and tip acceleration.

Based on the data types available, we define sets of thresholds. Events are defined as threshold crossings. Observing the data frames over time, the system creates a list of time-stamped events, such as the moment when a spatial region of interest (ROI) is entered or an instrument's jaws are fully closing. This list of events would typically be orders of magnitude smaller than the original data set.

From a detailed task analysis of relevant surgical scenarios, we define *gestures* as meaningful patterns of *events*. The system creates recursively higher order lists of gestures, subtasks, tasks, and ultimately, procedures, corresponding with the different levels of the tasks analysis hierarchy (Table 1,Figure 1).

Identifying actions at each level of the taxonomy provides the opportunity to provide the best evaluation metrics at the most appropriate moment during the scenario. Depending on the training goals, this may be evaluation of decision processes, confirmation of correct sequencing of sub-tasks or gestures, or, when required, detailed analysis of a subset of the motion data within a gesture. At the same time, it allows exclusion from the evaluation process of extraneous motions (e.g. interacting with other colleagues or with the environment).

Table 1. System Taxonomy

Classification	Definition	Examples
First order data	Raw sensor data	• Instruments positions/orientations • Instruments opening/closing • Instruments force
Second order data	Data derived from raw sensor data	• Instruments tip positions • Instrument velocity

[3] Recognition of specific paths, curves and other features by specific features extracted from the path followed by the surgical tool.

Event	A crossing of a defined threshold for a given stream of sensor data or second order data	• Tip of needle holder enters a ROI. • Forceps open • Scissor cut
Gesture	A pattern of events	• Needle holder tip is closed. • Forceps grasp with medium tension • Needle holder pitches 95 degrees about its axis. • Cut w/ scissors
Subtask	A pattern of gestures	• Pass Needle • Two-throw knot tie • One-throw knot tie
Task	A set of subtasks	• 2-1-1 knot placement • Interrupted suture • Running suture • Exploration w/ forceps
Procedure	A set of tasks	• Full thickness eyelid laceration repair

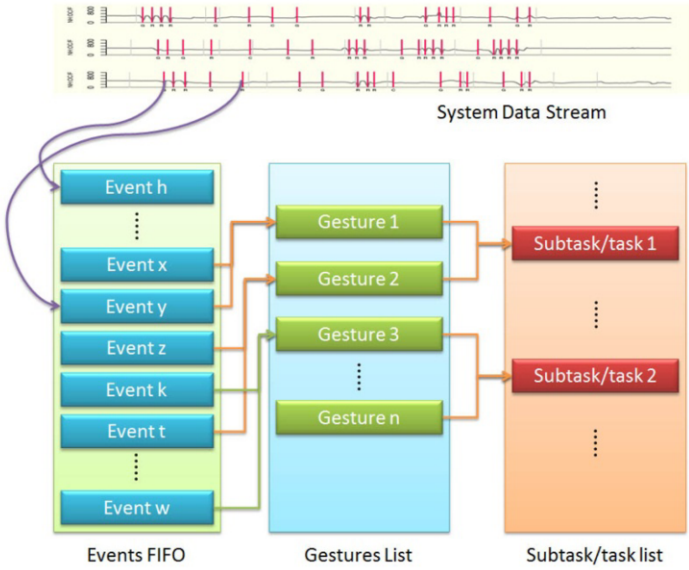

Figure 1. Organization structure of taxonomy.

3. Experimental Setup

The current approach was evaluated using the ocular trauma surgical simulator system that we are developing, described briefly below (Figure 2). The system is described in more detail in an accompanying paper [10].

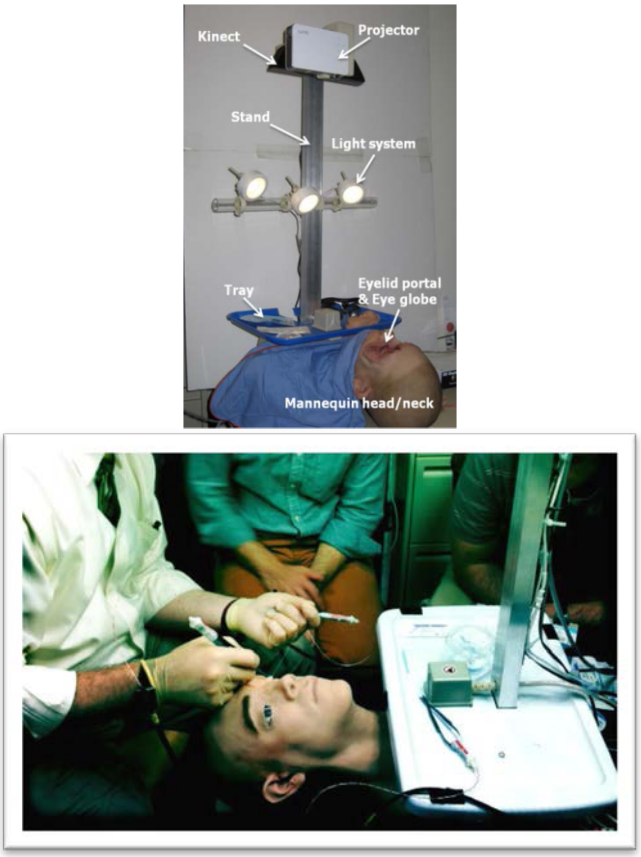

Figure 2. Simulation platform: mannequin head, instrument tray, tracking system, lighting system, overhead projector and Kinect tracker.

The platform is based on a silicone head attached to a vertical stand supporting a 3D camera (Microsoft Kinect™) used to track the interaction between the user and the simulation content, a set of lights, and a video projector. The mannequin head includes a set of interchangeable portals designed to simulate a range of trauma procedures (Figure 3, left). We are currently focusing on events related to repair of eyelid lacerations.

Figure 3. (left) Eye trauma portals and top view of instruments with position tracking sensors attached (right).

The system provides the user with a set of instruments necessary to perform relevant surgical tasks. Each instrument is connected to a magnetic tracking system (Figure 3, right), which measures instrument positions and orientations in six degrees of freedom

(DOF), and to a sensor circuit able to measure the opening/closing dynamics at the instrument tip and the force applied to the tip of the instrument. The sensors used on the surgical instruments are a set of strain gauges connected with a signal conditioning circuit board.

A series of opthalmic surgical instruments were connected to the magnetic tracking system for this evaluation (Figure 4)

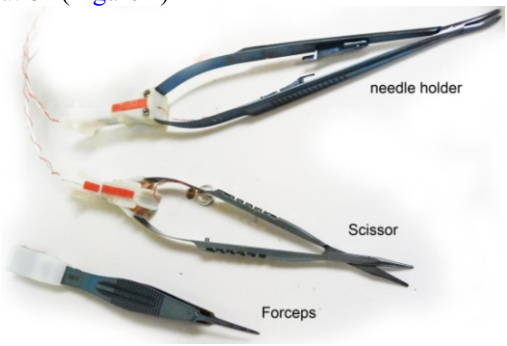

Figure 4. Surgical instruments set: 1-510 Westcott scissors curved tip, 2255T Castroviejo forceps, 4536T Castroviejo needle holder.

The system is controlled by data acquisition software (Figure 5, left), which provides capabilities to record data provided from the instruments/sensors and other environmental parameters. The Graphical User Interface (GUI) also provides real-time 3-dimensional (3D) displays of the mannequin and instrument positions, as well as configurable multi-track views of the recorded data.

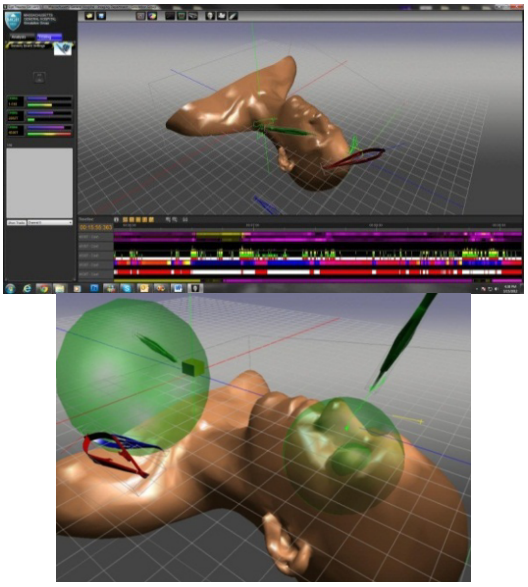

Figure 5. (left) GUI of data acquisition and analysis software. (right) Regions of Interest (ROIs) and instrument interactions with ROIs.

A significant feature provided by the software tool is the management of multiple spherical regions-of-interest (ROI), allowing the creation of maps and generating events for each crossing of an ROI boundary (Figure 5, right).

The software records the signals coming from the system (instrument position/orientation/state,) and displays this information in a timeline. To support the experimental design below, the interface also provides the capability to insert time-stamped markers, using an external interface device (mouse, keyboard, etc). The listing of these keystrokes is shown in Table 2.

Table 2. Direct Observation Markers

0. Null key
1. Needle point pierces tissue
2. Needle eye retrieved from tissue
3. Knot throws initiated
4. Knot pulled taught
5. Scissors retrieved from / returned to tray
6. Cut with scissors
7. Non-tracked hand action
8. User error or digression
9. Verbal comment

4. Experimental Design

The current prototype allowed collection of natural human interaction data in a highly-structured fashion to support initial investigation into our theory of event-driven gesture segmentation and subsequent task recognition.

To develop an understanding of how to parse the data collected by the simulator, it was initially necessary to identify what parameters constitute an *event*. Identification of the unique *types* of these events throughout a surgical procedure, currently focusing on suturing of an eyelid laceration, was also required.

4.1. Experimental apparatus

The subject matter experts (SMEs) were provided with one or two pairs of surgical gloves, depending on personal preference. Several varieties of suture and needle combinations were available to provide the SMEs with familiar interventional options. Across our three subject matter experts, preferences were for Ethicon 5-0 Perma-Hand silk with P-3 needles, Ethicon 6-0 Vicryl with P-3 needles, and Ethicon 6-0 Prolene sutures with P-3 needles. Task portals were inserted into the mannequin head, synthetic blood was applied to the wound, and the lacerated eye was covered with a Fox eye shield to hide the simulated injury until the beginning of the scenario. The prototype's LED lighting units were turned on, and were augmented with a Storz fiber optic Xenon surgical lamp, per the SME's request.

4.2. Protocol for Capturing Expert Data During a Simulated Eyelid Laceration Repair

In order to keep the SME's performance as natural as possible, the protocol was designed to minimize simulator-specific motions. Precautions were taken to avoid having the SME modify his or her natural gestures to accommodate discrepancies in the simulated procedure. Brief conversations with the engineers, comments on known issues with the prototype, and a general hesitation to break potentially fragile

components could have distorted how an SME would use the simulator. Surgeons are often also natural teachers and tend to explain their actions during the data capture process. Therefore, sessions began with strict guidance *not* to offer comments, illustrate thoughts by pointing with instruments, or teach using the simulator. The SMEs were instructed to remove the Fox eye shield, investigate the wound, and treat the injury as they would in real life. To ensure the session was as unbiased as possible, SMEs were asked to complete the full eyelid repair before focusing on repetitive tasks so as to avoid any simulator-specific learned behaviors. In addition to the unstructured surgical performance, the structured exercises recorded across all three experts were as follows:

1. Grasp suture from tray and load the needle in the needle holder.
2. Double-bite through both sides of incision, pull length of suture through
3. Double-bite with 2-1-1 surgeon's knot, excess cut with scissors
4. Single-bite through both sides of incision, pull length of suture through
5. Single-bite with 2-1-1 surgeon's knot, excess cut with scissors.
6. Suture placed, pull length of suture through until ready to tie knot
7. Suture placed, tying of 1-1-1 surgeon's knot.
8. **Suture placed, tying of 2-1-1 surgeon's knot.**
9. Suture placed, tying of 3-1-1 surgeon's knot.
10. Suture placed, tying of 3-1 granny-1 adjustable surgeon's knot.
11. Grasp tissue with forceps, light pressure.
12. Grasp tissue with forceps, normal pressure.
13. Grasp tissue with forceps, heavy pressure.
14. Vertical mattress suture.
15. Running suture.

Three eye portals were fabricated from our multi-layer multi-part molds that shared a similar laceration on the upper eyelid. The laceration was a full-thickness wound and was generally repaired with 6 to 8 interrupted sutures. Figure 6 shows the repairs and the sutures that were placed during the later discrete task sessions. Minimally guided performance by all three SMEs was found to be similar.

The system was configured to collect data from the SMEs on both a complete procedure, as well as a specific set of tasks. As the SMEs were performing both the open-ended eyelid laceration repair and the discrete event tasks, an observer manually recorded the data captured by using the keyboard attached to the simulator. These manual keystrokes facilitated the later synchronization of the multiple sources of data: overhead video, 3D path data, and the initial event recognition output. The manual keys were used when parsing the path data to begin to identify trends, distinct markings, and patterns while helping to ignore erroneous data.

Figure 6. Silicone eye portals illustrating the final suture patterns created by three different ocular surgeons.

5. Preliminary Data, Analysis and Discussion

The analysis below focuses on Exercise #8: the tying of a 2-1-1 surgeon's knot. The raw data collected by the simulator was parsed to begin to extract events that characterized this known task. Each track of data was analyzed using three different methods: visualization of the raw data, characterization of the recorded video, and normalization across all three sessions for each of the three SMEs.

Figure 7 shows the open/close position data collected from each of the three SMEs, overlaid with the corresponding manually identified needle grasp and release gestures. One can identify correspondence between the sensor data and the observations, which supports the proposition that an automated event detection and gesture recognition system can reproduce the manual observations.

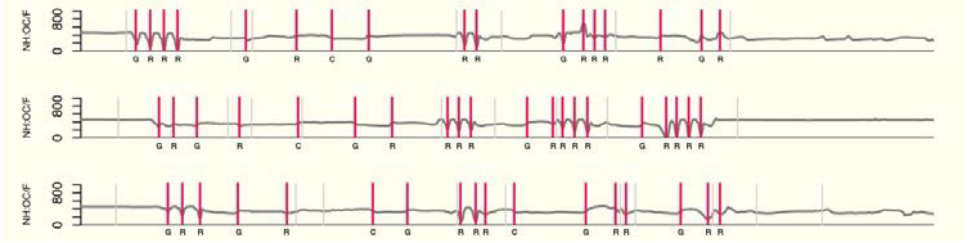

Figure 7. Raw needle holder open/close position data and overlaid observational event markings.

Figure 8 shows a schematic representation of the spatial ROIs around the eye. The radii of these spheres and their centers were established in relation to the real anatomy, and the raw position data processed to identify the boundary crossing events for each instrument. The time evolution of which ROI a given instrument occupies is shown in Figure 9, which presents the motion of scissors, from occupying the instrument tray to cutting a suture and returning. The sequence of events can be interpreted as the gestures: (A) "removal from tray," (B) "entry into working space," (C,C) "cutting of suture ends," (D) "exit from working area" and (E) "return to tray." Over multiple SMEs and multiple repetitions, this sequence of gestures was the same.

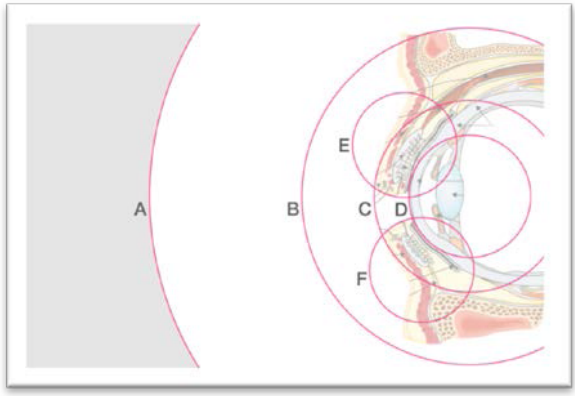

Figure 8. Regions of Interest (ROI) defining areas where the simulator begins to monitor instrument interaction to extract events for gesture segmentation:

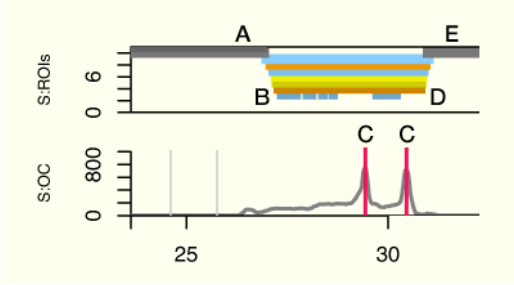

Figure 9. Use of scissors to cut suture ends

Using different combinations of event sequences and their derived gesture sequences, higher levels of the taxonomy can be identified, such as creating a 2-1-1 surgeon's knot. The full sequence is shown in Figure 10.

Both the forceps and the needle holder start within a relatively small ROI near the eye. During the process, the needle holder approaches more closely, entering a smaller ROI. Presence within the smallest ROI and the closure of the needle holder identifies the grasping gesture. The subsequent opening and closings are releases and re-grasping gestures as the needle passes through the tissue. The departure of the instruments from the nested ROIs suggests pulling the needle to draw the suture through the skin, and in combination with orientation thresholds (not shown) the forceps are palmed, pointing away from the suture site, hence apparently moving away, through the sequence of ROIs.

The re-approach and movement into and out of the small ROIs, followed by a needle holder closure (vs. grasp) signal the double wrap of suture around the needle holder and closing of the holder about the short end of the suture to form the knot, which is tightened at 10 seconds with the next passage outwards through the ROIs. The close-up closure and release gestures signal single wraps of suture and short tightening of the next two knot ties. Finally, the needle holder passes out of the eye centered ROIs and is palmed (orientation events not shown) and enters the instrument tray ROI, where the scissors are picked up brought inwards to cut the long end of the suture, to be returned and exchanged with the needle holder again. Together, these gestures constitute the 2-1-1 knot placement subtask.

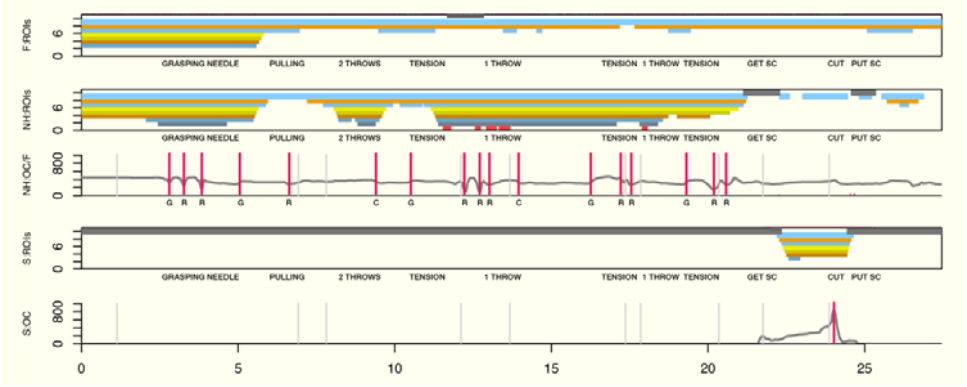

Figure 10. Full sequence of needle insertion and tying of 2-1-1 knot subtask.

This example presents the sequential re-composition of the raw data, events detected and gestures into a subtask. Longer sequences would be further composed into tasks making up a procedure. Similar observations of sets of expert performances will be parsed into the broad taxonomic library that the system under development will use to segment automatically trainee performance data sets, to identify where they perform sequences similarly to the experts, where and how they differ, and ultimately provide feedback in support of the learning process.

6. Conclusion / Ongoing Work

This paper presents the early stage development of a novel approach towards efficient and useful surgical task recognition and performance measurement. It reduces computational load compared with real-time motion trajectory analysis by identifying and operating on small numbers of discrete, low-level events, which are rebuilt into progressively higher level, meaningful taxonomic structures. This tiered system will permit the identification of key elements for evaluation, and trigger feedback appropriate to the level of analysis.

The next phases of the work focus on characterizing the remainder of subtasks that the SMEs performed; extracting additional thresholds to build the event library and the subsequent gesture and sub-task sequence libraries; validation of the analysis algorithms by comparing automated segmentation against manual recognition; and collecting extensive data sets from experts and novices to begin to distinguish how these two groups differ and when those differences rise to the level of triggering corrective feedback. A data collection protocol is currently under IRB review, in which military attending surgeons, fellows and residents will perform laceration repair and elementary exercised so their behavior can be compared. Ultimately, this will form a key element of the ocular trauma surgical simulator and provide new tools for developing other training systems.

Acknowledgements

We would like to express our grateful appreciation of our Subject Matter Experts: Dr. Robert Mazzoli, Dr. Suzanne Freitag, Dr. Daniel Lefebvre, Dr. Justin Kanoff, Dr. Maria Troulis, and Dr. Steven L. Dawson.

This material is based upon work supported by the U.S. Army Medical Research Acquisition Activity under Contract No. W81XWH-11-C-0095. The U.S. Army Medical Research Acquisition Activity, 820 Chandler Street, Fort Detrick MD 21702-5014 is the awarding and administering acquisition office.

Any opinions, findings and conclusions, or recommendations expressed in this material are those of the author(s) and do not necessarily reflect the views of the U.S. Army Medical Research Acquisition Activity.

References

[1] I. Hajshirmohammadi, S. Payandeh, Fuzzy Set Theory for performance Evaluation in Surgical Simulator, *Presence 2007*:16(6): 603-622.

[2] L. Moody, C. Baber, T.N. Arvanitis, Objective surgical performance evaluation based on haptic feedback. *Stud Health Technol Inform*. 2002;85:304-10.

[3] C. Sewell, Automatic Performance Evaluation in surgical Simulation, Doctoral thesis, Stanford University, 2007.

[4] C. Feng, H. Haniffa, J. Rozenblit, J. Peng, A. Hamilton, M. Salkini. Surgical Training and Performance Assesment Using a Motion Tracking System. *Proc. 18th European Modeling and Simulation Symposium*, EMSS06-4833796613, 2006.

[5] C.E. Reiley, G.D. Hager, Task versus subtask surgical skill evaluation of robotic minimally invasive surgery, *Med Image Comput Assist Interv. 2009*; 12(Pt 1):435-42.

[6] K. Kahol, N.C. Krishnan, V.N. Balasubramanian, S. Panchanathan, M. Smith, J. Ferrara, Measuring movement expertise in surgical tasks, *Proc. MULTIMEDIA '06, 14th annual ACM international conference on Multimedia*, 719-722, 2006.

[7] N. Padoy, T. Blum, I. Essa, H. Feussner, M.O. Berger, N. Navab, A boosted segmentation method for surgical workflow analysis. *Med Image Comput Comput Assist Interv*. 2007;10(Pt 1):102-9.

[8] S. Speidel, T. Zentek, G. Sudra, T. Gehrig, B.P. Müller-Stich, C. Gutt, R. Dillmann, Recognition of Surgical Skills using Hidden Markov Models, Medical Imaging 2009: Visualization, Image-Guided Procedures, and Modeling, edited by Michael I. Miga, Kenneth H. Wong, *Proc. of SPIE* Vol. 7261, 726125.

[9] N. Stylopoulos, S. Cotin, S.K. Maithel, M. Ottensmeyer, P.G. Jackson, R.S. Bardsley, P.F. Neuman, D.W. Rattner, S.L. Dawson, Computer-enhanced laparoscopic training system (CELTS): bridging the gap. *Surg Endosc.* 2004 May;18(5):782-9.

[10] M.P. Ottensmeyer, B. Ahn, J.C. Moore, E. Munteanu, S. Iorino, G. De Novi, R. Bardsley, R. Shah, P. Neumann, D. Langston, Ocular and Craniofacial Trauma Treatment Training System: Overview & Eyelid Laceration Module, *Proc. IMIASH 2012 - 1st International Workshop on Intelligent Multimodal Interfaces Applied in Skills Transfer, Healthcare and Rehabilitation*, Guanajuato, Mexico. Accepted for publication.